**Final Report – Work Packages 6 & 7**

# MMF/GSMA Phase 2: Scientific Basis for Base Station Exposure Compliance Standards

**IT'IS Foundation, Zurich, Switzerland**
**INTEC, Ghent University, Ghent, Belgium**
**Helsinki University of Technology, Helsinki, Finland**
**France Telecom Research & Development, Paris, France**
**Hokkaido University, Hokkaido, Japan**
**FDA, Silver Spring, Maryland, USA**
**ARC, Seiberdorf, Austria**
**EMSS, Stellenbosch, South Africa**

Zurich, June 2009
Version 21

# Contents

# Acronyms and Abbreviations

| | |
|---|---|
| 1 g SAR | 1 g Peak Spatial Average SAR |
| 10 g SAR | 10 g Peak Spatial Average SAR |
| BSA | Base Station Antenna |
| EMSS | Electromagnetic Software & Systems |
| FC | Fully Coupled |
| FDTD | Finite-Difference Time-Domain |
| FEM | Finite Elements Method |
| FTRD | France Telecom R&D |
| GHB | Generalized Huygens' Box |
| GSM | Global System for Mobile Communication |
| GSMA | GSM Association |
| HPBW | Half-Power Beamwidth |
| ICNIRP | International Commission on Non-Ionizing Radiation Protection |
| INTEC | Department of Information Technology, Ghent University / IBBT |
| IT'IS | Foundation for Research on Information Technologies in Society |
| MMF | Mobile Manufacturers Forum |
| MoM | Method of Moments |
| MPE | Maximum Permissible Exposure |
| NORMAN | Normalized Man |
| RF | Radio Frequency |
| rms | root-mean-squared |
| SAR | Specific Absorption Rate |
| UMTS | Universal Mobile Telecommunications System |
| UniH | Hokkaido University |
| VFB | Virtual Family Boy (6 years old) |
| VFF | Virtual Family Female |
| VFM | Virtual Family Male |
| VHM | Visible Human Male |
| wba SAR | Whole-Body Average SAR |
| WP | Work Package |

# 1  WP6: Full Wave SAR – Representative Base Station Antennas

**Conducted by IT'IS Foundation**

**Authors: Marie-Christine Gosselin, Valpré Kellermann, Günter Vermeeren, Stefan Benkler, Sven Kühn, Abdelhamid Hadjem, Azeddine Gati, Wout Joseph, Man Fai Wong, Joe Wiart, Frans Meyer, Luc Martens, Quirino Balzano, Niels Kuster**

**Executive Summary**

This study was initiated by the MMF/GSMA to support the development of the IEC standard PT62232.

The objective was to evaluate human (workers) exposure in front of various base station antennas operating in the frequency range of 300 MHz to 5 GHz. Further, estimation formulas for exposure based on the $95^{th}$ percentile worst-case principle have been developed in the considered exposure scenarios.

We assessed the exposure in various anatomical human models in front of base station antennas by performing full-wave numerical simulations using the finite difference time domain (FDTD) method implemented in the software platform SEMCAD X. A set of generic base station antennas has been developed from specifications of real base station antennas. The antennas were tuned to operate at 300, 450, 900, 2100, 3500, and 5000 MHz. Two antennas were developed for each frequency. Those models were simulated and validated using FDTD and the method of moments (MoM). Three members of the Virtual Family (male (VFM), female (VFF), and boy (VFB)) [Christ et al., 2009] were used. The human models were placed at distances of 10, 50, 300, 500, 1000 and 3000 mm from the antenna with both front and back sides facing the antenna.

Placement of the models at large distances in terms of wavelength causes the computational problem to become very large when using the traditional FDTD method. Thus, we developed a new method called the Generalized Huygens' Box (GHB) method. This method allows the separation of free-space antenna simulation and the human exposure evaluation. The incident fields from the antenna are simulated in free-space and recorded on the surface of the GHB surrounding the human model. For the purpose of the exposure evaluation, which requires a locally very fine grid resolution, the previously recorded fields are excited on the surface of the GHB with the model placed inside, and then the absorbed power in the model is calculated. The GHB method is only applicable to configurations where the decoupling between the human model and the antenna is sufficient. We evaluated the requirements in terms of separation distance by running GHB simulation in FDTD and the full-scenario (antenna and human model in place) using the MoM implemented in FEKO.

The simulated data points computed in function of antenna, distance and human model represent a complete data set to derive the absorption mechanism and to validate the developed estimation for the $95^{th}$ percentile exposure. It is obvious that the results cannot be used to assess the exposure distribution of adults since each applied human model only represents the average anatomy of its group.

The below estimation formula is based on the identified absorption mechanism derived from the simulated results combined with physical considerations.

$$SAR_{wb} = C(f)\frac{H_{eff}}{0.089\,\text{m}\cdot 1.54\,\text{m}}\frac{P_{rad}}{\Phi_{3\text{dB}}Ld}\left[1+\left(\frac{4\pi d}{\Phi_{3\text{dB}}G_A L}\right)^2\right]^{-1/2} \qquad (1)$$

$$SAR_{10g} = 25\cdot SAR_{wb}\frac{1.54\,\text{m}}{H_{eff}}\frac{1}{R_{wb/10g}} \qquad (2)$$

$$H_{eff} = \begin{cases} L & \text{if } H_{beam} < L,\ 1.54\,\text{m} \\ H_{beam} & \text{if } L \le H_{beam} < 1.54\,\text{m} \\ 1.54\,\text{m} & \text{if } 1.54\,\text{m} \le H_{beam} \\ 1.54\,\text{m} & \text{if } 1.54\,\text{m} \le L \end{cases} \qquad (3)$$

$$R_{wb/10g} = \begin{cases} 1.5 & \text{if } 300\,\text{MHz} < f < 2.5\,\text{GHz} \\ 1 & \text{if } 2.5\,\text{GHz} < f < 5\,\text{GHz} \end{cases} \qquad (4)$$

whereby $H_{beam} = 2d\tan(\Theta_{3\text{dB}}/2)$.

| $f$ MHz | $C(f)$ $10^{-4}\,\text{m}^3/\text{kg}$ |
|---|---|
| 300 | 6.3 |
| 900 - 5000 | 8.1 |

Table 1: Piecewise linear approximation of $C(f)$ resulting in a deviation of less than 5%. For frequencies between 300 MHz and 900 MHz, a linear interpolation should be used.

| | |
|---|---|
| $C(f)$ | frequency dependent coefficient |
| $d$ | distance between the antenna and the box bounding the human model |
| $f$ | frequency |
| $G_A$ | gain of the antenna |
| $H_{beam}$ | height of the beam at a distance $d$ from the antenna, based on far-field characteristics of the antenna |
| $H_{eff}$ | effective height of the cuboid, the irradiated section |
| $L$ | total length of the antenna |
| $P_{rad}$ | power radiated from the antenna |
| $R_{wb/10g}$ | worst-case ratio between the $SAR_{wb}$ to its limit and the $SAR_{10g}$ to its limit |
| $SAR_{10g}$ | peak spatial average SAR |
| $SAR_{wb}$ | whole-body average SAR |
| $\Phi_{3\text{dB}}$ | horizontal HPBW of the antenna |
| $\Theta_{3\text{dB}}$ | vertical HPBW of the antenna |

Equations (1) and (2) approximate the $95^{th}$ percentile whole body and peak spatial exposure of adults in the vicinity of base station antennas. The approximation formulas were successfully

validated with the bulk simulated data from this project as well as with data from the literature. The validation also demonstrates that the approximation is not always conservative for children. The available data do not allow the uncertainty of the approximation with respect to the $95^{th}$ percentile exposure to be determined. Nevertheless, the confidence is high due to the step-by-step approximation. The comparison with the simulated configurations does not provide indication for a strong overestimation nor underestimation of the $95^{th}$ percentile exposure.

In the reactive near field region, estimation formulas as well as full-wave simulations have been found to be problematic in estimating the human exposure due to the strong dependence of the localized absorption on the human anatomy. Furthermore, feedback of the human body on the antenna impedance, the feeding network in particular and possibly also the power amplifier, is not always predictable with state-of-the-art simulation tools. Thus, at close antenna-body distances of less than 200 mm, SAR measurements are strongly recommended for demonstrating compliance. An obvious choice for the phantom is the $95^{th}$ percentile cuboid.

| Model | Age | Weight kg | Height m |
|-------|-----|-----------|----------|
| VFM   | 34  | 72.2      | 1.80     |
| VFF   | 26  | 58.1      | 1.63     |
| VFB   | 6   | 19.4      | 1.18     |

Table 2: Characteristics of the human models

## 1.1 Exposure Configurations

All the possible combinations of these specifications have been simulated, leading to 432 exposure scenarios:

- 3 human models from the Virtual Family[1] (male (VFM), female (VFF), and boy (VFB))

- 12 base station antennas, 2 for each of 6 frequencies (300 MHz, 450 MHz, 900 MHz, 2100 MHz, 3500 MHz, and 5000 MHz)

- 6 distances (10 mm, 50 mm, 300 mm, 500 mm, 1000 mm, and 3000 mm)

- 2 sides (exposure from the front and the back of the model)

## 1.2 Human models

The three human models used for the simulations are members of the Virtual Family [Christ et al., 2009]. Table 2 presents their age, weight and height. The weight of the models varies with the density assigned to the content of the intestines and the stomach, in particular. The assignment of the dielectric properties and density of the tissues has been done according to the mapping presented in Section 3.

## 1.3 Specification of Generic Base Station Antennas

The antennas have been selected based on the experience of OrangeLabs (France Telecom RD) in order to represent typical wireless base station antennas. Two antenna models for each test frequency have been developed. Their specifications are summarized in Table 3. Detailed specifications are available in Appendix B. The antenna models are simplified generic antennas based on commercially available antennas. The models have been optimized to fit the specifications of the data sheets with respect to far-field radiation pattern. The 900MHz H65V7 X45V4 and the 2100MHz H65V7 OutdoorXPolV3 antenna models have further been validated with measurements in the radiating near-field of commercially available antenna samples (see Appendix B).

---

[1]The dielectric properties of the tissues have been assigned according to the parametric model described in [Gabriel et al., 1996].

| Frequency | Antenna | Type | Polarization | Number of elements | Height | Dir. | h-HPBW 3dB | v-HPBW 3dB | Example of commercial model |
|---|---|---|---|---|---|---|---|---|---|
| MHz | | | | | mm | dBi | degrees | degrees | |
| 300 | 300MHz H65V64 VPolV5 | Outdoor | vertical | 2 | 1000 | 9 | 66 | 60 | K 523057 |
| | 300MHz H116V32 VPolV2 | Outdoor | vertical | 2 | 1530 | 9 | 116 | 32 | K 739504 |
| 450 | 450MHz H118V35 VPolV4 | Outdoor | vertical | 2 | 1020 | 9.3 | 118 | 35 | K739504 |
| | 450MHz H180V19 VPolV4 | Outdoor | vertical | 4 | 1960 | 10 | 188 | 19 | DAPA 1280 |
| 900 | 900MHz H65V7 X45V4 | Outdoor | X | 8 | 2562 | 18.5 | 65 | 7 | K739 624 |
| | 900MHz H90V9 VPolV7 | Outdoor | vertical | 6 | 1922 | 15.9 | 90 | 9 | K736 863 |
| 2100 | 2100MHz H65V7 OutdoorXPolV3 | Outdoor | X | 10 | 1302 | 19.25 | 66 | 7 | K742 212 |
| | 2100MHz H90V80 IndoorVPolV4 | Indoor | vertical | 1 | 204 | 8.1 | 90 | 81 | K742 149 |
| 3500 | 3500MHz H18V18 VPol CPEV4 | CPE | vertical | 4×4 | 245 | 20 | 20 | 19 | Alvarion |
| | 3500MHz H65V9 VPol BTSV3 | BTS | vertical | 12 | 482 | 17.3 | 65 | 9 | Alvarion |
| 5000 | 5000MHz H65V35 VPol DirectionalV5 | Directional | vertical | 4 | 81 | 11.8 | 66 | 35 | Hubet & Suhner |
| | 5000MHz H360V7 VPol OmmiV4 | Ommi | vertical | 6 | 375 | 10.1 | 360 | 7 | SMCANT-00M10 |

Table 3: Specifications of the generic antennnas used in work packages 6 and 7.

## 1.4   Validation of Generic Base Station Antennas

The generic base station antennas presented in Section 1.3 have been modeled using the SEM-CAD X CAD modeling tool by OrangeLabs (France Telecom RD) based on the physical dimensions of the selected antennas. Those models have then been further optimized (tuned) by IT'IS in order to meet the specifications of Section 1.3 as well as showing a reasonable input impedance at the desired test frequencies using the FDTD method in SEMCAD X. In order to obtain further confidence in the correctness of the base station antennas, these have been independently validated by INTEC using the MoM. The comparison of the far-field results determined when using the MoM and FDTD compared to the nominal (target) values are displayed in Table 4. Good agreement with the nominal values and between the different methods was obtained.

Moreover, a good agreement has been found for the E- and H-fields from SEMCAD X and Feko in 4 vertical planes in front of the antennas. These results are shown in Section C.2

| Antenna | Nominal parameters | | | SEMCAD parameters | | | FEKO parameters | | |
|---|---|---|---|---|---|---|---|---|---|
| | Dir. dBi | h-HPBW deg | v-HPBW deg | Dir. dBi | h-HPBW deg | v-HPBW deg | Dir. dBi | h-HPBW deg | v-HPBW deg |
| 300MHz H65V64 VPolV5 | 9.0 | 60 | 66 | 9.7 | 58 | 63 | 9.7 | 59 | 64 |
| 300MHz H116V32 VPolV2 | 9.0 | 116 | 32 | 9.7 | 116 | 32 | 9.2 | 91 | 25 |
| 450MHz H118V35 VPolV4 | 9.3 | 118 | 35 | 9.7 | 114 | 30 | 9.7 | 120 | 33 |
| 450MHz H180V19 VPolV4 | 10.0 | 188 | 19 | 10.1 | 198 | 15 | 10.1 | 201 | 17 |
| 900MHz H65V7 X45V4 | 18.5 | 65 | 7 | 18.3 | 61 | 7 | 18.1 | 68 | 7.4 |
| 900MHz H90V9 VPolV7 | 15.9 | 90 | 9 | 16.1 | 88 | 8 | 15.6 | 91 | 10.2 |
| 2100MHz H65V7 OutdoorXPolV3 | 19.25 | 66 | 9 | 19.1 | 63 | 6 | 19.1 | 67 | 6.3 |
| 2100MHz H90V80 IndoorVPolV4 | 8.1 | 90 | 81 | 8.3 | 82 | 76 | 8.3 | 84 | 77 |
| 3500MHz H18V18 VPol CPEV4 | 20.0 | 20 | 19 | 20.0 | 17 | 18.5 | 20 | 18 | 19 |
| 3500MHz H65V9 VPol BTSV3 | 17.3 | 65 | 9 | 17.5 | 63 | 9 | 17.5 | 65 | 9 |
| 5000MHz H65V35 VPol DirectionalV5 | 11.8 | 66 | 35 | 11.6 | 66 | 35 | 11.6 | 67 | 36 |
| 5000MHz H360V7 VPol OmniV4 | 10.1 | 360 | 7 | 10.1 | 360 | 7 | 10.0 | 360 | 7.3 |

Table 4: Far-field characteristics of the generic antenna models: nominal values, and characteristics determined with MOM and FDTD methods.

|  | Difference (in %) between GHB and full scenario solutions | | |
|---|---|---|---|
| distance | wba SAR | 10 g SAR | 1 g SAR |
| 5 cm | 5.4 | -1.5 | -0.9 |
| 15 cm | 4.8 | 3.6 | 4.9 |
| 30 cm | 3.2 | 3.6 | 4.1 |
| 50 cm | -1.2 | -3.5 | -3.2 |
| 100 cm | -1.4 | -3.6 | -3.5 |

Table 5: Comparison of whole-body average and local SAR in the VFM for GHB and full scenario solutions using FDTD in SEMCAD X

## 1.5 Validation of Generalized Huygens' Box Approach

The numerical assessment of the local and whole-body SAR in a heterogeneous human body phantom for the considered configurations is an excessive task due to the limitations of computer hardware in terms of memory requirements. A new method was therefore used, called the Generalized Huygens' Box (GHB) method. It is based on the assumption that the coupling between the human body and the base station antenna can be neglected. In this approach, the complex incident field of the radiating near-field environment computed by MoM, FDTD or other methods is used as incident field input for the FDTD technique. In the FDTD platform SEMCAD X, the source is a box that uses the free-space electric and magnetic fields in a few planes adjacent each of its faces to interpolate the fields in the whole volume enclosed by the box. In our case, the human model was placed completely inside the source (Huygens' Box) and a few cells were left empty between the model and the box.

To verify the validity of this approach and to determine the limitations of its applicability, we performed a set of validation simulations in this work-package.

### 1.5.1 Generalized Huygens' Box Validation with FDTD

The initial verifications were performed with the FDTD method implemented in SEMCAD X. We selected the 2100 MHz H65V7 OutdoorXPolV3 antenna and the heterogeneous Virtual Family male (VFM) as models for these validation simulations. The simulations were run with the whole exposure scenario, i.e., the antenna in place, as well as with the GHB only (with the FDTD free-space incident fields from the antenna as input to the GHB). We evaluated the whole-body average and 1 g and 10 g average peak spatial SAR inside the body for separation distances of 5, 15, 30, 50 and 100 cm between the VFM and the antenna. The results are summarized in Table 5. The results indicated that the GHB seems to be applicable at least down to distances of $2\lambda$. Further validation with the MoM is presented in Section 1.5.2.

### 1.5.2 Generalized Huygens' Box Validation with MoM

The verification has been performed with the homogeneous Virtual Family model of the 6-year-old boy (VFB) in front of three generic base station antennas (300 MHz H65V64 VPolV5, 900 MHz H90V9 VPolV7, and 2100 MHz H90V80 IndoorVPolV4). For the verification of the method, the simulations were carried out with the GHB implementation in the FDTD method. The MoM (using FEKO) was used to simulate the whole exposure scenario with antenna and model in place. Additionally, the MoM was used to provide the free-space input fields for the GHB in FDTD.

For the validation setup, the following was specified:

- The antenna length was aligned with the z-axis, z plus pointing up. Its width was aligned with the y-axis and its depth with the x-axis. The direction of propagation was along x-negative. The vertical center of the antenna corresponded to z=0. The outer most point in x (towards x minus) corresponded to x=0. The position y=0 corresponded to the vertical symetry axis of the antenna. (see Figure 1)

- The model was placed facing the antenna, thus looking toward the positive x direction. Its vertical axis was aligned with the z-axis. The anatomical model is bounded by a box. The center of this box in the y- and z-directions corresponded to y=0 and z=0 respectively. The minimum distance (measured along the x-axis) between the antenna and the bounding box of the human model, $d$, was 0.3 m or 3 m.

- Every part of the human model was filled with an homogeneous medium (see dielectric properties in Table 7) with a density of 1000 kg/m$^3$.

- The antenna input power was normalized to 1 W.

- The whole-body average SAR was computed from the total absorbed power in the human model divided by its mass.

- The location of the maximum 10 g SAR was in center of cube. The 10 g SAR averaging was done according to IEEE C95.3. The maximum 10 g SAR value in the body was computed.

- The electric field along lines passing through the body center in $x$, $y$, and $z$ was extracted.

- The free-space E- and H-fields were computed using the MoM (EMSS). The coordinates of the GHB Source that were used in SEMCAD X are specified in Table 8. (The algorithm requires the input fields in 3 planes on each side of the faces of this source (see Figure 2)).

For the validation, we compared the whole-body average, 1 g and 10 g peak spatial SAR and their locations for the configurations computed with the MoM (FEKO) as well as with the GHB implementation in FDTD (SEMCAD X). The validation sheet of results completed by the participating groups is attached in Appendix J. The results of the comparison between the two methods, i.e. full scenario and GHB, are presented in Table 6. For the three frequencies used, the agreement of the whole-body SAR results is not good at a distance of 0.3 m, but satisfactory at 3 m. However, the comparison between the peak spatial average 10 g and 1 g SAR is not good for any distance and frequency. This is due to the differences in the averaging algorithms mentioned in Appendix D.

Additionally, we have compared the E-field along 1-d extraction lines within the volume of the GHB and at the same locations for the full scenario computed with MoM. The comparison graphs are presented in Appendix D. The fields agreed better at distances of 3 m than 0.3 m at 300 MHz, and agreed very well for both distances at 900 MHz and 2100 MHz. That confirms conclusions of Section 1.5.1, that the GHB method can be used at least for separation distances larger than 2λ.

|            |          | Difference (in %) between GHB and full scenario solutions | | |
|------------|----------|----------|----------|----------|
| frequency  | distance | wba SAR  | 10 g SAR | 1 g SAR  |
| 300 MHz    | 0.3 m    | -13.8    | -42.9    | -37.8    |
|            | 3 m      | -1.9     | 11.0     | -25.9    |
| 900 MHz    | 0.3 m    | 14.4     | 54.9     | 13.8     |
|            | 3 m      | 0.1      | -5.9     | 4.3      |
| 2100 MHz   | 0.3 m    | 7.6      | 3.7      | 2.9      |
|            | 3 m      | 2.0      | -18.9    | -9.8     |

Table 6: Comparison of whole-body average and local SAR in the VFB for GHB (FDTD) and full scenario (MoM) solutions
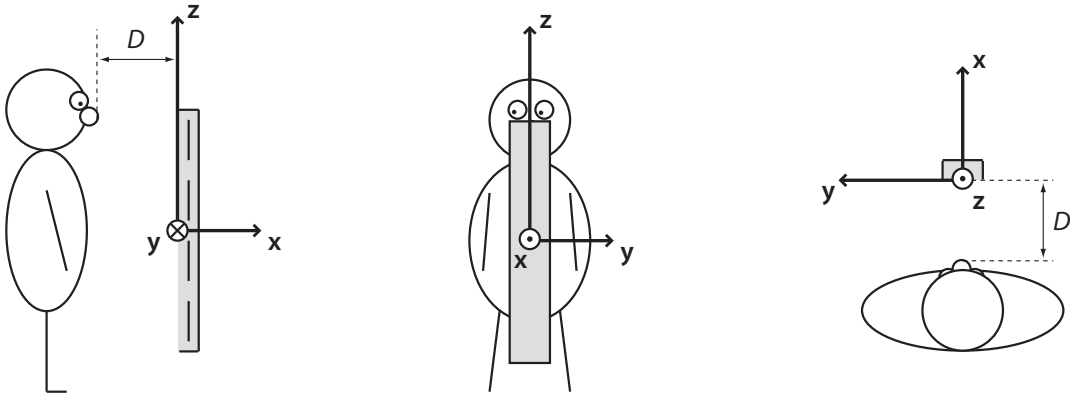


Figure 1: Axis definition for the GHB validation setup.

| Frequency MHz | Permittivity $\epsilon'_r$ | Conductivity $\sigma$ S/m |
|------------|--------------|--------------|
| 300        | 45.3         | 0.87         |
| 900        | 41.5         | 0.97         |
| 2100       | 39.8         | 1.49         |

Table 7: Dielectric properties of the human body model

|                            |          | for a distance of 0.3m | | | for a distance of 3m | | |
|----------------------------|----------|--------|--------|--------|--------|--------|--------|
|                            |          | x m    | y m    | z m    | x m    | y m    | z m    |
| GHB Source                 | corner 1 | -0.526 | -0.200 | -0.602 | -3.226 | -0.200 | -0.602 |
|                            | corner 2 | -0.284 | 0.200  | 0.602  | -2.984 | 0.200  | 0.602  |
| Human model bounding box   | corner 1 | -0.513 | -0.185 | -0.588 | -3.213 | -0.185 | -0.588 |
|                            | corner 2 | -0.300 | 0.185  | 0.588  | -3.000 | 0.185  | 0.588  |

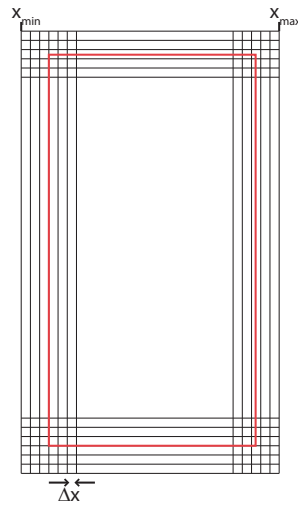Table 8: Coordinates of the GHB source and the human model bounding box

Figure 2: Input planes for GHB source.

| | VFB | VFM | VFF |
|---|---|---|---|
| 300MHz H65V64 VPolV5 | - | 3000 mm | 3000 mm |
| 300MHz H116V32 VPolV2 | - | ≥300 mm | 3000 mm |
| 450MHz H118V35 VPolV4 | - | ≥1000 mm | 3000 mm |
| 450MHz H180V19 VPolV4 | - | ≥1000 mm | 3000 mm |
| 900MHz H65V7 X45V4 | - | - | - |
| 900MHz H90V9 VPolV7 | 3000 mm | 3000 mm | - |
| 2100MHz H65V7 OutdoorXPolV3 | 3000 mm | 3000 mm | 3000 mm |
| 2100MHz H90V80 IndoorVPolV4 | 3000 mm | 3000 mm | - |
| 3500MHz H18V18 VPol CPEV4 | 3000 mm | ≥500 mm | ≥1000 mm |
| 3500MHz H65V9 VPol BTSV3 | 3000 mm | ≥500 mm | ≥1000 mm |
| 5000MHz H65V35 VPol DirectionalV5 | ≥300 mm | ≥300 mm | ≥300 mm |
| 5000MHz H360V7 VPol OmniV4 | ≥300 mm | ≥300 mm | ≥300 mm |

Table 9: List of configurations that have been simulated using the GHB

## 1.6   Bulk Simulation Setup

After the successful completion of the generic antennas and GHB approach validation, the bulk simulations have been set up for separation distances between the human and the antenna of 10 mm, 50 mm, 300 mm, 500 mm, 1000 mm, and 3000 mm. Simulations with the largest separation distances have been set up based on the outcome of the GHB validation (Section 1.5.2). Table 9 shows the configurations for which the GHB was used.

The orientation of the models relative to the antennas are equivalent to the definition in Section 1.5.2. This means that the vertical and horizontal centers of the antenna and the human model are aligned and the closest points between the antenna and the box bounding the model are spaced with the investigated distances.

Figure 3 displays the three models in front of a 900 MHz antenna at different distances. The dielectric properties have been assigned to all tissues according to [Gabriel et al., 1996] for all frequencies used. Five field sensors have been defined for every model, including the following parts of the body: right arm, left arm, head and trunk, legs and whole-body. Therefore, it was possible to distinguish the peak spatial average SAR in the limbs from the one in the trunk, and compare them to the appropriate ICNIRP basic restriction. The sensor including the whole body was used to extract the whole-body average SAR

The minimum grid step in the human models has been set depending on the frequency:

- at 300 MHz: 2 mm in the whole body

- at 450 MHz: 2 mm in the whole body

- at 900 MHz: 2 mm in the whole body

- at 2100 MHz: 2 mm in the whole body

- at 3500 MHz: 1.5 mm in the first half of the body, and 2 mm in the second half

- at 5000 MHz: 1 mm in the first half of the trunk, and 2 mm elsewhere.

Scripts for the automatic set up (including translation of the model and gridding of the simulation domain), running and post-processing of the simulations have been used.
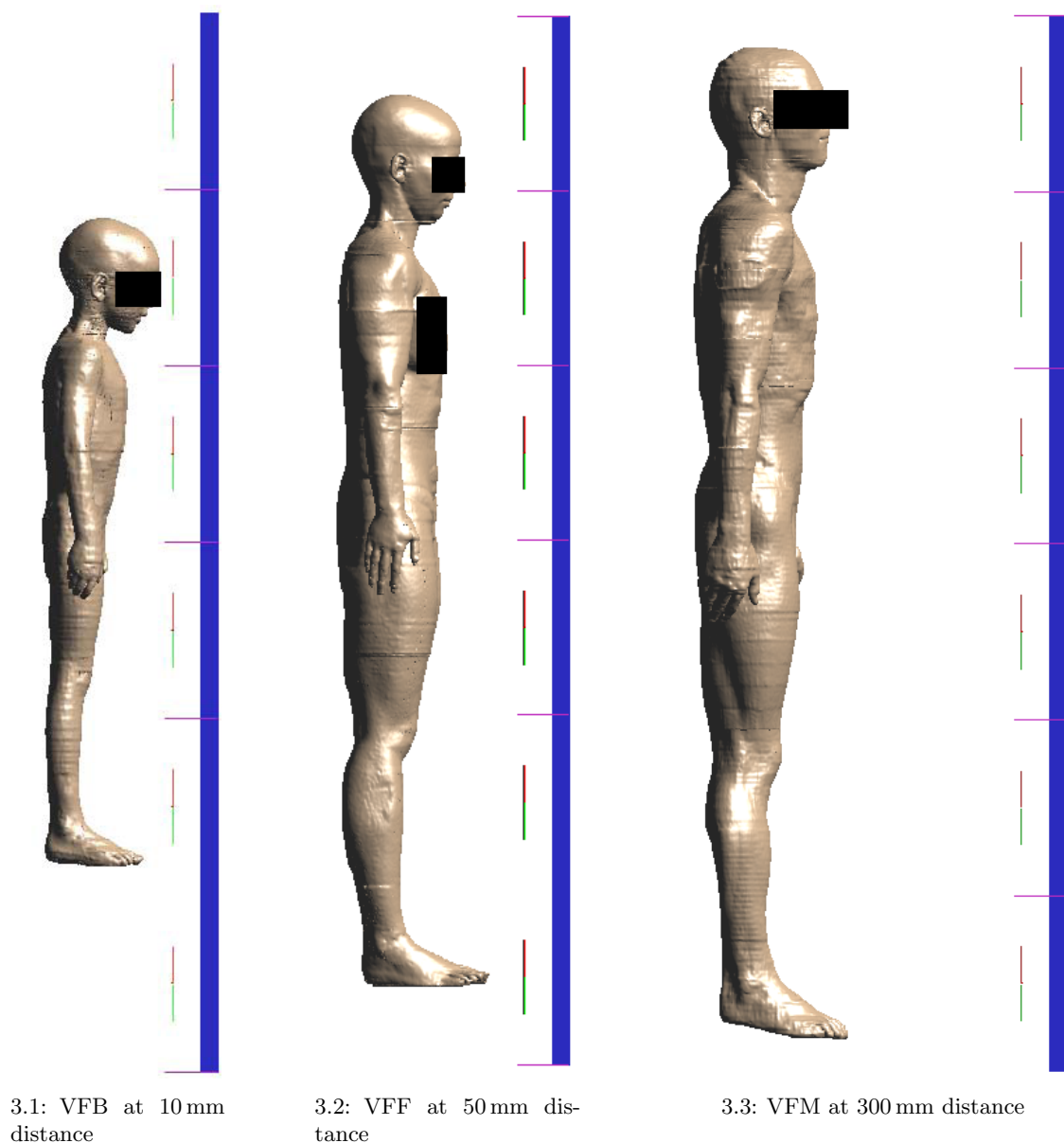
3.1: VFB at 10 mm distance

3.2: VFF at 50 mm distance

3.3: VFM at 300 mm distance

Figure 3: Simulation setups with the VFB, VFF, and VFM in front of an 900 MHz base station antenna.

## 1.7  $95^{th}$ Percentile Estimation Formula

### 1.7.1  Summary of the Method

WP 5 - WP 7 has defined a large number of simulations for 7 anatomical human models at specific frequencies covering the entire frequency range of interest. Despite the large number of data points, the results cannot be used to assess the $95^{th}$ percentile of exposures since each applied human model only represents the average anatomy of its group. Each member of the Virtual Family represents the average anatomy of its age group. The same applies for the Japanese couple. Norman is representative of the average European male. The Visible Human is taler and slightly fatter than the average of his height group. In other words, the applied models do not cover the required anatomical variation space and the statistical evaluation of the data for

estimation of the $95^{th}$ percentile exposure would be scientifically faulty.

On the other hand, the collected data provided a good basis to investigate the major absorption mechanism of humans exposed to base station antennas and to derive a generic approach to compute the $95^{th}$ percentile exposure as a function of the distance and the antenna parameters available in the data sheets. The simulated SAR results are particularly important to validate the approximation formula.

The elegant and sound approach to derive the $95^{th}$ percentile exposure consists of the following steps, the details of which are described in the next paragraphs:

- Generic human model: cuboid

- Statistical data of the human population

- Transmitted electric field into the cuboid as a function of the incident power density

- General form of the whole-body average SAR

- Enhancement on the whole-body average SAR from the tissue layering

- Whole-body average SAR from plane-wave exposure

- Peak spatial average SAR from plane-wave simulation results and the estimation of the whole-body average SAR

- Average power density from the properties of the antenna

- Whole-body average SAR from base-station antennas

- Issues at short antenna-body distances

The results of the estimation formula are validated by comparing to bulk simulation results in Section 1.8.

### 1.7.2   Generic Human Model

As a first approximation, the human phantom is considered to be a cuboid with the same height, weight, and skin surface as the human it represents. The cuboid is homogeneous with a density $\rho = 1000 \, \text{kg/m}^3$. However, the surface of a human is not trivial to determine. A few approximations exist, giving a relation between the surface of a human body, its weight, $m$, and its height, $H$, for example [DuBois and DuBois, 1916]

$$S_{DuBois}(\text{cm}) = 71.84 \, (m\,[\text{kg}])^{0.425} \, (H\,[\text{cm}])^{0.725} \, . \tag{5}$$

The cuboid is built using the height and the weight of the human model. It's total surface is calculated using (5) and the volume is found considering a uniform density ($\rho = 1000 \, \text{kg/m}^3$). The surface and the volume can also be expressed as a function of the dimensions of the cuboid (height, width and depth). Its width and depth are found by resolving this system of 2 equations and 2 unknowns. The largest of the two is associated to the width and the smallest to the depth. Each model can thus be represented by a unique cuboid. The cross-section is then calculated from the width times the height of the cuboid.

|        |     |     | $95^{th}$ percentile cuboid |
|--------|-----|-----|-----------------------------|
| weight | $m$ | kg  | 46.7                        |
| height | $H$ | m   | 1.54                        |
| width  | $W$ | m   | 0.339                       |
| depth  | $D$ | m   | 0.089                       |

Table 10: Dimensions of the cuboid representing the $95^{th}$ percentile human body

### 1.7.3   $95^{th}$ Percentile Human Body

Instead of basing the cuboid on the dimensions of a specific human body, a more general approach of the estimation formula consists of using the dimensions of a realistic human body which would lead to a worst-case exposure covering 95 % of the adult human population. For a uniform exposure over the entire cross-section of the cuboid, the whole-body average SAR, $SAR_{wb}$, can be estimated by

$$SAR_{wb} = \frac{S_{cs}}{m} P_{D,t},\tag{6}$$

where $S_{cs}$ is the cross-section of the cuboid (its height times its width) and $P_{D,t}$ is the power density transmitted in the solid. The highest wba SAR will be reached for a maximum ratio of $\frac{S_{cs}}{m}$. This has already been observed in [Kühn et al., 2009] and [Gosselin et al., 2009], as well as in the results of the bulk simulations of WP 6 (Section 1.8), where the whole-body average SAR is higher for smaller bodies, like children.

[Diverse Populations Collaborative Group, 2005] provides anthropometric data (mean and standard deviation of weight, height and bmi) of several groups of adults from the US, Europe and Asia. Assuming that these data are representative of the global population, 95% of the population have their weight, height and bmi included in the range 'mean $\pm$ 2 $\times$ standard deviation'. Figure 4 shows the cross-section on mass ratio of cuboids based on weights and heights within the range containing 95% of the population. The highest cross-section on mass ratio of $11.97 \cdot 10^{-3}\,\mathrm{m^2/kg}$ is obtained for the lightest human and its highest height (limited such that the bmi is also within the 95% range).

However, under base-station antenna exposure, the entire body is typically not exposed uniformly; the power density is higher around the vertical center of the antenna. In this case, a shorter but wider human body will be absorbing more radiation. According to Figure 4, the highest cross-section on mass ratio for the shortest human is also found for the minimum mass. Its value of $11.23 \cdot 10^{-3}\,\mathrm{m^2/kg}$ is 94% of the cross-section on mass ratio found for the tallest and lightest human. In the case of exposure to base-station antennas, this is more likely to lead to the highest whole-body average SAR. Furthermore, this value of cross-section on mass ratio can be reached for the whole range of heights representing 95% of the population. Thus, the cuboid representing the $95^{th}$ percentile representative human (the lightest and shortest one) has the dimensions listed in Table 10.

If the base station antenna is such that the exposure is uniform over the entire height of the model, we expect this cuboid to lead to a conservative estimation of the exposure for 90% of the adults. Otherwise, the estimation will be conservative for 95% of the adults in the population. The human models developed for the Virtual Family are representative of the average human in the population (based on statistical data from [Diverse Populations Collaborative Group, 2005]). Since the estimation formulas have been developed based on the premise to be conservative for 95% of the adult population, we do not expect the simulation results from the Virtual Family models to exceed the exposure predicted by the estimation formulas.
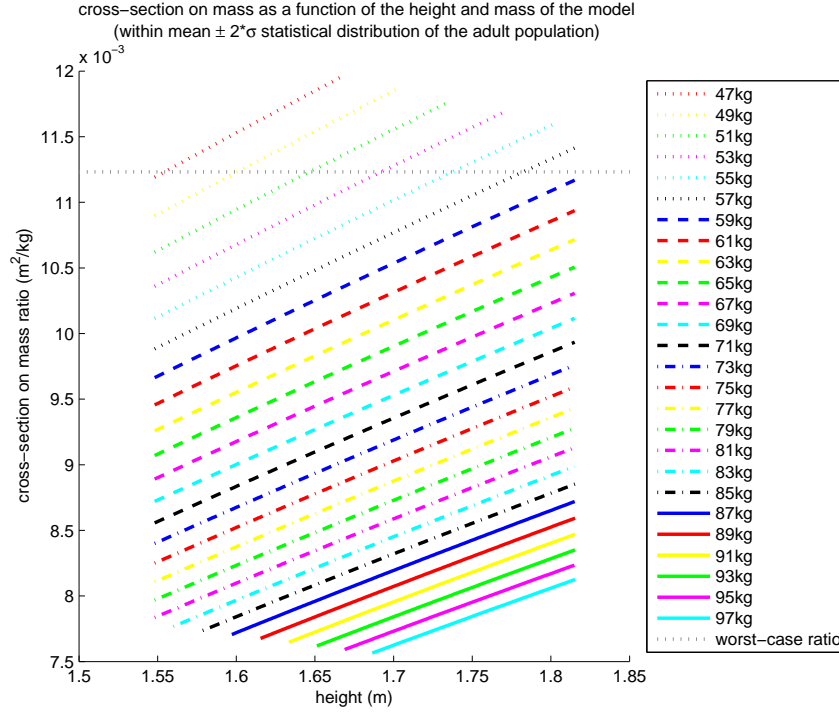
Figure 4: Cross-section on mass ratio as a function of the mass and height of the body

### 1.7.4   Induced Power Density

The relation between the power density, $P_D$, and the electric and magnetic fields of a propagating wave, $E$ and $H$ respectively, is

$$\vec{P}_D = \Re\{\vec{E}_{rms} \times \vec{H}_{rms}^*\}. \tag{7}$$

Assuming plane-wave propagation, the electric and magnetic fields are perpendicular and the impedance of the wave is defined as $Z = |E|/|H| = \sqrt{\frac{\mu}{\epsilon}}$, where $|E|$ and $|H|$ are the norm of the electric and magnetic fields, respectively, $\mu$, the complex permeability, and $\epsilon$, the complex permittivity. Thus (7) can be written as

$$P_D = \Re\left\{ E_{rms} \cdot \left( \frac{E_{rms}}{Z} \right)^* \right\}. \tag{8}$$

For a plane wave coming from free space at normal incidence to a non-magnetic medium of complex permittivity $\epsilon_2$, the transmitted electric field, $E_t$, is related to the incident electric field, $E_i$, via the transmission coefficient, $t$.

$$E_t = tE_i \tag{9}$$

$$= \frac{2}{1 + \sqrt{\epsilon_2}} E_i. \tag{10}$$

The transmitted power density, $P_{D,t}$, can then be written

$$P_{D,t} = \Re\left\{E_{rms,t}\left(\frac{E_{rms,t}}{Z_t}\right)^*\right\} \tag{11}$$

$$= \Re\left\{tE_{rms,i}\left(\frac{tE_{rms,i}}{Z_t}\right)^*\right\} \tag{12}$$

$$= \Re\left\{\frac{|E_{rms,i}|^2\,|t|^2}{Z_t^*}\right\} \tag{13}$$

$$= |E_{rms,i}|^2\,|t|^2\,\Re\left\{\frac{1}{Z_t^*}\right\}. \tag{14}$$

And using (8) for the definition of the incident power density to replace $E_{rms,i}$, it becomes

$$P_{D,t} = Z_i\,|t|^2\,\Re\left\{\frac{1}{Z_t^*}\right\}P_{D,i}, \tag{15}$$

or under the form

$$|E_{rms,t}|^2 = Z_i\,|t|^2\,P_{D,i}. \tag{16}$$

### 1.7.5   Whole-Body Average SAR

Based on the same type of development as in [Kanda et al., 2004] for the 10 g SAR, the SAR in the whole body of volume $V_{tot}$ can be estimated from the SAR at the surface of the model. The definition of the whole-body average SAR, $SAR_{wb}$, from the position-dependant local SAR, $SAR(x, y, z)$, is

$$SAR_{wb} = \frac{1}{V_{tot}}\iiint\limits_{vol} SAR(x,y,z)dxdydz. \tag{17}$$

For a wave propagating in the $x$-direction, we assume that the SAR in the $yz$-plane is uniform over the 'exposed region', $R_{yz}$, and zero outside. The SAR decays exponentially along $x$ from the surface of the medium to its depth, $x_d$, so (17) becomes

$$SAR_{wb} = \frac{1}{V_{tot}}\iiint\limits_{vol} SAR(x)dxdydz \tag{18}$$

$$= \frac{1}{V_{tot}}\iiint\limits_{vol} SAR(0)e^{\frac{-2x}{\delta}}dxdydz \tag{19}$$

$$= \frac{1}{V_{tot}}\iint\limits_{R_{yz}} dydz\int_0^{x_d} SAR(0)e^{\frac{-2x}{\delta}}dx \tag{20}$$

$$= \frac{1}{V_{tot}}\iint\limits_{R_{yz}} dydz\left[\frac{\delta}{2}SAR(0)\left(1 - e^{\frac{-2x_d}{\delta}}\right)\right], \tag{21}$$

where $\delta$ is the penetration depth. Worst-case will be reached for a thick model that will absorb all the power ($x_d \gg \delta$). Thus, the exponential term in (21) will be negligible:

$$SAR_{wb} = \frac{1}{V_{tot}}\frac{\delta}{2}SAR(0)\iint\limits_{R_{yz}} dydz. \tag{22}$$

For plane waves, the penetration depth is expressed as a function of the angular frequency, $\omega$, the real part of the relative permittivity, $\epsilon'_r$, and the conductivity, $\sigma$:

$$\delta = \frac{1}{\omega} \left[ \left( \frac{\mu_0 \epsilon'_r \epsilon_0}{2} \right) \left( \sqrt{1 + \left( \frac{\sigma}{\omega \epsilon'_r \epsilon_0} \right)^2} - 1 \right) \right]^{-1/2}. \tag{23}$$

### 1.7.6   Tissue Layering

The work of [Christ et al., 2006a] and [Christ et al., 2006b] have shown that standing waves in the layers of tissues can increase the local SAR by as much as 5 dB. Based on their work, calculations of layered half-spaces with different configurations of layers of tissue types exposed to incident plane waves from 30 MHz to 5.8 GHz have been performed. The layer thicknesses were based on human anatomical data. The effect of layers on the total absorbed power has been determined, comparing the total absorption in the layered body to the one in the homogeneous body with dielectric properties set according to [IEC, 2009]. The tissue layering configuration resulting in the maximum absorbed power has been determined by a 1d numerical simulation based on analytical equations. Those results have been validated using FDTD for the determined layering configuration in the abdomen compared to the homogeneous case.
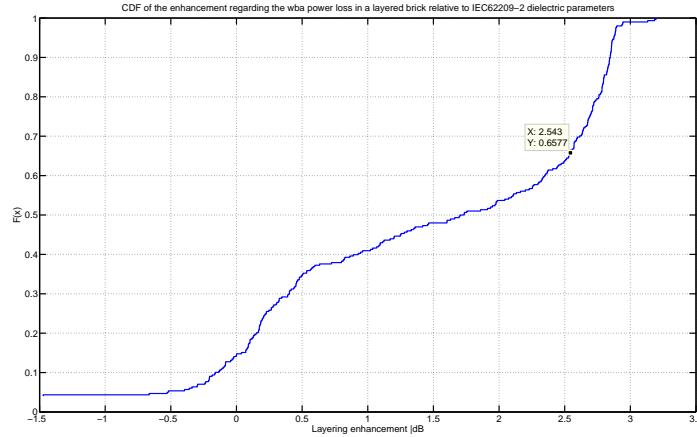


Figure 5: Cumulative distribution function of the enhancement of the absorbed power in a layered volume compared to an homogeneous volume

Figure 5 shows the cumulative distribution function of the enhancement of the total absorbed power in the different configurations of layers compared to an homogeneous solid, i.e. the fraction of configurations of layers conservatively estimated as a function of the layer enhancement factor. From these results, we have chosen an enhancement factor of 2.5 dB due to the tissue layers. This factor includes about 65% of the layers configurations. The highest enhancements are found for layers configurations including a lot of fat. However, the $95^{th}$ percentile human with respect to wba SAR (see Section 1.7.3) is rather a skinny person. Also the layering will not be homogeneous in a real human as assumed in the half-space model. Thus, a worst-case enhancement value (3 dB according to Figure 5) would not be realistic when considering a worst-case human and would lead to an over-conservative estimation. The whole-body average SAR including the layer enhancement factor will be a factor $10^{2.5/10}$ higher than the whole-body average SAR of a homogeneous volume.

### 1.7.7   Whole-Body Average SAR – Plane-Wave Exposure

For a cuboid under uniform plane-wave exposure, the exposed region $R_{yz}$ is simply the area of the surface of incidence, and (22) becomes

$$SAR_{wb} = \frac{1}{V_{tot}} \frac{\delta}{2} W_{body} H_{body} SAR(0) \tag{24}$$

$$= \frac{1}{D_{body} W_{body} H_{body}} \frac{\delta}{2} W_{body} H_{body} SAR(0) \tag{25}$$

$$= \frac{1}{2} \frac{\delta}{D_{body}} \frac{W_{body}}{W_{body}} \frac{H_{body}}{H_{body}} SAR(0) \tag{26}$$

$$= \frac{\delta}{2 D_{body}} SAR(0), \tag{27}$$

where $D_{body}$, $W_{body}$, and $H_{body}$ are the depth, width, and height of the cuboid used as an approximation of the body, respectively.

Knowing that the SAR is given by

$$SAR = \frac{\sigma |E_{rms,t}|^2}{\rho}, \tag{28}$$

where $\sigma$ is the conductivity, one can find the SAR at $x = 0$ inside a medium, $SAR(0)$, using (16), if the incident face of the medium is perpendicular to the direction of propagation of the wave:

$$SAR(0) = \frac{\sigma}{\rho} Z_i |t|^2 P_{D,i}(0). \tag{29}$$

To validate the cuboid approach, simulation results of vertically polarized plane waves have been compared to the estimation of the whole-body SAR from (27) and (29). Figure 6 shows the results from plane-wave exposure of the VFB from [Kühn et al., 2009] and WP 5 [Uusitupa et al., 2009]. The results are expressed as the percentage of the whole-body average SAR basic restriction reached for a plane-wave exposure at the reference level (according to ICNIRP, see Tables 11 and 12). Additional plane-wave simulations have been performed using an homogeneous cuboid based on the height and weight of the VFB (cuboid: 19.4 kg, 0.065 m × 0.253 m × 1.176 m). These dimensions have also been used to estimate the whole-body average SAR from (27) and (29). The dielectric properties have been set according to [IEC, 2009], which are based on a 95% requirement for near-field exposure.

Figure 6 shows that the simulation of the cuboid as well as the estimation of the whole-body average SAR based on its dimensions underestimate the whole-body average SAR for the whole frequency range. An estimation of the whole-body average SAR including the layering effect (Section 1.7.6) has also been plotted on Figure 6. This curve represents the simulation results in a more accurate way. However, at low frequencies (around 100 MHz), the simulation results are much higher than the approximation, due to the whole-body resonance that is not taken into account into the estimation formula. For higher frequencies ($> 2$ GHz), the dielectric properties of the uniform liquid lead to more conservative results from the cuboid simulations, as well as from the approximation including the layering enhancement. We can conclude that equation (27) is a good approximation for frequencies between 100 MHz and 2000 MHz and more conservative for higher frequencies.

### 1.7.8   Peak Spatial Average SAR

From the results of [Kühn et al., 2009], it can be shown that for frontal plane-wave exposure of vertical polarization, the ratio between the whole-body average SAR and the peak spatial

|                        | SAR W/kg |
|------------------------|----------|
| Whole-body average     | 0.4      |
| 10 g in head and trunk | 10       |
| 10 g in limbs          | 20       |

Table 11: ICNIRP basic restrictions for occupational exposure, for frequencies between 10 kHz and 10 GHz

| Frequency range | plane-wave power density W/m$^2$ |
|-----------------|----------------------------------|
| 10-400 MHz      | 10                               |
| 400-2000 MHz    | $f/40$                           |
| 2-300 GHz       | 50                               |

Table 12: ICNIRP reference levels for occupational exposure
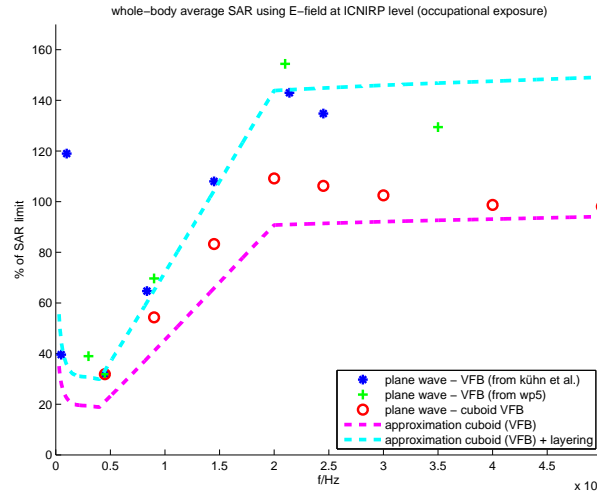


Figure 6: Comparison between whole-body average SAR of the heterogeneous VFB from plane-wave exposure and the cuboid approximation

average SAR does not vary a lot for frequencies between 50 MHz and 2.5 GHz. The ratio leading to the highest peak spatial average SAR for a given value of whole-body average SAR is found for the Visible Human model. In this case, the ratio between the whole-body average SAR to ICNIRP limit, $R_{wb}$, and the 10 g peak spatial average SAR to ICNIRP limit, $R_{10g}$, is roughly equal to 2.

In [Djafarzadeh et al., 2009], plane-wave exposure of six child models between 5 and 14 years of age at 2 GHz, 4 GHz, and 6 GHz show that the previously mentioned ratio is twice as small at 4 GHz and 6 GHz than it is at 2 GHz.

The peak spatial average SAR is highly dependent on the anatomical properties and posture of the phantom. The position of the potential local enhancement parts of the body relatively to the antenna and the beam is also of great influence. Thus, the spatial peak average SAR for a specific configuration of antenna and phantom is hard to evaluate without a simulation. However, the ratio between the whole-body average SAR and the peak spatial average SAR

allows a rough but simple worst-case estimation. Figure 7 uses plane-wave exposure data from WP 5 [Uusitupa et al., 2009] to show the ratio between the whole-body average SAR (to its ICNIRP basic restriction, $SAR_{wb}^{icnirp}$) and the peak spatial average SAR (to its ICNIRP basic restriction, $SAR_{10g}^{icnirp}$).
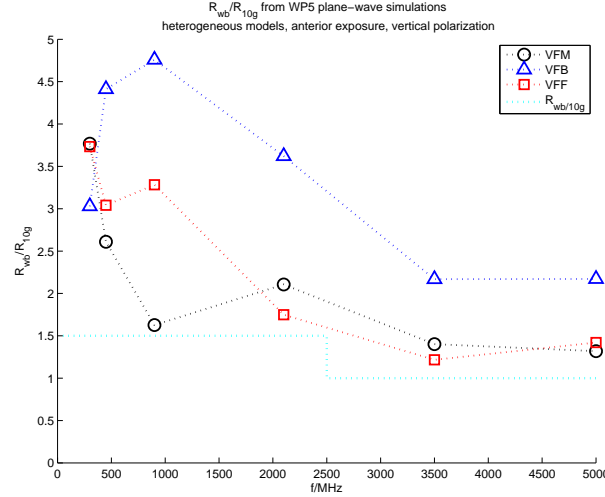


Figure 7: Ratio of the whole-body average SAR to the peak spatial average SAR from data of WP 5 [Uusitupa et al., 2009]. The curve described in (30) is also represented.

A ratio adjusted depending on the frequency range is used to estimate the peak spatial average SAR from the estimation of the whole-body average SAR:

$$R_{wb/10g} = \begin{cases} 1.5 & \text{if} \quad 50\,\text{MHz} < f < 2.5\,\text{GHz} \\ 1 & \text{if} \quad 2.5\,\text{GHz} < f < 6\,\text{GHz} \end{cases}, \tag{30}$$

where $R_{wb} = SAR_{wb}/SAR_{wb}^{icnirp}$ is the ratio of the whole-body SAR result on its ICNIRP basic restriction and $R_{10g} = SAR_{10g}/SAR_{10g}^{icnirp}$ is the ratio of the peak spatial average SAR result on its ICNIRP basic restriction. The frequency range has been extended to lower frequencies based on results from [Kühn et al., 2009] and to higher frequencies based on [Djafarzadeh et al., 2009]. This frequency dependent ratio is based on plane-wave results. Thus, it is not considering the eventual local enhancements due to the radiation pattern of the antenna. It should at least be conservative enough to include all the results in our possession for plane-wave exposure. Our results are based only on a few orientations of the models, and, as shown in WP 5 [Uusitupa et al., 2009], there can be strong enhancements of the local SAR due to the posture and orientation of the model.

The expression of the 10 g peak spatial average SAR based on these ratios and the value of whole-body SAR is

$$SAR_{10g} = \frac{1}{R_{wb/10g}} \frac{SAR_{10g}^{icnirp}}{SAR_{wb}^{icnirp}} SAR_{wb} \tag{31}$$

$$= \frac{1}{2R_{wb/10g}} \frac{SAR_{10g}^{icnirp}}{SAR_{wb}^{icnirp}} \frac{\delta}{D_{body}} SAR(0). \tag{32}$$

### 1.7.9   Cylindrical Propagation – Radiating Near Field

It was shown in [Faraone et al., 2000] that cylindrical propagation could be assumed in the radiating near field of a collinear array antenna. The power flux is then confined within the

horizontal half-power beamwidth, $\Phi_{3\text{dB}}$, and the overall height of the antenna, $L$. The average power density, $\overline{P_D}$, along a vertical line of length $L$, at a distance $d$ from the antenna is given by

$$\overline{P_D}(d, |\xi| < \Phi_{3\text{dB}}/2; L) = \frac{P_{rad}}{\Phi_{3\text{dB}} L d \sqrt{1 + (d/d_0)^2}} \tag{33}$$

$$d_0 = \frac{\Phi_{3\text{dB}}}{\pi} \frac{G_A L}{4},$$

where $P_{rad}$ is the power radiated from the antenna, $G_A$, the directivity, and $\xi$, the azimuthal angle.

Equation (33) and the physical characteristics of the antennas have been used to compute the average power density along a vertical line parallel to the axis of the 12 antennas described in Section 1.3. Figure 8 compares the results of (33) with the computation of the average power density from free-space simulations. Equation (33) is conservative for most cases for the evaluated distances from 0 to 3 m. The equation is only a poor approximation of the average power density if the assumption of cylindrical propagation is violated, e.g., in the close near-field of the antennas, 300MHz H65V64 VPolV5 and 3500MHz H18V18 VPol CPEV4 that have a large width compared to length. For these antennas, (33) overestimates the free-space simulation results for distances closer than 200 mm. This is of little relevance since experimental dosimetric evaluations are needed for these close distances since interactions of the human body with the source cannot be excluded.
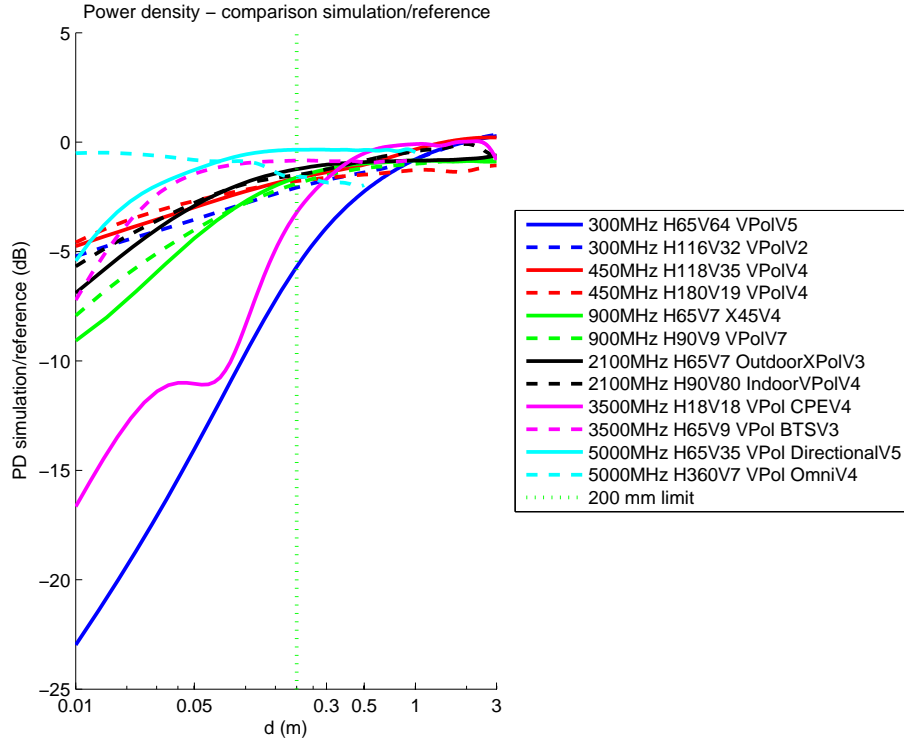


Figure 8: Comparison of average power density from simulations and calculated from (33)

### 1.7.10    Whole-Body Average SAR – Base-Station Antennas

In equation (22), the exposed region, $R_{yz}$, depends a lot on the human model in front of the antenna and the characteristics of the antenna itself. Once again, a simple case is to approximate

the human body by a cuboid of depth $D_{body}$, width $W_{body}$, and height $H_{body}$. However, the entire height or width of its cross-section might not be homogeneously exposed by the wave coming from the antenna. The exposed fraction of its width and height are named $W_{eff}$ and $H_{eff}$, respectively. In this case, equation (22) for the whole-body average SAR can be written as

$$SAR_{wb} = \frac{1}{V_{tot}} \frac{\delta}{2} W_{eff} H_{eff} SAR(0) \tag{34}$$

$$= \frac{1}{D_{body} W_{body} H_{body}} \frac{\delta}{2} W_{eff} H_{eff} SAR(0) \tag{35}$$

$$= \frac{1}{2} \frac{\delta}{D_{body}} \frac{W_{eff}}{W_{body}} \frac{H_{eff}}{H_{body}} SAR(0). \tag{36}$$

We consider that the model is exposed over its entire width ($W_{eff} = W_{body}$). The exposed fraction of its height, $H_{eff}$, varies with the distance between the body and the antenna. As shown in Figure 9, $H_{eff}$ depends also on the height of the beam, $H_{beam}$, calculated from the far-field characteristics of the antenna (vertical HPBW):

$$H_{beam} = 2d \tan(\Theta_{3dB}/2), \tag{37}$$

and the height of the phantom, $H_{body}$:

$$H_{eff} = \begin{cases} L & \text{if } H_{beam} < L, H_{body} & \text{(A)} \\ H_{beam} & \text{if } L \leq H_{beam} < H_{body} & \text{(B)} \\ H_{body} & \text{if } H_{body} \leq H_{beam} & \text{(C)} \\ H_{body} & \text{if } H_{body} \leq L \end{cases} \tag{38}$$

If the phantom is taller than the antenna and the beam (example, position p1), $H_{eff}$ is equal to the height of the antenna. If the beam is taller than the antenna, but still shorter than the phantom (example, position p2), the height of the beam is taken for $H_{eff}$. And if the phantom is shorter than the beam, the entire height of the body is exposed (example, position p3), so $H_{eff}$ is equal to $H_{body}$. Finally, if the phantom is shorter than the antenna (not shown in Figure 9), $H_{eff}$ is also equal to $H_{body}$.
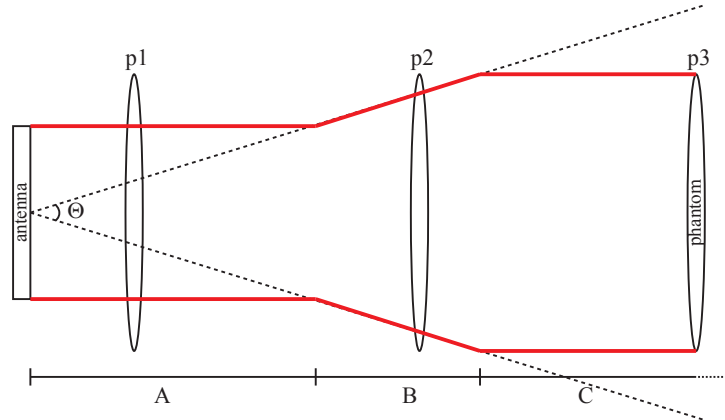


Figure 9: Exposed vertical length at various distances from the antenna, depending on its vertical opening angle. The red line indicates $H_{eff}$ taken into account. (side view)

### 1.7.11   Issues at Short Antenna-Body Distances

The distance between the antenna and the human body is calculated between the box bounding the antenna and the box bounding the human, along the direction of propagation of the antenna. When the body is facing the antenna, the body part that typically determines the closest face of the bounding box is the toes or the forehead (see Figure 3). The position of the peak spatial average SAR is typically located in the trunk, the face or the wrists. Thus, the distance between the antenna and the location of the peak spatial average SAR is different than the distance to the bounding box of the body. For short antenna-body distances, this implies an important uncertainty on the distance. An approximation based on these results would not be conservative since the same values of SAR should be associated with larger distances.

Moreover, very close to the antenna ($d < \lambda/2\pi$), the assumptions made in the last paragraphs are no longer valid. The field is complex and no general equation can easily be assumed or derived. The feedback from the presence of the human can possibly be very strong, changing the impedance of the sources, thus the radiating properties of the antenna [Christ et al., 2006a]. [IEC, 2007] and [FCC, 2001] suggest measurements for distances up to 200 mm from the antenna. We also propose that dosimetric measurements are made closer than 200 mm to ensure compliance with the guidelines.

### 1.7.12   Final Form of the Estimation Formula

This section presents the final form of the estimation formulas in their general form and in a more compact form based on the premise to cover 95% of the adult human population. These two representations of the estimation formulas can also be found in Appendix A. The frequency range has been restricted to the range within which we could validate the formula with the bulk simulation results, i.e. 300 MHz to 5 GHz. In particular, the formulas will not be conservative at low frequencies for which whole-body resonances occur.

**General Form**

The final form of the estimation formulas, for the whole-body average and 10 g peak spatial average SAR, from (23), (29), (30), (32), (33), (36), (37), and (38), and including all the effects discussed earlier, is

$$SAR_{wb} = \frac{10^{0.25}}{2} \frac{\delta}{D_{body}} \frac{W_{eff}}{W_{body}} \frac{H_{eff}}{H_{body}} SAR(0) \tag{39}$$

$$SAR_{10g} = \frac{10^{0.25}}{2R_{wb/10g}} \frac{SAR_{10g}^{icnirp}}{SAR_{wb}^{icnirp}} \frac{\delta}{D_{body}} SAR(0), \tag{40}$$

with

$$SAR(0) = \frac{\sigma Z_i |t|^2 P_{rad}}{\rho \Phi_{3dB} L d} \left[ 1 + \left( \frac{4\pi d}{\Phi_{3dB} G_A L} \right)^2 \right]^{-1/2} \tag{41}$$

$$R_{wb/10g} = \begin{cases} 1.5 & \text{if} \quad 300\,\text{MHz} < f < 2.5\,\text{GHz} \\ 1 & \text{if} \quad 2.5\,\text{GHz} < f < 5\,\text{GHz} \end{cases} \tag{42}$$

$$H_{eff} = \begin{cases} L & \text{if } H_{beam} < L,\, H_{body} \\ H_{beam} & \text{if } L \le H_{beam} < H_{body} \\ H_{body} & \text{if } H_{body} \le H_{beam} \\ H_{body} & \text{if } H_{body} \le L \end{cases} \tag{43}$$

$$H_{beam} = 2d \tan(\Theta_{3dB}/2) \tag{44}$$

$$W_{eff} = W_{body} \tag{45}$$

$$t = \frac{2}{1 + \sqrt{\epsilon}} \tag{46}$$

$$\delta = \frac{1}{\omega} \left[ \left( \frac{\mu_0 \epsilon_r' \epsilon_0}{2} \right) \left( \sqrt{1 + \left( \frac{\sigma}{\omega \epsilon_r' \epsilon_0} \right)^2} - 1 \right) \right]^{-1/2}. \tag{47}$$

It should be noted that this estimation formula does not take into account reflections from the environment; these environmental conditions are treated in Section 2.5.

**Compact Form – Worst-case Human**

A more compact form of the estimation formula can be found using the dimensions of the cuboid based on the worst case human:

$$SAR_{wb} = C(f) \frac{H_{eff}}{0.089\,\mathrm{m} \cdot 1.54\,\mathrm{m}} \frac{P_{rad}}{\Phi_{3\mathrm{dB}} L d} \left[ 1 + \left( \frac{4\pi d}{\Phi_{3\mathrm{dB}} G_A L} \right)^2 \right]^{-1/2} \tag{48}$$

$$SAR_{10g} = SAR_{wb} \frac{1.54\,\mathrm{m}}{H_{eff}} \frac{SAR_{10g}^{icnirp}}{R_{wb/10g} SAR_{wb}^{icnirp}} = 25 \cdot SAR_{wb} \frac{1.54\,\mathrm{m}}{H_{eff}} \frac{1}{R_{wb/10g}} \tag{49}$$

$$H_{eff} = \begin{cases} L & \text{if } H_{beam} < L,\ 1.54\,\mathrm{m} \\ H_{beam} & \text{if } L \le H_{beam} < 1.54\,\mathrm{m} \\ 1.54\,\mathrm{m} & \text{if } 1.54\,\mathrm{m} \le H_{beam} \\ 1.54\,\mathrm{m} & \text{if } 1.54\,\mathrm{m} \le L \end{cases} \tag{50}$$

$$H_{beam} = 2d \tan(\Theta_{3\mathrm{dB}}/2) \tag{51}$$

$$R_{wb/10g} = \begin{cases} 1.5 & \text{if} \quad 300\,\mathrm{MHz} < f < 2.5\,\mathrm{GHz} \\ 1 & \text{if} \quad 2.5\,\mathrm{GHz} < f < 5\,\mathrm{GHz} \end{cases} \tag{52}$$

$$C(f) = \frac{10^{0.25}}{2} \delta(f) \left| t(f) \right|^2 \frac{\sigma(f)}{\rho} \sqrt{\frac{\mu_0}{\epsilon_0}} \tag{53}$$

The coefficient $C(f)$ is frequency dependent. It can be evaluated using the values of conductivity and permittivity from [IEC, 2009]. Table 13 shows the approximation of $C(f)$. The deviation between $C(f)$ calculated from (53) with the dielectric properties specified in [IEC, 2009] and $C(f)$ from Table 13 is less than 5%.

| $f$ | $C(f)$ |
|:---:|:---:|
| MHz | $10^{-4}\,\mathrm{m}^3/\mathrm{kg}$ |
| 300 | 6.3 |
| 900 - 5000 | 8.1 |

Table 13: Piecewise linear approximation of $C(f)$ resulting in a deviation of less than 5%. For frequencies between 300 MHz and 900 MHz, a linear interpolation should be used.

The comparison between the SAR obtained from this set of equations and the bulk simulation results is presented in Section 1.8.

## 1.8 Validation – Bulk Simulation Results

Figures 10 to 21 show the results from the bulk simulations of WP 6 for the adult models, as well as the estimation formulas developed to cover 95% of the adult human population for the whole-body average SAR and 10 g peak spatial average SAR given in Equations (48) to (53). The ratio of the average power density from (33) to the ICNIRP power density limit, given in Table 12, is also represented. Vertical lines show the single-dipole near-field limit $(d = \lambda/(2\pi))$ as well as the 200 mm limit. The results related to all models, including the child, are shown in Figures 158 to 169 of Appendix E. They show that the estimation formula (covering 95% of the adult population) is not always conservative compared to the FDTD simulation results with the VFB. This confirms that the formulas are only valid to insure safety of adults.

It can be observed in these figures that the estimation formula is conservative for distances further than 200 mm. At low frequency, the ICNIRP power density limit is more conservative than the estimation formulas of the whole-body average and the 10 g peak spatial average SAR. For higher frequencies, the ICNIRP power density limit is more conservative than the whole-body average SAR estimation formula in almost every case and the 10 g peak spatial average SAR estimation formula is only about 1 dB more conservative than the ICNIRP power density limit.

[Thors et al., 2008] presented an estimation formula based on simulation results of many different groups, using mainly large or average male and average female models, for frequencies ranging from 800 MHz to 2200 MHz. We have plotted our results included in this frequency range with the estimation formula that they propose in Appendix F, as well as the results they collected with our estimation formula in Appendix G.
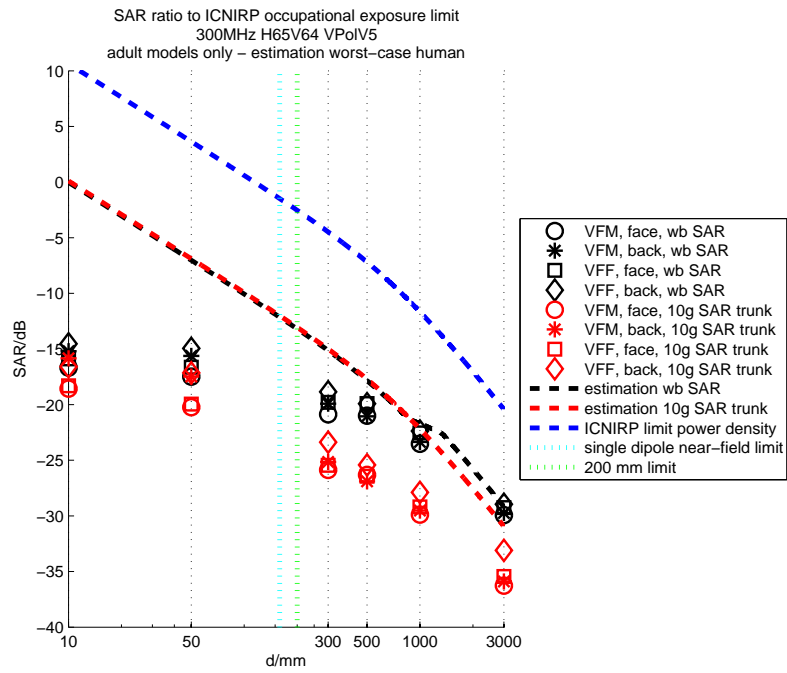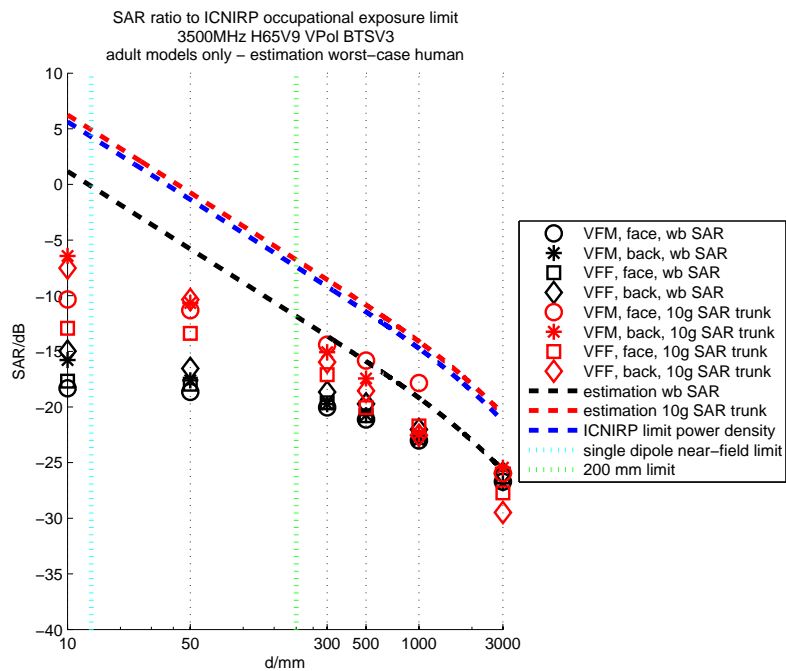
Figure 10: Bulk simulation results of the adult models in front of the antenna 300MHz H65V64 VPolV5 and approximation formula using the dimensions of the worst-case human, for 1W radiated power
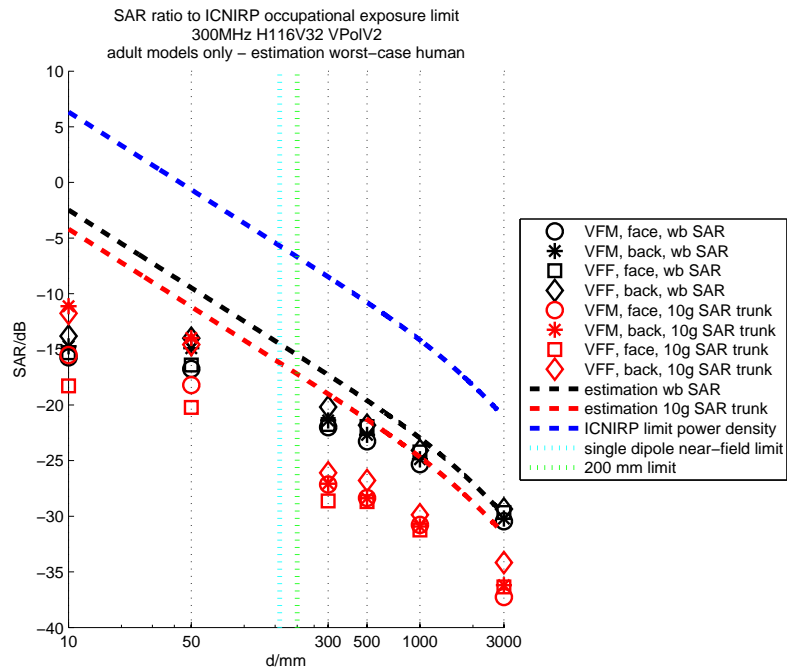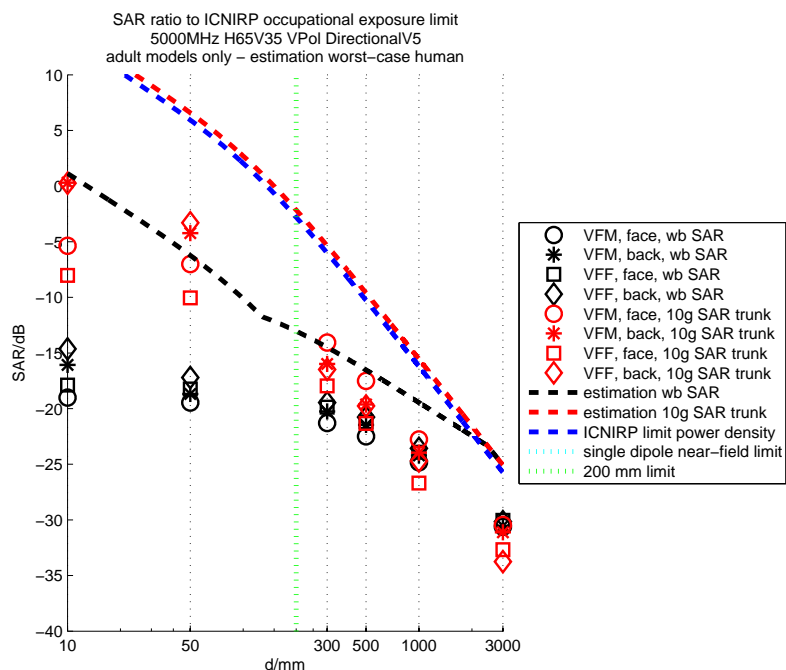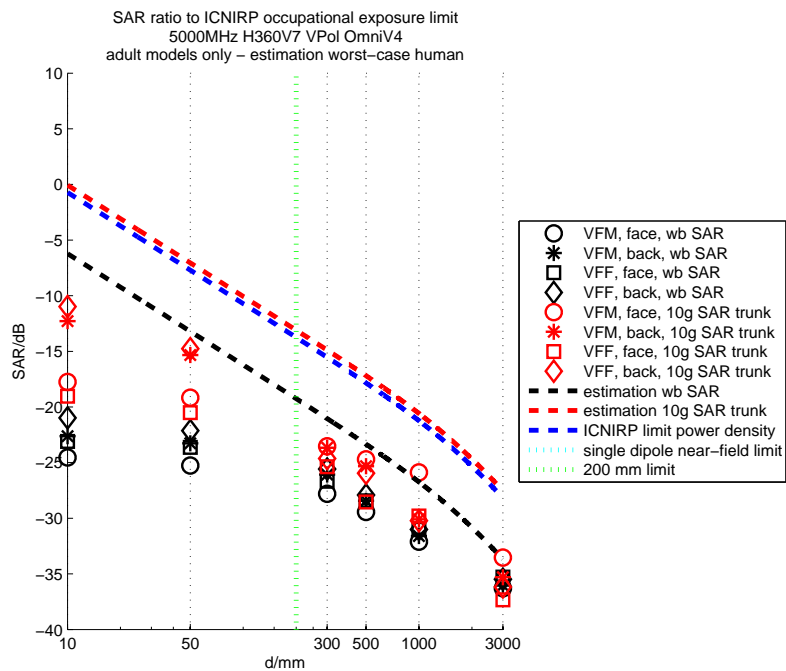


Figure 11: Bulk simulation results of the adult models in front of the antenna 300MHz H116V32 VPolV2 and approximation formula using the dimensions of the worst-case human, for 1W radiated power
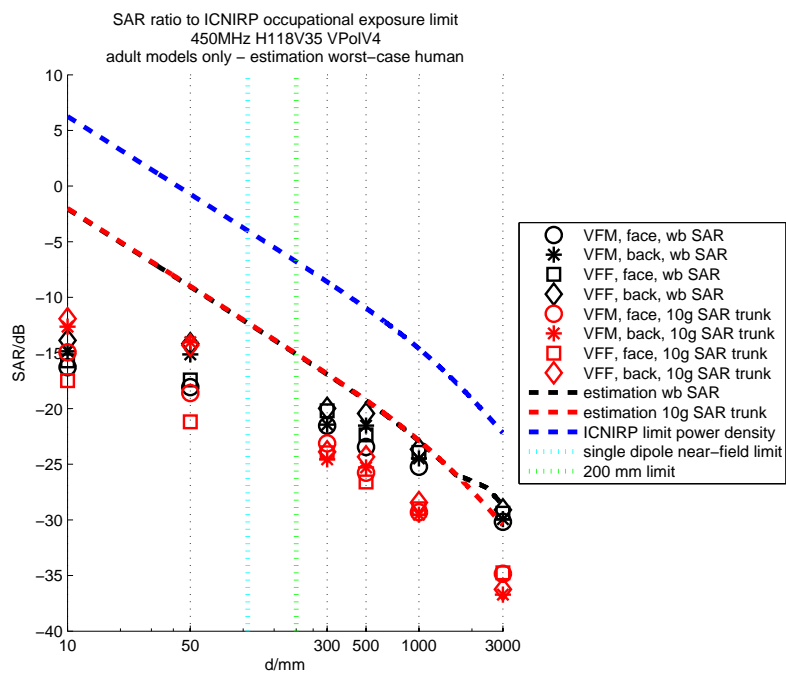
Figure 12: Bulk simulation results of the adult models in front of the antenna 450MHz H118V35 VPolV4 and approximation formula using the dimensions of the worst-case human, for 1W radiated power
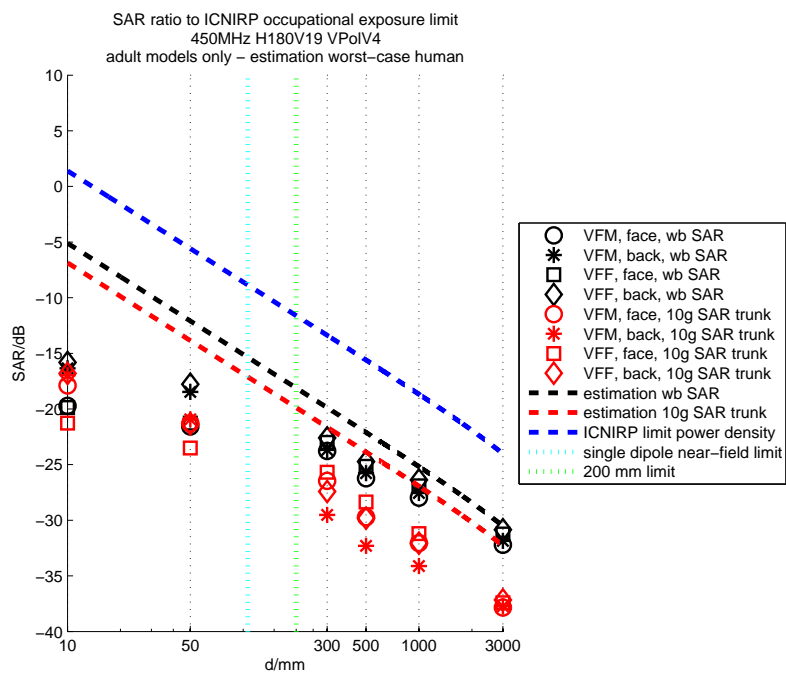


Figure 13: Bulk simulation results of the adult models in front of the antenna 450MHz H180V19 VPolV4 and approximation formula using the dimensions of the worst-case human, for 1W radiated power
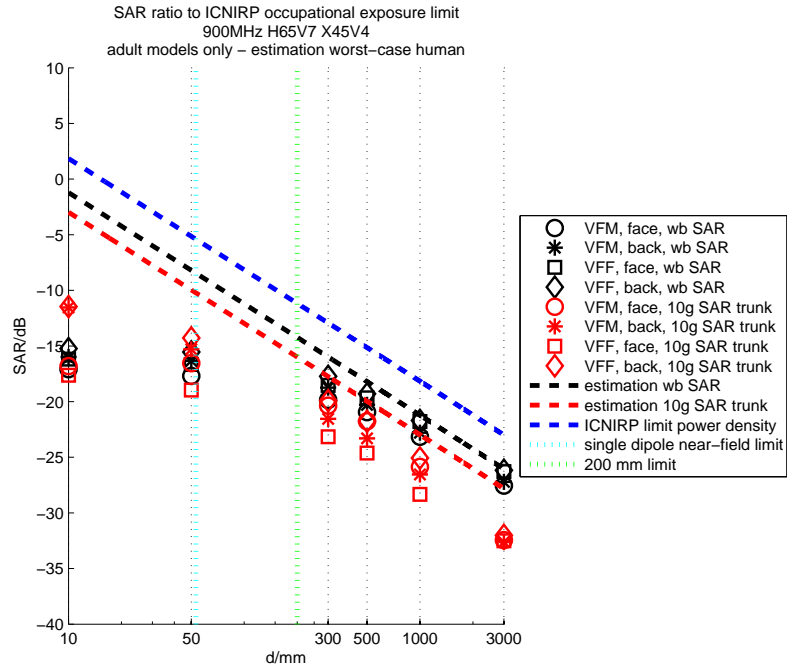
Figure 14: Bulk simulation results of the adult models in front of the antenna 900MHz H65V7 X45V4 and approximation formula using the dimensions of the worst-case human, for 1W radiated power
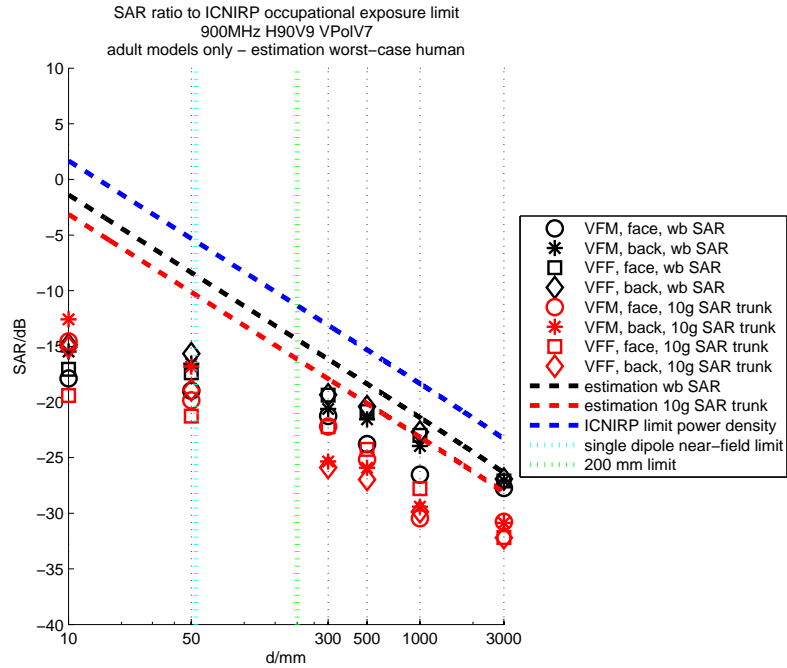


Figure 15: Bulk simulation results of the adult models in front of the antenna 900MHz H90V9 VPolV7 and approximation formula using the dimensions of the worst-case human, for 1W radiated power
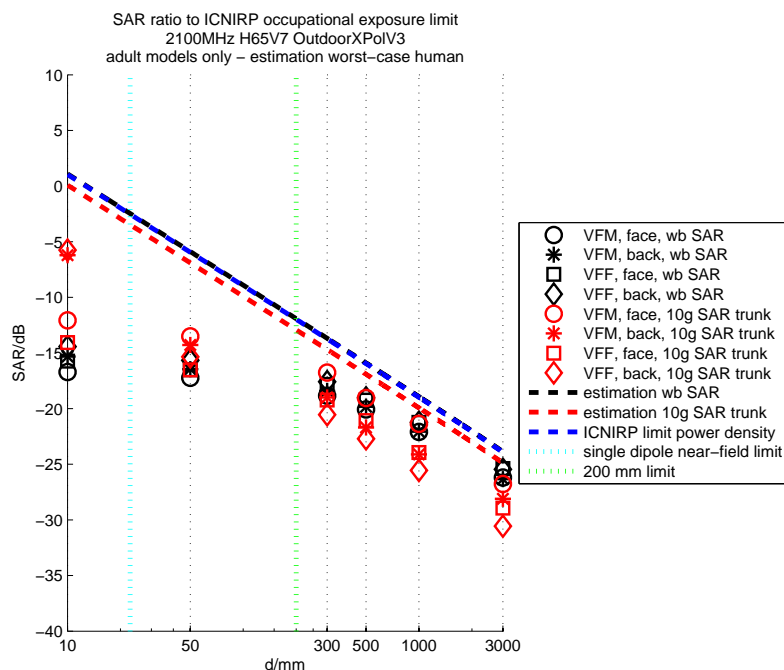
Figure 16: Bulk simulation results of the adult models in front of the antenna 2100MHz H65V7 OutdoorXPolV3 and approximation formula using the dimensions of the worst-case human, for 1W radiated power
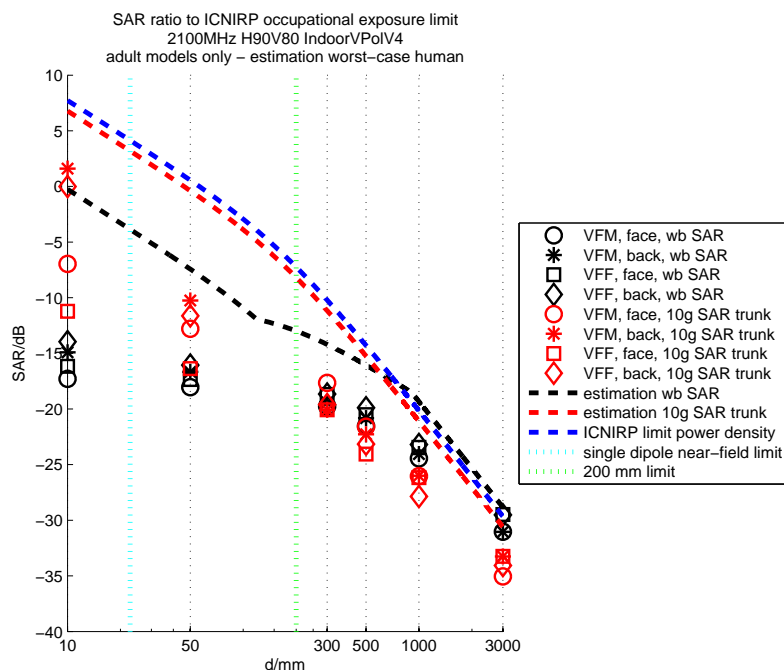


Figure 17: Bulk simulation results of the adult models in front of the antenna 2100MHz H90V80 IndoorVPolV4 and approximation formula using the dimensions of the worst-case human, for 1W radiated power
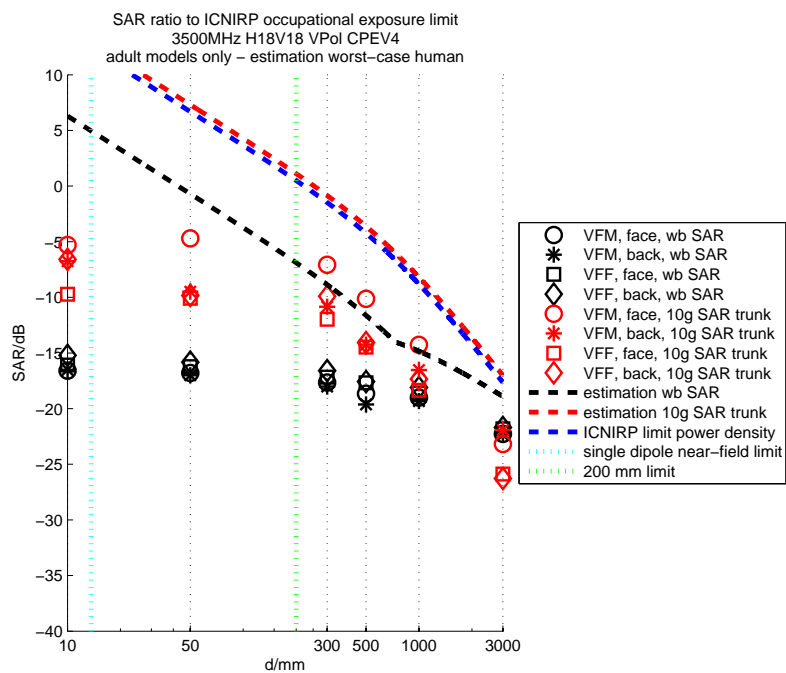
Figure 18: Bulk simulation results of the adult models in front of the antenna 3500MHz H18V18 VPol CPEV4 and approximation formula using the dimensions of the worst-case human, for 1W radiated power



Figure 19: Bulk simulation results of the adult models in front of the antenna 3500MHz H65V9 VPol BTSV3 and approximation formula using the dimensions of the worst-case human, for 1W radiated power

Figure 20: Bulk simulation results of the adult models in front of the antenna 5000MHz H65V35 VPol DirectionalV5 and approximation formula using the dimensions of the worst-case human, for 1W radiated power



Figure 21: Bulk simulation results of the adult models in front of the antenna 5000MHz H360V7 VPol OmniV4 and approximation formula using the dimensions of the worst-case human, for 1W radiated power

## 1.9 Conservativeness Study

The histograms presented in Figures 22 and 23 show that the estimation formula is more conservative than the results of the bulk simulations using the VFM and the VFF (for distances higher than 200 mm) in most of the cases.

- layering enhancement: probably includes close to 95% of the possible layers configurations of a skinny model

- $95^{th}$ percentile human: from statistical data, includes 95% of the population

- $R_{wb/10g}$: conservative for 100% of the plane-wave results in our possession, all with the human in the upright standing position, but we evaluate that it is conservative in less than 95% of all the possible configurations of humans, distances, antennas, field distributions, etc.



22.1: histogram 22.2: cumulative distribution function
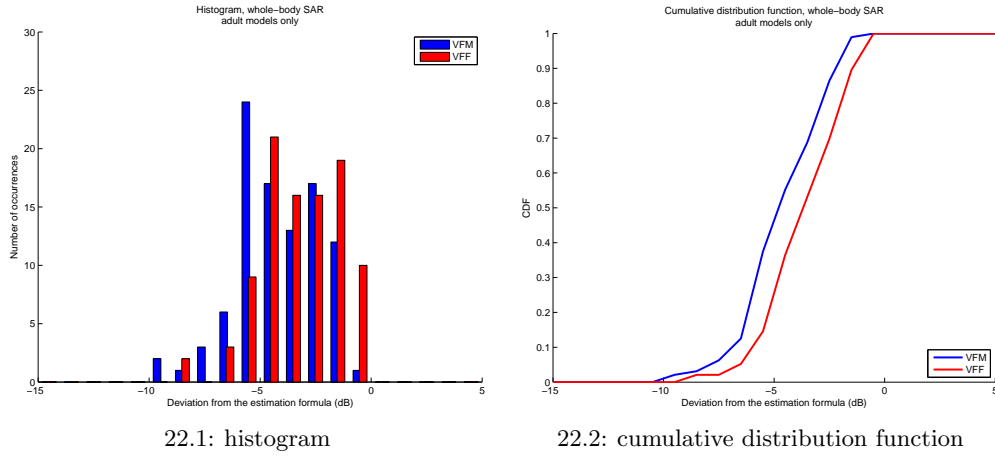
Figure 22: Histogram and cumulative distribution function of the deviation between the bulk simulation whole-body SAR results of the adult models ($> 200$ mm) and the estimation formula based on the $95^{th}$ percentile human body cuboid



23.1: histogram 23.2: cumulative distribution function
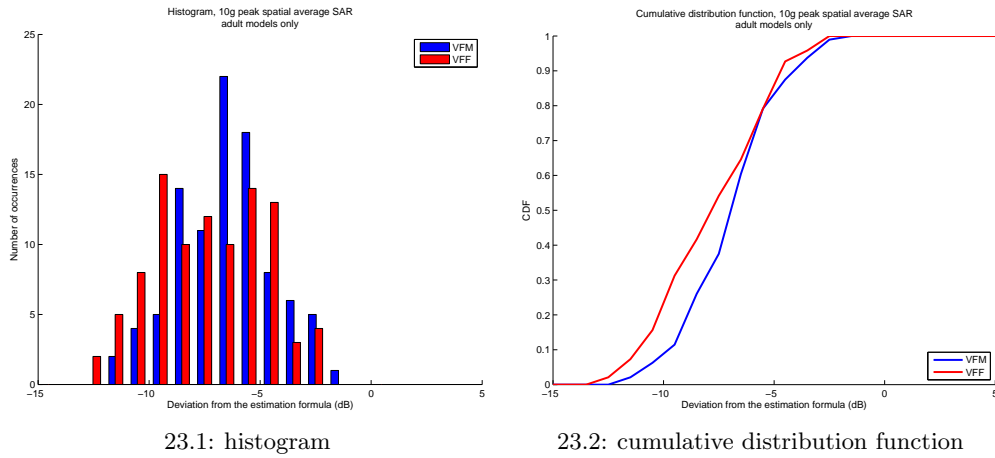
Figure 23: Histogram and cumulative distribution function of the deviation between the bulk simulation 10 g peak spatial average SAR results of the adult models ($> 200$ mm) and the estimation formula based on the $95^{th}$ percentile human body cuboid

## 1.10 Conclusions

The developed estimation formulas are based on the identified absorption mechanism derived from the simulated configurations combined with physical considerations. They estimate the $95^{th}$ percentile whole body and peak spatial exposure of adults in the vicinity of base station antennas. The estimation formulas were validated with the bulk simulated data from this project as well as from data in the literature. The validation also demonstrates that the approximation is not always conservative for children. The available data do not allow to determine the uncertainty of the approximation with respect to the $95^{th}$ percentile exposure. Nevertheless, the confidence is high due to the step-by-step approximation. The comparison with the simulated configurations does not provide indication for a strong overestimation nor underestimation of the $95^{th}$ percentile exposure.

In the reactive near field region, estimation formulas as well as full-wave simulations have been found to be problematic in estimating the human exposure due to the strong dependence of the localized absorption on the human anatomy. Furthermore, feedback of the human body on the antenna impedance, the feeding network in particular and possibly also the power amplifier, is not always predictable with state-of-the-art simulation tools. Thus, at close antenna-body distances of less than 200 mm, SAR measurements are strongly recommended for demonstrating compliance. An obvious choice for the phantom is the $95^{th}$ percentile cuboid.

## 2  WP7: Full Wave Field & SAR – Representative Base Station Antennas with Reflections

**Conducted by INTEC, Ghent University**

**Authors: Günter Vermeeren, Marie-Christine Gosselin, Valpre Kellerman, Sven Kühn, Abdelhamid Hadjem, Louis-Ray Harris, Azeddine Gati, Wout Joseph, Takashi Hikage, Toshio Nojima, Joe Wiart, Frans Meyer, Niels Kuster, Luc Martens**

### 2.1  Executive summary

#### 2.1.1  Introduction

Work Package 7 (WP7) of the 'MMF-GSMA Dosimetry Program Phase 2' project investigates numerically the whole-body Specific Absorption Rate (SAR) and peak spatial averaged SAR in the Virtual Family Man (VFM) exposed by representative base station antennas in a reflective environment. The aim of this work package is to assist the development of the IEC standard 62232 in evaluating the uncertainties of the induced SAR in the human body with respect to a variation of the environment. In this study, only perfectly conducting environments are considered in view of a worst-case approach. The uncertainties of the SAR have been studied by reviewing the literature and by performing simulations on the VFM exposed to representative base station antennas in different reflective environments.

#### 2.1.2  Methodology

The literature database has been thoroughly scanned, but only a limited number of papers have been found regarding the influence of perfectly conducting ground on the electromagnetic absorption in a human body. Therefore, the literature review has been extended to plane wave exposure and non-perfectly conducting reflectors. A total of 8 publications have been discussed.

The numerical investigation of the influence of a reflecting ground and a vertical wall on the SAR in a human body near a base station antenna (BSA) has been investigated using 3D full wave electromagnetic solvers, i.e., an FDTD based (SEMCAD X) and MoM/FEM based tool (FEKO). Three typical reflecting (perfectly conducting) environments have been considered: 'ground', 'vertical wall', and 'ground + vertical wall'. Representative base station antennas have been developed for the frequencies of 300 MHz, 450 MHz, 900 MHz, 2100 MHz, 3500 MHz, and 5000 MHz. The localized and whole-body SAR has been investigated in the inhomogeneous Virtual Family Man (VFM) [Christ et al., 2009]. The dielectric properties of the VFM have been set as specified for the inter-laboratory comparison (Section 3). The distance between the human body model and the antenna varied from 0.3 m to 10 m. Only frontal exposure of the human body has been studied. The vertical wall has been placed at the left side of the human body. The minimum distance between the vertical wall and the human body and antenna was 10 cm. The ground was placed 5 cm below the feet of the human body. The absorption in the reflective environments has been compared to the absorption in free space. To reduce computational resources, the generalized huygens' box method has been used for the configurations at higher frequencies and larger distances. In this approach the complex incident field of the reflecting near field environment, over the area where the human body is placed, computed by the MoM/Fem technique is used as incident for the FDTD technique. The generalized huygens' box method has been validated before it has been used for the computations.

### 2.1.3 Conclusions

From the literature review it is clear that worst-case exposure scenarios can be expected in an environment consisting of a perfectly conducting walls and ground, because at a reflector all the power is reflected back in the domain. Considering realistic walls and grounds decreases the variation on the calculation of the SAR. With respect to exposure in free space, an increase of up to 5 dB for the whole-body absorption has been reported in the literature.

The validation of the generalized huygens' box method has shown that the coupling between the environment and the human body cannot be neglected at 300 MHz. Therefore, the generalized huygens' box method has not been used at frequencies below 900 MHz.

The whole-body SAR and peak spatial averaged SAR have been investigated in the Virtual Family Man in a perfectly conducting environment for representative base station antennas operating in the frequency range of 300 MHz to 5000 MHz. The perfectly conducting environment consisted of an infinite ground and / or an infinite vertical wall. The vertical was placed at the left side of the human body model. The huygens' box method has been used for an efficient calculation of the absorption for the larger simulations. This huygens' box method is a hybrid method using the MoM/FEM for calculating the incident fields and the FDTD method for assessing numerically the absorption in an inhomogeneous human body model. It has been shown that the huygens' box method is applicable for the configurations with an operating frequency of 900 MHz and above.

From the bulk simulations, one can conclude that the whole-body and local absorption vary a lot with respect to the absorption in the VFM in free space. The ratio of the SAR in the VFM in a reflective environment and the SAR in the VFM in the free space environment ranged from -8.71 dB up to 8.01 dB. The whole-body absorption correlated very well with the rms incident fields averaged over a bounding box around the body, whereas for the peak spatial SAR in 1 g and 10 g a good correlation has been observed with the peak rms incident electric field over the bounding box around the body. So, worst-case exposure can be determined from an investigation of the rms incident field in a certain environment. The location where the rms field achieves the highest value, the highest absorption can be expected. A worst-case reflective environment could not be determined.

## 2.2   Introduction

Work Package 7 (WP7) of the "MMF-GSMA Dosimetry Program Phase 2" project investigates numerically the whole-body Specific Absorption Rate (SAR) and peak spatial averaged SAR in the Virtual Family Man (VFM) exposed by representative base station antennas in a reflective environment.

The aim of this work package is to assist the development of the IEC standard 62232 in evaluating the uncertainties of the induced SAR in the human body with respect to a variation of the environment. In this study, only perfectly conducting environments are considered in view of a worst-case approach. The uncertainties of the SAR have been studied by reviewing the literature and by performing simulations on the VFM exposed to representative base station antennas in different reflective environments.

## 2.3   Literature review

Due to the limited amount of papers found regarding the influence of perfectly conducting ground on the electromagnetic absorption in a human body, the literature review has been extended to plane wave exposure and non-perfectly conducting reflectors.

Grounding and reflector effects on the absorption of electromagnetic energy caused by RF transmitters have already been studied in the late 70's by amongst others Hagmann and Ghandi [Hagmann and Gandhi, 1979]. These studies assumed that human body was in the farfield of the antenna, so that incident plane wave exposure could be applied. More recently, the influence of grounding effects on the SAR for a plane wave exposure have been studied by Vermeeren [Vermeeren et al., 2007] and Findlay [Findlay and Dimbylow, 2008].

Hagmann et al. [Hagmann and Gandhi, 1979] studied the electromagnetic absorption in a standard man standing on or above an infinite ground plane and near an infinite flat and 90° corner reflector. The incident electric field was vertically polarized with a propagation directed from the front to the back of the human body model. They reported that grounding effects are most prominent at low frequencies and disappear for frequencies above 200 MHz. A perfectly conducting ground plane reduces the resonance frequency to 0.610 times the resonance frequency in free space. So, the SAR in a standing man on a ground plane increases considerably at low frequencies with respect to the standing man in free space. At the reduced resonance frequency the SAR was 32 % higher than the SAR at the resonance in free space. With respect to the local absorption they found an increase of a factor 60 in the area of the heel in case of a ground reflector. Besides a ground reflector, Hagmann et al. also studied an infinite flat and 90° corner reflector. The numerical solutions indicated that for frequencies near resonance, the enhancement in SAR due to a reflector is approximately equal to the enhancement in gain of half-wavelength dipole with the same reflector configuration. SAR values of up to 17 times the SAR in a man in free space have been observed. The enhancement in absorption due to reflector effects becomes small for small values of separation between human body model and reflector, or for high frequencies.

Durney et al. derived semiempirical relations for irradiation near a ground plane [Durney et al., 1986]. This formula is used for calculating the whole-body SAR of a half-spheroid placed over, but at a distance from, an infinitely large ground plane. They found that the presence of a ground plane shifts the resonance frequency, but it does not significantly effect the maximum value of the whole-body SAR. However, at a given frequency below resonance the presence of the ground plane increases the whole-body SAR by an order of magnitude over the free space value.

Vermeeren at al. [Vermeeren et al., 2007] investigated the influence of a perfectly conducting ground on the whole-body SAR in the spheriod average man [Durney et al., 1986] for a TE- and TM polarized incident plane wave at the GSM downlink frequency of 950 MHz. The elevation

angle of the incident plane wave was varied between 0° (vertically propagating plane wave) and 90° (horizontally propagating plane wave). They found that above a perfectly conducting ground the whole-body SAR can be twice as high as due to the reflections of the incident plane waves at the ground. The whole-body SAR did not vary significantly with increasing separation between the spheroid model and the ground. Consequently, the increase in whole-body SAR can be completely attributed to the reflections of the incident plane waves at the ground plane and the impact of capacitive effects and conducting effects can be neglected. They also reported that whole-body SAR increased with increasing elevation angle for a TE-polarized incident plane wave.

Findlay at al. [Findlay and Dimbylow, 2008] investigated numerically the SAR distributions in NORMAN due to the reflections of electromagnetic fields from a ground plane between 65 MHz and 2 GHz. Five different single incident plane wave exposures have been considered. It turned out that for the considered exposure configurations the current ICNIRP reference levels and the IEEE MPE were not exceeded. Moreover, for the frequency range studied, Findlay et al. noted that field reflections from the ground plane generally failed to produce SAR values higher than those calculated when reflection did not occur. At frequencies above 200 MHz, the location of the field absorption in the body is influenced by the location of the peaks and troughs of the standing waves caused by the reflections of the incident electromagnetic field.

Bernardi et al. studied the human exposure to rooftop mounted base station antennas operating around 900 MHz in an urban environment. Three particular configurations have been considered: a person standing on the roof, a person standing on the balcony, and a person standing in the street [Bernardi et al., 2000]. The heterogeneous Visible Human Male (VHM) [Ackerman, 1998] has been selected as the human body model. Analysis of the SAR distributions showed that the power absorption characteristics vary considerably in the three investigated configurations. The highest whole-body and local absorption was obtained when the VHM is standing on the balcony. The lowest values were found for the VHM standing in the street. The authors also remarked that the obtained results depend strongly upon the dielectric characteristics of the building walls and ground. They noted that considering a reflection coefficient of 0.7 results in a doubling of the whole-body SAR compared to the configuration in free space. With respect to a perfectly conducting reflector, the walls in an urban environment reflect less than 50 % of the incident power. They reported that incident field levels and SAR values were far below the safety levels.

In 2003 Bernardi et al. published a paper about the human exposure to cellular base station antennas for a person standing in a room with a window facing a roof-top base station antenna [Bernardi et al., 2003] for GSM and UMTS. Two configurations were examined. Again, the VHM was selected as the human body model. The rms fields in the room were analyzed and the VFM was placed in the room where the exposure was the highest. They reported peak SARs that were twice as high as in the corresponding free space configuration. They also found that the whole-body SAR correlates with the volume averaged field values.

Recently, Vermeeren et al. investigated the whole-body averaged SAR in spheroid child and adult phantoms in an urban-macrocell environment at the GSM downlink frequency of 900 MHz using a statistical approach [Vermeeren et al., 2008]. They found that the whole-body SAR increases with decreasing size of the human body. Furthermore, they reported that in a realistic environment the 99th-percentile of the whole-body SAR can be up to 5 dB higher than the worst-case single incident plane wave exposure. They also showed that the ICNIRP reference levels don not always ensure compliance with the basic restrictions in case of a realistic exposure.

From the literature review it is clear that worst-case exposure scenarios can be expected in an environment consisting of a perfectly conducting walls and ground, because at a perfectly conducting reflector all the power is reflected back in the domain. Considering realistic walls and grounds decreases the variation on the calculation of the SAR. With respect to exposure

in free space, an increase of up to 5 dB for the whole-body absorption has been reported in the literature.

## 2.4  Numerical evaluation of typical reflection scenarios near base station antennas

The influence of a reflecting environment near base station antennas on the induced SAR in a human body has been numerically investigated.

In WP 7 a set of base station antennas, developed in WP 6, have been placed in different reflective environments. The selected base station antennas as well as their corresponding radiation frequency are listed in Table 14. Three reflecting scenarios were considered: perfectly conducting ground (denoted as 'Ground'), perfectly conducting wall (denoted as 'Wall'), and the combination of the perfectly conducting ground and wall (denoted as 'Ground + Wall'). The ground has been placed at a distance of 5 cm below the feet of the human body model for numerical reasons. The wall has been placed at a distance of 10 cm from the combination of human body and base station antenna.

Table 14: The selected base station antennas from WP 6.

| Operating Frequency (MHz) | Base Station Antenna |
|---|---|
| 300 | 300MHz_H65V64_VPolV5 |
| 450 | 450MHz_H180V19_VPolV4 |
| 900 | 900MHz_H65V7_X45V4 |
| 2100 | 2100MHz_H65V7_OutdoorXpolV3 |
| 3500 | 3500MHz_H65V9_VPol_BTSV3 |
| 5000 | 5000MHz_H65V35_VPol_DirectionalV5 |

The inhomogeneous VFM has been selected as the human body model. The dielectric properties of the body tissues have been set according to the parametric model described in [Gabriel et al., 1996]. The separation distances between VFM and the base station antenna were 0.3 m, 1 m, 3 m and 10 m. The vertical center of the VFM was aligned with the vertical center of the base station antenna if the height of the antenna was smaller than the length of the VFM. The bottom (feet) of the VFM was aligned with the bottom of the antenna if the height of the antenna was larger than the length of the VFM. The investigated configurations are depicted in Figure 24.

The whole-body SAR and peak spatial averaged SAR in the inhomogeneous VFM has been determined for all exposure configurations, i.e., all possible combinations of base station antenna, reflecting environment, and separation distance between human body model and antenna. The total antenna input power for all the simulations performed within this work package was 1 W unless otherwise specified.

The finite-difference time-domain (FDTD) method has been used to assess the SAR for all the configurations. However, a disadvantage of the FDTD technique is the discretization of the free space between the antenna and the human body model. For large distances and high frequencies running the simulations is an excessive task due to the limitations of the computer hardware in terms of memory requirement. Therefore, in order to reduce the memory requirements and to speed up the simulations, a new hybrid technique, called the generalized huygen's box method (GHB), has been used for the larger configurations, i.e. the configurations that exceeded the memory limits of the simulation computer. The huygen's box method combines the Method of Moments / Finite Elements Method (MoM/FEM) and the FDTD technique.
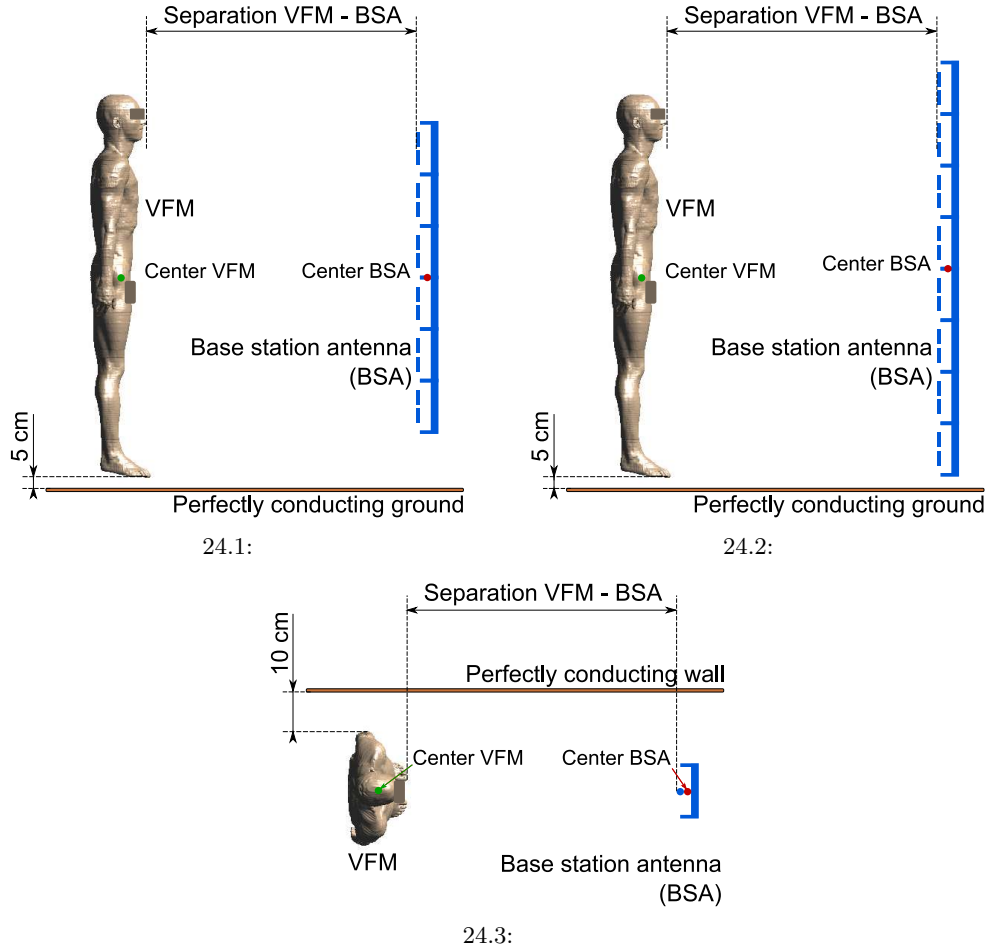
Figure 24: The investigated configurations for the bulk simulations: (a) perfectly conducting ground with antenna aligned with the center of the VFM, (b) perfectly conducting ground with the antenna aligned with the feet of the VFM and (c) perfectly conducting wall.

Section 2.4.1 and section 2.4.2 discuss the results of the validation of the generalized huygens' box method and the bulk simulations, respectively.

### 2.4.1 Validation of the Huygen's box method in a reflective environment

The MoM/FEM is an efficient tool to determine the incident fields in a location at any distance from the antenna. The FDTD, on the other hand, is generally known as the most efficient method to calculate the electromagnetic power deposition in a large inhomogeneous human body, such as the VFM. The huygen's box method is a hybrid method using the MoM/FEM and FDTD method to determine the absorption in a human body exposed to an antenna at a large distance. This hybrid method is based on the assumption that the coupling between the human body, on the one hand, and the reflective environment and the base station antenna, on the other hand, can be neglected. In this approach the complex incident field of the reflecting near-field environment computed by MoM technique is used as incident for the FDTD technique.

The huygens' box method has been validated for a free space environment in WP 6. In WP 7 the validity of this method in a reflective environment has been investigated. The huygen's box method has been validated using four 3D full wave electromagnetic solvers, i.e., FDTD based and MoM/FEM based tools. Several research groups participated in this validation. Three different FDTD solvers and a single MoM/FEM tool were used. The FDTD solvers were the

commercially available SEMCAD X, and the in-house FDTD solvers of France Telecom R&D and Hokkaido University (Japan). The commercial package FEKO has been used as the MoM/FEM tool. Table 15 lists the tools used by the groups which participated in the validation.

Table 15: The 3D electromagnetic solvers used by the participating research groups.

| Research Group | 3D EM solver | Technique |
|---|---|---|
| INTEC | SEMCAD X | FDTD |
| IT'IS | SEMCAD X | FDTD |
| FTRD | In-house | FDTD |
| UniH | In-house | FDTD |
| EMSS | FEKO | MoM / FEM |

**Configurations and methodology**

To verify the applicability and uncertainty of the huygen's box approach, verification simulations have been performed. In these simulations the homogeneous 6-year old Virtual Family Boy (VFB) has been exposed to the electromagnetic fields irradiated by the base station antennas listed in Table 16 with an operating frequency of 300 MHz, 900 MHz, and 2100 MHz. Only anterior exposure has been considered. The tissues have been assigned the dielectric properties as specified in IEC62209 [IEC, 2009]. The separation between VFB and base station antenna was 0.3 m, 3 m, and 10 m. The vertical center of the VFB has been aligned to the verical center of the base station antennna if the antenna height was smaller than the length of the VFB. In the configurations for which the antenna was larger than the VFB, the bottom of the antenna has been aligned to the feet of the VFB. Two reflective environments have been selected: a perfectly conducting ground placed 5 cm below the feet of the boy, and a perfectly conducting vertical wall 10 cm behind the back of the boy. Both reflective environments were infinite in extent. The investigated configurations are shown in Figure 25. A total of 18 validation simulations have been performed.

Table 16: The selected base station antennas from WP 6 used for the validation of the GHB.

| Operating Frequency (MHz) | Base Station Antenna |
|---|---|
| 300 | 300MHz_H65V64_VPolV5 |
| 900 | 900MHz_H90V9_VPolV7 |
| 2100 | 2100MHz_H90V80_IndoorVPolV4 |

All the configurations have been simulated taking full coupling into account and using the presented huygens' box method. The whole-body SAR and the peak spatial SAR in 1 g and 10 g have been determined and compared for all the considered configurations. The fully coupled simulations were performed by the groups EMSS, IT'IS, and UniH. The huygens box simulations were executed by the groups IT'IS, FTRD, and INTEC. The incident fields for these huygens' box simulations were generated by EMSS using the hybrid MoM/FEM code FEKO and distributed the E and H fields over the huygens' box to IT'IS and FTRD. INTEC generated the incident fields using the FDTD method (SEMCAD X). The tools used by the different research groups are listed in Table 15. These validation simulations not only verify the applicability of the huygens' box method in a reflective environment, but also allow to estimate the uncertainty on the calculated SAR between the participating groups and different solvers.

25.1:

25.2:

25.3:
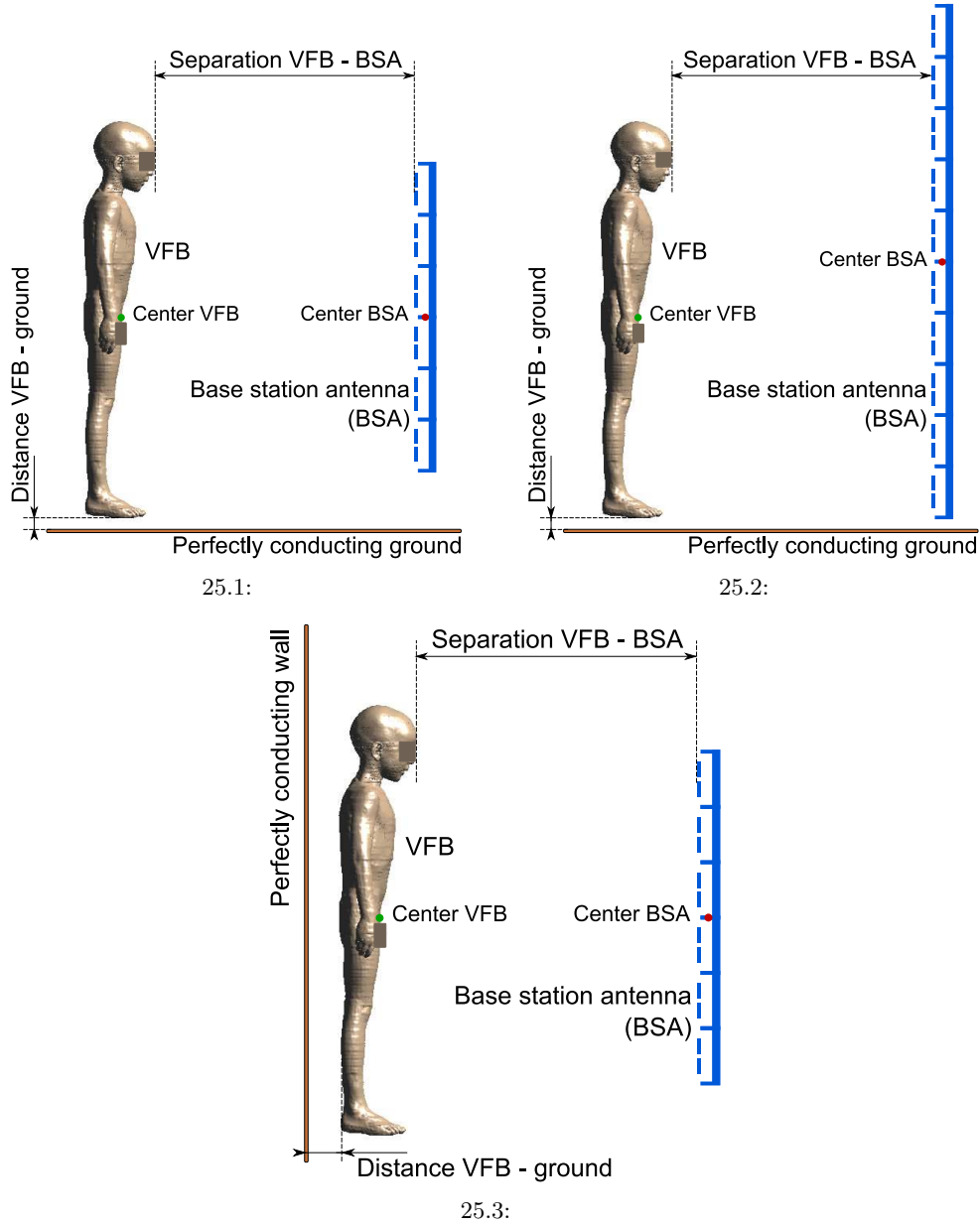
Figure 25: The investigated configurations for the validation of the generalized huygens' box method in a reflective environment: (a) perfectly conducting ground with antenna aligned with the center of the VFB, (b) perfectly conducting ground with the antenna aligned with the feet of the VFB and (c) perfectly conducting wall.

## Results

The results of the validation are shown in Figure 26 to Figure 31. The fully coupled simulations are designated as FC whereas the huygens' box simulations are indicated by GHB. Table 17 summarizes the results in terms of the relative standard deviation $\sigma_{rel}$. The relative standard deviation $\sigma_{rel}$ for a quantity $Q$ is defined as follows:

$$\sigma_{rel}(Q) = \frac{\sigma(Q)}{\mu(Q)} \tag{54}$$

with $\sigma(Q)$, $\mu(Q)$ the standard deviation, mean of $Q$, respectively.

First, the results for the ground plane are discussed. A good agreement for the whole-body SAR has been observed in Figure 26 between the fully coupled and huygens' box results for the 900 MHz and 2100 MHz base station antennas except from UniH that reported a significantly higher $SAR_{wb}$ for the 2100 MHz base station antenna and an antenna-body separation of 3 m. The relative standard deviation $\sigma_{rel}$ varies from 0.68 % (900 MHz, 10 m) to 24.2 % (2100 MHz, 3 m). The strong variation at 300 MHz for the $SAR_{wb}$ is also reflected in $\sigma_{rel}$ which varies from 11.85 % (3 m) to 25.72 % (10 m). This might be due to the fact that coupling between the human body model and the environment cannot be neglected. Therefore, for the bulk simulations the huygens' box method has been used for frequencies of 900 MHz and above.

The relative standard deviations for the peak spatial averaged SARs are in line with the observations made for the whole-body SAR. However, $\sigma_{rel}$ is higher for the peak spatial averaged SAR than for the whole-body SAR. Again, UniH reports a much higher $SAR_{1g}$ and $SAR_{10g}$ at 2100 MHz but now for a separation of 0.3 m and 3 m. The main reason for the larger deviations in the peak spatial averaged SAR is a difference in the determination of the local averaging volume by the averaging routines of the different numerical tools as reported by EMSS in WP 5.

For the vertical reflectors no good agreement has been obtained between the huygens' box simulations and the fully coupled simulations. This can be addressed to the shadowing of the human body in the fully coupled simulations. This shadowing is not taken into account in the huygens' box simulations as the radiated fields from the antenna will be reflected all at the vertical reflector, and, thus, incident on the human body. Furthermore, it is also observed that a vertical reflector behind the back of the VFB does not result in significantly higher SAR values than the ground. Therefore, the vertical reflector will be positioned at the left side of the VFB for the bulk simulations.

Table 17 also lists the relative standard deviation for the mass $m$ of the body. $\sigma_{rel}(m)$ quantifies the correct assignment of the dielectric properties to the human body tissues. Excellent agreement has been observed because $\sigma_{rel}(m)$ is below 1 %.

The electric field has also been compared along lines passing through the model. The results are shown in Section H. The agreement between the fully coupled and GHB simulations is good for the ground plane for 900 MHz and 2100 MHz. For 300 MHz and for all the cases with a vertical wall, the results of the GHB simulations are not equivalent to the fully coupled ones.

## Conclusions

In view of the bulk simulations the following conclusions were drawn from the validation of the huygens' box method in a reflective environment: firstly, at 300 MHz and 450 MHz all the simulations have been performed taking full coupling into account. Secondly, for the simulations at the other frequencies of interest, i.e., 900 MHz, 2100 MHz, 3500 MHz, and 5000 MHz, we have only used the huygens' box if the memory requirements exceeded the limits of the computer hardware. Finally, the infinite vertical reflector has been placed at the left side of the human body model in order to find a worst-case reflective environment.

26.1: 0.3 m



26.2: 3 m



26.3: 10 m
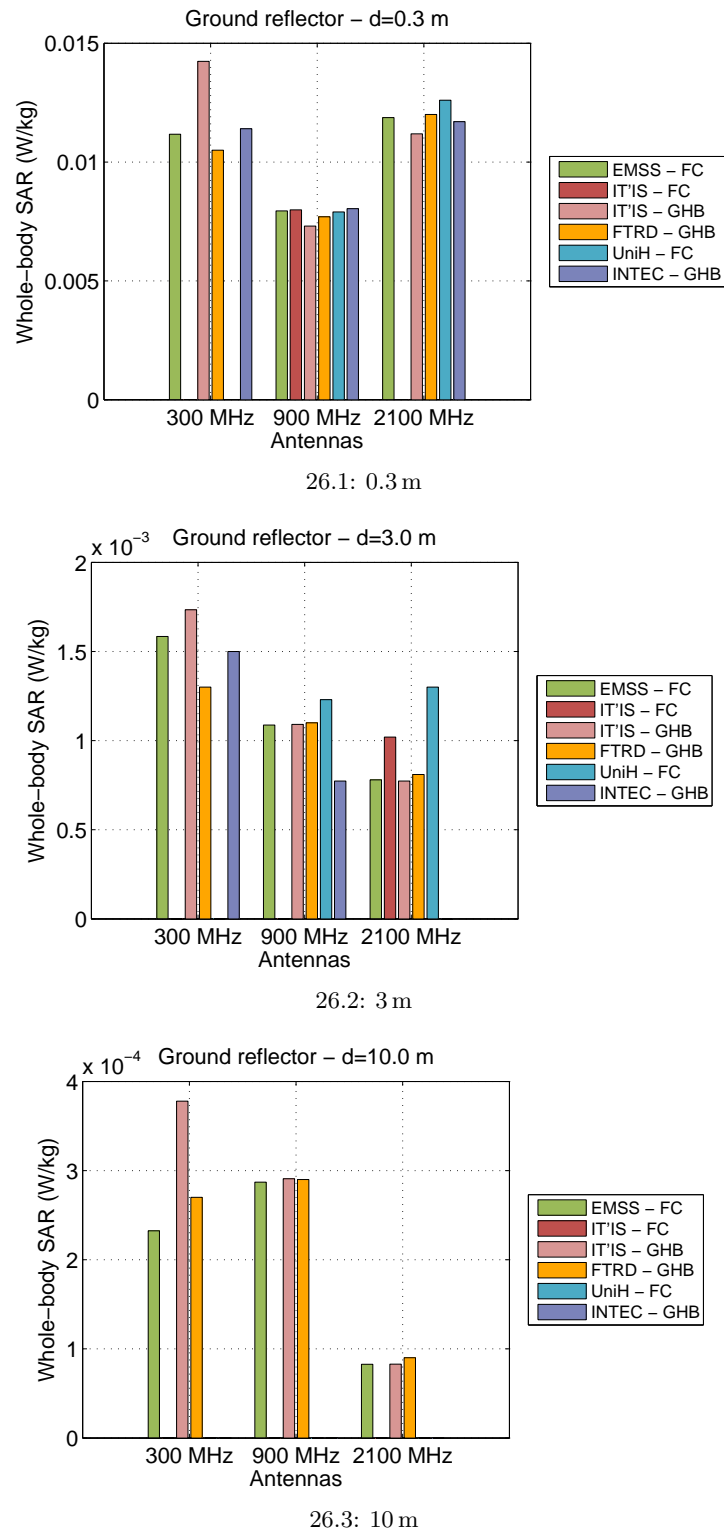
Figure 26: The whole-body SAR in the VFB placed at 5 cm above a perfectly conducting ground of infinite extent and for a separation of (a) 0.3 m, (b) 3 m, and (c) 10 m.

27.1: 0.3 m



27.2: 3 m



27.3: 10 m
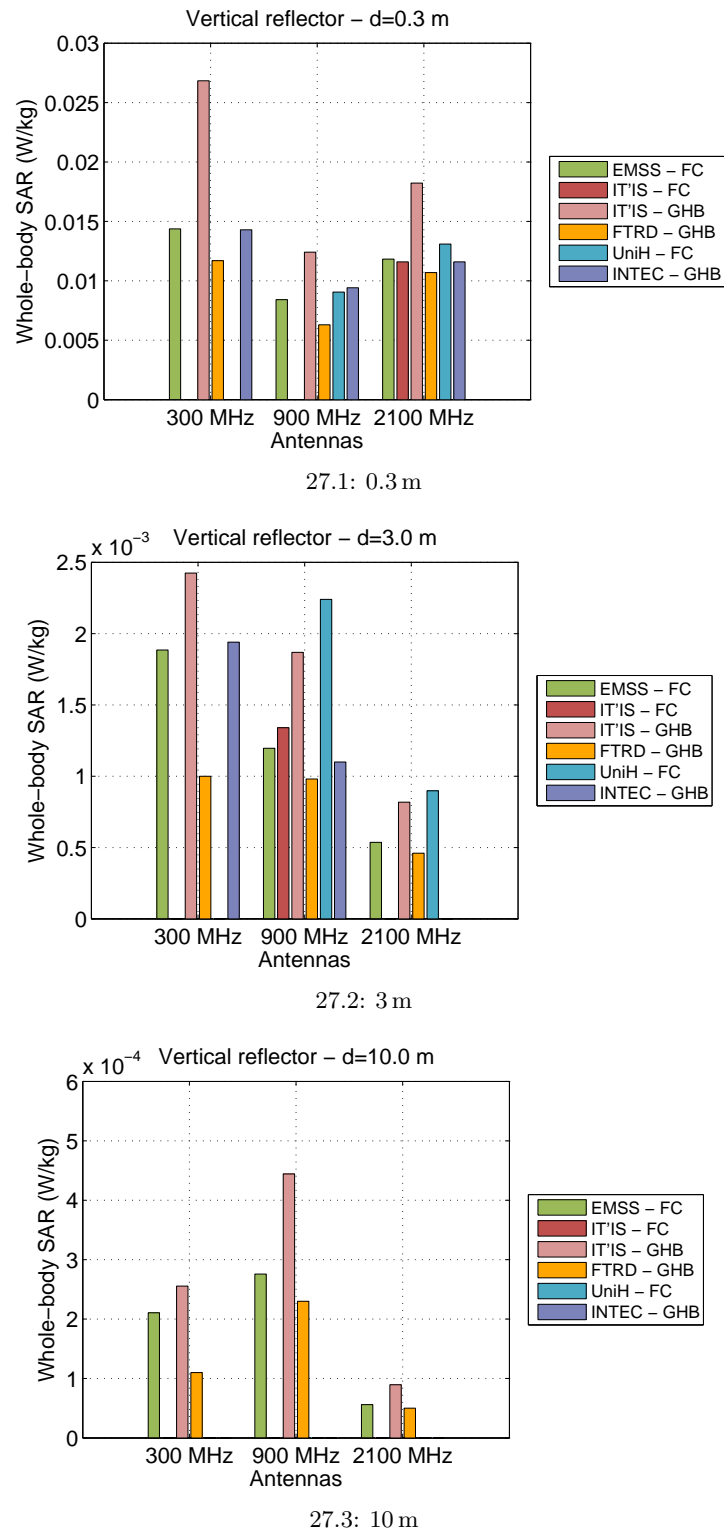
Figure 27: The whole-body SAR in the VFB with a perfectly conducting wall of infinite extent at the left side of the phantom at a distance of 10 cm and for a separation of (a) 0.3 m, (b) 3 m, and (c) 10 m.

28.1: 0.3 m



28.2: 3 m



28.3: 10 m
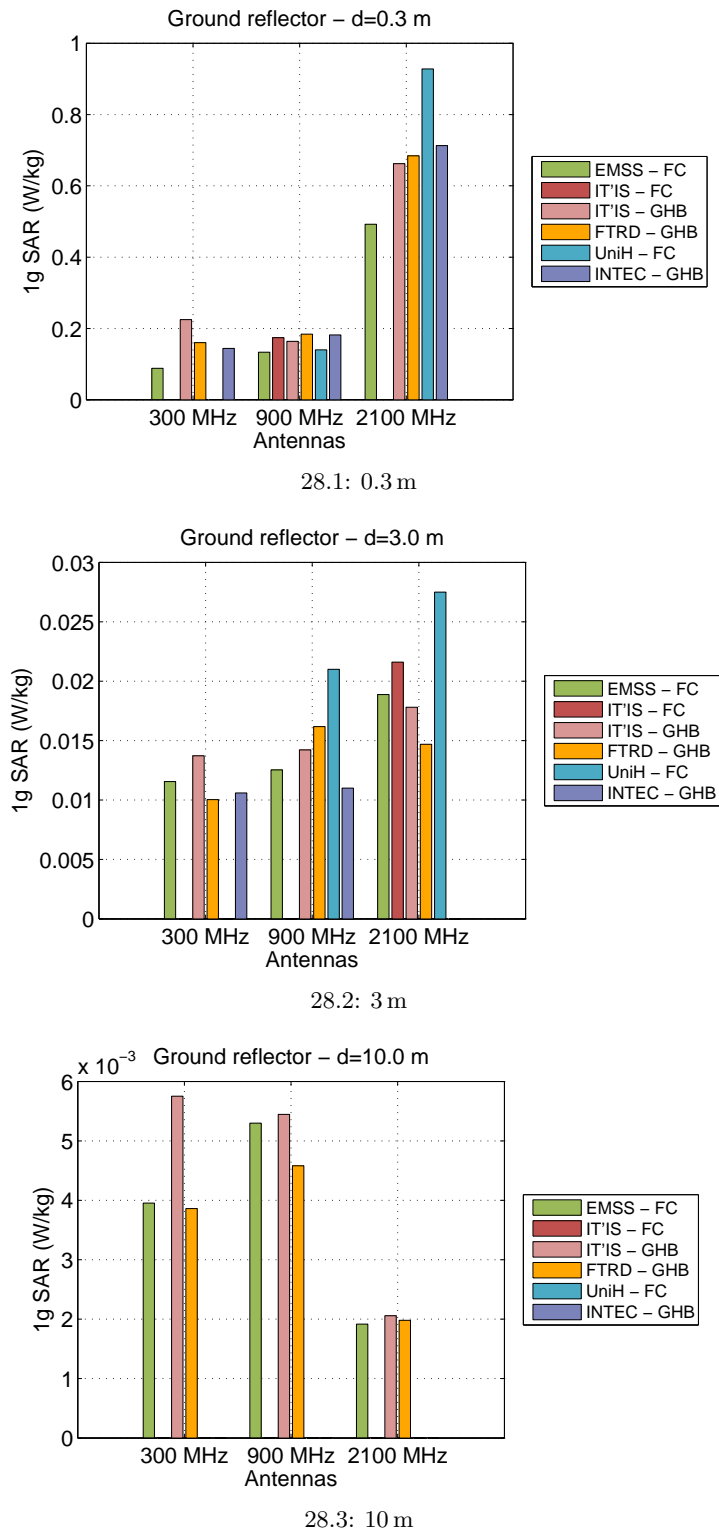
Figure 28: $SAR_{1g}$ in the VFB placed at $5\,cm$ above a perfectly conducting ground of infinite extent and for a separation of (a) $0.3\,m$, (b) $3\,m$, and (c) $10\,m$.

29.1: 0.3 m



29.2: 3 m



29.3: 10 m
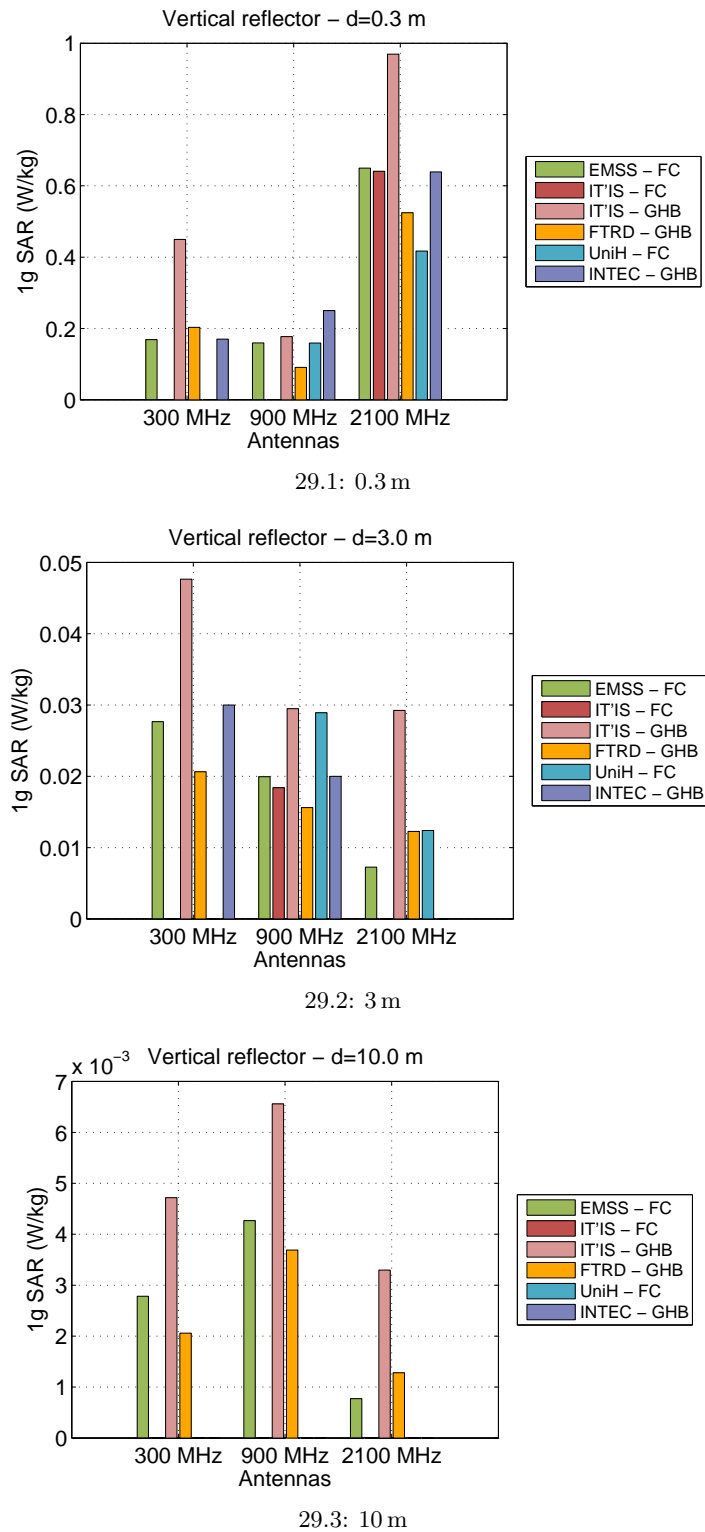
Figure 29: $SAR_{1g}$ in the VFM with a perfectly conducting wall of infinite extent at the left side of the phantom at a distance of 10 cm and for a separation of (a) 0.3 m, (b) 3 m, and (c) 10 m.

30.1: 0.3 m



30.2: 3 m



30.3: 10 m
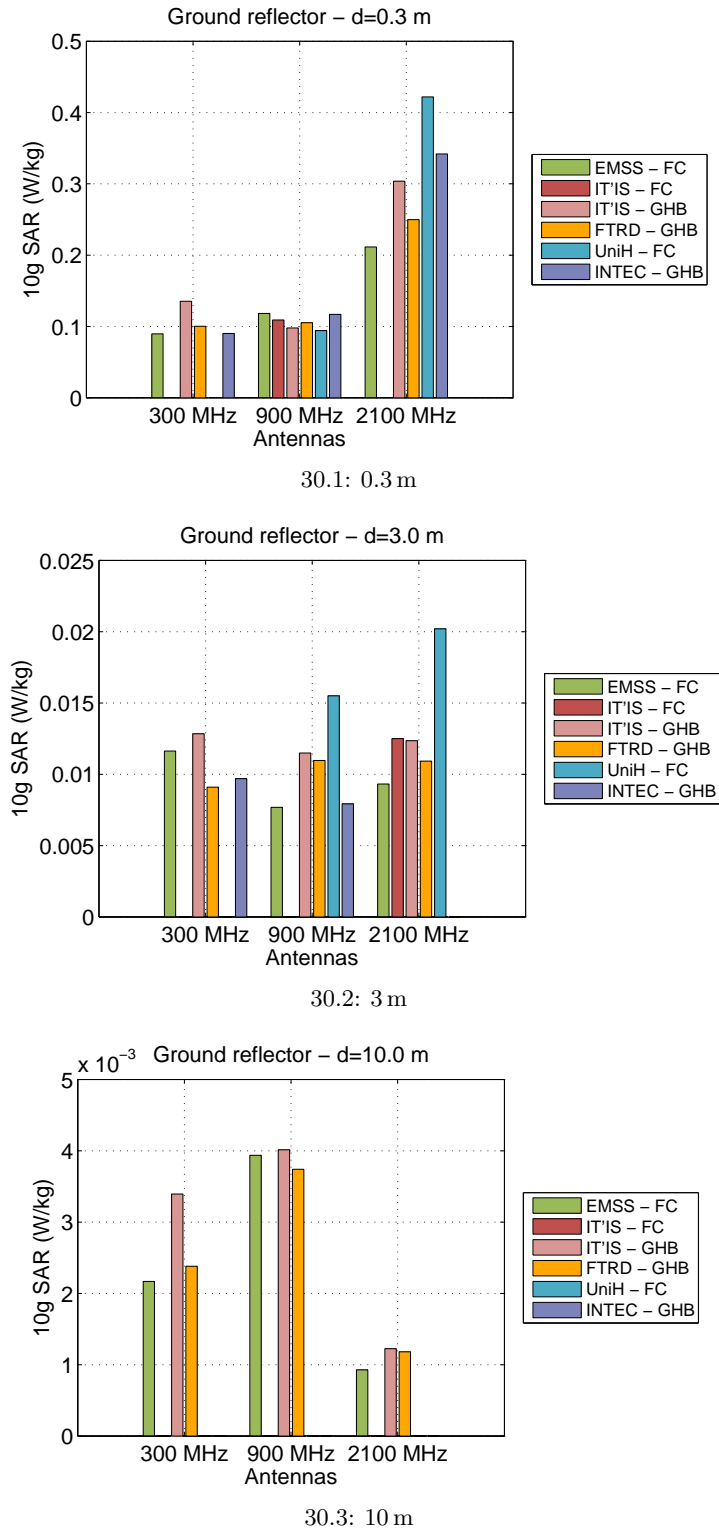
Figure 30: $SAR_{10g}$ in the VFM placed at $5\,\mathrm{cm}$ above a perfectly conducting ground of infinite extent and for a separation of (a) $0.3\,\mathrm{m}$, (b) $3\,\mathrm{m}$, and (c) $10\,\mathrm{m}$.

31.1: 0.3 m



31.2: 3 m



31.3: 10 m
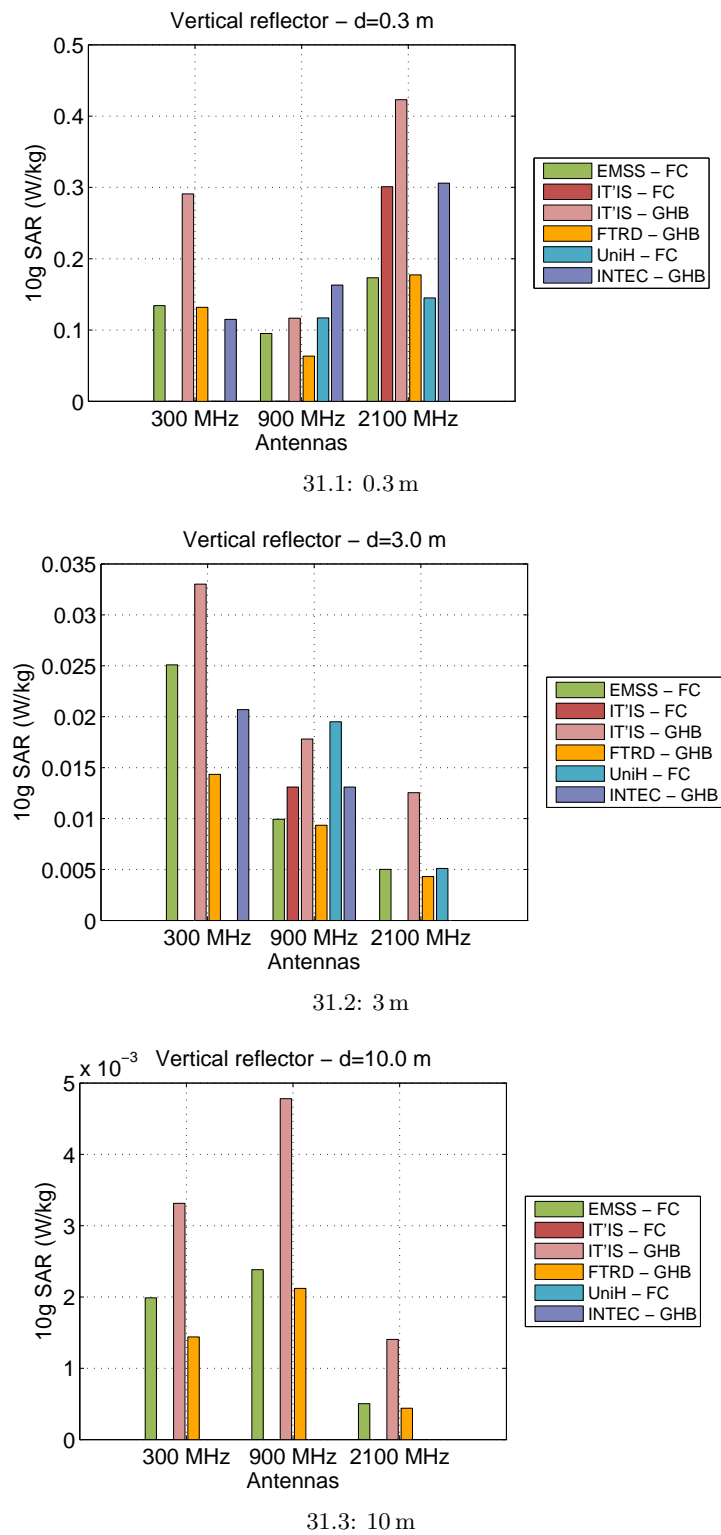
Figure 31: $SAR_{10g}$ in the VFM with a perfectly conducting wall of infinite extent at the left side of the phantom at a distance of 10 cm and for a separation of (a) 0.3 m, (b) 3 m, and (c) 10 m.

Table 17: The relative standard deviation of the mass, whole-body SAR, peak spatial averaged SAR in 1 g, and 10 g.

| Antenna | Environment | d (m) | $\sigma_{rel}(m)$ (%) | $\sigma_{rel}(SAR_{wb})$ (%) | $\sigma_{rel}(SAR_{1g})$ (%) | $\sigma_{rel}(SAR_{10g})$ (%) |
|---|---|---|---|---|---|---|
| 300MHz_H65V64_VPolV5 | Ground reflector | 0.3 | 0.72 | 14.05 | 36.34 | 20.83 |
| | | 3.0 | 0.72 | 11.85 | 14.04 | 15.98 |
| | | 10.0 | 0.84 | 25.72 | 23.58 | 24.76 |
| | Vertical reflector | 0.3 | 0.72 | 40.46 | 54.63 | 49.05 |
| | | 3.0 | 0.72 | 32.72 | 36.47 | 33.69 |
| | | 10.0 | 0.84 | 38.80 | 43.11 | 42.84 |
| 900MHz_H90V9_VPolV7 | Ground reflector | 0.3 | 0.52 | 3.49 | 13.23 | 9.13 |
| | | 3.0 | 0.57 | 7.10 | 19.95 | 24.43 |
| | | 10.0 | 0.74 | 0.68 | 9.08 | 3.62 |
| | Vertical reflector | 0.3 | 0.57 | 24.13 | 33.87 | 33.65 |
| | | 3.0 | 0.52 | 33.99 | 26.07 | 29.72 |
| | | 10.0 | 0.74 | 35.64 | 31.36 | 47.39 |
| 2100MHz_H90V80_IndoorVPolV4 | Ground reflector | 0.3 | 0.52 | 4.03 | 22.34 | 26.80 |
| | | 3.0 | 0.40 | 24.22 | 24.02 | 32.07 |
| | | 10.0 | 0.52 | 4.87 | 3.55 | 14.40 |
| | Vertical reflector | 0.3 | 0.46 | 21.83 | 28.92 | 42.24 |
| | | 3.0 | 0.45 | 31.34 | 62.80 | 57.61 |
| | | 10.0 | 0.52 | 32.58 | 74.93 | 68.92 |

### 2.4.2 Bulk simulations

**Configurations**

The investigated configurations have been discussed in section 2.4. Two research groups participated in performing the batch of simulations: INTEC and IT'IS. The FDTD solver SEMCAD X has been used to determine the SAR in the VFM. For the largest simulations with an operating frequency above 900 MHz the generalized huygens' box method has been applied to obtain a reasonable simulation time. Table 18 shows the list of configurations for which the huygens' box has been used. The incident fields for the huygens' box have been determined with SEMCAD X for all configurations except from the configurations with a separation distance of 10 m and operating frequencies of 2100 MHz and above. For the latter configurations the incident fields were calculated by INTEC using the hybrid MoM/FEM tool FEKO and used in SEMCAD X using the GHB method.

Table 18: The configurations for which the generalized huygens' box method has been used.

| Base Station Antenna | Separation distance |
|---|---|
| 900MHz_H65V7_X45V4 | $\geq 1\,\mathrm{m}$ |
| 2100MHz_H65V7_OutdoorXpolV3 | $\geq 3\,\mathrm{m}$ |
| 3500MHz_H65V9_VPol_BTSV3 | $\geq 1\,\mathrm{m}$ |
| 5000MHz_H65V35_VPol_DirectionalV5 | $\geq 0.3\,\mathrm{m}$ |

**Results**

The results are shown with frequency in Figure 32 and with distance in Figure 33 to Figure 38. In Figure 32 the whole-body SAR decreases with frequency above 2100 MHz, whereas the peak spatial SAR increases with increasing frequency. Both observations are due to the fact that for increasing frequency the electromagnetic energy in the body is absorbed closer to the surface of the body (skin effect). It is also observed that the highest SAR values are obtained at short distances between the base station antenna and the VFM.

**Comparison with the free space results**

To compare the SAR between the different reflective environments and free space, the ratio $R$ of the SAR in the VFM in a reflective environment and the SAR in the VFM in a free space environment has been plotted against the separation distance between the antenna and human body in Figures 33 to 38. Table 19 lists the minimum and the maximum values of the ratio $R$ for the investigated reflective environments with respect to the free space environment. The ratio $R$ varies between -8.71 dB (wall, 300 MHz, 10 m) and 5.62 dB (ground and wall, 450 MHz, 0.3 m), -7.85 dB (wall, 300 MHz, 10 m) and 8.01 dB (ground and wall, 450 MHz, 1 m), -7.39 dB (wall, 300 MHz, 10 m) and 7.77 dB (ground and wall, 450 MHz, 10 m) for $SAR_{wb}$, $SAR_{1g}$, and $SAR_{10g}$, respectively. So, the minimum and maximum $R$ occurs for the base station antennas with the lower operating frequencies of 300 MHz and 450 MHz except from the minimum for $SAR_{wb}$ and $SAR_{10g}$ in the environments 'ground' and 'ground + wall', respectively.

For the majority of the configurations, the highest SAR values with respect to the free space environment are found for the reflective environments with a wall. However, for the 300 MHz and 450 MHz base station antenna and a separation of 10 m, the highest SAR values are obtained for the ground environment (see Figures 33 and 34). Moreover, it is also observed that the SAR in a reflective environment is not always higher than the SAR in the free space environment. So, a worst-case (reflective) environment could not be determined.

Table 19: The minimum and maximum ratio $R$ of the whole-body and localized absorption in a reflective environment with respect to the absorption in free space environment.

| Reflective environment | $R_{wb} = \frac{SAR_{wb,reflect.env.}}{SAR_{wb,freespace}}$ (dB) | scenario |
|---|---|---|
| Ground | -2.91 (min) | 2100 MHz BSA at 10 m |
| | 2.99 (max) | 450 MHz BSA at 10 m |
| Wall | -8.71 (min) | 300 MHz BSA at 10 m |
| | 5.62 (max) | 450 MHz BSA at 0.3 m |
| Ground + wall | -5.95 (min) | 300 MHz BSA at 10 m |
| | 5.67 (max) | 450 MHz BSA at 0.3 m |

| Reflective environment | $R_{1g} = \frac{SAR_{1g,reflect.env.}}{SAR_{1g,freespace}}$ (dB) | scenario |
|---|---|---|
| Ground | -3.97 (min) | 900 MHz BSA at 1 m |
| | 6.61 (max) | 450 MHz BSA at 10 m |
| Wall | -7.85 (min) | 300 MHz BSA at 10 m |
| | 6.94 (max) | 450 MHz BSA at 0.3 m |
| Ground + wall | -4.72 (min) | 300 MHz BSA at 10 m |
| | 8.01 (max) | 450 MHz BSA at 1 m |

| Reflective environment | $R_{10g} = \frac{SAR_{10g,reflect.env.}}{SAR_{10g,freespace}}$ (dB) | scenario |
|---|---|---|
| Ground | -3.22 (min) | 3500 MHz BSA at 10 m |
| | 6.41 (max) | 450 MHz BSA at 10 m |
| Wall | -7.39 (min) | 300 MHz BSA at 10 m |
| | 7.07 (max) | 450 MHz BSA at 0.3 m |
| Ground + wall | -4.33 (min) | 300 MHz BSA at 10 m |
| | 7.77 (max) | 450 MHz BSA at 1 m |

**Correlation between incident fields and absorption**

To better compare the absorption between the investigated configurations, the rms incident electric field spatially averaged over the bounding box enclosing the human body model ($\langle E_{rms}\rangle_{bounding\ box\ body}$) and the peak spatial rms electric field over the bounding box of the body ($E_{rms,peak,bounding\ box\ body}$) have been determined when the human body is not present. The results are shown in Figures 39 - 40 and Figures 41 - 42 for $\langle E_{rms}\rangle_{bounding\ box\ body}$ and $E_{rms,peak,bounding\ box\ body}$, respectively. Comparing Figures 33 - 38 (SAR results) to Figures 39 - 42 ($E_{rms}$ results), it is observed that, generally, high field values over the bounding box of the human body result in high values for the absorption. To further investigate this, the correlation coefficient has been calculated between the whole-body SAR, peak local averaged SAR and $\langle E_{rms}\rangle_{bounding\ box\ body}$, $E_{rms,peak,bounding\ box\ body}$, respectively. The correlation between $SAR_{wb}$ and $\langle E_{rms}\rangle_{bouning\ box\ body}$ varies from 89.0 % at 5000 MHz and 99.1 % at 2100 MHz. The correlation between $SAR_{1g}$, $SAR_{10g}$ and $E_{rms,peak,bounding\ box\ body}$ ranges from 90.3 % (300 MHz), 92.2 % (3500 MHz) to 99.1 % (2100 MHz), 99.7 % (5000 MHz), respectively. For the investigated configurations a strong correlation has been observed between the whole-body SAR and the rms incident electric field averaged over the bounding box around the human body model, and between the peak spatial averaged SAR and the peak rms incident electric field over the bounding box of the human body. Previously, it was already reported that

the whole-body SAR correlates well with the rms electric field averaged over the bounding box of the human body. For the peak spatial SAR a good correlation has been reported with the peak rms electric field found inside the bounding box of the human body [Bernardi et al., 2000].
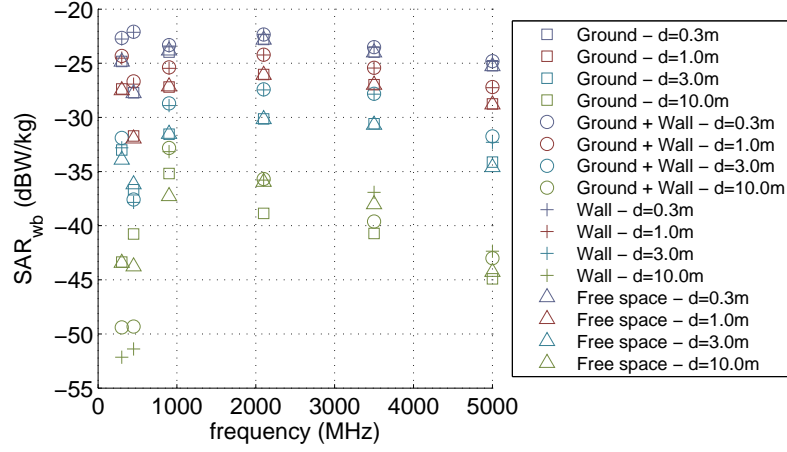


32.1: $SAR_{wb}$
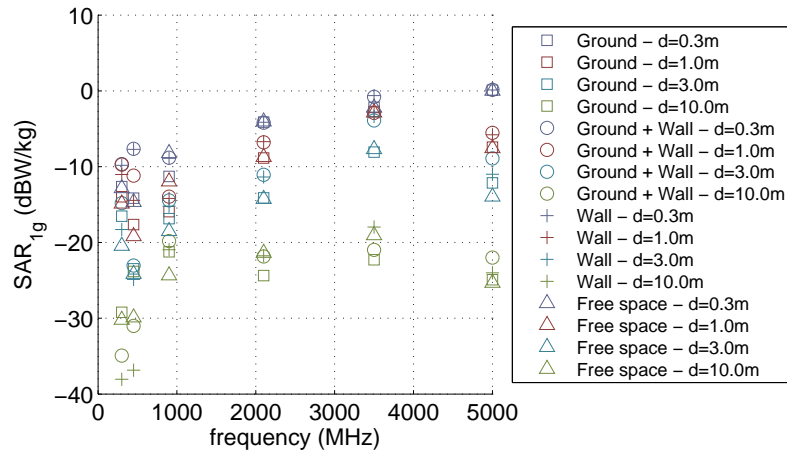


32.2: $SAR_{1g}$
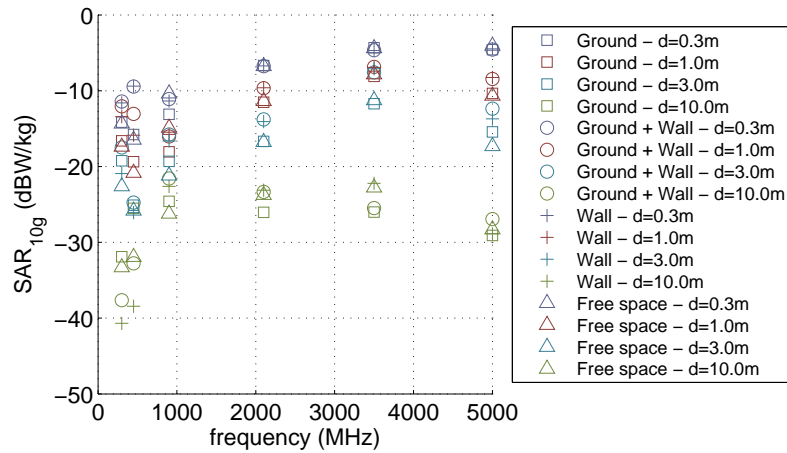


32.3: $SAR_{10g}$

Figure 32: The (a) whole-body SAR, (b) peak spatial SAR in 1 g, and (c) peak spatial SAR in 10 g as a function of frequency for a total antenna input power of 1 W.
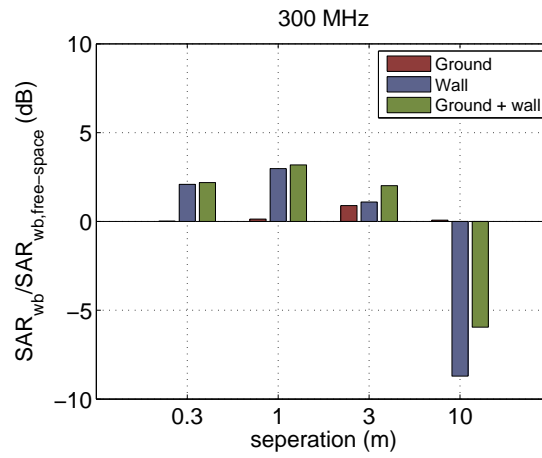
33.1: $SAR_{wb}$
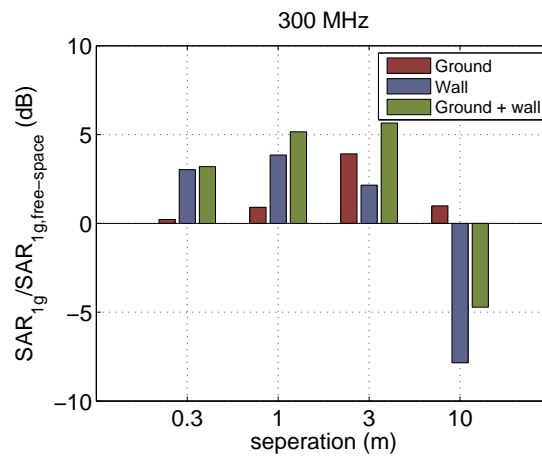


33.2: $SAR_{1g}$
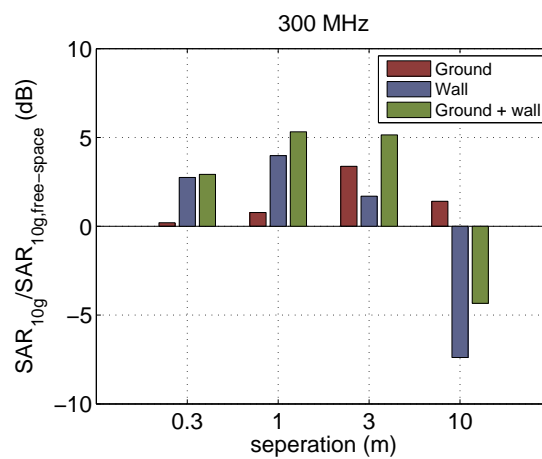


33.3: $SAR_{10g}$

Figure 33: The ratio $R$ of the SAR in VFM in a reflective environment and the SAR in VFM in free space as a function of the separation between VFM and base station antenna at 300 MHz for (a) whole-body SAR, (b) peak spatial SAR in 1 g, and (c) peak spatial SAR in 10 g.

34.1: $SAR_{wb}$



34.2: $SAR_{1g}$



34.3: $SAR_{10g}$
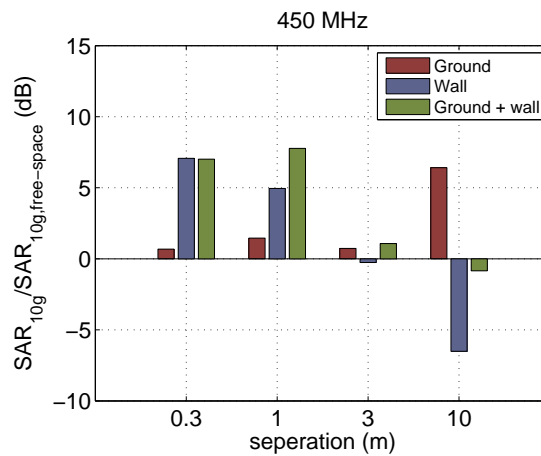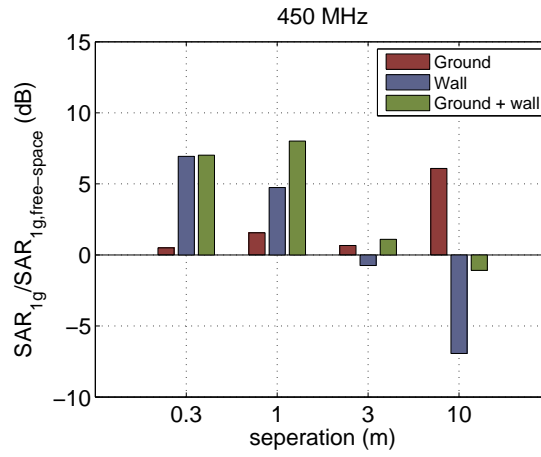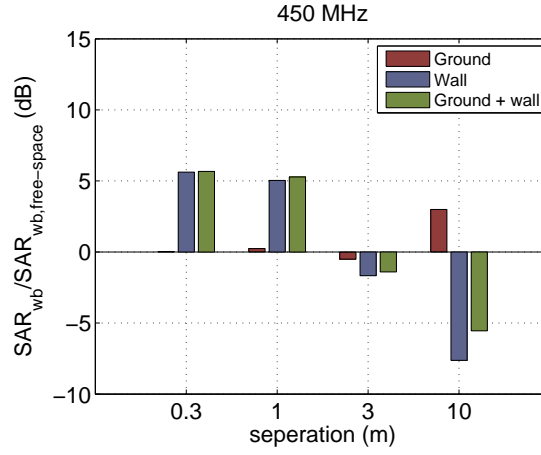
Figure 34: The ratio $R$ of the SAR in VFM in a reflective environment and the SAR in VFM in free space as a function of the separation between VFM and base station antenna at $450\,\mathrm{MHz}$ for (a) whole-body SAR, (b) peak spatial SAR in $1\,\mathrm{g}$, and (c) peak spatial SAR in $10\,\mathrm{g}$.
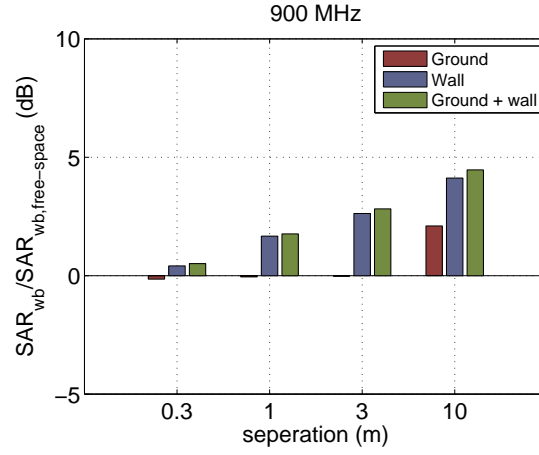
35.1: $SAR_{wb}$
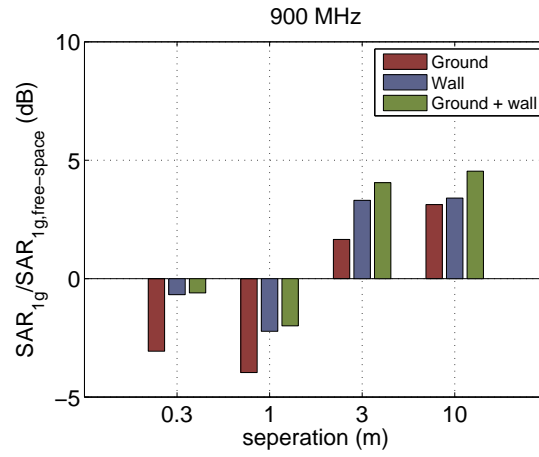


35.2: $SAR_{1g}$
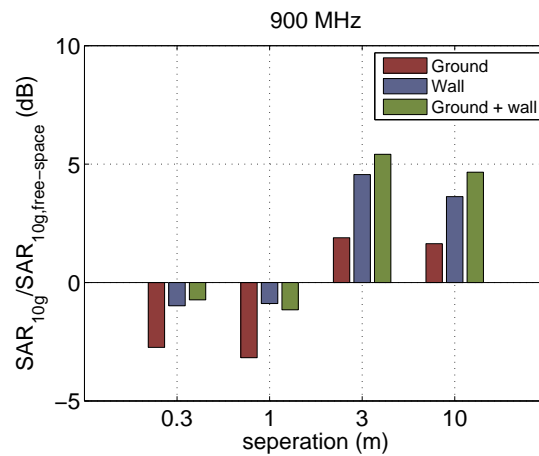


35.3: $SAR_{10g}$

Figure 35: The ratio $R$ of the SAR in VFM in a reflective environment and the SAR in VFM in free space as a function of the separation between VFM and base station antenna at 900 MHz for (a) whole-body SAR, (b) peak spatial SAR in 1 g, and (c) peak spatial SAR in 10 g.
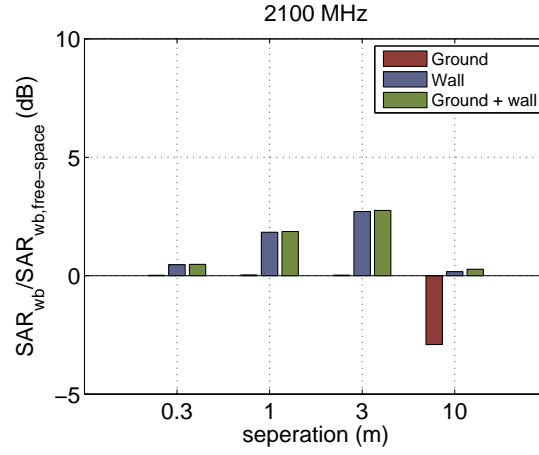
36.1: $SAR_{wb}$
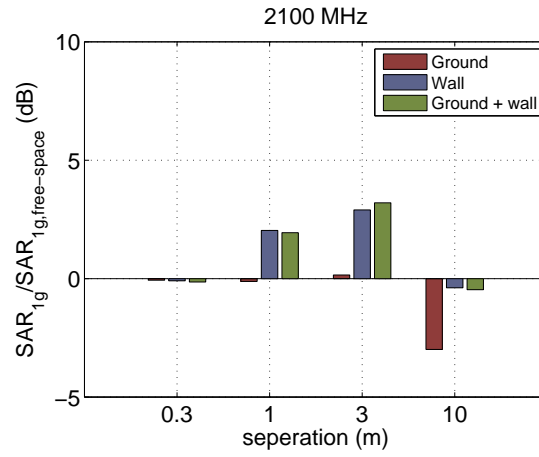


36.2: $SAR_{1g}$
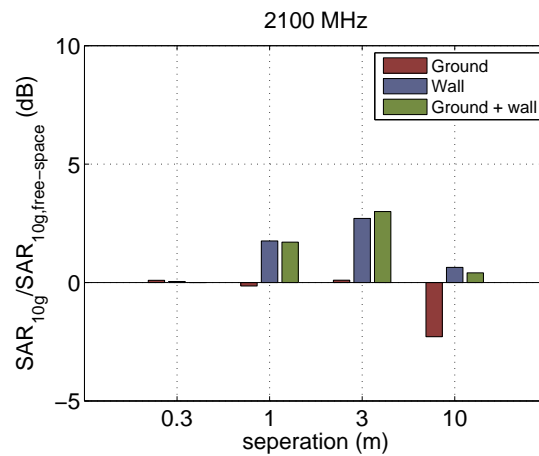


36.3: $SAR_{10g}$

Figure 36: The ratio $R$ of the SAR in VFM in a reflective environment and the SAR in VFM in free space as a function of the separation between VFM and base station antenna at 2100 MHz for (a) whole-body SAR, (b) peak spatial SAR in 1 g, and (c) peak spatial SAR in 10 g.
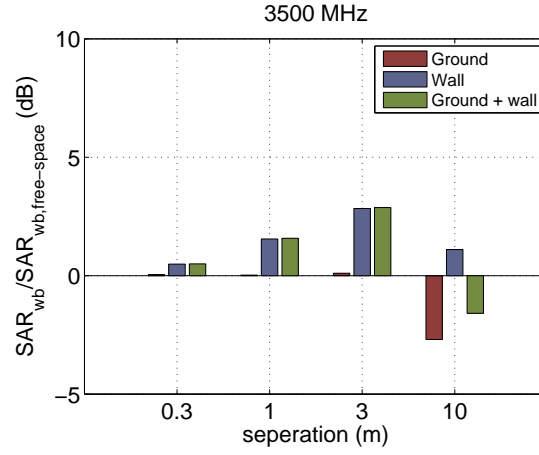
37.1: $SAR_{wb}$
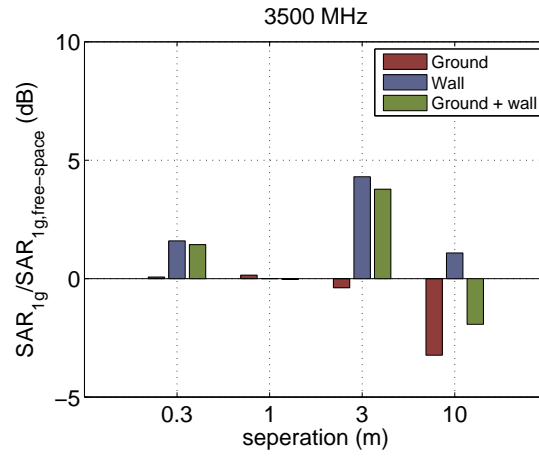


37.2: $SAR_{1g}$
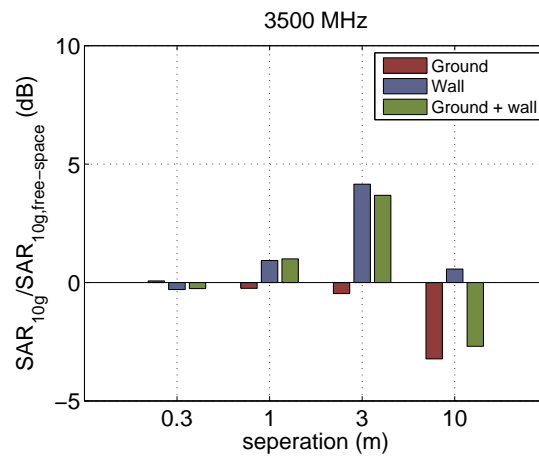


37.3: $SAR_{10g}$

Figure 37: The ratio $R$ of the SAR in VFM in a reflective environment and the SAR in VFM in free space as a function of the separation between VFM and base station antenna at 3500 MHz for (a) whole-body SAR, (b) peak spatial SAR in 1 g, and (c) peak spatial SAR in 10 g.
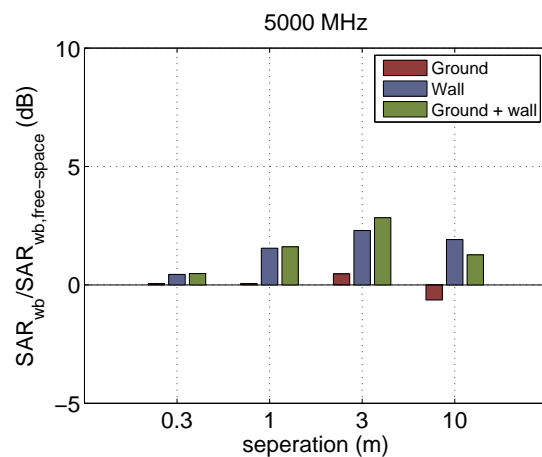
38.1: whole-body averaged
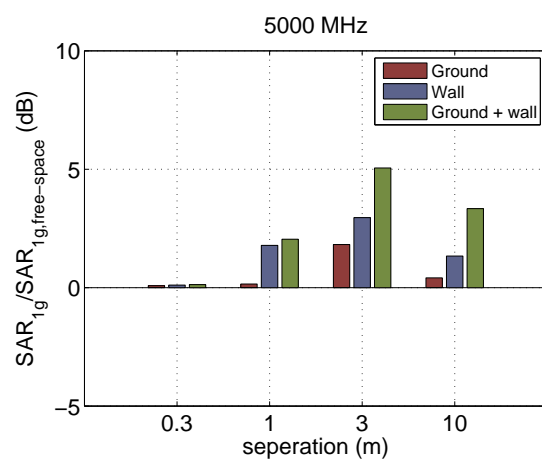


38.2: 1 g averaged
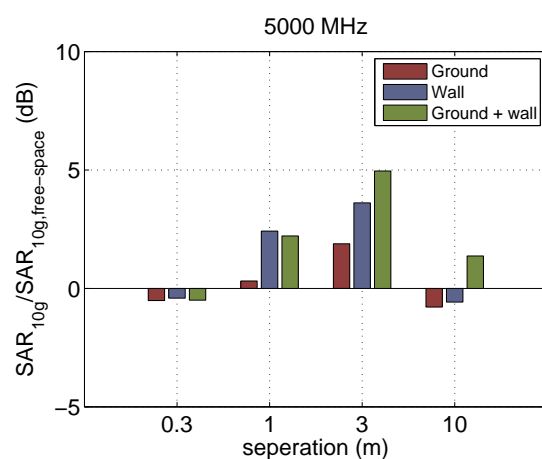


38.3: 10 g averaged

Figure 38: The ratio $R$ of the SAR in VFM in a reflective environment and the SAR in VFM in free space as a function of the separation between VFM and base station antenna at $5000\,\mathrm{MHz}$ for (a) whole-body SAR, (b) peak spatial SAR in $1\,\mathrm{g}$, and (c) peak spatial SAR in $10\,\mathrm{g}$.
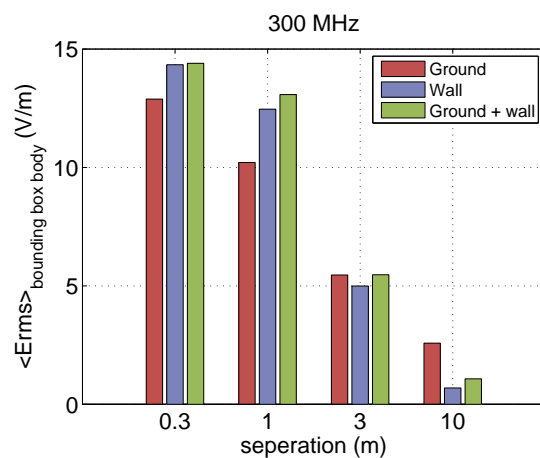
39.1: 300 MHz
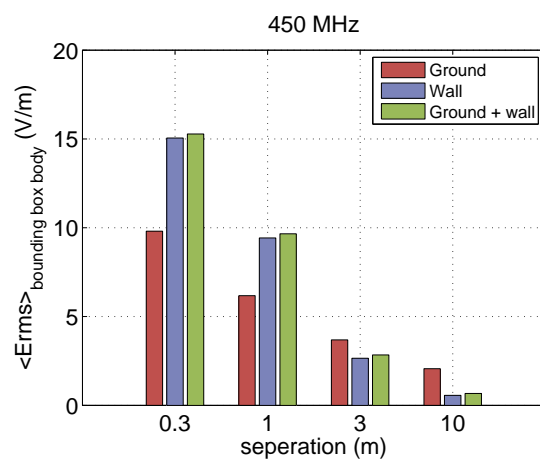


39.2: 450 MHz
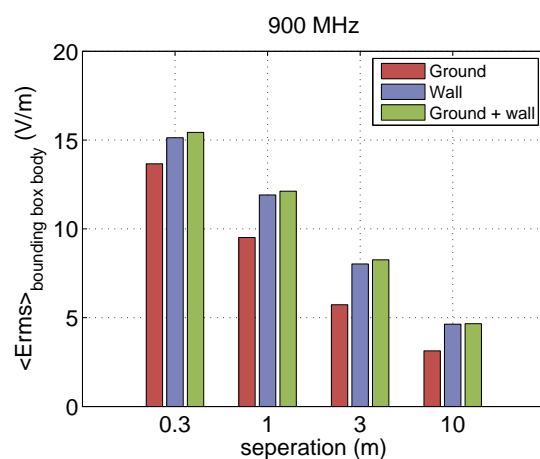


39.3: 900 MHz

Figure 39: The rms electric field averaged over the box around the human body model if the model is not present for the base station antennas with operating frequencies of (a) 300 MHz, (b) 450 MHz, and (c) 900 MHz and a total antenna input power of 1 W.

40.1: 2100 MHz

40.2: 3500 MHz
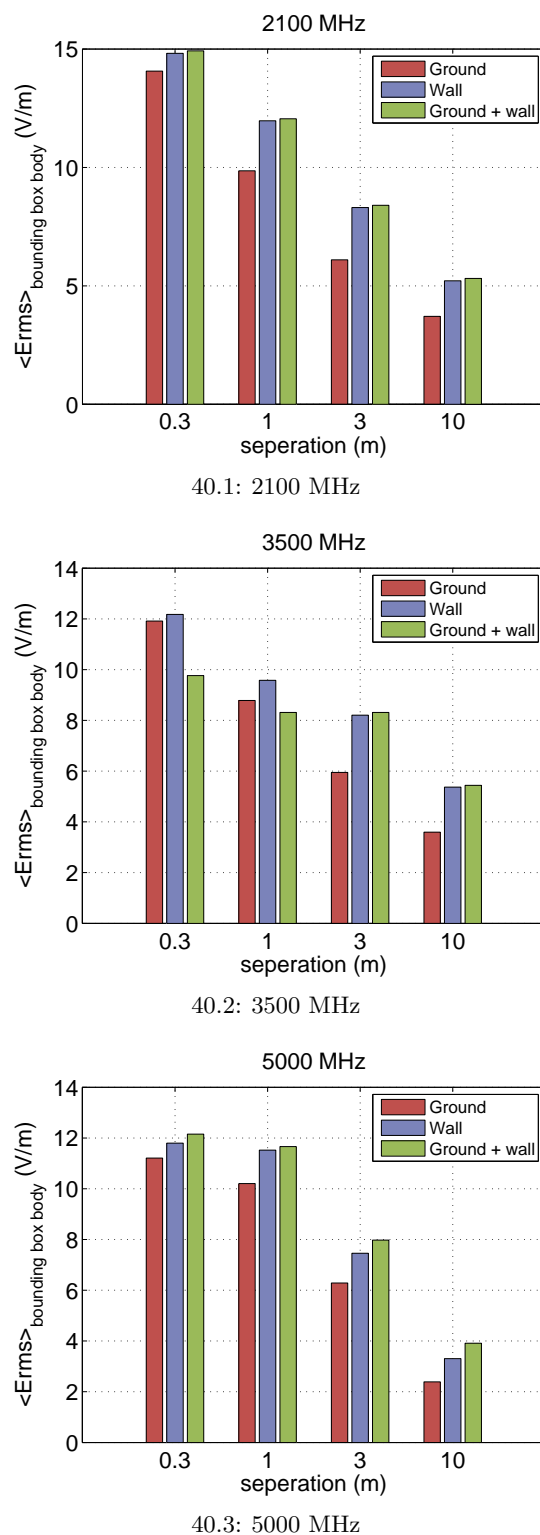
40.3: 5000 MHz

Figure 40: The rms electric field averaged over the box around the human body model if the model is not present for the base station antennas with operating frequencies of (a) 2100 MHz, (b) 3500 MHz, and (c) 5000 MHz and a total antenna input power of 1 W.
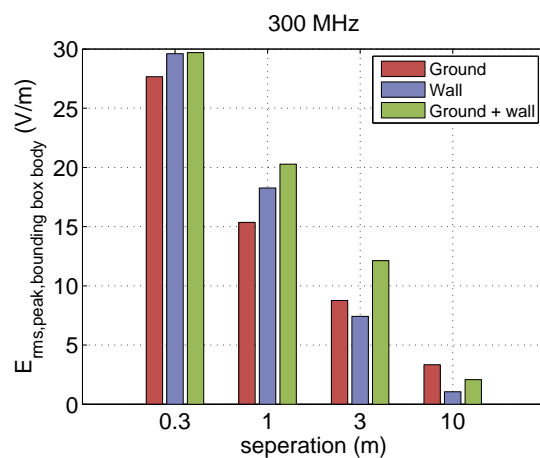
41.1: 300 MHz
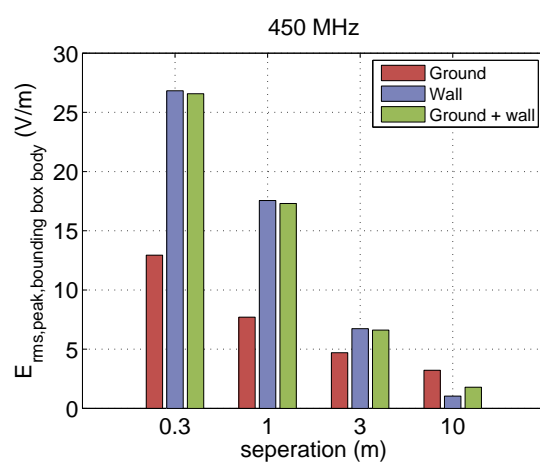


41.2: 450 MHz
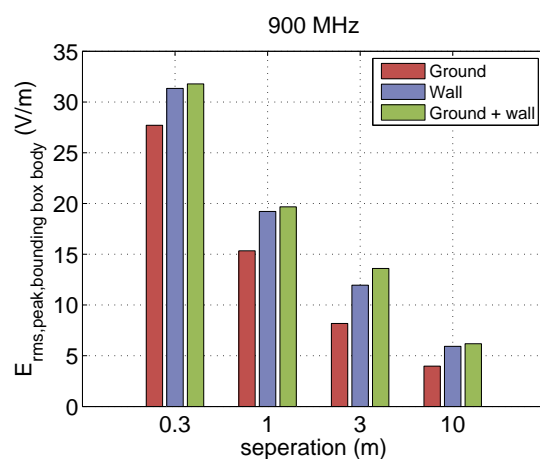


41.3: 900 MHz

Figure 41: The spatial peak rms electric field over the box around the human body model if the model is not present for the base station antennas with operating frequencies of (a) 300 MHz, (b) 450 MHz, and (c) 900 MHz and a total antenna input power of 1 W.

42.1: 2100 MHz



42.2: 3500 MHz
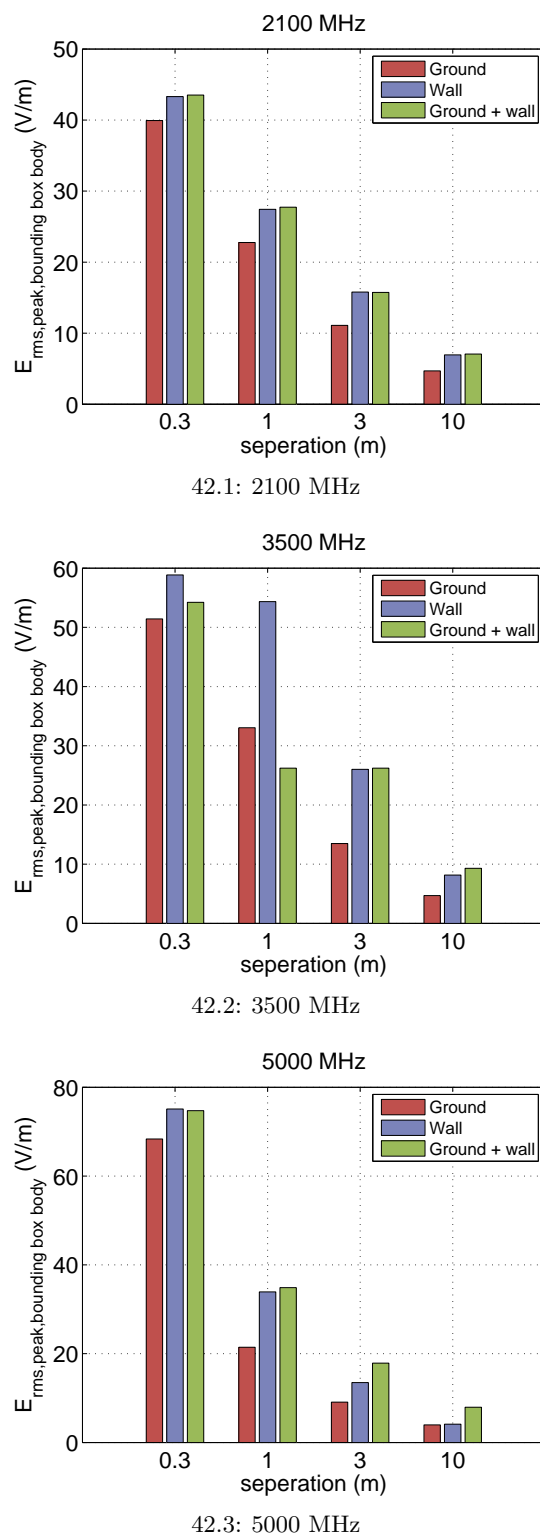


42.3: 5000 MHz

Figure 42: The spatial peak rms electric field over the box around the human body model if the model is not present for the base station antennas with operating frequencies of (a) 2100 MHz, (b) 3500 MHz, and (c) 5000 MHz and a total antenna input power of 1 W.
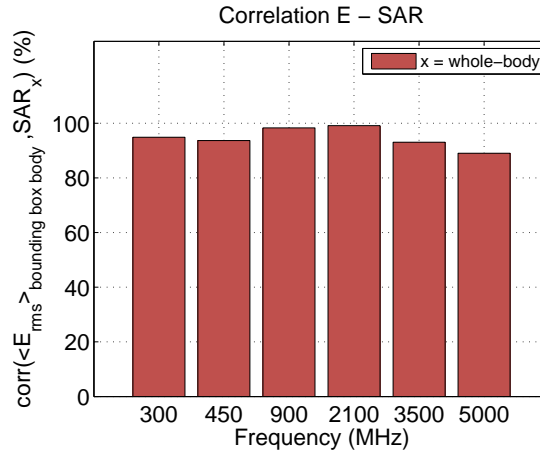
Figure 43: The correlation between the rms electric field averaged over the box around the human body model if the model is not present and the whole-body averaged SAR.
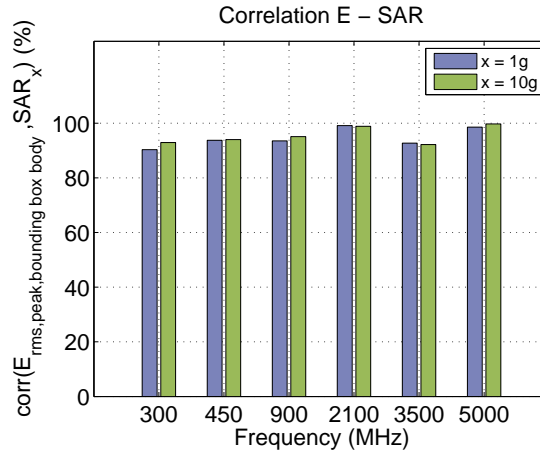


Figure 44: The correlation between the peak spatial rms electric field over the box around the human body model if the model is not present and the peak spatial SAR in 1 g and 10 g.

## 2.5 Conclusions

The whole-body SAR and peak spatial averaged SAR have been investigated in the Virtual Family Man in a perfectly conducting environment for representative base station antennas operating in the frequency range of 300 MHz to 5000 MHz. The perfectly conducting environment consisted of an infinite ground and / or an infinite vertical wall. The wall has been placed at the left side of the human body model.

From the literature review it is clear that worst-case exposure scenarios can be expected in an environment consisting of a perfectly conducting walls and ground, because at a perfectly conducting reflector all the power is reflected back in the domain. Considering realistic walls and grounds decreases the variation on the calculation of the SAR. With respect to exposure in free space, an increase of up to 5 dB for the whole-body absorption has been reported in the literature.

The huygens' box method has been used for an efficient calculation of the absorption for the larger simulations. This huygens' box method is a hybrid method using the MoM/FEM for calculating the incident fields and the FDTD method for assessing numerically the absorption in an inhomogeneous human body model. It has been shown that the huygens' box method is applicable for the configurations with an operating frequency of 900 MHz and above.

From the bulk simulations, one can conclude that the whole-body and local absorption vary a lot with respect to the absorption in the VFM in free space. The ratio of the SAR in the VFM in a reflective environment and the SAR in the VFM in the free space environment ranged from -8.71 dB up to 8.01 dB. The whole-body absorption correlated very well with the rms incident fields averaged over a bounding box around the body, whereas for the peak spatial SAR in 1 g and 10 g a good correlation has been observed with the peak rms incident electric field over the bounding box around the body. So, worst-case exposure can be determined from an investigation of the rms incident field in a certain environment. The location where the rms field achieves the highest value, the highest absorption can be expected. A worst-case reflective environment could not be determined.

# 3 Inter-Laboratory Comparison

**Conducted by FDA**

**Authors: Wolfgang Kainz, Gonzalo Mendoza, Valpré Kellermann, Stefan Cecil, Louis-Ray Harris, Takashi Hikage, Toshio Nojima, Abdelhamid Hadjem, Azeddine Gati, Marie-Christine Gosselin, Tero Uusitupa, Sven Kühn**

**Executive Summary**

Seven different groups used two different anatomical models (homogeneous and in-homogeneous) to calculate the 1 g averaged SAR (1 g SAR), the 10 g averaged SAR (10 g SAR) and whole-body averaged SAR (wba SAR) when exposed to plane waves and base station antennas at 0.9, 2.1, and 5.0 GHz. The goal was to assess the variability of these values when different numerical codes were used which use different numerical methods. SAR averaging is based on a standardized method outlined in the standard IEEE C95.3 [IEEE, 2002]. We found that the standard deviation for the wba SAR is less than 16% for base station exposure and less than 3% for plane wave exposure. The 1 g and 10 g averaged SAR is less than 36% for base station exposure and less than 28% for plane wave exposure. The use of an homogeneous or in-homogeneous model has insignificant influence on the SAR results. For the free-space simulations, the standard deviation of the electric and magnetic field values and the directivity of the base station antennas is less than 9%. The Method of Moments (MoM) implementation of the SAR averaging algorithm showed the largest deviation from the other SAR averaging implementations which are all written for FDTD codes. This can be expected due and the reasons for these difference are presented in Section 3.4.3.

## 3.1 Exposure Configurations

Anatomical human models have been exposed to plane waves and base station antennas. The exposure parameters for the plane-wave simulations were:

- 2 human models (VFM and VFB)

- 2 sets of dielectric properties for human tissues[2] (homogeneous liquid [IEC, 2009] and heterogeneous tissues [Gabriel et al., 1996])

- 3 frequencies (0.9, 2.1, and 5 GHz)

- frontal exposure

The parameters for the exposure to base station antennas were:

- 2 human models (VFM and VFB)

- 2 sets of dielectric properties for human tissues[2] (homogeneous liquid [IEC, 2009] and heterogeneous tissues [Gabriel et al., 1996])

- 3 base station antennas, 1 for each frequency (0.9, 2.1, and 5 GHz[3]):
    - 900 MHz H90V9 VPolV7
    - 2100 MHz H90V80 Indoor VPolV4
    - 5000 MHz H65V35 VPol DirectionalV5

- distance of 1 m between the antenna and the human model

- frontal exposure

## 3.2 Participating Groups

The seven participants involved in this project were: FDA (leader), ARCS, IT'IS, EMSS, Hokkaido University, TKK and France Telecom. The methods used were different 3D EM computational techniques either implemented as Finite Difference Time Domain (FDTD) code or based on the Method of Moments (MoM). The EM solver and computational technique used by each participating group are presented in Table 20. Tables 21 and 22 show the different configurations simulated by the different groups, with plane waves and base station antennas, respectively. The participants that have performed simulations using base station antennas also ran free-space simulation up to 50 cm to validate the numerical representations of the antennas.

## 3.3 Methodology

The following setup was used by all participants to run the computational simulations to calculate the 1 g averaged SAR, the 10 g averaged SAR and whole-body averaged SAR:

- Each anatomical model is bounded by a rectangular box[4]. Looking from the front into the eyes of the model, the lower, left, back corner of this bounding box is the origin of a right handed coordinate system. In other words, the z-axis has to be aligned with the vertical

---

[2]The dielectric properties assigned to the tissues are detailed in Figure 45

[3]The base station antennas are presented in Appendix B and validated in Appendix C. They are part of the set of antennas used in WP6.

[4]This lead to differences between the different participating groups, depending on the presence or not of air padding around the human model.

| # | Organ or Tissue Label as in Model | Tissue Type as in Internet Databases http://niremf.ifac.cnr.it/tissprop/ http://www.fcc.gov/fcc-bin/dielec.sh | Density [kg/m3] | NON-HOMOGENEOUS 0.9 GHz σ [S/m] | ε_r [1] | 2.1 GHz σ [S/m] | ε_r [1] | 5.0 GHz σ [S/m] | ε_r [1] | HOMOGENEOUS 0.9 GHz σ [S/m] | ε_r [1] | 2.1 GHz σ [S/m] | ε_r [1] | 5.0 GHz σ [S/m] | ε_r [1] |
|---|---|---|---|---|---|---|---|---|---|---|---|---|---|---|---|
| 1 | Adrenal_gland | Gland | 1025 | 1.0385 | 59.684 | 1.7033 | 57.705 | 4.6614 | 53.342 | 0.97 | 41.50 | 1.49 | 39.82 | 4.40 | 36.20 |
| 2 | Air_internal | Air | 0 | 0 | 1 | 0 | 1 | 0 | 1 | 0.97 | 41.50 | 1.49 | 39.82 | 4.40 | 36.20 |
| 3 | Artery | Blood | 1060 | 1.5379 | 61.36 | 2.2614 | 58.851 | 5.3951 | 53.95 | 0.97 | 41.50 | 1.49 | 39.82 | 4.40 | 36.20 |
| 4 | Bladder | Bladder | 1040 | 0.38308 | 18.936 | 0.60049 | 18.182 | 1.5308 | 16.674 | 0.97 | 41.50 | 1.49 | 39.82 | 4.40 | 36.20 |
| 5 | Blood_vessel | Blood | 1060 | 1.5379 | 61.36 | 2.2614 | 58.851 | 5.3951 | 53.95 | 0.97 | 41.50 | 1.49 | 39.82 | 4.40 | 36.20 |
| 6 | Bone | BoneCortical | 1990 | 0.14331 | 12.454 | 0.32813 | 11.592 | 0.96228 | 10.04 | 0.97 | 41.50 | 1.49 | 39.82 | 4.40 | 36.20 |
| 7 | Brain_grey_matter | BrainGreyMatter | 1039 | 0.94227 | 52.725 | 1.5738 | 49.51 | 4.0995 | 45.147 | 0.97 | 41.50 | 1.49 | 39.82 | 4.40 | 36.20 |
| 8 | Brain_white_matter | BrainWhiteMatter | 1043 | 0.59079 | 38.886 | 1.0466 | 36.6 | 2.8588 | 33.444 | 0.97 | 41.50 | 1.49 | 39.82 | 4.40 | 36.20 |
| 9 | Breast | Fat/Gland(average) | 928 | 0.5447715 | 32.573 | 0.8965795 | 31.51095 | 2.45181 | 29.18555 | 0.97 | 41.50 | 1.49 | 39.82 | 4.40 | 36.20 |
| 10 | Bronchi | BloodVessel | 1063 | 0.69612 | 44.775 | 1.2262 | 42.963 | 3.533 | 39.295 | 0.97 | 41.50 | 1.49 | 39.82 | 4.40 | 36.20 |
| 11 | Bronchi_lumen | Air | 0 | 0 | 1 | 0 | 1 | 0 | 1 | 0.97 | 41.50 | 1.49 | 39.82 | 4.40 | 36.20 |
| 12 | Cartilage | Cartilage | 1100 | 0.78239 | 42.653 | 1.4939 | 39.535 | 4.0855 | 33.63 | 0.97 | 41.50 | 1.49 | 39.82 | 4.40 | 36.20 |
| 13 | Cerebellum | Cerebellum | 1040 | 1.2628 | 49.444 | 1.8822 | 45.462 | 4.1943 | 41.053 | 0.97 | 41.50 | 1.49 | 39.82 | 4.40 | 36.20 |
| 14 | Cerebrospinal_fluid | CerebroSpinalFluid | 1007 | 2.4126 | 68.638 | 3.1541 | 66.764 | 6.5969 | 61.952 | 0.97 | 41.50 | 1.49 | 39.82 | 4.40 | 36.20 |
| 15 | Commissura_anterior | BrainWhiteMatter | 1043 | 0.59079 | 38.886 | 1.0466 | 36.6 | 2.8588 | 33.444 | 0.97 | 41.50 | 1.49 | 39.82 | 4.40 | 36.20 |
| 16 | Commissura_posterior | BrainWhiteMatter | 1043 | 0.59079 | 38.886 | 1.0466 | 36.6 | 2.8588 | 33.444 | 0.97 | 41.50 | 1.49 | 39.82 | 4.40 | 36.20 |
| 17 | Connective_tissue | Fat/Tendon(average) | 1013 | 0.3847165 | 25.6435 | 0.7506795 | 24.52595 | 2.27156 | 21.66405 | 0.97 | 41.50 | 1.49 | 39.82 | 4.40 | 36.20 |
| 18 | Cornea | Cornea | 1076 | 1.3943 | 55.235 | 2.0495 | 52.21 | 4.7223 | 47.733 | 0.97 | 41.50 | 1.49 | 39.82 | 4.40 | 36.20 |
| 19 | Diaphragm | Muscle | 1041 | 0.94294 | 55.032 | 1.5135 | 53.163 | 4.0448 | 49.54 | 0.97 | 41.50 | 1.49 | 39.82 | 4.40 | 36.20 |
| 20 | Ear_cartilage | Cartilage | 1100 | 0.78239 | 42.653 | 1.4939 | 39.535 | 4.0855 | 33.63 | 0.97 | 41.50 | 1.49 | 39.82 | 4.40 | 36.20 |
| 21 | Ear_skin | SkinDry | 1100 | 0.86674 | 41.405 | 1.3075 | 38.431 | 3.0608 | 35.774 | 0.97 | 41.50 | 1.49 | 39.82 | 4.40 | 36.20 |
| 22 | Epididymis | Gland | 1050 | 1.0385 | 59.684 | 1.7033 | 57.705 | 4.6614 | 53.342 | 0.97 | 41.50 | 1.49 | 39.82 | 4.40 | 36.20 |
| 23 | Esophagus | Oesophagus | 1040 | 1.1867 | 65.062 | 1.9204 | 62.727 | 5.1565 | 57.89 | 0.97 | 41.50 | 1.49 | 39.82 | 4.40 | 36.20 |
| 24 | Esophagus_lumen | Air | 0 | 0 | 1 | 0 | 1 | 0 | 1 | 0.97 | 41.50 | 1.49 | 39.82 | 4.40 | 36.20 |
| 25 | Eye_lens | Lens | 1090 | 0.7934 | 46.573 | 1.302 | 45.014 | 3.5606 | 41.671 | 0.97 | 41.50 | 1.49 | 39.82 | 4.40 | 36.20 |
| 26 | Eye_Sclera | EyeSclera | 1032 | 1.1668 | 55.271 | 1.7892 | 53.125 | 4.4985 | 48.996 | 0.97 | 41.50 | 1.49 | 39.82 | 4.40 | 36.20 |
| 27 | Eye_vitreous_humor | VitreousHumor | 1009 | 1.6362 | 68.902 | 2.2218 | 68.418 | 5.411 | 65.81 | 0.97 | 41.50 | 1.49 | 39.82 | 4.40 | 36.20 |
| 28 | Fat | Fat | 916 | 0.051043 | 5.462 | 0.089859 | 5.3169 | 0.24222 | 5.0291 | 0.97 | 41.50 | 1.49 | 39.82 | 4.40 | 36.20 |
| 29 | Gallbladder | GallBladderBile | 1026 | 1.8383 | 70.188 | 2.5147 | 68.742 | 5.9127 | 64.915 | 0.97 | 41.50 | 1.49 | 39.82 | 4.40 | 36.20 |
| 30 | Heart_lumen | Blood | 1060 | 1.5379 | 61.36 | 2.2614 | 58.851 | 5.3951 | 53.95 | 0.97 | 41.50 | 1.49 | 39.82 | 4.40 | 36.20 |
| 31 | Heart_muscle | Heart | 1060 | 1.2298 | 59.893 | 1.9849 | 55.579 | 4.8626 | 50.274 | 0.97 | 41.50 | 1.49 | 39.82 | 4.40 | 36.20 |
| 32 | Hippocampus | BrainGreyMatter | 1039 | 0.94227 | 52.725 | 1.5738 | 49.51 | 4.0995 | 45.147 | 0.97 | 41.50 | 1.49 | 39.82 | 4.40 | 36.20 |
| 33 | Hypophysis | Gland | 1066 | 1.0385 | 59.684 | 1.7033 | 57.705 | 4.6614 | 53.342 | 0.97 | 41.50 | 1.49 | 39.82 | 4.40 | 36.20 |
| 34 | Hypothalamus | Gland | 1050 | 1.0385 | 59.684 | 1.7033 | 57.705 | 4.6614 | 53.342 | 0.97 | 41.50 | 1.49 | 39.82 | 4.40 | 36.20 |
| 35 | Intervertebral_disc | Cartilage | 1100 | 0.78239 | 42.653 | 1.4939 | 39.535 | 4.0855 | 33.63 | 0.97 | 41.50 | 1.49 | 39.82 | 4.40 | 36.20 |
| 36 | Kidney_cortex | Kidney | 1049 | 1.3921 | 58.675 | 2.1623 | 53.586 | 4.9423 | 48.059 | 0.97 | 41.50 | 1.49 | 39.82 | 4.40 | 36.20 |
| 37 | Kidney_medulla | Kidney | 1044 | 1.3921 | 58.675 | 2.1623 | 53.586 | 4.9423 | 48.059 | 0.97 | 41.50 | 1.49 | 39.82 | 4.40 | 36.20 |
| 38 | Large_intestine | Colon | 1044 | 1.0799 | 57.94 | 1.7787 | 54.531 | 4.5845 | 49.723 | 0.97 | 41.50 | 1.49 | 39.82 | 4.40 | 36.20 |
| 39 | Large_intestine_lumen | Muscle | 1041 | 0.94294 | 55.032 | 1.5135 | 53.163 | 4.0448 | 49.54 | 0.97 | 41.50 | 1.49 | 39.82 | 4.40 | 36.20 |
| 40 | Larynx | Cartilage | 1082 | 0.78239 | 42.653 | 1.4939 | 39.535 | 4.0855 | 33.63 | 0.97 | 41.50 | 1.49 | 39.82 | 4.40 | 36.20 |
| 41 | Liver | Liver | 1050 | 0.85497 | 46.833 | 1.4637 | 43.638 | 3.8278 | 39.26 | 0.97 | 41.50 | 1.49 | 39.82 | 4.40 | 36.20 |
| 42 | Lung | Lung:Deflated/Inflated(avg) | 655 | 0.65734 | 36.712 | 1.08284 | 34.81 | 2.83165 | 31.9125 | 0.97 | 41.50 | 1.49 | 39.82 | 4.40 | 36.20 |
| 43 | Mandible | BoneCortical | 1990 | 0.14331 | 12.454 | 0.32813 | 11.592 | 0.96228 | 10.04 | 0.97 | 41.50 | 1.49 | 39.82 | 4.40 | 36.20 |
| 44 | Marrow_red | BoneMarrow | 1027 | 0.040208 | 5.5043 | 0.080159 | 5.3362 | 0.23379 | 5.0379 | 0.97 | 41.50 | 1.49 | 39.82 | 4.40 | 36.20 |
| 45 | Medulla_oblongata | Brain:Gray/White(average) | 1039 | 0.76653 | 45.8055 | 1.3102 | 43.055 | 3.47915 | 39.2955 | 0.97 | 41.50 | 1.49 | 39.82 | 4.40 | 36.20 |
| 46 | Meniscus | Cartilage | 1098 | 0.78239 | 42.653 | 1.4939 | 39.535 | 4.0855 | 33.63 | 0.97 | 41.50 | 1.49 | 39.82 | 4.40 | 36.20 |
| 47 | Midbrain | Brain:Gray/White(average) | 1039 | 0.76653 | 45.8055 | 1.3102 | 43.055 | 3.47915 | 39.2955 | 0.97 | 41.50 | 1.49 | 39.82 | 4.40 | 36.20 |
| 48 | Mucosa | MucousMembrane | 1050 | 0.84465 | 46.08 | 1.3897 | 43.365 | 3.5744 | 39.611 | 0.97 | 41.50 | 1.49 | 39.82 | 4.40 | 36.20 |
| 49 | Muscle | Muscle | 1041 | 0.94294 | 55.032 | 1.5135 | 53.163 | 4.0448 | 49.54 | 0.97 | 41.50 | 1.49 | 39.82 | 4.40 | 36.20 |
| 50 | Nerve | Nerve | 1038 | 0.57369 | 32.531 | 0.95085 | 30.514 | 2.426 | 27.89 | 0.97 | 41.50 | 1.49 | 39.82 | 4.40 | 36.20 |
| 51 | Ovary | Ovary | 1048 | 1.2904 | 50.471 | 2.0167 | 45.556 | 4.4803 | 39.961 | 0.97 | 41.50 | 1.49 | 39.82 | 4.40 | 36.20 |
| 52 | Pancreas | Pancreas | 1045 | 1.0385 | 59.684 | 1.7033 | 57.705 | 4.6614 | 53.342 | 0.97 | 41.50 | 1.49 | 39.82 | 4.40 | 36.20 |
| 53 | Patella | BoneCortical | 1990 | 0.14331 | 12.454 | 0.32813 | 11.592 | 0.96228 | 10.04 | 0.97 | 41.50 | 1.49 | 39.82 | 4.40 | 36.20 |
| 54 | Penis | Blood | 1060 | 1.5379 | 61.36 | 2.2614 | 58.851 | 5.3951 | 53.95 | 0.97 | 41.50 | 1.49 | 39.82 | 4.40 | 36.20 |
| 55 | Pharynx | Air | 0 | 0 | 1 | 0 | 1 | 0 | 1 | 0.97 | 41.50 | 1.49 | 39.82 | 4.40 | 36.20 |
| 56 | Pinealbody | Gland | 1050 | 1.0385 | 59.684 | 1.7033 | 57.705 | 4.6614 | 53.342 | 0.97 | 41.50 | 1.49 | 39.82 | 4.40 | 36.20 |
| 57 | Pons | Brain:Gray/White(average) | 1039 | 0.76653 | 45.8055 | 1.3102 | 43.055 | 3.47915 | 39.2955 | 0.97 | 41.50 | 1.49 | 39.82 | 4.40 | 36.20 |
| 58 | Prostate | Prostate | 1045 | 1.2096 | 60.553 | 1.8984 | 58.107 | 4.8833 | 53.526 | 0.97 | 41.50 | 1.49 | 39.82 | 4.40 | 36.20 |
| 59 | SAT | Fat | 916 | 0.051043 | 5.462 | 0.089859 | 5.3169 | 0.24222 | 5.0291 | 0.97 | 41.50 | 1.49 | 39.82 | 4.40 | 36.20 |
| 60 | Skin | SkinDry | 1100 | 0.86674 | 41.405 | 1.3075 | 38.431 | 3.0608 | 35.774 | 0.97 | 41.50 | 1.49 | 39.82 | 4.40 | 36.20 |
| 61 | Skull | BoneCortical | 1990 | 0.14331 | 12.454 | 0.32813 | 11.592 | 0.96228 | 10.04 | 0.97 | 41.50 | 1.49 | 39.82 | 4.40 | 36.20 |
| 62 | Small_intestine | SmallIntestine | 1044 | 2.1652 | 59.488 | 2.906 | 55.114 | 5.7533 | 49.977 | 0.97 | 41.50 | 1.49 | 39.82 | 4.40 | 36.20 |
| 63 | Small_intestine_lumen | Muscle | 1041 | 0.94294 | 55.032 | 1.5135 | 53.163 | 4.0448 | 49.54 | 0.97 | 41.50 | 1.49 | 39.82 | 4.40 | 36.20 |
| 64 | Spinal_cord | SpinalChord | 1038 | 0.57369 | 32.531 | 0.95085 | 30.514 | 2.426 | 27.89 | 0.97 | 41.50 | 1.49 | 39.82 | 4.40 | 36.20 |
| 65 | Spleen | Spleen | 1054 | 1.2727 | 57.178 | 1.9815 | 53.159 | 4.7178 | 48.195 | 0.97 | 41.50 | 1.49 | 39.82 | 4.40 | 36.20 |
| 66 | Stomach | Stomach | 1050 | 1.1867 | 65.062 | 1.9204 | 62.727 | 5.1565 | 57.89 | 0.97 | 41.50 | 1.49 | 39.82 | 4.40 | 36.20 |
| 67 | Stomach_lumen | Muscle | 1041 | 0.94294 | 55.032 | 1.5135 | 53.163 | 4.0448 | 49.54 | 0.97 | 41.50 | 1.49 | 39.82 | 4.40 | 36.20 |
| 68 | Teeth | Tooth | 2160 | 0.14331 | 12.454 | 0.32813 | 11.592 | 0.96228 | 10.04 | 0.97 | 41.50 | 1.49 | 39.82 | 4.40 | 36.20 |
| 69 | Tendon_Ligament | Tendon | 1110 | 0.71839 | 45.825 | 1.4115 | 43.735 | 4.3009 | 38.299 | 0.97 | 41.50 | 1.49 | 39.82 | 4.40 | 36.20 |
| 70 | Testis | Testis | 1044 | 1.2096 | 60.553 | 1.8984 | 58.107 | 4.8833 | 53.526 | 0.97 | 41.50 | 1.49 | 39.82 | 4.40 | 36.20 |
| 71 | Thalamus | BrainGreyMatter | 1039 | 0.94227 | 52.725 | 1.5738 | 49.51 | 4.0995 | 45.147 | 0.97 | 41.50 | 1.49 | 39.82 | 4.40 | 36.20 |
| 72 | Thymus | Thymus | 1026 | 1.0385 | 59.684 | 1.7033 | 57.705 | 4.6614 | 53.342 | 0.97 | 41.50 | 1.49 | 39.82 | 4.40 | 36.20 |
| 73 | Thyroid_gland | Gland | 1050 | 1.0385 | 59.684 | 1.7033 | 57.705 | 4.6614 | 53.342 | 0.97 | 41.50 | 1.49 | 39.82 | 4.40 | 36.20 |
| 74 | Tongue | Tongue | 1041 | 0.93631 | 55.271 | 1.5587 | 53.125 | 4.268 | 48.996 | 0.97 | 41.50 | 1.49 | 39.82 | 4.40 | 36.20 |
| 75 | Trachea | Cartilage | 1100 | 0.78239 | 42.653 | 1.4939 | 39.535 | 4.0855 | 33.63 | 0.97 | 41.50 | 1.49 | 39.82 | 4.40 | 36.20 |
| 76 | Trachea_lumen | Air | 0 | 0 | 1 | 0 | 1 | 0 | 1 | 0.97 | 41.50 | 1.49 | 39.82 | 4.40 | 36.20 |
| 77 | Ureter_Urethra | BloodVessel | 1056 | 0.69612 | 44.775 | 1.2262 | 42.963 | 3.533 | 39.295 | 0.97 | 41.50 | 1.49 | 39.82 | 4.40 | 36.20 |
| 78 | Uterus | Uterus | 1052 | 1.2699 | 61.115 | 1.9741 | 58.403 | 4.979 | 53.681 | 0.97 | 41.50 | 1.49 | 39.82 | 4.40 | 36.20 |
| 79 | Vagina | Colon | 1044 | 1.0799 | 57.94 | 1.7787 | 54.531 | 4.5845 | 49.723 | 0.97 | 41.50 | 1.49 | 39.82 | 4.40 | 36.20 |
| 80 | Vein | Blood | 1060 | 1.5379 | 61.36 | 2.2614 | 58.851 | 5.3951 | 53.95 | 0.97 | 41.50 | 1.49 | 39.82 | 4.40 | 36.20 |
| 81 | Vertebrae | BoneCortical | 1990 | 0.14331 | 12.454 | 0.32813 | 11.592 | 0.96228 | 10.04 | 0.97 | 41.50 | 1.49 | 39.82 | 4.40 | 36.20 |

Figure 45: Dielectric properties for in-homogeneous [Gabriel et al., 1996] and homogeneous [IEC, 2009] for anatomical human models.

| Group | 3D EM solver | Technique |
|---|---|---|
| FDA | X-FDTD | FDTD |
| ARCS | SEMCAD X | FDTD |
| ITIS | SEMCAD X | FDTD |
| EMSS | FEKO | MoM |
| Hokkaido | in-house | FDTD |
| TKK | in-house | FDTD |
| Telecom | in-house | FDTD |

Table 20: 3D EM solver and computational technique used by each participating group in the inter-laboratory comparison study

| Group | Homogeneous | | | | In-homogeneous | | | |
|---|---|---|---|---|---|---|---|---|
| | VFM | VFB | | | VFM | VFB | | |
| | 0.9 GHz | 0.9 GHz | 2.1 GHz | 5 GHz | 0.9 GHz | 0.9 GHz | 2.1 GHz | 5 GHz |
| FDA | × | × | × | × | × | × | × | × |
| ARCS | × | × | × | × | × | × | × | × |
| ITIS | | | | | | | | |
| EMSS | × | × | × | × | | | | |
| Hokkaido | | | | × | | | | × |
| TKK | × | × | × | × | × | × | × | × |
| Telecom | × | × | × | | × | × | × | |

Table 21: Plane-wave configurations simulated by each group

| Group | Homogeneous | | | | In-homogeneous | | | |
|---|---|---|---|---|---|---|---|---|
| | VFM | VFB | | | VFM | VFB | | |
| | 0.9 GHz | 0.9 GHz | 2.1 GHz | 5 GHz | 0.9 GHz | 0.9 GHz | 2.1 GHz | 5 GHz |
| FDA | × | × | × | × | × | × | × | × |
| ARCS | × | × | × | × | × | × | × | × |
| ITIS | × | × | × | × | × | × | × | × |
| EMSS | × | × | × | × | | | | |
| Hokkaido | | | | × | | | | × |
| TKK | | | | | | | | |
| Telecom | × | × | × | | × | × | × | |

Table 22: Base station antenna configurations simulated by each group

axis of the anatomical model. The positive direction of the z-axis is oriented from the legs to the head. The positive direction of the y-axis has to point to the left hand side of the anatomical model (from right hand to the left hand). Finally, the x-axis positive direction has to be oriented from the back to the front of the model.

- All locations are according to the above defined coordinate system. All units are set according to the International System of units (SI).

- The incident field for plane-wave exposures has to be oriented towards the front of the anatomical model, in other words its pointing vector has to be aligned and follow the negative x-direction of the coordinate system. The E-field is parallel to the body axis. The amplitude of the incident field is $1 \, \mathrm{V/m}$ (peak).

- The base station antennas are placed in front of the anatomical model so that the minimum free-space distance between antenna and the bounding box of the human model is exactly 1 m. The vertical center of the antenna is aligned with the vertical center of the anatomical model. The vertical symmetry axis of the antenna is aligned with the vertical symmetry axis of the anatomical model (z-axis). All results for the representative base station antennas are normalized to an antenna net-input power of 1 W.

- Location of the 1 g and 10 g averaged SAR is in the center of 1 g or 10 g cube. The 1 g and 10 g SAR averaging shall be done according to IEEE C95.3.

- Tissue parameters for homogeneous and in-homogenous human models can be found in Figure 45.

## 3.4   Results including EMSS calculations
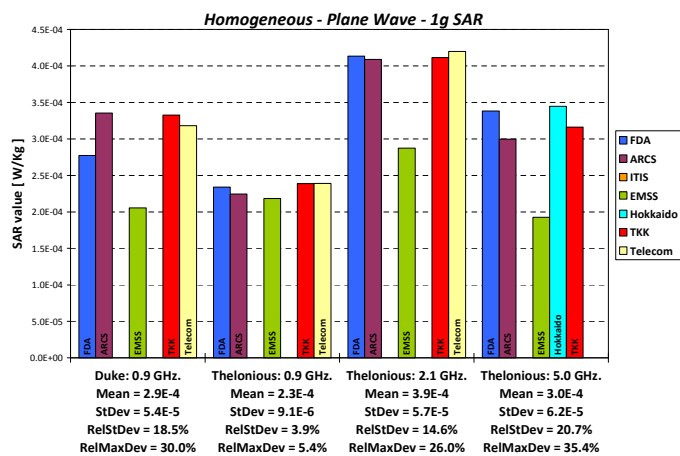


46.1: 1 g SAR
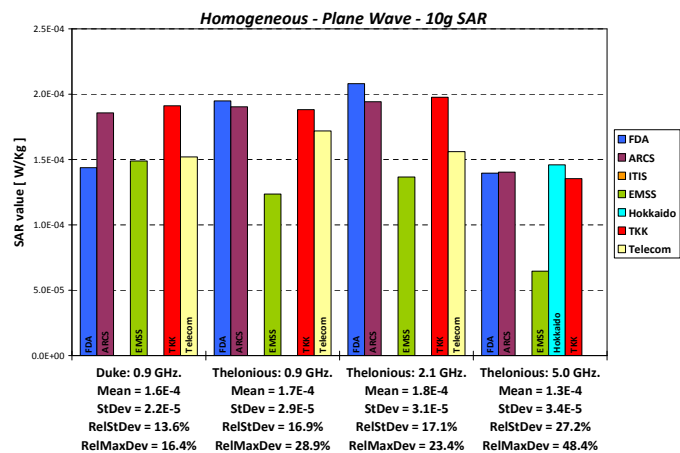


46.2: 10 g SAR
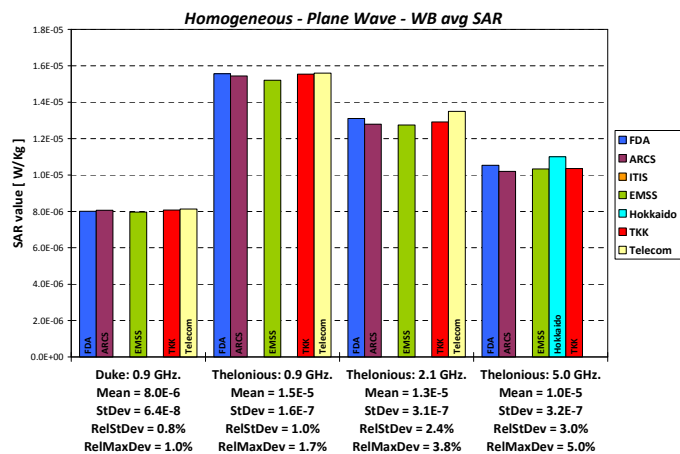


46.3: wba SAR

Figure 46: SAR in homogeneous models exposed to plane waves, including EMSS calculations
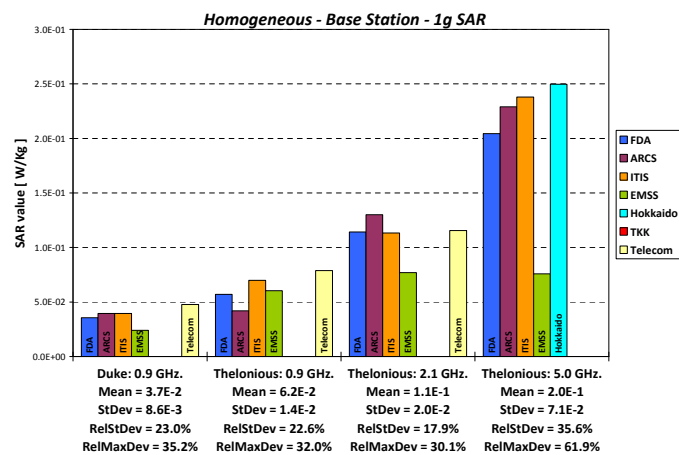
47.1: 1 g SAR
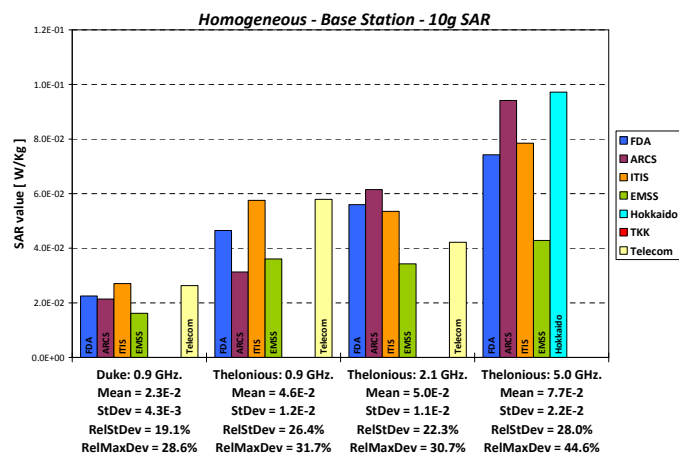


47.2: 10 g SAR
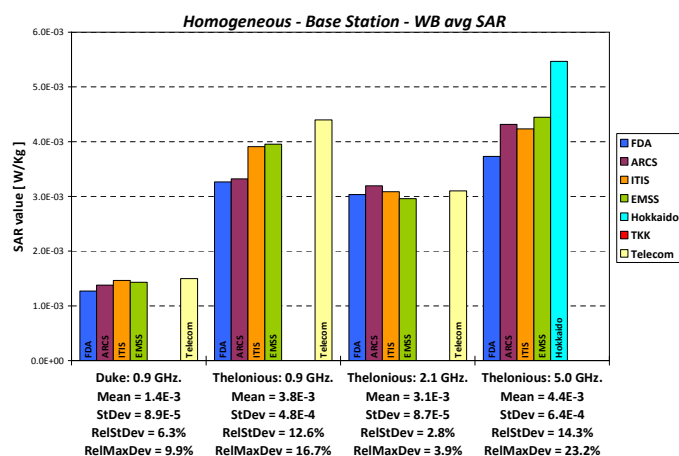


47.3: wba SAR

Figure 47: SAR in homogeneous models exposed to base station antennas, including EMSS calculations
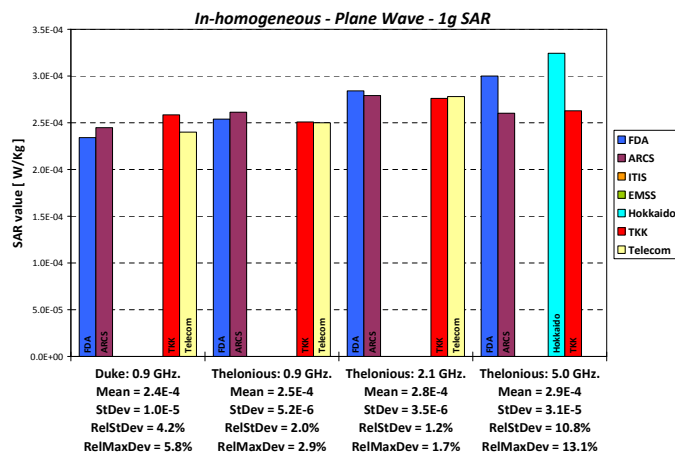
48.1: 1 g SAR
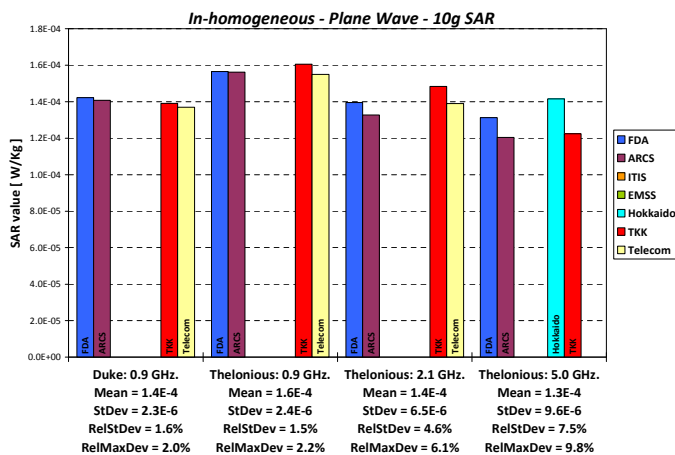


48.2: 10 g SAR
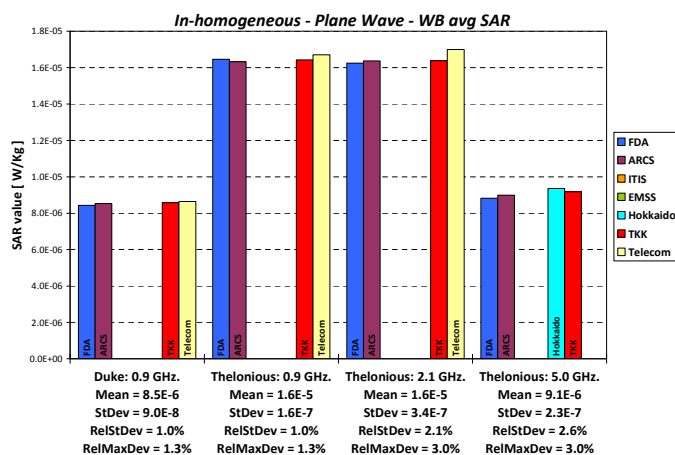


48.3: wba SAR

Figure 48: SAR in in-homogeneous models exposed to plane waves
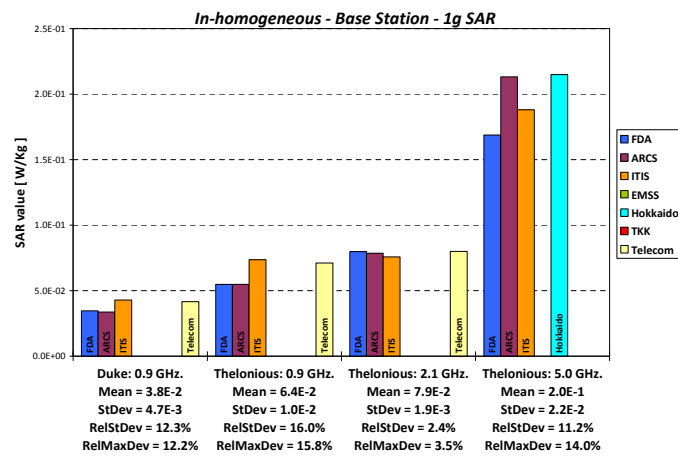
49.1: 1 g SAR
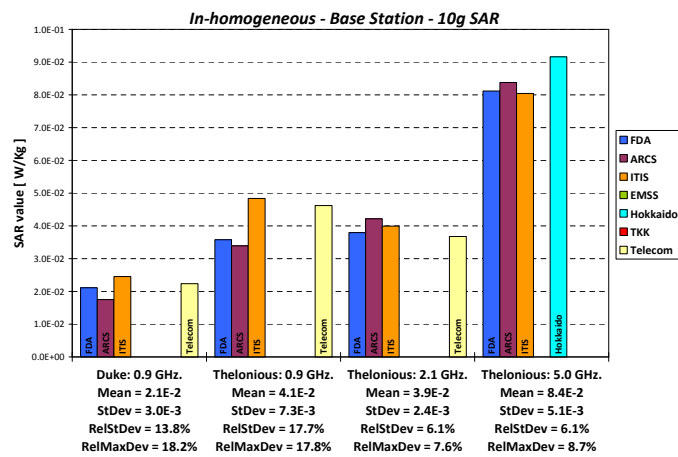


49.2: 10 g SAR
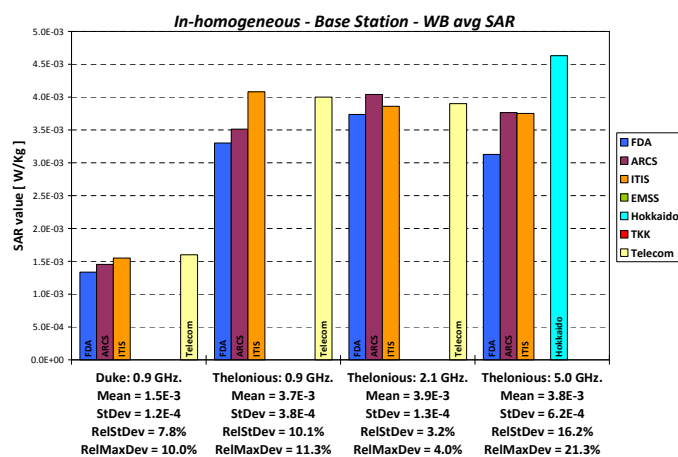


49.3: wba SAR

Figure 49: SAR in in-homogeneous models exposed to base station antennas

### 3.4.1 Mean, Standard Deviation, Relative Standard Deviation and Relative Maximum Deviation final results including EMSS calculations

**Mean, Standard Deviation, Relative Standard Deviation & Relative Maximum Deviation (with EMSS)**

**Homogeneous**

**Full Wave SAR Evaluations – Plane Waves**

| Anatomical Model from Virtual Family | Antenna | Resolution (mm) | Statistics | 1g SAR (W/kg) | 10g SAR (W/kg) | Whole Body Averaged SAR (W/kg) |
|---|---|---|---|---|---|---|
| male adult: Duke | Plane Wave Freq.= 0.9 GHz | 2 | Mean | 2.9E-04 | 1.6E-04 | 8.0E-06 |
| | | | StDev | 5.4E-05 | 2.2E-05 | 6.4E-08 |
| | | | RelStDev | 18.5% | 13.6% | 0.8% |
| | | | RelMaxDev | 30.0% | 16.4% | 1.0% |
| child boy 6y: Thelonious | Plane Wave Freq.= 0.9 GHz | 2 | Mean | 2.3E-04 | 1.7E-04 | 1.5E-05 |
| | | | StDev | 9.1E-06 | 2.9E-05 | 1.6E-07 |
| | | | RelStDev | 3.9% | 16.9% | 1.0% |
| | | | RelMaxDev | 5.4% | 28.9% | 1.7% |
| child boy 6y: Thelonious | Plane Wave Freq.= 2.1 GHz | 2 | Mean | 3.9E-04 | 1.8E-04 | 1.3E-05 |
| | | | StDev | 5.7E-05 | 3.1E-05 | 3.1E-07 |
| | | | RelStDev | 14.6% | 17.1% | 2.4% |
| | | | RelMaxDev | 26.0% | 23.4% | 3.8% |
| child boy 6y: Thelonious | Plane Wave Freq.= 5.0 GHz | 1 | Mean | 3.0E-04 | 1.3E-04 | 1.0E-05 |
| | | | StDev | 6.2E-05 | 3.4E-05 | 3.2E-07 |
| | | | RelStDev | 20.7% | 27.2% | 3.0% |
| | | | RelMaxDev | 35.4% | 48.4% | 5.0% |

**Full Wave SAR Evaluations – Representative Base Station Antenna**

| Anatomical Model from Virtual Family | Antenna | Resolution (mm) | Statistics | 1g SAR (W/kg) | 10g SAR (W/kg) | Whole Body Averaged SAR (W/kg) |
|---|---|---|---|---|---|---|
| male adult: Duke | 900MHz-H90V9 VPol Outdoor Freq.= 0.9 GHz | 2 | Mean | 3.7E-02 | 2.3E-02 | 1.4E-03 |
| | | | StDev | 8.6E-03 | 4.3E-03 | 8.9E-05 |
| | | | RelStDev | 23.0% | 19.1% | 6.3% |
| | | | RelMaxDev | 35.2% | 28.6% | 9.9% |
| child boy 6y: Thelonious | 900MHz-H90V9 VPol Outdoor Freq.= 0.9 GHz | 2 | Mean | 6.2E-02 | 4.6E-02 | 3.8E-02 |
| | | | StDev | 1.4E-02 | 1.2E-02 | 4.8E-04 |
| | | | RelStDev | 22.6% | 26.4% | 12.6% |
| | | | RelMaxDev | 32.0% | 31.7% | 16.7% |
| child boy 6y: Thelonious | 2100MHz-H90V80 VPol Indoor base station Freq.= 2.1 GHz | 2 | Mean | 1.1E-01 | 5.0E-02 | 3.1E-03 |
| | | | StDev | 2.0E-02 | 1.1E-02 | 8.7E-05 |
| | | | RelStDev | 17.9% | 22.3% | 2.8% |
| | | | RelMaxDev | 30.1% | 30.7% | 3.9% |
| child boy 6y: Thelonious | 5000MHz-H65V35 VPol Directional Panel Freq.= 5.0 GHz | 1 | Mean | 2.0E-01 | 7.7E-02 | 4.4E-03 |
| | | | StDev | 7.1E-02 | 2.2E-02 | 6.4E-04 |
| | | | RelStDev | 35.6% | 28.0% | 14.3% |
| | | | RelMaxDev | 61.9% | 44.6% | 23.2% |

**In-homogeneous**

**Full Wave SAR Evaluations – Plane Waves**

| Anatomical Model from Virtual Family | Antenna | Resolution (mm) | Statistics | 1g SAR (W/kg) | 10g SAR (W/kg) | Whole Body Averaged SAR (W/kg) |
|---|---|---|---|---|---|---|
| male adult: Duke | Plane Wave Freq.= 0.9 GHz | 2 | Mean | 2.4E-04 | 1.4E-04 | 8.5E-06 |
| | | | StDev | 1.0E-05 | 2.3E-06 | 9.0E-08 |
| | | | RelStDev | 4.2% | 1.6% | 1.0% |
| | | | RelMaxDev | 5.8% | 2.0% | 1.3% |
| child boy 6y: Thelonious | Plane Wave Freq.= 0.9 GHz | 2 | Mean | 2.5E-04 | 1.6E-04 | 1.6E-05 |
| | | | StDev | 5.2E-06 | 2.4E-06 | 1.6E-07 |
| | | | RelStDev | 2.0% | 1.5% | 1.0% |
| | | | RelMaxDev | 2.9% | 2.2% | 1.3% |
| child boy 6y: Thelonious | Plane Wave Freq.= 2.1 GHz | 2 | Mean | 2.8E-04 | 1.4E-04 | 1.6E-05 |
| | | | StDev | 3.5E-06 | 6.5E-06 | 3.4E-07 |
| | | | RelStDev | 1.2% | 4.6% | 2.1% |
| | | | RelMaxDev | 1.7% | 6.1% | 3.0% |
| child boy 6y: Thelonious | Plane Wave Freq.= 5.0 GHz | 1 | Mean | 2.9E-04 | 1.3E-04 | 9.1E-06 |
| | | | StDev | 3.1E-05 | 9.6E-06 | 2.3E-07 |
| | | | RelStDev | 10.8% | 7.5% | 2.6% |
| | | | RelMaxDev | 13.1% | 9.8% | 3.0% |

**Full Wave SAR Evaluations – Representative Base Station Antenna**

| Anatomical Model from Virtual Family | Antenna | Resolution (mm) | Statistics | 1g SAR (W/kg) | 10g SAR (W/kg) | Whole Body Averaged SAR (W/kg) |
|---|---|---|---|---|---|---|
| male adult: Duke | 900MHz-H90V9 VPol Outdoor Freq.= 0.9 GHz | 2 | Mean | 3.8E-02 | 2.1E-02 | 1.5E-03 |
| | | | StDev | 4.7E-03 | 3.0E-03 | 1.2E-04 |
| | | | RelStDev | 12.3% | 13.8% | 7.8% |
| | | | RelMaxDev | 12.2% | 18.2% | 10.0% |
| child boy 6y: Thelonious | 900MHz-H90V9 VPol Outdoor Freq.= 0.9 GHz | 2 | Mean | 6.4E-02 | 4.1E-02 | 3.7E-02 |
| | | | StDev | 1.0E-02 | 7.3E-03 | 3.8E-04 |
| | | | RelStDev | 16.0% | 17.7% | 10.1% |
| | | | RelMaxDev | 15.8% | 17.8% | 11.3% |
| child boy 6y: Thelonious | 2100MHz-H90V80 VPol Indoor base station Freq.= 2.1 GHz | 2 | Mean | 7.9E-02 | 3.9E-02 | 3.9E-03 |
| | | | StDev | 1.9E-03 | 2.4E-03 | 1.3E-04 |
| | | | RelStDev | 2.4% | 6.1% | 3.2% |
| | | | RelMaxDev | 3.5% | 7.6% | 4.0% |
| child boy 6y: Thelonious | 5000MHz-H65V35 VPol Directional Panel Freq.= 5.0 GHz | 1 | Mean | 2.0E-01 | 8.4E-02 | 3.8E-03 |
| | | | StDev | 2.2E-02 | 5.1E-03 | 6.2E-04 |
| | | | RelStDev | 11.2% | 6.1% | 16.2% |
| | | | RelMaxDev | 14.0% | 8.7% | 21.3% |

Figure 50: Final statistical results including EMSS

### 3.4.2   Conclusions

- Max. RelStdDev on plane wave 1 g and 10 g avg. SAR is ∼28%; wba SAR is about 1-3%

- Base station 1 g and 10 g SAR has a RelStdDev of up to ∼36%; max. wba SAR is about 16%

- Homogeneous and in-homogeneous has similar RelStdDev for 1 g, 10 g SAR and wba SAR

We obtained considerable different final results for 1 g and 10 g SAR when including data from EMSS. The explanation given by them is as follows:

### 3.4.3   Discussion

EMSS has reviewed the way FEKO calculates local peak SAR and again looked at the C95.3 and IEEE P1528.1 standards for calculating SAR in a 1 g and 10 g cube. They have focused on IEEE P1528.1 because the instruction with the MMF project was that SAR should be calculated in accordance with IEEE P1528.1 (see communication regarding validation test sent out to partners on this project).

EMSS cannot implement the standard *exactly* as it is written because it has been written for SAR calculations with an FDTD code. FEKO is based on the MoM and FEM and obviously there are no voxels to extend and expand, etc. EMSS has developed a local peak SAR algorithm in FEKO which are similar and have the same goals as the algorithm proposed in P1528.1, and also that takes the intentions of P1528.1, ICNIRP and the IEEE (when they set the basic restrictions) into account.

The aim of the FEKO algorithm is to find the maximum local peak SAR as averaged over any 1 g (or 10 g) human tissue material in the shape of a cube. Allowing some air in the cube (but not a high percentage of air) and requiring that the majority of the cube is situated in the human body – and not outside the human body.

The most important differences between the FEKO algorithm and the P1528.1 algorithm are:

1. FEKO's algorithm requires that the centre of each *face* of the cube lies inside the human body. (There are exceptions in P1528.1 where the 'entire faces in air' restrictions are relaxed).

2. FEKO's algorithm always requires that the centre of *the cube itself* lies inside the human body. (There are exceptions in P1528.1 where the SAR associated with a FDTD voxel is calculated by expanding the volume from a voxel on a face, which could result in the centre of the cube – with a valid SAR value – positioned outside the human body).

3. FEKO's algorithm rotates the cube to find the maximum SAR, which ICNIRP and IEEE probably had in mind but P1528.1 does not require (because of the FDTD Cartesian grid).

Difference (1) above is the result of the fact that for the MoM and FEM different algorithms must be found to check if part of a face of the cube lies inside the human body. (There is no VOXEL attached to a face!) Difference (2) above is because with MoM and FEM models, there are no voxels that can have strange extensions outside the body (as catered for in P1528.1 for the extreme cases in an FDTD model).

Even with these differences, the local peak SAR results obtained with FEKO should compare well with those calculated with the FDTD strictly in accordance with P1528.1. This should be true for most scenarios and we've validated the results from FEKO against SEMCAD and other FDTD codes on many occasions before with excellent agreement.

EMSS has recalculated the SAR values allowing up to 20% of AIR as specified in P1528.1 (previously 0% air was allowed for the runs of this specific project, not in FEKO in general).

The results from EMSS presented in Section 3.4 are the ones where the algorithm was allowing up to 20% of air. The agreement between FEKO results and FDTD codes results is much better when allowing 20% of air. However, FEKO still gives, in general, a lower local peak SAR than most FDTD codes.

The reasons for this are:

- The FDTD codes allow much more than 20% air in the local peak SAR cube. So although P1528.1 clearly states that: 'No valid volume should contain more than twenty percent air' – unless you have the occurrence where a VOXEL has NOT been used in any averaging volume. So we assume this is what happens with the fingers and the FDTD codes.

- We assume the FDTD codes then apply this special occurrence rule of P1528.1 around the fingers, but the rule says the 'unused' voxels should be expanded from the surface in all directions and the SMALLEST cube should then be used. We doubt if this is done.

    - To support this argument various 10 g SAR values have been calculated with FEKO at various positions in the hand. This is shown in Figure 51. FEKO does rotate the cube (see difference (3) mentioned above) but ALL the positions results in a SAR volume with MUCH more than 20% air. It is unlikely (just looking at the size and hand shape) that with the cubes NOT rotated (along FDTD grid) the volume would contain 80% or more tissue.
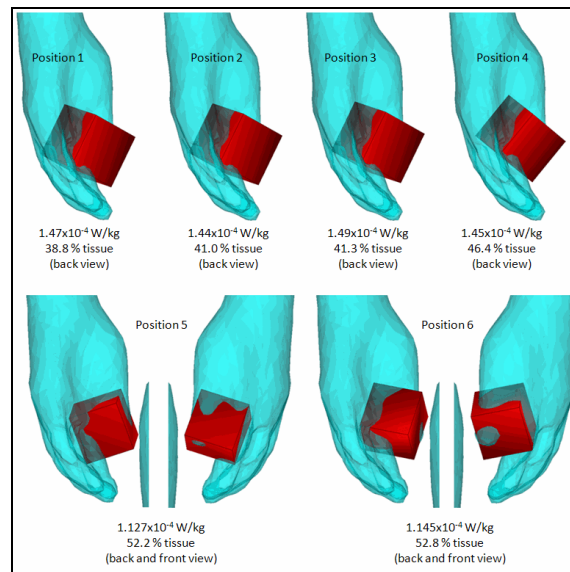


Figure 51: Variation of the 10 g SAR with the amount of air allowed inside

    - Finally, Figure 52 points out a specific scenario. With the cube at exactly the position where ARCS found the peak SAR we've positioned a FEKO 10 g SAR cube. We've forced the FEKO SAR cube to be aligned with the Cartesian grid. The percentage air in this cube is 71%.

In conclusion:

- The local peak SAR algorithm used in FEKO is not exactly the algorithm proposed in P1528.1 because the P1528.1 algorithm has specifically been written for FDTD solutions. FEKO uses the MoM and FEM, which does not have voxels associated with the model or field solution.
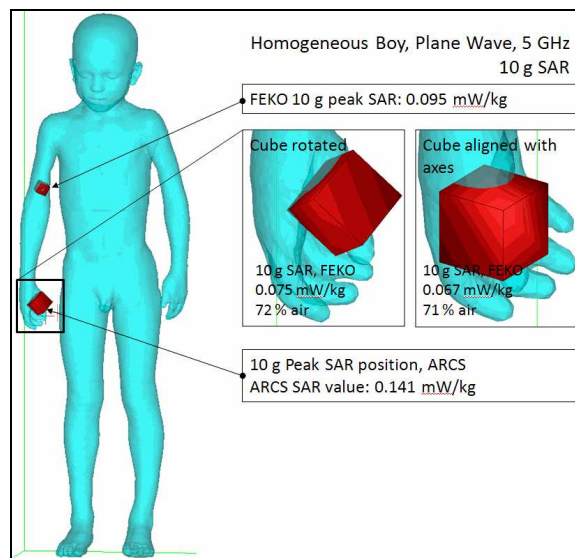
Figure 52: Variation of the 10 g SAR with its rotation

- Nonetheless, the algorithm implemented in FEKO follows the general guidance on implementation proposed in P1528.1, also taking into account the intentions of ICNIRP and the IEEE's when they set the basic restrictions.

- Due to the specific algorithm, FEKO will calculate the maximum local peak SAR in any 1 g or 10 g cube, for any cube that is situated predominantly inside the human body. FEKO will NOT allow a cube that has more than 10% air (which has been increased to 20% of air in the results presented here).

- The FEKO SAR algorithm has been verified extensively against the SAR algorithm of SEMCAD, for canonical shapes, but also for problems involving the visible human phantom. The agreement found in these cases was typically very good (less than 20% difference in extreme cases).

- The excellent agreement between FEKO and the FDTD codes used in the MMF project in terms of whole body SAR and antenna pattern results indicates that the local peak SAR differences observed are most probably associated with the specific local peak SAR algorithms employed.

- After a detailed investigation the reasons for the differences are most probably related to the amount of air allowed in the averaging cube. It seems that the SAR algorithms of the different FDTD codes allow much more air in the peak SAR cubes than the FEKO algorithm – and even much more air than allowed by P1528.1 (20%maximum). It should be noted that the project instructions was to calculate SAR in accordance with P1528.1. We thus assume the special algorithm for occurrence of 'unused' voxels was used around the fingers by the FDTD codes. If this is the case, the FDTD codes will find considerably higher local peak SAR values in extremities (e.g., in the fingers) and FEKO would disregard local peak SAR values here because of the high percentage of air in the cube.

Other differences between results reported by FEKO and the FDTD codes are probably due to differences in the MoM *model geometry and the FDTD model geometry* and small differences due to the rotation of the cube allowed by FEKO. These differences will be relatively small and

typically within the same range of differences found between the results of the different FDTD codes.

The following section presents the results and the statistics without the results from MoM, i.e. excluding the results from EMSS. Figures 53 and 54 present the same results than Figures 46 to 47, respectively, however without the results from EMSS. EMSS did not perform any simulation with the in-homogeneous human model, so Figures 48 to 49 remain unchanged.

## 3.5 Results excluding EMSS calculations
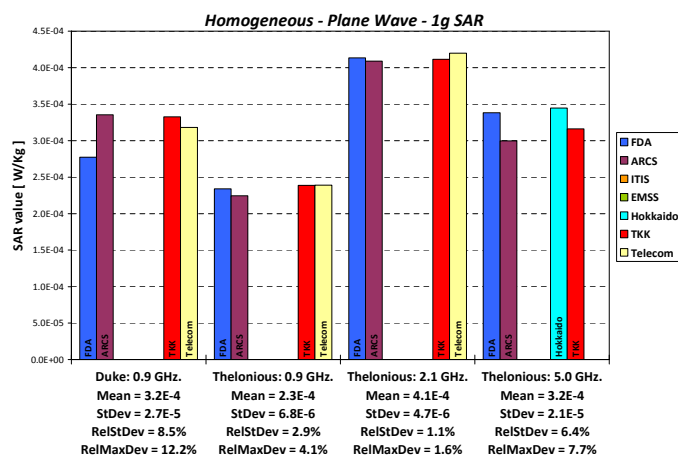


53.1: 1 g SAR
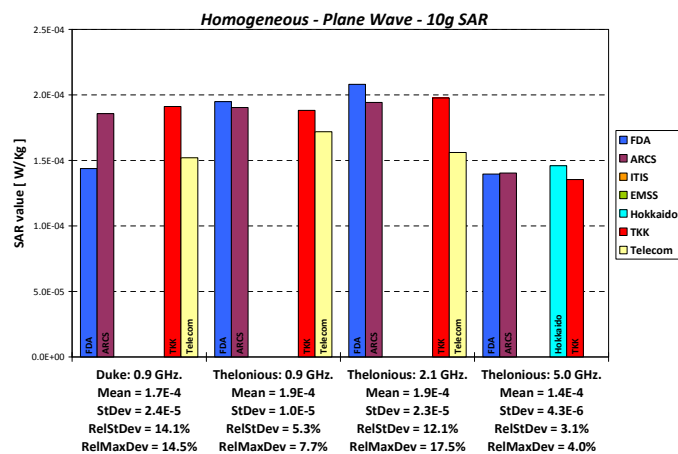


53.2: 10 g SAR
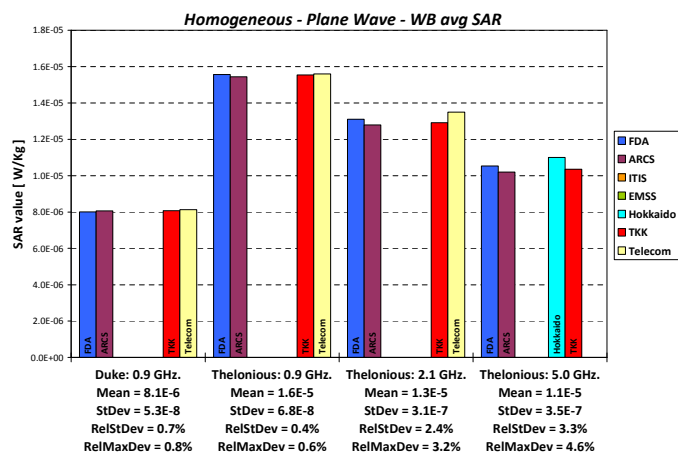


53.3: wba SAR

Figure 53: SAR in homogeneous models exposed to plane waves, excluding EMSS calculations
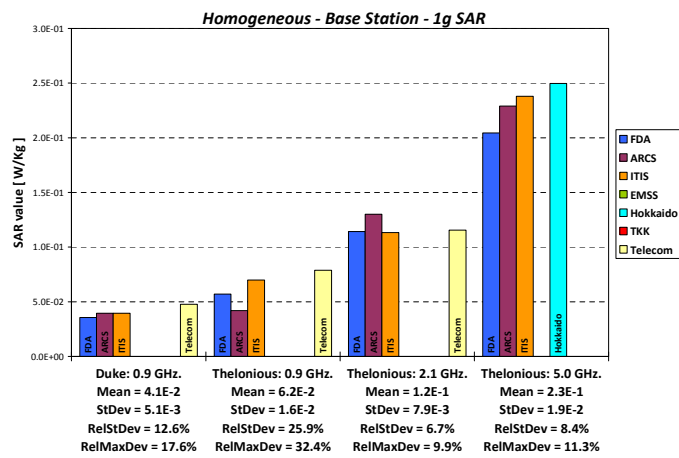
54.1: 1 g SAR
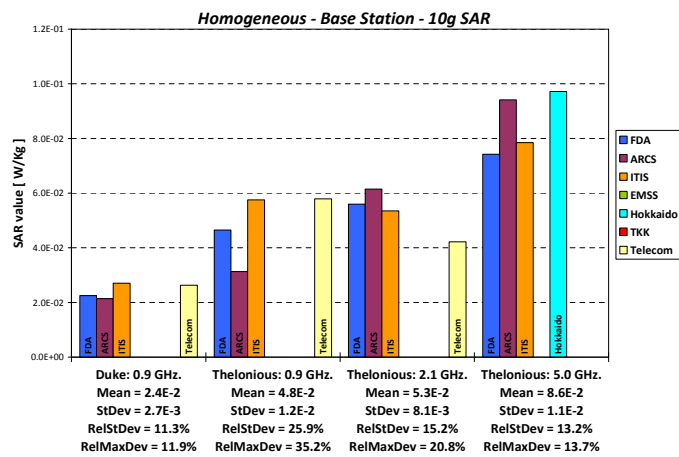


54.2: 10 g SAR
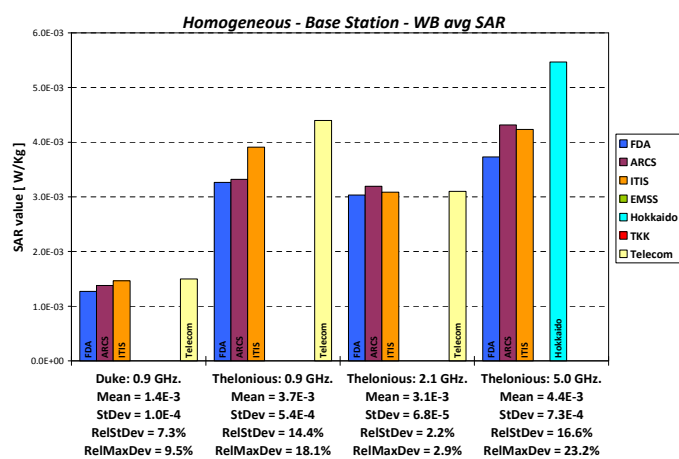


54.3: wba SAR

Figure 54: SAR in homogeneous models exposed to base station antennas, excluding EMSS calculations

### 3.5.1 Mean, Standard Deviation, Relative Standard Deviation and Relative Maximum Deviation final results excluding EMSS calculations

Mean, Standard Deviation, Relative Standard Deviation & Relative Maximum Deviation (without EMSS)

**Homogeneous**

**Full Wave SAR Evaluations – Plane Waves**

| Anatomical Model from Virtual Family | Antenna | Resolution (mm) | Statistics | 1g SAR (W/kg) | 10g SAR (W/kg) | Whole Body Averaged SAR (W/kg) |
|---|---|---|---|---|---|---|
| male adult: Duke | Plane Wave Freq.= 0.9 GHz | 2 | Mean | 3.2E-04 | 1.7E-04 | 8.1E-06 |
| | | | StDev | 2.7E-05 | 2.4E-05 | 5.3E-08 |
| | | | RelStDev | 8.5% | 14.1% | 0.7% |
| | | | RelMaxDev | 12.2% | 14.5% | 0.8% |
| child boy 6y: Thelonious | Plane Wave Freq.= 0.9 GHz | 2 | Mean | 2.3E-04 | 1.9E-04 | 1.6E-05 |
| | | | StDev | 6.8E-06 | 1.0E-05 | 6.8E-08 |
| | | | RelStDev | 2.9% | 5.3% | 0.4% |
| | | | RelMaxDev | 4.1% | 7.7% | 0.6% |
| child boy 6y: Thelonious | Plane Wave Freq.= 2.1 GHz | 2 | Mean | 4.1E-04 | 1.9E-04 | 1.3E-05 |
| | | | StDev | 4.7E-06 | 2.3E-05 | 3.1E-07 |
| | | | RelStDev | 1.1% | 12.1% | 2.4% |
| | | | RelMaxDev | 1.6% | 17.5% | 3.2% |
| child boy 6y: Thelonious | Plane Wave Freq.= 5.0 GHz | 1 | Mean | 3.2E-04 | 1.4E-04 | 1.1E-05 |
| | | | StDev | 2.1E-05 | 4.3E-06 | 3.5E-07 |
| | | | RelStDev | 6.4% | 3.1% | 3.3% |
| | | | RelMaxDev | 7.7% | 4.0% | 4.6% |

**Full Wave SAR Evaluations – Representative Base Station Antenna**

| Anatomical Model from Virtual Family | Antenna | Resolution (mm) | Statistics | 1g SAR (W/kg) | 10g SAR (W/kg) | Whole Body Averaged SAR (W/kg) |
|---|---|---|---|---|---|---|
| male adult: Duke | 900MHz-H90V9 VPol Outdoor Freq.= 0.9 GHz | 2 | Mean | 4.1E-02 | 2.4E-02 | 1.4E-03 |
| | | | StDev | 5.1E-03 | 2.7E-03 | 1.0E-04 |
| | | | RelStDev | 12.6% | 11.3% | 7.3% |
| | | | RelMaxDev | 17.6% | 11.9% | 9.5% |
| child boy 6y: Thelonious | 900MHz-H90V9 VPol Outdoor Freq.= 0.9 GHz | 2 | Mean | 6.2E-02 | 4.8E-02 | 3.7E-03 |
| | | | StDev | 1.6E-02 | 1.2E-02 | 5.4E-04 |
| | | | RelStDev | 25.9% | 25.9% | 14.4% |
| | | | RelMaxDev | 32.4% | 35.2% | 18.1% |
| child boy 6y: Thelonious | 2100MHz-H90V80 VPol Indoor base station Freq.= 2.1 GHz | 2 | Mean | 1.2E-01 | 5.3E-02 | 3.1E-03 |
| | | | StDev | 7.9E-03 | 8.1E-03 | 6.8E-05 |
| | | | RelStDev | 6.7% | 15.2% | 2.2% |
| | | | RelMaxDev | 9.9% | 20.8% | 2.9% |
| child boy 6y: Thelonious | 5000MHz-H65V35 VPol Directional Panel Freq.= 5.0 GHz | 1 | Mean | 2.3E-01 | 8.6E-02 | 4.4E-03 |
| | | | StDev | 1.9E-02 | 1.1E-02 | 7.3E-04 |
| | | | RelStDev | 8.4% | 13.2% | 16.6% |
| | | | RelMaxDev | 11.3% | 13.7% | 23.2% |

**In-homogeneous**

**Full Wave SAR Evaluations – Plane Waves**

| Anatomical Model from Virtual Family | Antenna | Resolution (mm) | Statistics | 1g SAR (W/kg) | 10g SAR (W/kg) | Whole Body Averaged SAR (W/kg) |
|---|---|---|---|---|---|---|
| male adult: Duke | Plane Wave Freq.= 0.9 GHz | 2 | Mean | 2.4E-04 | 1.4E-04 | 8.5E-06 |
| | | | StDev | 1.0E-05 | 2.3E-06 | 9.0E-08 |
| | | | RelStDev | 4.2% | 1.6% | 1.0% |
| | | | RelMaxDev | 5.8% | 2.0% | 1.3% |
| child boy 6y: Thelonious | Plane Wave Freq.= 0.9 GHz | 2 | Mean | 2.5E-04 | 1.6E-04 | 1.6E-05 |
| | | | StDev | 5.2E-06 | 2.4E-06 | 1.6E-07 |
| | | | RelStDev | 2.0% | 1.5% | 1.0% |
| | | | RelMaxDev | 2.9% | 2.2% | 1.3% |
| child boy 6y: Thelonious | Plane Wave Freq.= 2.1 GHz | 2 | Mean | 2.8E-04 | 1.4E-04 | 1.6E-05 |
| | | | StDev | 3.5E-06 | 6.5E-06 | 3.4E-07 |
| | | | RelStDev | 1.2% | 4.6% | 2.1% |
| | | | RelMaxDev | 1.7% | 6.1% | 3.0% |
| child boy 6y: Thelonious | Plane Wave Freq.= 5.0 GHz | 1 | Mean | 2.9E-04 | 1.3E-04 | 9.1E-06 |
| | | | StDev | 3.1E-05 | 9.6E-06 | 2.3E-07 |
| | | | RelStDev | 10.8% | 7.5% | 2.6% |
| | | | RelMaxDev | 13.1% | 9.8% | 3.0% |

**Full Wave SAR Evaluations – Representative Base Station Antenna**

| Anatomical Model from Virtual Family | Antenna | Resolution (mm) | Statistics | 1g SAR (W/kg) | 10g SAR (W/kg) | Whole Body Averaged SAR (W/kg) |
|---|---|---|---|---|---|---|
| male adult: Duke | 900MHz-H90V9 VPol Outdoor Freq.= 0.9 GHz | 2 | Mean | 3.8E-02 | 2.1E-02 | 1.5E-03 |
| | | | StDev | 4.7E-03 | 3.0E-03 | 1.2E-04 |
| | | | RelStDev | 12.3% | 13.8% | 7.8% |
| | | | RelMaxDev | 12.2% | 18.2% | 10.0% |
| child boy 6y: Thelonious | 900MHz-H90V9 VPol Outdoor Freq.= 0.9 GHz | 2 | Mean | 6.4E-02 | 4.1E-02 | 3.7E-03 |
| | | | StDev | 1.0E-02 | 7.3E-03 | 3.8E-04 |
| | | | RelStDev | 16.0% | 17.7% | 10.1% |
| | | | RelMaxDev | 15.8% | 17.8% | 11.3% |
| child boy 6y: Thelonious | 2100MHz-H90V80 VPol Indoor base station Freq.= 2.1 GHz | 2 | Mean | 7.9E-02 | 3.9E-02 | 3.9E-03 |
| | | | StDev | 1.9E-03 | 2.4E-03 | 1.3E-04 |
| | | | RelStDev | 2.4% | 6.1% | 3.2% |
| | | | RelMaxDev | 3.5% | 7.6% | 4.0% |
| child boy 6y: Thelonious | 5000MHz-H65V35 VPol Directional Panel Freq.= 5.0 GHz | 1 | Mean | 2.0E-01 | 8.4E-02 | 3.8E-03 |
| | | | StDev | 2.2E-02 | 5.1E-03 | 6.2E-04 |
| | | | RelStDev | 11.2% | 6.1% | 16.2% |
| | | | RelMaxDev | 14.0% | 8.7% | 21.3% |

Figure 55: Final statistical results excluding EMSS

### 3.5.2    Conclusions

- Max. RelStdDev on plane wave 1 g and 10 g SAR is ∼14%; wba SAR is about 1-3%

- Base station antennas 1 g and 10 g SAR has a RelStdDev of up to 26%; max. wba SAR is ∼16%

- Homogeneous and inhomogeneous has similar RelStdDev for 1 g, 10 g SAR and wba SAR

## 3.6    Free space simulations

The three base station antennas used for the exposure of humans have also been simulated in free space. This section presents the comparison of the free-space results obtained by the various participating groups:

- directivity

- maximum of E-rms and H-rms in planes (1900 mm high and 600 mm wide), 1, 5, 30 and 50 cm from the antennas[5], normalized to an antenna input power of 1 W
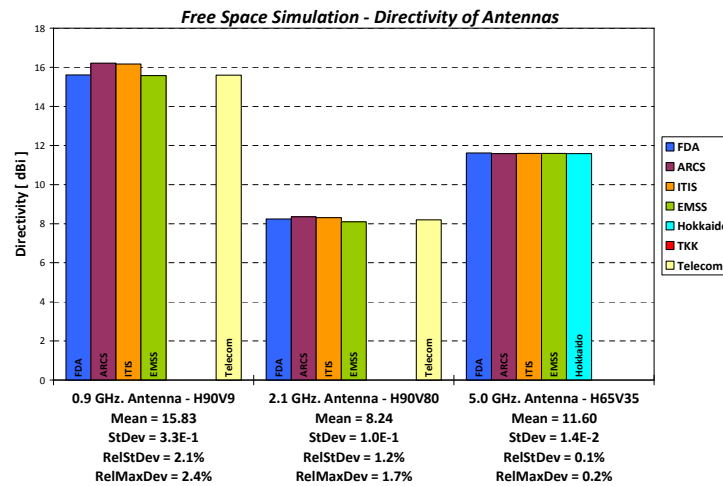


Figure 56: Directivity of the antennas

---

[5]The E- and H-fields were plotted in the planes and the agreement between the various participating groups was very good. To make this report more concise, we only report here the maximum value of E- and H-fields in each plane.
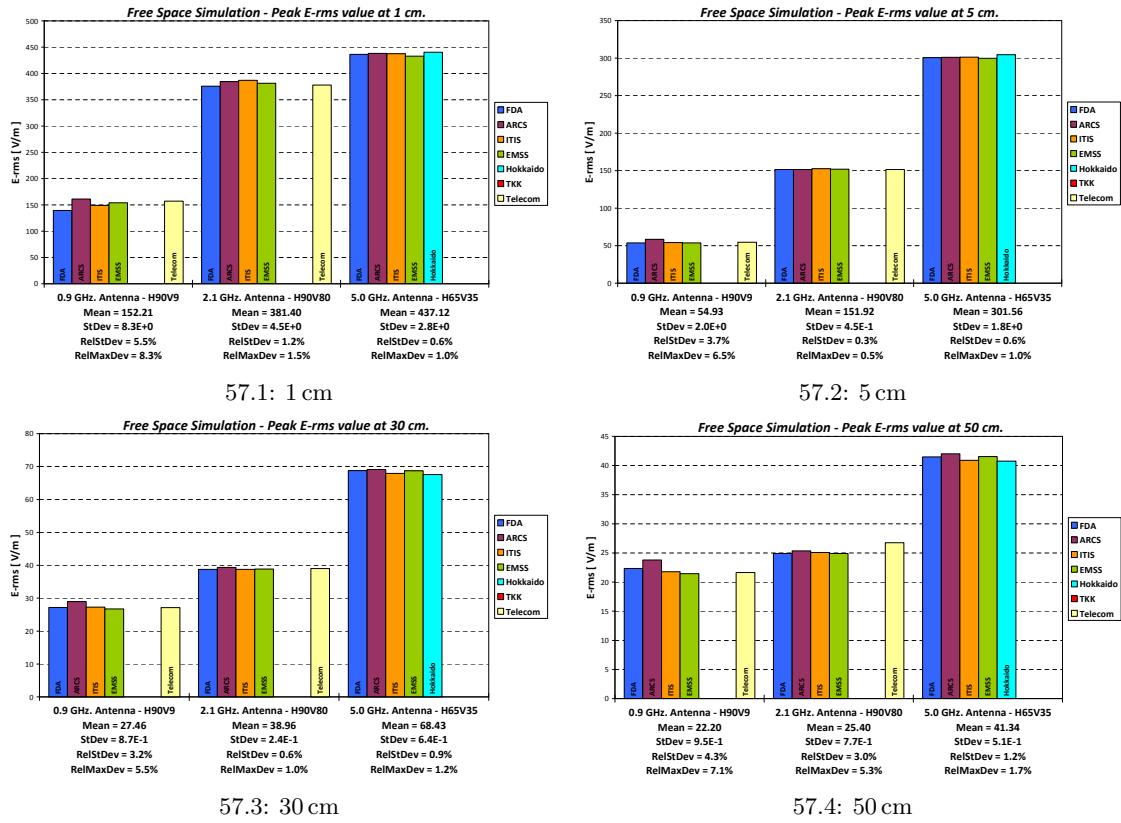
Figure 57: Maximum of E-rms in 4 planes at various distances from the antennas in free-space
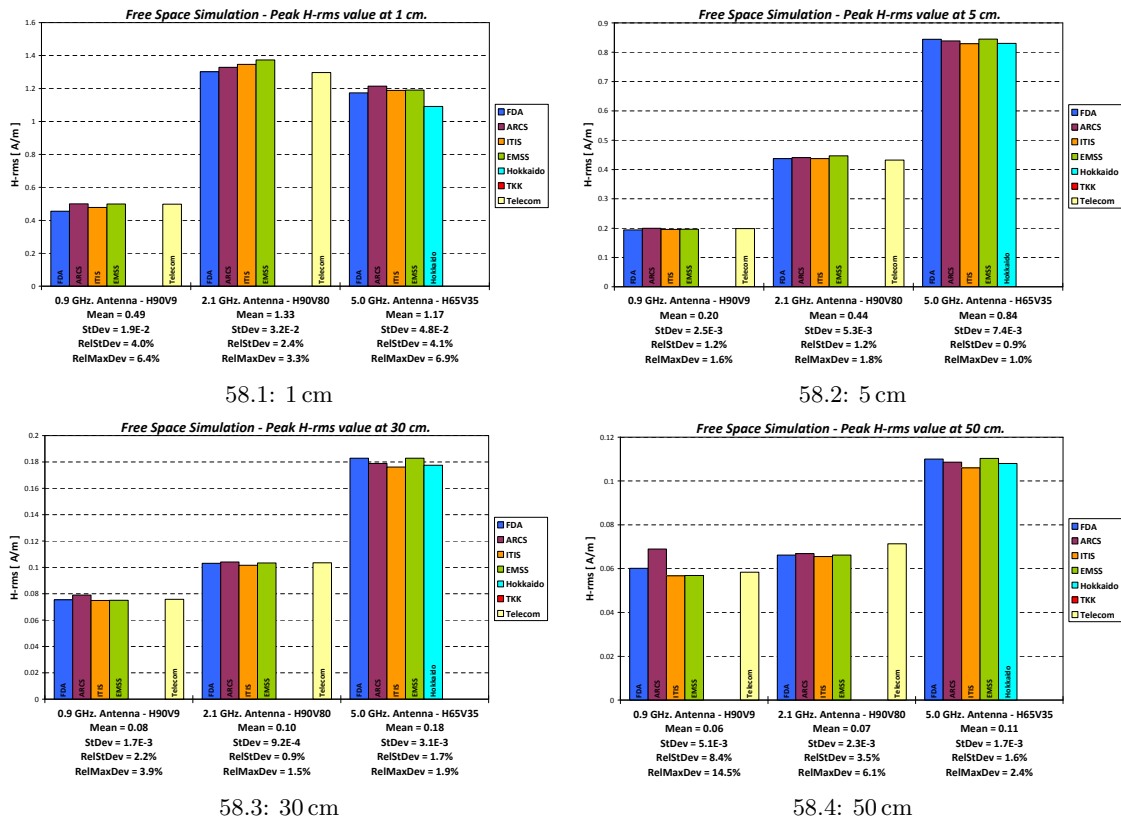


Figure 58: Maximum of H-rms in 4 planes at various distances from the antennas in free-space

### 3.6.1    Mean, Standard Deviation, Relative Standard Deviation and Relative Maximum Deviation final results

Mean, Standard Deviation, Relative Standard Deviation & Relative Maximum Deviation

| | Antenna | Statistics | | Peak value of Erms in a plane with a height of | | | | Peak value of Hrms in a plane with a height of | | | |
|---|---|---|---|---|---|---|---|---|---|---|---|
| | | | directivity | 1cm | 5cm | 30cm | 50cm | 1cm | 5cm | 30cm | 50cm |
| | | | dBi | V/m | V/m | V/m | V/m | A/m | A/m | A/m | A/m |
| Free Space Simultions | 900MHz-H90V9 VPol Outdoor Freq. = 0.9 GHz | Mean | 15.83 | 152.21 | 54.93 | 27.46 | 22.20 | 0.49 | 0.20 | 0.08 | 0.06 |
| | | StDev | 3.3E-01 | 8.3E+00 | 2.0E+00 | 8.7E-01 | 9.5E-01 | 1.9E-02 | 2.5E-03 | 1.7E-03 | 5.1E-03 |
| | | RelStDev | 2.1% | 5.5% | 3.7% | 3.2% | 4.3% | 4.0% | 1.2% | 2.2% | 8.4% |
| | | RelMaxDev | 2.4% | 8.3% | 6.5% | 5.5% | 7.1% | 6.4% | 1.6% | 3.9% | 14.5% |
| | 2100MHz-H90V80 VPol Indoor base station Freq. = 2.1 GHz | Mean | 8.24 | 381.40 | 151.92 | 38.96 | 25.40 | 1.33 | 0.44 | 0.10 | 0.07 |
| | | StDev | 1.0E-01 | 4.5E+00 | 4.5E-01 | 2.4E-01 | 7.7E-01 | 3.2E-02 | 5.3E-03 | 9.2E-04 | 2.3E-03 |
| | | RelStDev | 1.2% | 1.2% | 0.3% | 0.6% | 3.0% | 2.4% | 1.2% | 0.9% | 3.5% |
| | | RelMaxDev | 1.7% | 1.5% | 0.5% | 1.0% | 5.3% | 3.3% | 1.8% | 1.5% | 6.1% |
| | 5000MHz-H65V35 VPol Directional Panel Freq. = 5.0 GHz | Mean | 11.60 | 437.12 | 301.56 | 68.43 | 41.34 | 1.17 | 0.84 | 0.18 | 0.11 |
| | | StDev | 1.4E-02 | 2.8E+00 | 1.8E+00 | 6.4E-01 | 5.1E-01 | 4.8E-02 | 7.4E-03 | 3.1E-03 | 1.7E-03 |
| | | RelStDev | 0.1% | 0.6% | 0.6% | 0.9% | 1.2% | 4.1% | 0.9% | 1.7% | 1.6% |
| | | RelMaxDev | 0.2% | 1.0% | 1.0% | 1.2% | 1.7% | 6.9% | 1.0% | 1.9% | 2.4% |

Figure 59: Final statistical results of free-space results

### 3.6.2    Conclusions

- Antenna directivity RelStdDev: 0.1 - 2.1%

- E field RelStdDev: 0.1 - 5.5%

- H field RelStdDev: 0.9 - 8.4%

## 3.7    Conclusions

Excellent agreement between the participants using FDTD-based codes has been obtained for the wba SAR results. Slightly higher differences have be found for the 1 g and 10 g spatial average peak SAR values for plane wave incidence. Since all participants have been using the same grid resolution (pre-voxelled model), tissue assignment, and orientation, the error has to be attributed to one of the following sources:

1. implementation differences in the peak spatial average SAR algorithm, due to different interpretations of the current standard, which probably is the biggest contributor;

2. reflections from the absorbing boundary condition; and

3. the simulation not having reached 100% steady state.

The difference of the wba, 1 g, and 10 g SAR for the compared cases in front of the base station antennas are larger than for plane-wave incidence. The expected sources of errors are:

1. again the implementation of the spatial averaging algorithm, which is also influenced for these cases directly in front of the antennas by the different resolutions used;

2. different resolutions which has an impact on the effect of tissue layering as well as on the accuracy of the antenna model

3. boundary conditions; especially for simulation in front of base station antennas, it is crucial that the absorbing boundary conditions are set high enough to sufficiently attenuate non-orthonally incident fields to them (upper and lower and lateral boundaries), otherwise reflections from the boundaries might be present

4. the simulation not having reached 100% steady state;

5. possible difference in the positioning of the models with respect to the antennas, due to some participants might have taken the air padding around the voxel models into account.

# References

[Ackerman, 1998] Ackerman, M. J. (1998). The Visible Human Project. *Proceedings of the IEEE*, 86(3):504–511.

[Bernardi et al., 2003] Bernardi, P., Cavagnaro, M., Cicchetti, R., Pisa, S., Piuzzi, E., and Testa, O. (2003). A UTD/FDTD investigation on procedures to assess the compliance of cellular base-station antennas with human-exposure limits in a realistic human urban environment. *IEEE Transactions on Microwave Theory and Techniques*, 51(12):2409–2417.

[Bernardi et al., 2000] Bernardi, P., Cavagnaro, M., Pisa, S., and Piuzzi, E. (2000). Human exposure to radio base-station antennas in urban environment. *IEEE Transactions on Microwave Theory and Techniques*, 48(11):1996–2002.

[Christ et al., 2009] Christ, A., Kainz, W., Hahn, E. G., Honegger, K., Zefferer, M., Neufeld, E., Rascher, W., Janka, R., Bautz, W., Chen, J., Kiefer, B., Schmitt, P., Hollenbach, H.-P., Shen, J., Oberle, M., Szczerba, D., Kam, A., Guag, J. W., and Kuster, N. (2009). The Virtual Family – development of anatomical CAD models of two adults and two children for dosimetric simulations. *Physics in Medicine and Biology.* submitted.

[Christ et al., 2006a] Christ, A., Klingenböck, A., Samaras, T., Goiceanu, C., and Kuster, N. (2006a). The dependence of electromagnetic far-field absorption on body tissue composition in the frequency range from 300 MHz to 6 GHz. *IEEE Transactions on Microwave Theory and Techniques*, 54(5):2188–2195.

[Christ et al., 2006b] Christ, A., Samaras, T., Klingenböck, A., and Kuster, N. (2006b). Characterization of the electromagnetic near-field absorption in layered biological tissue in the frequency range from 30 MHz to 6000 MHz. *Physics in Medicine and Biology*, 51(19):4951–4965.

[Diverse Populations Collaborative Group, 2005] Diverse Populations Collaborative Group (2005). Weight-height relationships and body mass index: Some observations from the diverse populations collaboration. *American Journal of Physical Anthropology*, 128(1):220–229.

[Djafarzadeh et al., 2009] Djafarzadeh, R., Zefferer, M., Honegger, K., Bühlmann, B., Bouterfas, M., and Kuster, A. C. N. (2009). Abschlussbericht: Numerische bestimmung der spezifischen absorptionsrate bei ganzkörperexposition von kindern. Technical report, in preparation, IT'IS Foundation.

[DuBois and DuBois, 1916] DuBois, D. and DuBois, E. F. (1916). A formula to estimate the approximate surface area if height and weight be known. *Archives of Internal Medicine*, 17:863–871.

[Durney et al., 1986] Durney, C. H., Massoudi, H., and Iskander, M. F. (1986). *Radiofrequency Radiation Dosimetry Handbook*. Brooks Air Force Base, TX 78235-5301, USAF School of Aerospace Medicine, Aerospace Medical Division (AFSC).

[Faraone et al., 2000] Faraone, A., Tay, R. Y.-S., Joyner, K. H., and Balzano, Q. (2000). Estimation of the average power density in the vicinity of cellular base-station collinear array antennas. *IEEE Transactions on Vehicular Technology*, 49(3):984–996.

[FCC, 2001] FCC (2001). *Evaluating Compliance with FCC Guidelines for Human Exposure to Radiofrequency Electromagnetic Fields, Supplement C to OET Bulletin 65*. Washington, D.C. 20554.

[Findlay and Dimbylow, 2008] Findlay, R. P. and Dimbylow, P. J. (2008). Calculated SAR distributions in a human voxel phantom due to the reflection of electromagnetic fields from a ground plane between 65 MHz and 2 GHz. *Physics in Medicine and Biology*, 53:2277–2289.

[Gabriel et al., 1996] Gabriel, S., Lau, R. W., and Gabriel, C. (1996). The dielectric properties of biological tissues: III. Parametric models for the dielectric spectrum of tissues. *Physics in Medicine and Biology*, 41(11):2271–2293.

[Gosselin et al., 2009] Gosselin, M. C., Christ, A., Kühn, S., and Kuster, N. (2009). Dependence of the occupational exposure to mobile phone base station on the properties of the antenna and the human body. *IEEE Transactions on Electromagnetic Compatibility*. in press.

[Hagmann and Gandhi, 1979] Hagmann, M. J. and Gandhi, O. P. (1979). Numerical calculation of electromagnetic energy deposition in models of man with grounding and reflector effects. *Radio Science*, 14(6S):23–29.

[IEC, 2007] IEC (2007). *IEC 62209 Part 2, Human Exposure to Radio Frequency Fields from Handheld and Body-Mounted Wireless Communication Devices - Human Models, Instrumentation and Procedures, Part 2: Procedure to determine the Specific Absorption Rate (SAR) for mobile wireless communication devices used in close proximity to the human body (frequency range of 30 MHz to 6 GHz), Draft.* International Electrotechnical Commission (IEC), IEC Technical Committee 106, Geneva, Switzerland.

[IEC, 2009] IEC (2009). *IEC 62209-2 Ed.1, Human Exposure to Radio Frequency Fields from Handheld and Body-Mounted Wireless Communication Devices - Human Models, Instrumentation and Procedures, Part 2: Procedure to determine the Specific Absorption Rate (SAR) for mobile wireless communication devices used in close proximity to the human body (frequency range of 30 MHz to 6 GHz), Draft.* International Electrotechnical Commission (IEC), IEC Technical Committee 106, Geneva, Switzerland.

[IEEE, 2002] IEEE (2002). *IEEE Std C95.3 Recommended Practice for Measurements and Computations of Radio Frequency Electromagnetic Fields With Respect to Human Exposure to Such Fields, 100 kHz-300 GHz.* IEEE Standards Department, International Committee on Electromagnetic Safety, The Institute of Electrical and Electronics Engineers, Inc. 3 Park Avenue, New York, NY 10016-5997, USA.

[Kanda et al., 2004] Kanda, M., Douglas, M., Mendivil, E., Ballen, M., Gessner, A., and Chou, C.-K. (2004). Faster determination of mass-averaged SAR from 2-d area scans. *IEEE Transactions on Microwave Theory and Techniques*, 52(8):2013–2020.

[Kühn et al., 2009] Kühn, S., Jennings, W., Christ, A., and Kuster, N. (2009). Assessment of induced radio-frequency electromagnetic fields in various anatomical human body models. *Physics in Medicine and Biology*, 54(4):875–890.

[Thors et al., 2008] Thors, B., Strydom, M., Hansson, B., Meyer, F., Karkkainen, K., Zollman, P., Ilvonen, S., and Tornevik, C. (2008). On the estimation of SAR and compliance distance related to RF exposure from mobile communication base station antennas. *IEEE Transactions on Electromagnetic Compatibility*, 50(4):837–848.

[Uusitupa et al., 2009] Uusitupa, T., Laakso, I., Ilvonen, S., and Nikoskinen, K. (2009). MMF-GSMA dosimetry program phase 2: Scientific basis for base station exposure compliance standards – Project work package 5 'plane-wave sar evaluations'. Technical report, Department of Radio Science and Engineering, Helsinki University of Technology (TKK).

[Vermeeren et al., 2008] Vermeeren, G., Joseph, W., and Martens, L. (2008). Whole-body SAR in spheroidal adult and child phantoms in realistic exposure environment. *Electronics Letters*, 44(13):790–791.

[Vermeeren et al., 2007] Vermeeren, G., Joseph, W., Martens, L., Preiner, P., Cecil, S., Mitrevski, N., Neubauer, G., Kuehn, S., and Kuster, N. (2007). Influence of a perfectly conducting ground on the whole-body SAR. In *Book of Abstracts of the 8th International Congress of the European BioElectromagnetics Association (EBEA 2007)*, Bordeaux, France.

# A    Estimation Formula

This appendix presents the estimation formula that has been developed in the context of this work, as well as the definition of the variables used. The general form of the formula and the compact form, based on the worst-case human, can be found in Section 1.7.12. The rationales leading to this formula are presented in Section 1.7.

## A.1    General Form

$$SAR_{wb} = \frac{10^{0.25}}{2} \frac{\delta}{D_{body}} \frac{W_{eff}}{W_{body}} \frac{H_{eff}}{H_{body}} SAR(0) \tag{55}$$

$$SAR_{10g} = \frac{10^{0.25}}{2R_{wb/10g}} \frac{SAR_{10g}^{icnirp}}{SAR_{wb}^{icnirp}} \frac{\delta}{D_{body}} SAR(0), \tag{56}$$

with

$$SAR(0) = \frac{\sigma Z_i \left|t\right|^2 P_{rad}}{\rho \Phi_{3dB} L d} \left[ 1 + \left( \frac{4\pi d}{\Phi_{3dB} G_A L} \right)^2 \right]^{-1/2} \tag{57}$$

$$R_{wb/10g} = \begin{cases} 1.5 & \text{if} \quad 300\,\text{MHz} < f < 2.5\,\text{GHz} \\ 1 & \text{if} \quad 2.5\,\text{GHz} < f < 5\,\text{GHz} \end{cases} \tag{58}$$

$$H_{eff} = \begin{cases} L & \text{if } H_{beam} < L,\, H_{body} \\ H_{beam} & \text{if } L \leq H_{beam} < H_{body} \\ H_{body} & \text{if } H_{body} \leq H_{beam} \\ H_{body} & \text{if } H_{body} \leq L \end{cases} \tag{59}$$

$$H_{beam} = 2d \tan(\Theta_{3dB}/2) \tag{60}$$

$$W_{eff} = W_{body} \tag{61}$$

$$t = \frac{2}{1 + \sqrt{\epsilon}} \tag{62}$$

$$\delta = \frac{1}{\omega} \left[ \left( \frac{\mu_0 \epsilon_r' \epsilon_0}{2} \right) \left( \sqrt{1 + \left( \frac{\sigma}{\omega \epsilon_r' \epsilon_0} \right)^2} - 1 \right) \right]^{-1/2}. \tag{63}$$

## A.2 Compact Form – Worst-case Human

$$SAR_{wb} = C(f)\frac{H_{eff}}{0.089\,\text{m} \cdot 1.54\,\text{m}}\frac{P_{rad}}{\Phi_{3\text{dB}}Ld}\left[1 + \left(\frac{4\pi d}{\Phi_{3\text{dB}}G_A L}\right)^2\right]^{-1/2} \tag{64}$$

$$SAR_{10g} = 25 \cdot SAR_{wb}\frac{1.54\,\text{m}}{H_{eff}}\frac{1}{R_{wb/10g}} \tag{65}$$

$$H_{eff} = \begin{cases} L & \text{if } H_{beam} < L,\ 1.54\,\text{m} \\ H_{beam} & \text{if } L \le H_{beam} < 1.54\,\text{m} \\ 1.54\,\text{m} & \text{if } 1.54\,\text{m} \le H_{beam} \\ 1.54\,\text{m} & \text{if } 1.54\,\text{m} \le L \end{cases} \tag{66}$$

$$H_{beam} = 2d\tan(\Theta_{3\text{dB}}/2) \tag{67}$$

$$R_{wb/10g} = \begin{cases} 1.5 & \text{if} & 300\,\text{MHz} < f < 2.5\,\text{GHz} \\ 1 & \text{if} & 2.5\,\text{GHz} < f < 5\,\text{GHz} \end{cases} \tag{68}$$

| $f$ MHz | $C(f)$ $10^{-4}\,\text{m}^3/\text{kg}$ |
|---------|--------|
| 300 | 6.3 |
| 900 - 5000 | 8.1 |

Table 23: Piecewise linear approximation of $C(f)$ resulting in a deviation of less than 5%. For frequencies between 300 MHz and 900 MHz, a linear interpolation should be used.

## A.3 Definition of the Variables

| | |
|---|---|
| $d$ | distance between the antenna and the box bounding the human model (m) |
| $D_{body}$ | depth of the cuboid representing the human body model (m) |
| $f$ | frequency (MHz) |
| $G_A$ | gain of the antenna |
| $H_{beam}$ | height of the beam at a distance $d$ from the antenna, based on far-field characteristics of the antenna (m) |
| $H_{body}$ | height of the cuboid representing the human body model (m) |
| $H_{eff}$ | effective height of the cuboid, the irradiated section (m) |
| $L$ | total length of the antenna (m) |
| $P_{rad}$ | power radiated from the antenna (W) |
| $SAR_{10g}$ | peak spatial average SAR (W/kg) |
| $SAR_{10g}^{icnirp}$ | ICNIRP limit on the $SAR_{10g}$ (W/kg) |
| $SAR_{wb}$ | whole-body average SAR (W/kg) |
| $SAR_{wb}^{icnirp}$ | ICNIRP limit on the $SAR_{wb}$ (W/kg) |
| $SAR(0)$ | local SAR at the surface of a material (W/kg) |
| $t$ | transmission coefficient |
| $W_{body}$ | width of the cuboid representing the human body model (kg) |
| $W_{eff}$ | effective width of the cuboid, the irradiated section (m) |
| $Z_i$ | impedance of the incoming wave ($\Omega$) |
| $\delta$ | penetration depth (m) |
| $\epsilon_0$ | permittivity of vaccum (F/m) |
| $\epsilon_r'$ | real part of the relative permittivity |
| $\Phi_{3dB}$ | horizontal HPBW of the antenna (rad) |
| $\mu_0$ | permeability of vaccum (H/m) |
| $\omega$ | angular frequency (rad/s) |
| $\Theta_{3dB}$ | vertical HPBW of the antenna (rad) |
| $\rho$ | density (kg/m$^3$) |
| $\sigma$ | conductivity (S/m) |

# B    WP6 – Generic Antenna Specifications

This appendix presents the detailed characteristics of the generic base station antennas used in WP6 and WP7.

## B.1    Models @ 300MHz

### B.1.1    300MHz H65V64 VPolV5

**Main characteristics**

| Model | 300MHz |
|---|---|
| Type | Macrocell |
| Polarization | vertical |
| max Gain/Directivity | 9 dBi |
| h-HPBW 3dB | $66° \pm 5°$ |
| v-HPBW 3dB | $60° \pm 5°$ |

| | |
|---|---|
| $L_y$ | 1000 mm |
| $L_z$ | 750 mm |
| $D_x$ | 188 mm |
| $D_y$ | 414 mm |
| $D_z$ | 440 mm |
| H | 1000 mm |
| Dipoles radius | 15 mm |
| Dipoles gap | 10 mm |
| Background plane thickness | 20 mm |
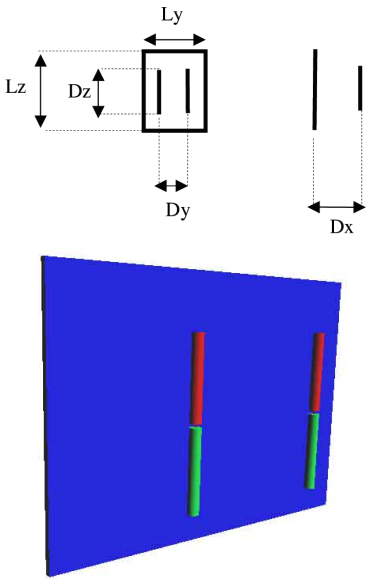
**Dipoles excitation**

| | Excitation/Voltage Amplitude | Excitation/Voltage Phase (deg) |
|---|---|---|
| Dipole 1 | 1 | 0 |
| Dipole 2 | 1 | 0 |

**Far-field pattern**
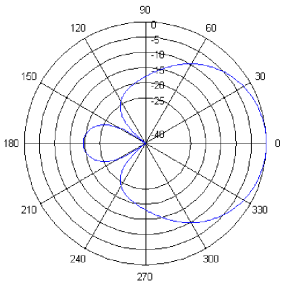
60.1: Horizontal
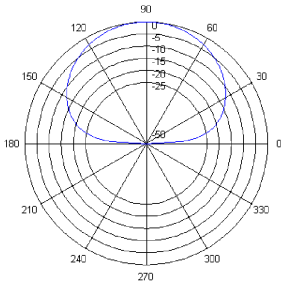
60.2: Vertical

## B.2 Models @ 450MHz - PMR

### B.2.1 450MHz H118V35 VPolV4

**Main characteristics**

| Model | GSM 400 |
|---|---|
| Type | Array panel - Macrocell |
| Polarization | vertical |
| max Gain/Directivity | 9.3 dBi |
| h-HPBW 3dB | $118° \pm 5°$ |
| v-HPBW 3dB | $35° \pm 5°$ |

| | |
|---|---|
| $L_y$ | 280 mm |
| $L_z$ | 510 mm |
| $D_x$ | 140 mm |
| $D_y$ | 140 mm |
| $D_z$ | 310 mm |
| H | 1020 mm |
| Dipoles radius | 2 mm |
| Dipoles gap | 2 mm |
| Background plane thickness | 2 mm |
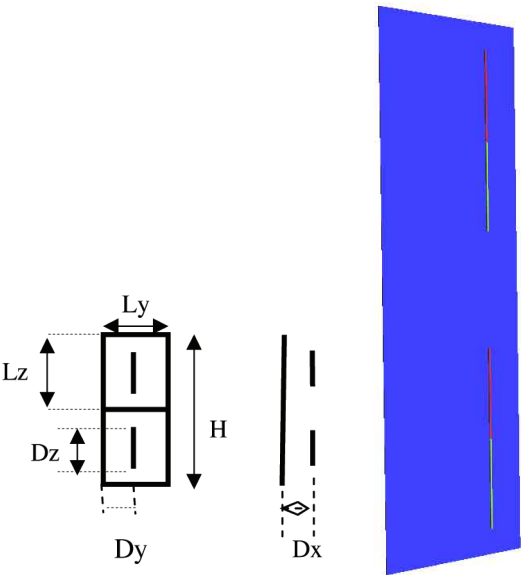
**Dipoles excitation**

| | Excitation/Voltage Amplitude | Excitation/Voltage Phase (deg) |
|---|---|---|
| Dipole 1 | 1 | 0 |
| Dipole 2 | 1 | 0 |

**Far-field pattern**
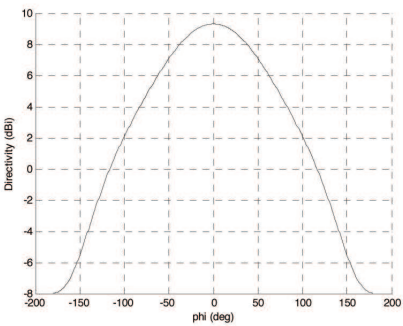


60.3: Horizontal
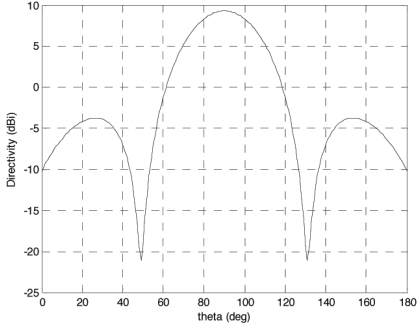


60.4: Vertical

## Specification sheet from the manufacturer

**Eurocell Panel Antenna**

**KATHREIN**
Antennen · Electronic

| | Panel 390/420 115° 8.5dBi | Panel 390/420 115° 11.5dBi |
|---|---|---|
| Type No. | 739 594 | 739 596 |
| Input | 7-16 female | |
| Frequency range | 380 – 430 MHz | |
| VSWR | < 1.5 | |
| Gain | 8.5 dBi | 11.5 dBi |
| Impedance | 50 Ω | |
| Polarization | Vertical | |
| Front-to-back ratio | > 18 dB | |
| Half-power beam width | H-plane: 115° / E-plane: 33° | H-plane: 115° / E-plane: 18° |
| Max. power | 500 Watt (at 50 °C ambient temperature) | |
| Weight | 4.5 kg | 9 kg |
| Wind load Frontal | 160 N (at 150 km/h) | 340 N (at 150 km/h) |
| Lateral | 100 N (at 150 km/h) | 220 N (at 150 km/h) |
| Rearside | 360 N (at 150 km/h) | 760 N (at 150 km/h) |
| Max. wind velocity | 200 km/h | |
| Packing size | 1102 x 272 x 160 mm | 2062 x 272 x 160 mm |
| Height/width/depth | 974 / 258 / 103 mm | 1934 / 258 / 103 mm |

Material: Radiator: Copper, tin-plated.
Reflector screen: Weather-resistant aluminum.
Radome: Fiberglass, colour: Grey.
All screws and nuts: Stainless steel.

Attachment: See the „Mounting Hardware" part of this catalogue.

Ice protection: Due to the very sturdy antenna construction and the protection of the radiating system by the radome, the antenna remains operational even under icy conditions.

Grounding: All metal parts of the antenna including the mounting kit and the inner conductor are DC grounded.

Horizontal Pattern

Vertical Pattern 739 594

Vertical Pattern 739 596
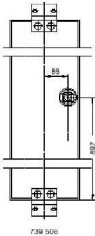
## B.2.2    450MHz H180V19 VPolV4

### Main characteristics

| | |
|---|---|
| Frequency | 450 MHz |
| Type | Array panel - Macrocell |
| Polarization | vertical |
| max Gain/Directivity | 10 dBi |
| h-HPBW 3dB | $188° \pm 5°$ |
| v-HPBW 3dB | $19° \pm 5°$ |

| | |
|---|---|
| $L_y$ | 140 mm |
| $L_z$ | 490 mm |
| $D_x$ | 210 mm |
| $D_y$ | 70 mm |
| $D_z$ | 310 mm |
| H | 1960 mm |
| Dipoles radius | 6 mm |
| Dipoles gap | 2 mm |
| Background plane thickness | 2 mm |
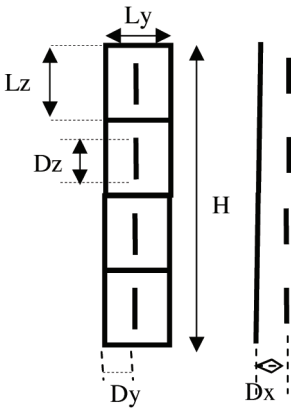
### Dipoles excitation

| | Excitation/Voltage Amplitude | Excitation/Voltage Phase (deg) |
|---|---|---|
| Dipole 1 | 1 | 0 |
| Dipole 2 | 1 | 0 |
| Dipole 3 | 1 | 0 |
| Dipole 4 | 1 | 0 |

### Far-field pattern
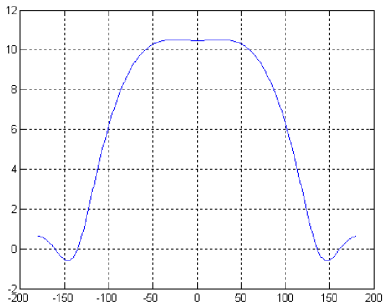
60.5: Horizontal
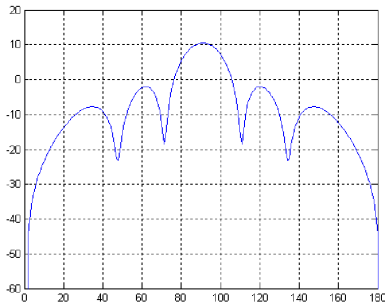
60.6: Vertical

**Specification sheet from the manufacturer**



DAPA TECHNOLOGY
dapa.info@dapa.fr

**Model 2680-130S, 180°, 10.5 dBi (8.4 dBd) Pane**
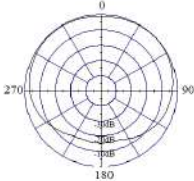
**ELECTRICAL CHARACTERISTICS**

| | |
|---|---|
| Frequency Range | 380 - 430 MHz |
| Beamwidth: Horizontal-plane | 180° ± 5° (at -3 dB) |
| Vertical-plane | 20° ± 1° (at -3 dB) |
| Gain | 10.5 dBi (8.4 dBd) |
| Electrical Downtilt | 0° (available -6°, -10°) |
| Front-to-Back Ratio | ≤ -15 dB |
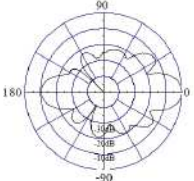
**GENERAL CHARACTERISTICS**

| | |
|---|---|
| Impedance | 50 Ω |
| VSWR | ≤ 1.3:1 |
| Polarization | Vertical |
| Rated Power | 1000 W |

HORIZONTAL - PLANE

VERTICAL - PLANE

DAPA • FRANCE, Les Ulis

## B.3    Models @ GSM 900

### B.3.1    900MHz H65V7 X45V4

**Main characteristics**

| Frequency | GSM 900 |
|---|---|
| Type | Array panel - Macrocell |
| Polarization | cross polarized |
| max Gain/Directivity | 18.5 dBi |
| h-HPBW 3dB | $65° \pm 5°$ |
| v-HPBW 3dB | $7° \pm 5°$ |

| | |
|---|---|
| $L_x$ | 60 mm |
| $L_y$ | 300 mm |
| $L_z$ | 320 mm |
| $D_x$ | 82 mm |
| $D_y$ | 99 mm |
| $D_z$ | 99 mm |
| H | 2560 mm |
| W | 40 mm |
| Dipoles radius | 3 mm |
| Dipoles gap | 2 mm |
| All metallic planes thickness | 2 mm |
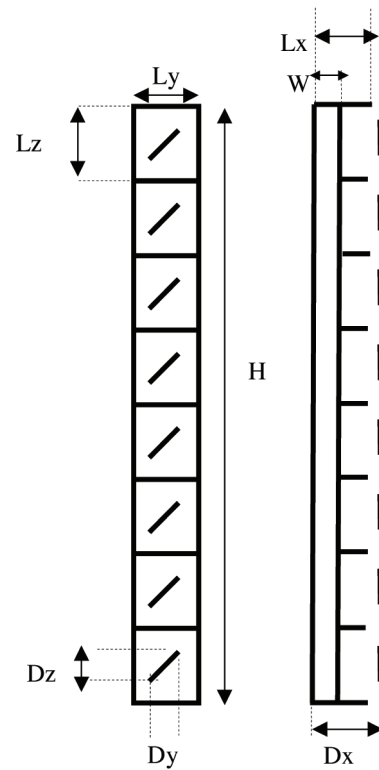
**Dipoles excitation**

| | Excitation/Voltage Amplitude | Excitation/Voltage Phase (deg) |
|---|---|---|
| Dipole 1 | 1 | 0 |
| Dipole 2 | 1 | 0 |
| Dipole 3 | 1 | 0 |
| Dipole 4 | 2 | 0 |
| Dipole 5 | 2 | 0 |
| Dipole 6 | 1 | 0 |
| Dipole 7 | 1 | 0 |
| Dipole 8 | 1 | 0 |
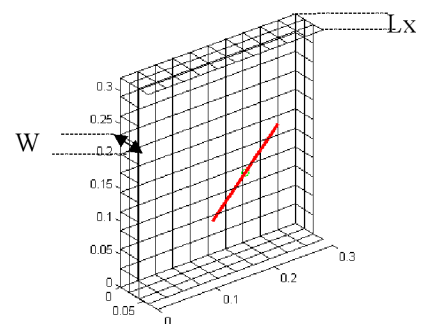
## Far-field pattern
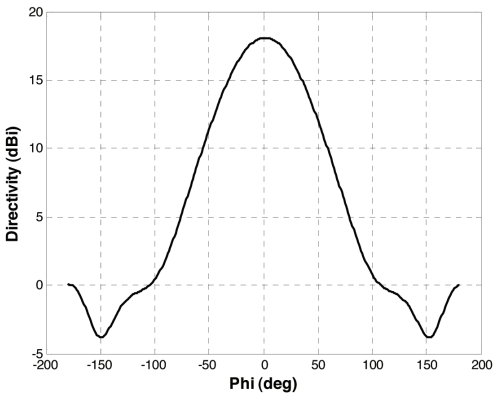


60.7: Horizontal
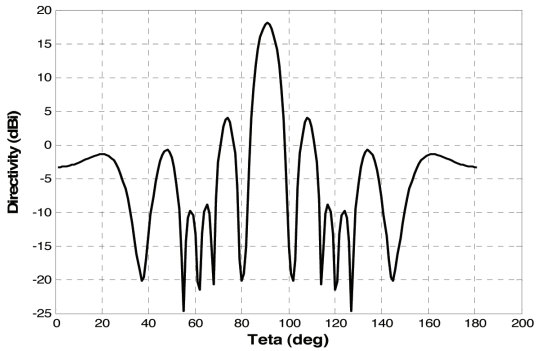


60.8: Vertical

**Comparison of the model to measurements**

A set of BTS 900 have been measured and compared to the model proposed in this subsection.
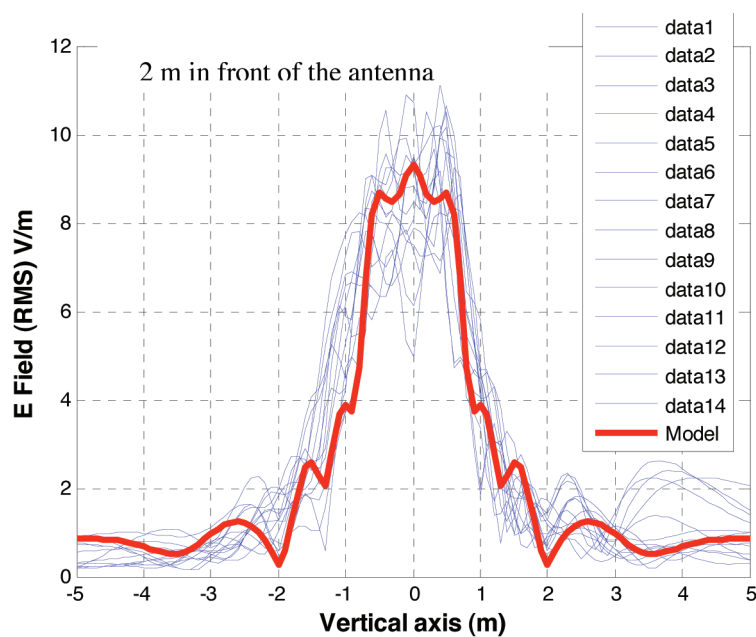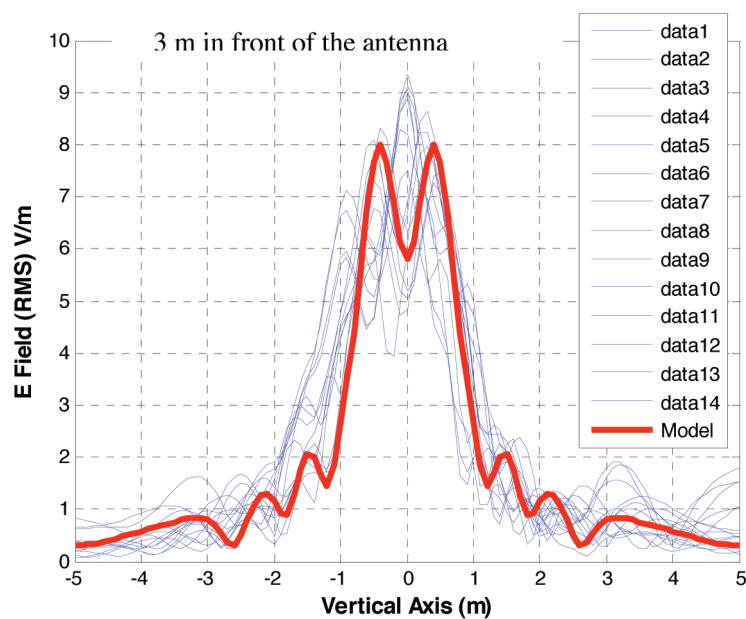
### B.3.2 900MHz H90V9 VPolV7

**Main characteristics**

| Frequency | GSM 900 |
|---|---|
| Type | Array panel - Macrocell |
| Polarization | vertical |
| max Gain/Directivity | 15.9 dBi |
| h-HPBW 3dB | $90° \pm 5°$ |
| v-HPBW 3dB | $9° \pm 5°$ |

| | |
|---|---|
| $L_x$ | 96 mm |
| $L_y$ | 240 mm |
| $L_z$ | 320 mm |
| $D_x$ | 82 mm |
| $D_y$ | 120 mm |
| $D_z$ | 136 mm |
| H | 1920 mm |
| W | 32 mm |
| Dipoles radius | 3 mm |
| Dipoles gap | 2 mm |
| All metallic planes thickness | 2 mm |
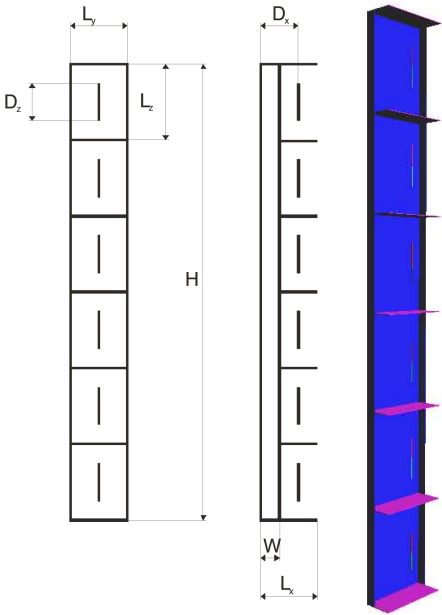
**Dipoles excitation**

| | Excitation/Voltage Amplitude | Excitation/Voltage Phase (deg) |
|---|---|---|
| Dipole 1 | 0.5 | 0 |
| Dipole 2 | 0.5 | 0 |
| Dipole 3 | 1 | 0 |
| Dipole 4 | 1 | 0 |
| Dipole 5 | 0.5 | 0 |
| Dipole 6 | 0.5 | 0 |
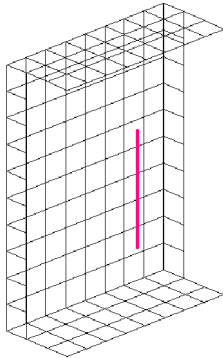
## Far-field pattern
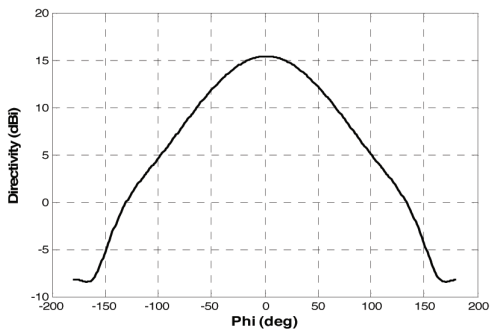


60.9: Horizontal
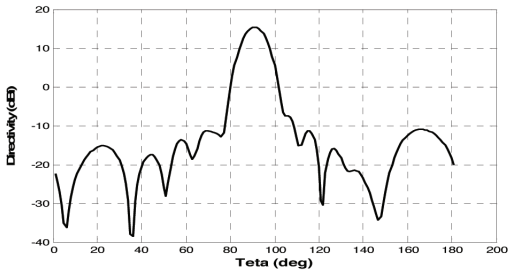


60.10: Vertical

## Specification sheet from the manufacturer



**VPol F-Panel 872–960 90° 15.5dBi**

| Type No. | 736 863 |
|---|---|
| Frequency range | 872 – 960 MHz |
| Polarization | Vertical |
| Gain | 15.5 dBi |
| Half-power beam width | H-plane: 90°<br>E-plane: 8.5° |
| Sidelobe suppression | above horizon for first sidelobe<br>better or equal 14 dB below maximum gain |
| Front-to-back ratio | > 20 dB |
| Impedance | 50 Ω |
| VSWR | < 1.3 |
| Intermodulation IM3<br>(2 x 43 dBm carrier) | < −150 dBc |
| Max. power | 400 W (at 50 °C ambient temperature) |
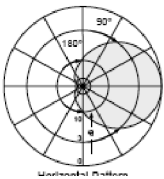
## B.4 Models @ 2100MHz - UMTS

### B.4.1 2100MHz H65V7 OutdoorXPolV3

**Main characteristics**

| Frequency | GSM 2100 |
|---|---|
| Type | Array panel - Macrocell |
| Polarization | cross polarized |
| max Gain/Directivity | 19.25 dBi |
| h-HPBW 3dB | $66° \pm 5°$ |
| v-HPBW 3dB | $7° \pm 5°$ |

| | |
|---|---|
| $L_x$ | 27 mm |
| $L_y$ | 130 mm |
| $L_z$ | 130 mm |
| $D_x$ | 37 mm |
| $D_y$ | 65 mm |
| $D_z$ | 41 mm |
| H | 1300 mm |
| W | 18 mm |
| Dipoles radius | 3 mm |
| Dipoles gap | 1.5 mm |
| All metallic planes thickness | 2 mm |
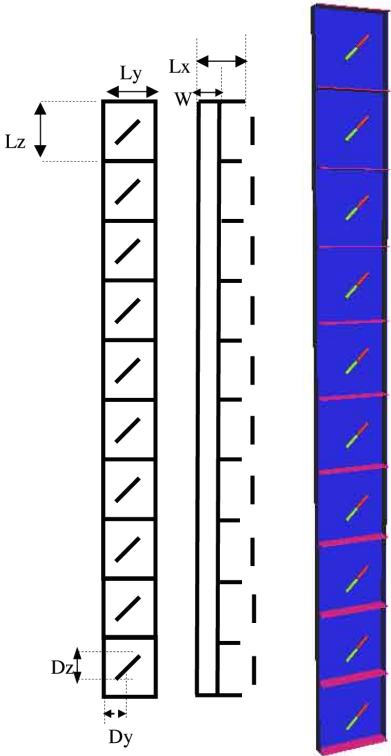
**Dipoles excitation**

| | Excitation/Voltage Amplitude | Excitation/Voltage Phase (deg) |
|---|---|---|
| Dipole 1 | 1 | 0 |
| Dipole 2 | 1 | 0 |
| Dipole 3 | 1 | 0 |
| Dipole 4 | 1.5 | 0 |
| Dipole 5 | 2 | 0 |
| Dipole 6 | 2 | 0 |
| Dipole 7 | 1.5 | 0 |
| Dipole 8 | 1 | 0 |
| Dipole 9 | 1 | 0 |
| Dipole 10 | 1 | 0 |

**Far-field pattern**
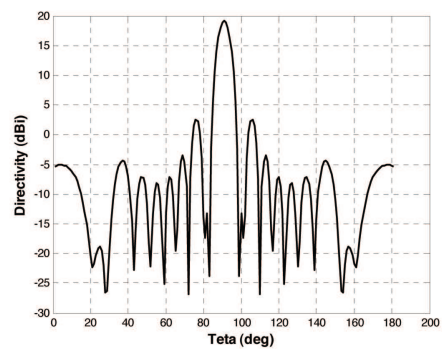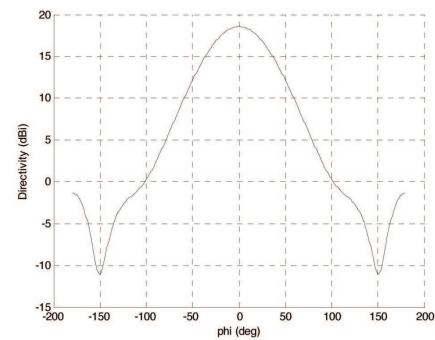


| 60.11: Horizontal | 60.12: Vertical |

**Specification sheet from the manufacturer**

XPol F-Panel 1710–2170 65° 18dBi 0°–8°T

| Type No. | 742 212 | | |
|---|---|---|---|
| Frequency range | | [1710–2170] | |
| | 1710 – 1880 MHz | 1850 – 1990 MHz | 1920 – 2170 MHz |
| Polarization | +45°, –45° | +45°, –45° | +45°, –45° |
| Gain | 2 x 17.5 dBi | 2 x 17.7 dBi | 2 x 18 dBi |
| Half-power beam width Copolar +45°/–45° | Horizontal: 67° Vertical: 7° | Horizontal: 66° Vertical: 6.7° | Horizontal: 63° Vertical: 6.5° |
| Electrical tilt continuously adjustable | 0°–8° | 0°–8° | 0°–8° |
| Sidelobe suppression for first sidelobe above horizon | 0° ... 2° ... 5° ... 8°T 17 ... 17 ... 15 .... 15 dB | 0° ... 2° ... 5° ... 8°T 20 ... 20 ... 18 ... 18 dB | 0° ... 2° ... 5° ... 8°T 20 ...20 ... 18 ... 16 dB |
| Front-to-back ratio (180° ± 30°) | Copolar: > 30 dB Total power: > 25 dB | Copolar: > 30 dB Total power: > 25 dB | Copolar: > 30 dB Total power: > 25 dB |
| Cross polar ratio Maindirection 0° Sector ±60° | Typically: 26 dB > 10 dB | Typically: 25 dB > 10 dB | Typically: 26 dB > 10 dB |
| Isolation, between ports | > 30 dB | > 30 dB | > 30 dB |
| Impedance | 50 Ω | 50 Ω | 50 Ω |
| VSWR | < 1.5 | < 1.5 | < 1.5 |
| Intermodulation IM3 (2 x 43 dBm carrier) | < –150 dBc | | |
| Max. power per input | 300 W (at 50 °C ambient temperature) | | |

## Comparison of the model to measurements

The measurements are performed on a set of BTS in UMTS band. The results show as expected a shift of the field due to the positioning problems of the antennas. In some cases (triple band antennas) the UMTS/GSM1800 dipoles are in the upper or lower part of the antenna.

**Near Field in front of the antenna (2m)**

**Near field in front of the antenna at (3m)**
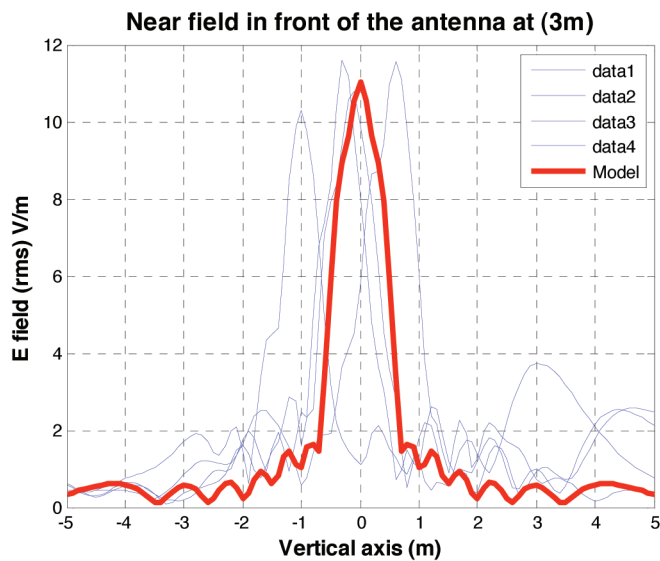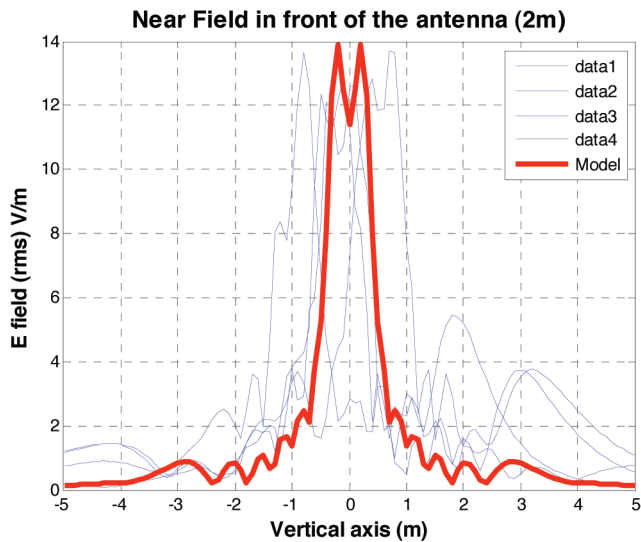
| **Measured antenna** |
|:---:|
| **Data1** : 'all18-2146T2 |
| **Data2**    'arial65xmdgww21-7_2157 |
| **Data3**    'arialcom2157 |
| **Data4**: 'insnec808580_T8_2000_m_2155 |

### B.4.2   2100MHz H90V80 IndoorVPolV4

**Main characteristics**



| Frequency | GSM 2100 |
|---|---|
| Polarization | cross polarized |
| max Gain/Directivity | 8.1 dBi |
| h-HPBW 3dB | $90° \pm 5°$ |
| v-HPBW 3dB | $81° \pm 5°$ |

| | |
|---|---|
| $L_x$ | 40 mm |
| $L_y$ | 160 mm |
| $L_z$ | 200 mm |
| $D_x$ | 35 mm |
| $D_z$ | 60 mm |
| W | 20 mm |
| Dipoles radius | 1 mm |
| Dipoles gap | 1 mm |
| All metallic planes thickness | 2 mm |
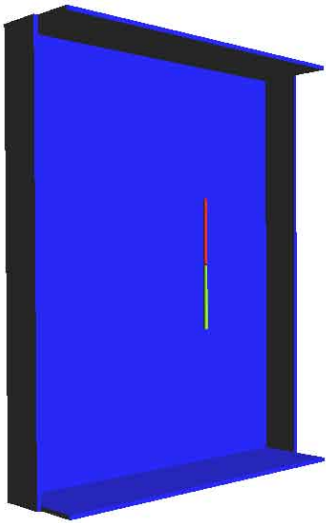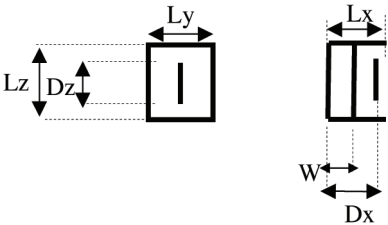
**Far-field pattern**
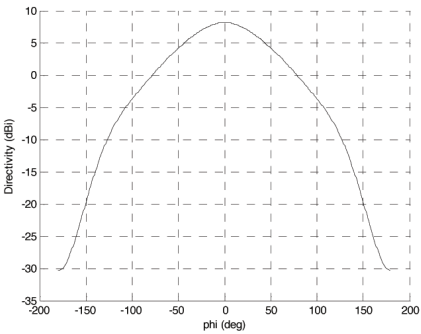


60.13: Horizontal
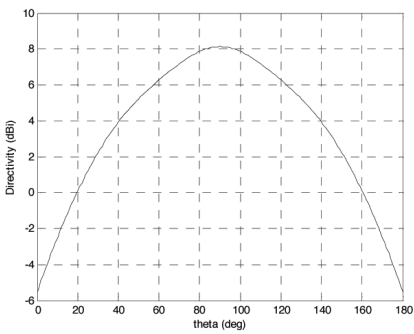


60.14: Vertical

## B.5 Models @ 3500MHz - Wimax

### B.5.1 3500MHz H18V18 VPol CPEV4

**Main characteristics**

| Frequency | GSM 3500 |
|---|---|
| Type | Array panel - Macrocell |
| Polarization | vertical |
| max Gain/Directivity | 20 dBi |
| h-HPBW 3dB | $20° \pm 5°$ |
| v-HPBW 3dB | $19° \pm 5°$ |

| | |
|---|---|
| $L_y$ | 250 mm |
| $L_z$ | 240 mm |
| $D_x$ | 22 mm |
| $D_y$ | 23 mm |
| $D_z$ | 35 mm |
| hor. distance between dipoles | 68 mm |
| vert. distance between dipoles | 60 mm |
| R: distance to limit | 23 mm |
| Dipoles radius | 1 mm |
| Dipoles gap | 1 mm |
| Reflectors thickness | 2 mm |

**Dipoles excitation**

| | Excitation/Voltage Amplitude | Excitation/Voltage Phase (deg) |
|---|---|---|
| Dipole 1 | 1 | 0 |
| Dipole 2 | 1 | 0 |
| Dipole 3 | 1 | 0 |
| Dipole 4 | 1 | 0 |
| Dipole 5 | 1 | 0 |
| Dipole 6 | 1.5 | 0 |
| Dipole 7 | 1.5 | 0 |
| Dipole 8 | 1 | 0 |
| Dipole 9 | 1 | 0 |
| Dipole 10 | 1.5 | 0 |
| Dipole 11 | 1.5 | 0 |
| Dipole 12 | 1 | 0 |
| Dipole 13 | 1 | 0 |
| Dipole 14 | 1 | 0 |
| Dipole 15 | 1 | 0 |
| Dipole 16 | 1 | 0 |
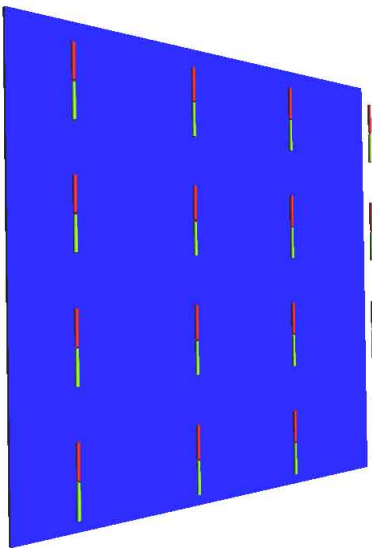
**Far-field pattern**
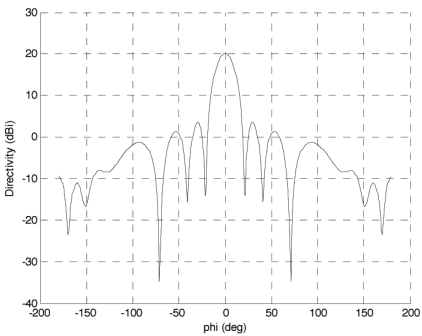


60.15: Horizontal
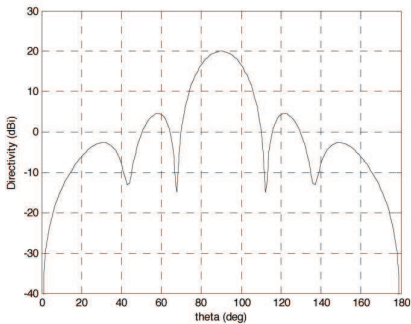


60.16: Vertical

**Specification sheet from the manufacturer**



## TS ANT 3.4 - 3.7GHz V/H - P/N 872457

### Technical Specification

| | |
|---|---|
| Marketing P.N | 872457 |
| Production P.N | AN1125 |
| ANT.TYPE | Subscriber 3.4 -3.7GHz V/H 18dBi |
| REG. COMP. | ETSI EN 302 085 V1.1.2 TS3, TS4. |
| | |
| **1. ELECTRICAL** | |
| | |
| FREQ. RANGE | 3.4 - 3.7GHz |
| GAIN | 18dBi |
| VSWR | 1.5:1 |
| AZ. B.W (3dB) | $18^0$ |
| EL. B.W (3dB) | $18^0$ |
| ELEC. DOWNTILT | $0^0$ |
| POLARIZATION | Vertical or Horizontal |
| MAX INPUT POWER | 10W |
| INPUT IMPEDANCE | 50 Ohms |
| | |
| **2. MECHANICAL** | |
| | |
| DIMENSION (HxWxD) | 261.3x261.3x30 mm |
| WEIGHT | 1.0Kg. |
| CONNECTOR | N - Type female. |

### B.5.2   3500MHz H65V9 VPol BTSV3

**Main characteristics**

| Frequency | Wimax BTS 3500 MHz |
|---|---|
| Type | Array panel - Macrocell |
| Polarization | vertical |
| max Gain/Directivity | 17.3 dBi |
| h-HPBW 3dB | $65° \pm 5°$ |
| v-HPBW 3dB | $9° \pm 5°$ |

| | |
|---|---|
| $L_x$ | 16 mm |
| $L_y$ | 60 mm |
| $L_z$ | 80 mm |
| $D_x$ | 16 mm |
| $D_y$ | 12 mm |
| $D_z$ | 34.6 mm |
| H | 480 mm |
| W | 11 mm |
| Dipoles radius | 1 mm |
| Dipoles gap | 1 mm |
| Reflectors thickness | 2 mm |
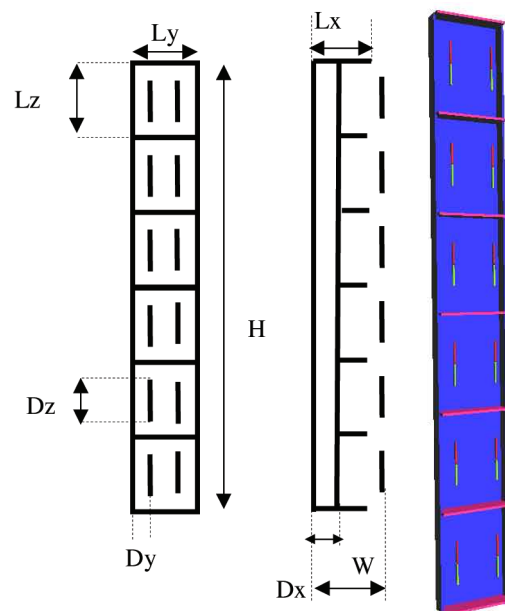


**Dipoles excitation**

| | Excitation/Voltage Amplitude | Excitation/Voltage Phase (deg) |
|---|---|---|
| Dipoles cell 1 | 1 | 0 |
| Dipoles cell 2 | 1 | 0 |
| Dipoles cell 3 | 1 | 0 |
| Dipoles cell 4 | 1 | 0 |
| Dipoles cell 5 | 1 | 0 |
| Dipoles cell 6 | 1 | 0 |
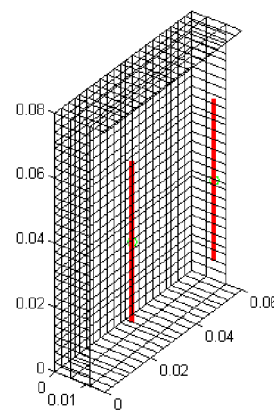
## Far-field pattern
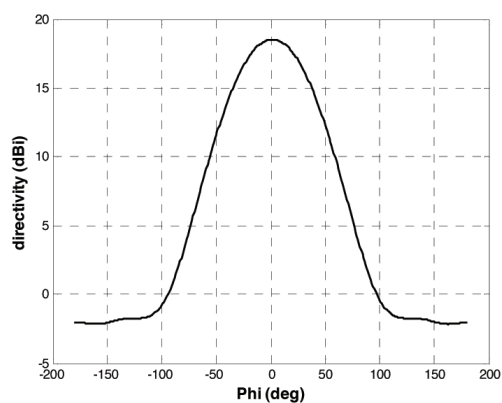


60.17: Horizontal
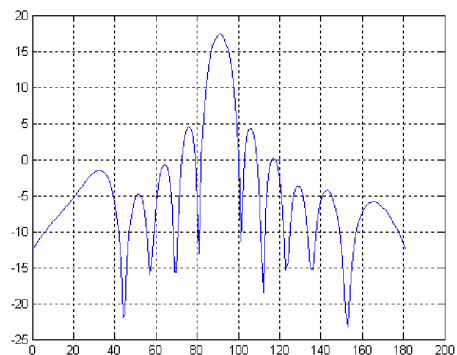


60.18: Vertical

## Specification sheet from the manufacturer



**BS ANT 3.3-3.8GHz/60V - P/N 835350**

**Technical Specification**

| | |
|---|---|
| **Marketing P.N** | 835350 |
| **Production P.N** | AN1164 |
| **ANT.TYPE** | SECTOR 3.3-3.8GHz /60V 16dBi |
| **REG. COMP.** | ETSI EN 302 085 V1.1.2 CS3. EL-Symmetrical mask |
| | |
| **1. ELECTRICAL** | |
| | |
| **FREQ. RANGE** | 3.3 - 3.8GHz |
| **GAIN** | 16dBi |
| **VSWR** | 1.5:1 |
| **AZ. B.W (3dB)** | $60^0$ |
| **EL. B.W (3dB)** | $10^0$ |
| **ELEC. DOWNTILT** | $0^0$ |
| **POLARIZATION** | Vertical |
| **MAX INPUT POWER** | 20W |
| **INPUT IMPEDANCE** | 50 Ohms |
| **F/B RATIO** | 30dB |
| **CROSS POLAR. (XPD)** | 25dB |
| | |
| **2. MECHANICAL** | |
| | |
| **DIMENSION (HxWxD)** | 590x265x50 mm |
| **WEIGHT** | 1.8Kg. |
| **CONNECTOR** | N- Type female. |
| **RADOME** | |

## B.6　Models @ 5000MHz

### B.6.1　5000MHz H65V35 VPol DirectionalV5

**Main characteristics**

| Frequency | Wifi 5 GHz |
|---|---|
| Type | Panel |
| Polarization | vertical |
| max Gain/Directivity | 11.8 dBi |
| h-HPBW 3dB | $66° \pm 5°$ |
| v-HPBW 3dB | $35° \pm 5°$ |

| | |
|---|---|
| $L_x$ | 11 mm |
| $L_y$ | 40 mm |
| $L_z$ | 40 mm |
| $D_x$ | 11 mm |
| $D_y$ | 24 mm |
| $D_z$ | 24 mm |
| H | 80 mm |
| W | 8 mm |
| Dipoles radius | 0.5 mm |
| Dipoles gap | 1 mm |
| All metallic planes thickness | 1 mm |
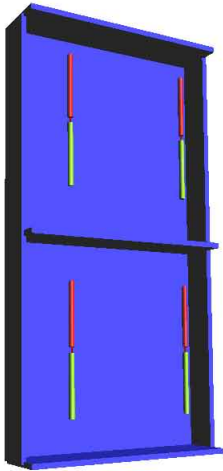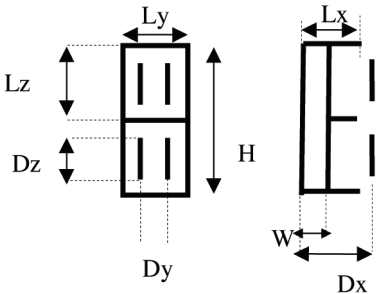


**Dipoles excitation**

| | Excitation/Voltage Amplitude | Excitation/Voltage Phase (deg) |
|---|---|---|
| Dipoles cell 1 | 1 | 0 |
| Dipoles cell 2 | 1 | 0 |

## Far-field pattern
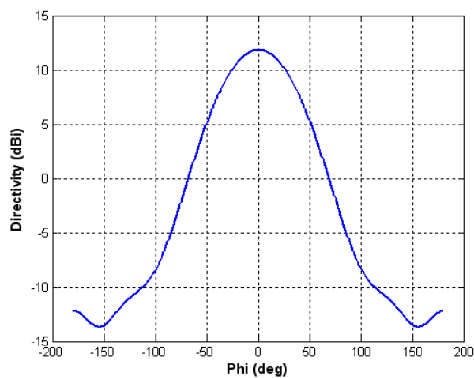


60.19: Horizontal
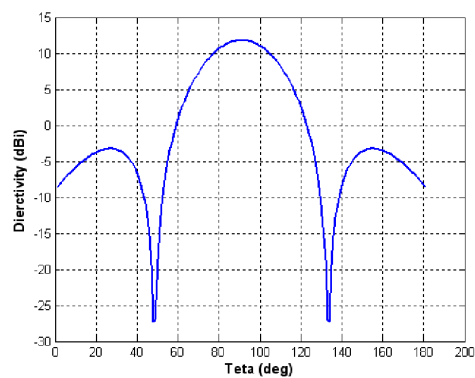


60.20: Vertical

## Specification sheet from the manufacturer



HUBER+SUHNER®
PLANAR ANTENNA
FOR WIRELESS COMMUNICATION

### SPA 5600/65/12/0/V

**Technical Data**

**Electrical Properties**

| | |
|---|---|
| Frequency range | 5150 – 5875 MHz |
| Impedance | 50 Ω |
| VSWR | 1.5 |
| Polarization | linear, vertical |
| Gain | 11.5 dBi |
| 3 dB beamwidth horizontal | 65° |
| 3 dB beamwidth vertical | 35° |
| Downtilt | 0° |
| Front to back ratio | 18 dB |
| Max. power | 80 W (CW) at 50°C |

**Mechanical & Environmental Properties**

| | |
|---|---|
| Dimensions | 101 x 80 x 20 mm |
| | (3.97" x 3.15" x 0.79") |
| Weight | 0.13 kg (0.29 lbs.) |
| Radome material | ASA |
| Radome colour | RAL 7035 (light grey) |
| 2002/95/EC (RoHS) | compliant |
| Operating temperature range | - 40°C to + 80°C |
| Storage temperature range | - 40°C to + 80°C |
| Windload | 15 N at 160km/h (100mph) |

| Available Types | Article no. | |
|---|---|---|
| 1356.19.0002 | 23041806 | SMA female |
| 1356.26.0002 | 23041809 | TNC female |

Wall and mast mounting bracket (1 metal band) included, mast diameter 40-60 mm (1.57" – 2.36")

| Mounting Hardware | Article no. | |
|---|---|---|
| 9091.99.0191 | 84011560 | Optional wall mounting bracket |

| Documents | | |
|---|---|---|
| 01.02.0777 | security instruction | |
| 01.02.1033 | mounting instruction | |
| 01.02.1111 | mounting instruction (9091.99.0191) | |

**Radiation Pattern**

horizontal
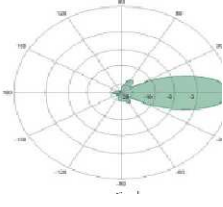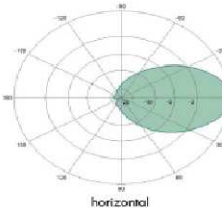
### B.6.2   5000MHz H360V7 VPol OmniV4

**Main characteristics**

| Frequency | Wifi 5 GHz |
|---|---|
| Type | Panel |
| Polarization | vertical |
| max Gain/Directivity | 10.1 dBi |
| h-HPBW 3dB | 360° |
| v-HPBW 3dB | 7° ± 5° |

| | |
|---|---|
| $L_z$ | 70 mm |
| $D_z$ | 25 mm |
| H | 380 mm |
| Dipoles radius | 1 mm |
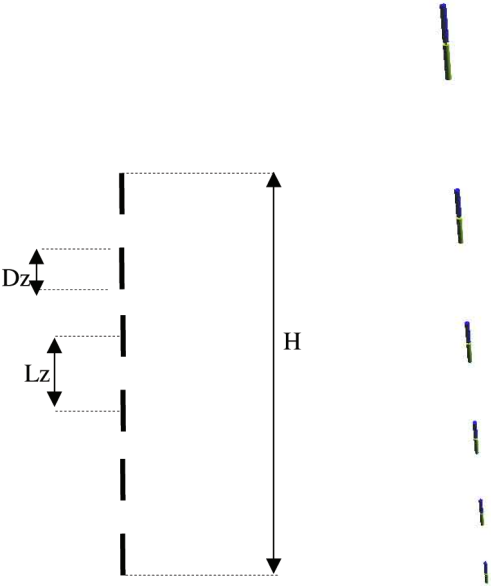
**Dipoles excitation**

| | Excitation/Voltage Amplitude | Excitation/Voltage Phase (deg) |
|---|---|---|
| Dipole 1 | 1 | 0 |
| Dipole 2 | 1 | 0 |
| Dipole 3 | 1 | 0 |
| Dipole 4 | 1 | 0 |
| Dipole 5 | 1 | 0 |
| Dipole 6 | 1 | 0 |

**Far-field pattern**
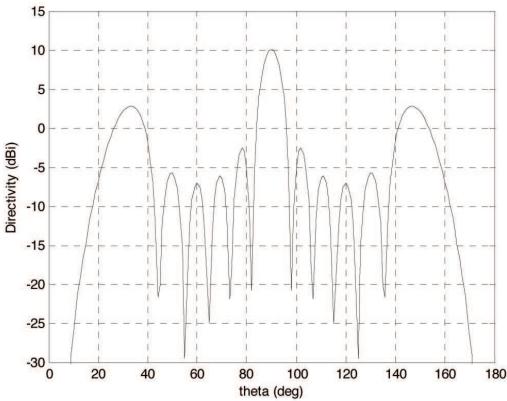
60.21: Vertical

# C  WP6 – Generic Antenna Validation Results

This appendix presents the results of the validation of the FEKO and SEMCAD X models of the 12 generic base station antennas. Their impedances and S11 parameters are compared. The electric and magnetic fields in vertical planes at 4 distances from each antenna are also compared. Finally, their directivity is plotted from the far-field results obtained with SEMCAD X (for comparison of HPBW, see Section 1.4).

## C.1  Impedances and S11

### C.1.1  300MHz H65V64 VPolV5



60.22: Impedance                                    60.23: S11
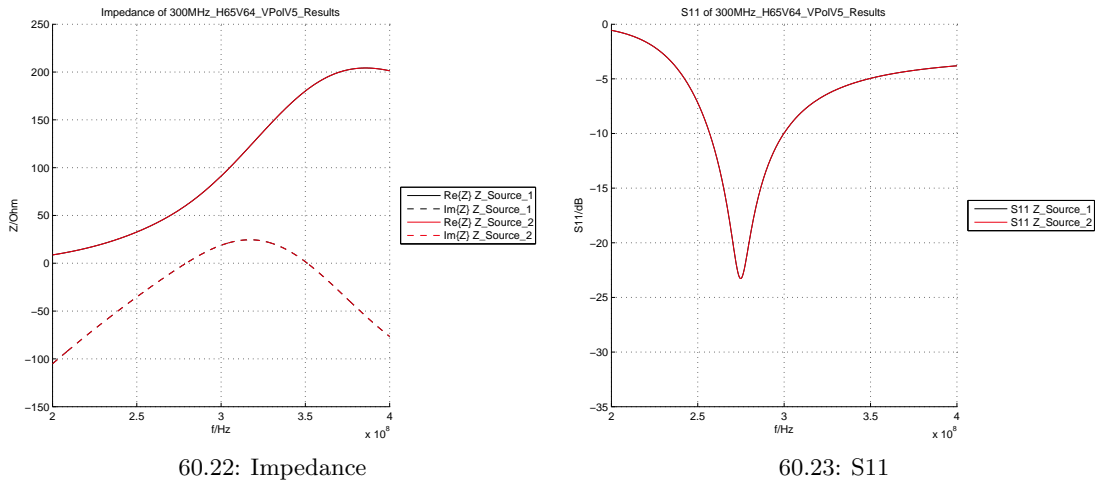
Figure 60: Results from SEMCAD 300MHz H65V64 VPolV5



61.1: Impedance                                    61.2: S11
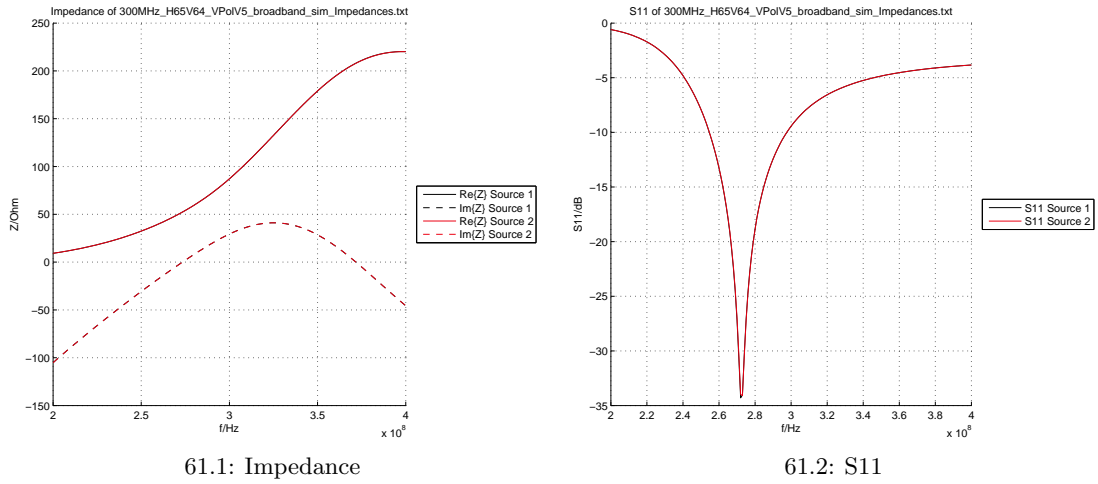
Figure 61: Results from FEKO 300MHz H65V64 VPolV5

### C.1.2 300MHz H116V32 VPolV2



62.1: Impedance

62.2: S11
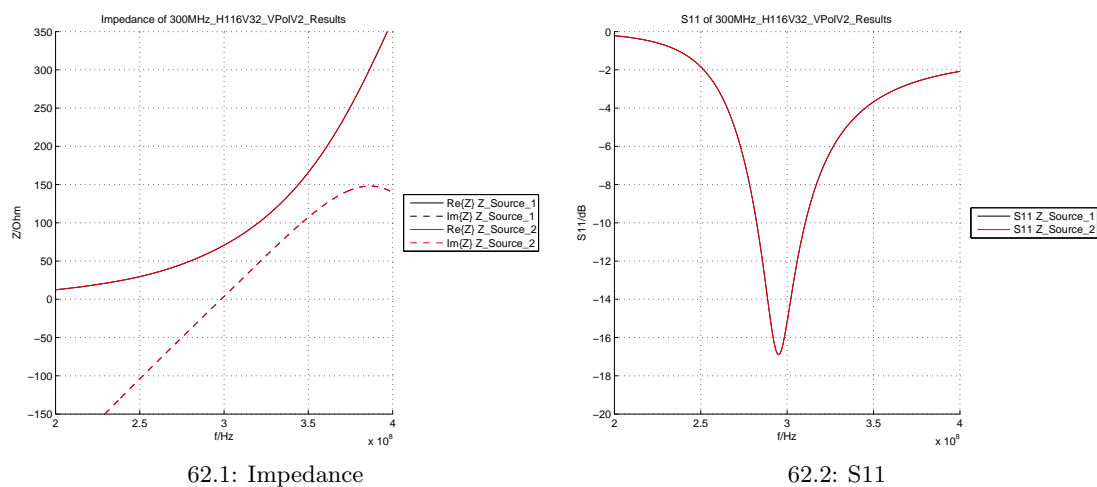
Figure 62: Results from SEMCAD 300MHz H116V32 VPolV2



63.1: Impedance

63.2: S11
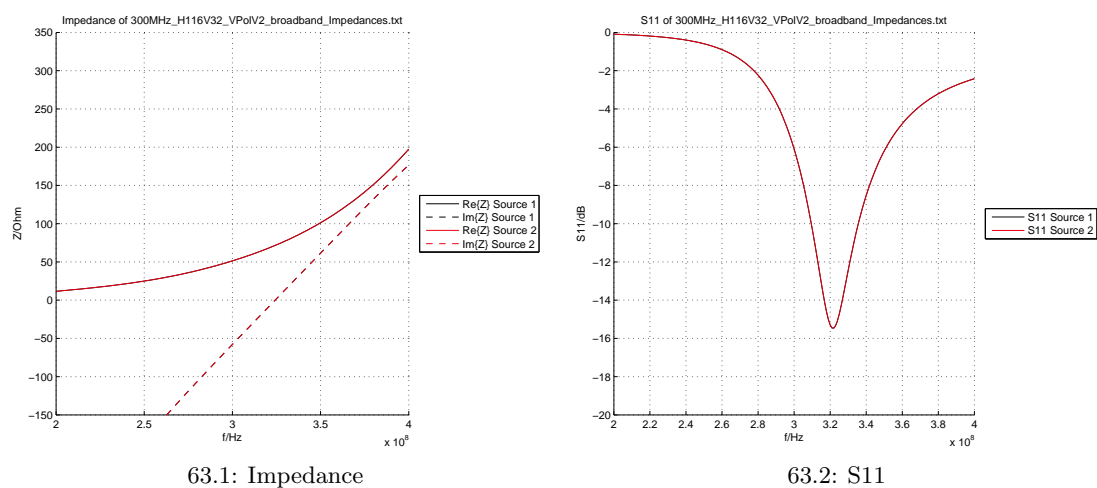
Figure 63: Results from FEKO 300MHz H116V32 VPolV2

### C.1.3   450MHz H118V35 VPolV4



64.1: Impedance



64.2: S11
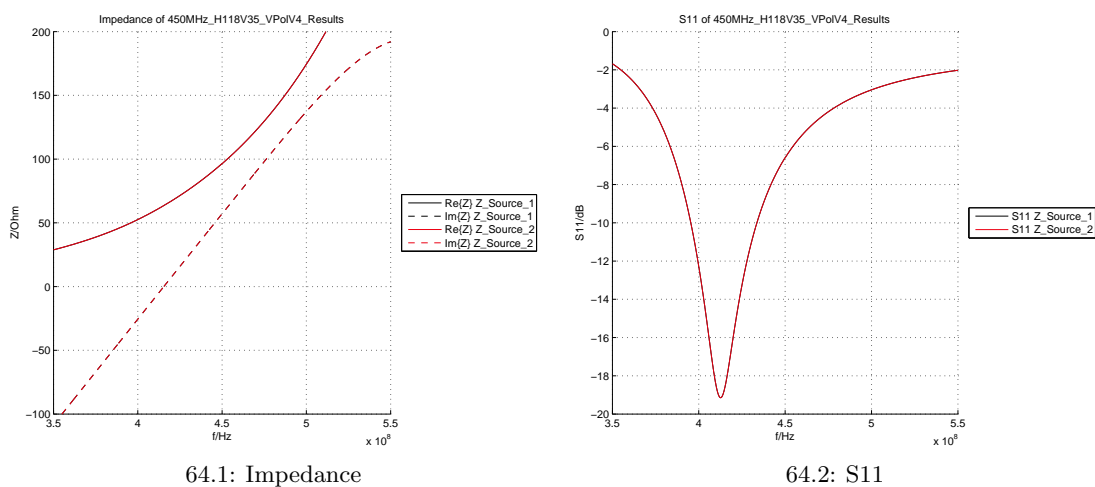
Figure 64: Results from SEMCAD 450MHz H118V35 VPolV4



65.1: Impedance



65.2: S11
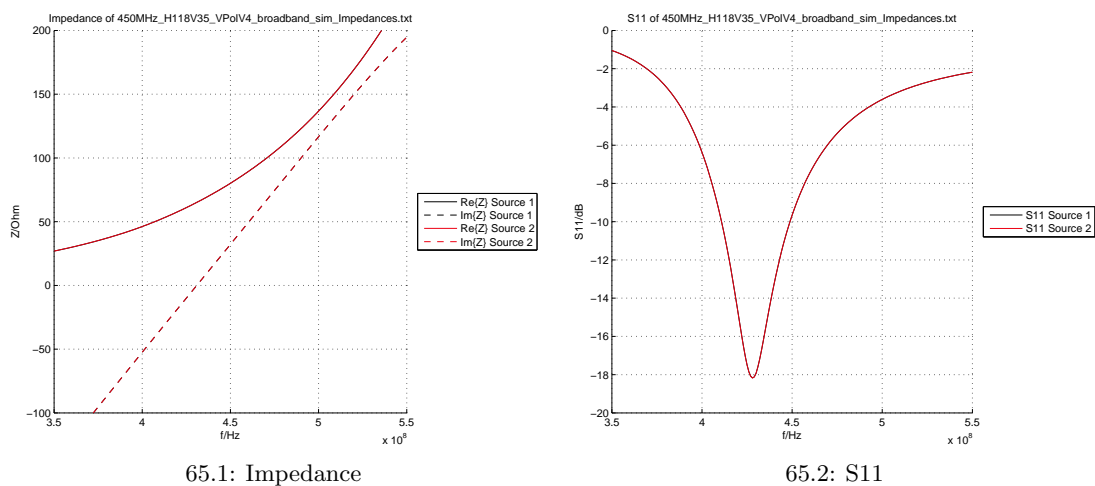
Figure 65: Results from FEKO 450MHz H118V35 VPolV4

### C.1.4    450MHz H180V19 VPolV4
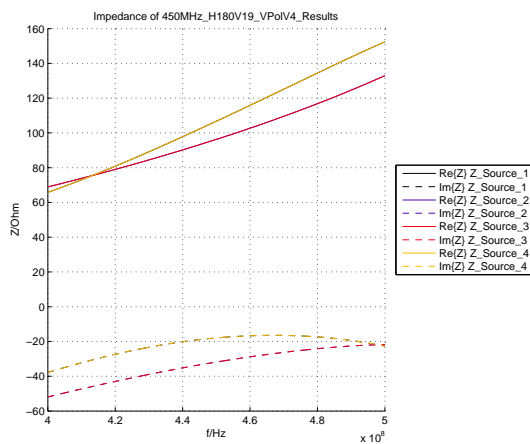


66.1: Impedance
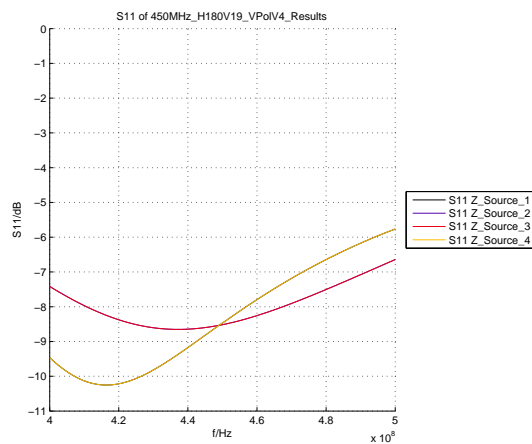
66.2: S11

Figure 66: Results from SEMCAD 450MHz H180V19 VPolV4
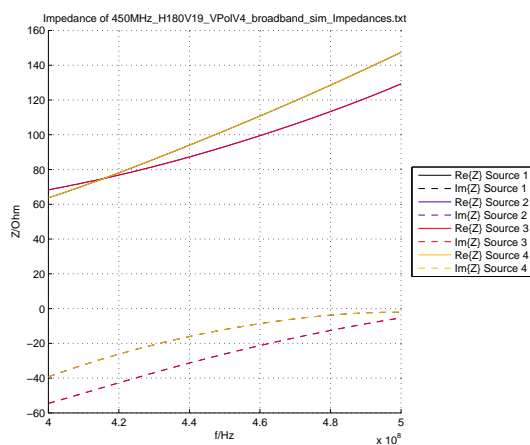


67.1: Impedance
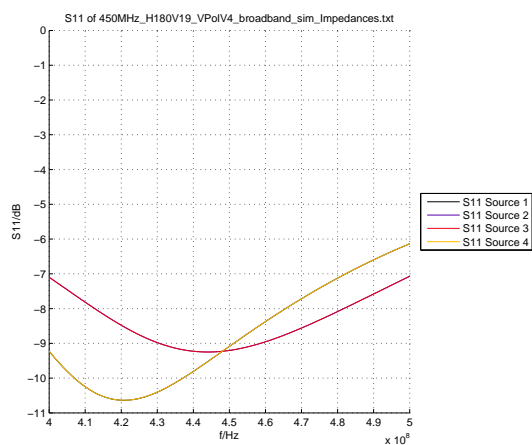
67.2: S11

Figure 67: Results from FEKO 450MHz H180V19 VPolV4

### C.1.5 900MHz H65V7 X45V4



68.1: Impedance

68.2: S11
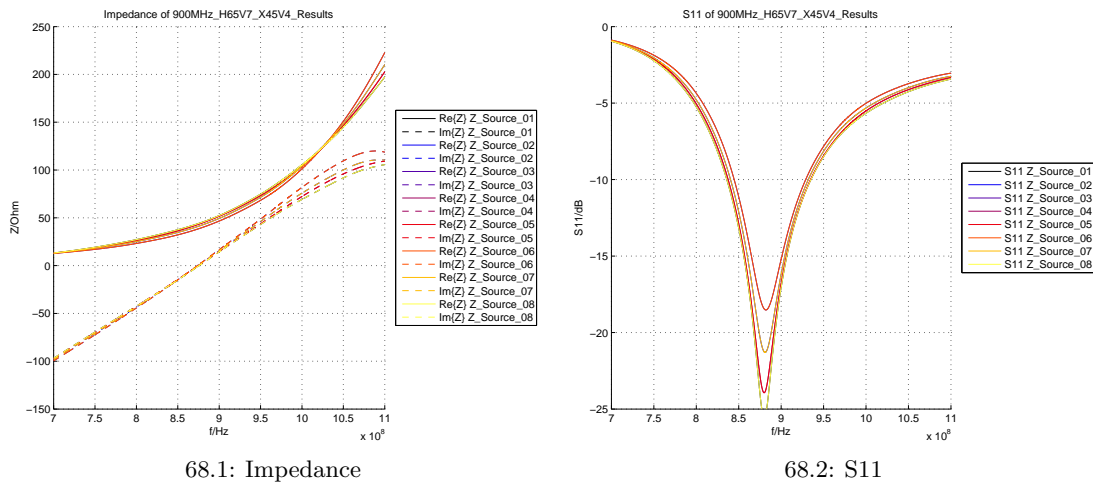
Figure 68: Results from SEMCAD 900MHz H65V7 X45V4



69.1: Impedance

69.2: S11
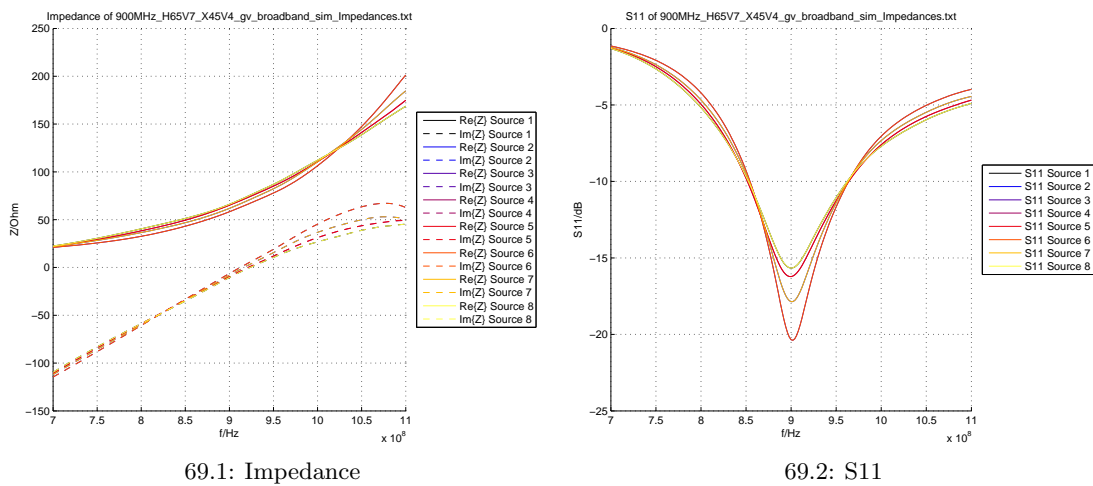
Figure 69: Results from FEKO 900MHz H65V7 X45V4

### C.1.6   900MHz H90V9 VPolV7



70.1: Impedance                                      70.2: S11
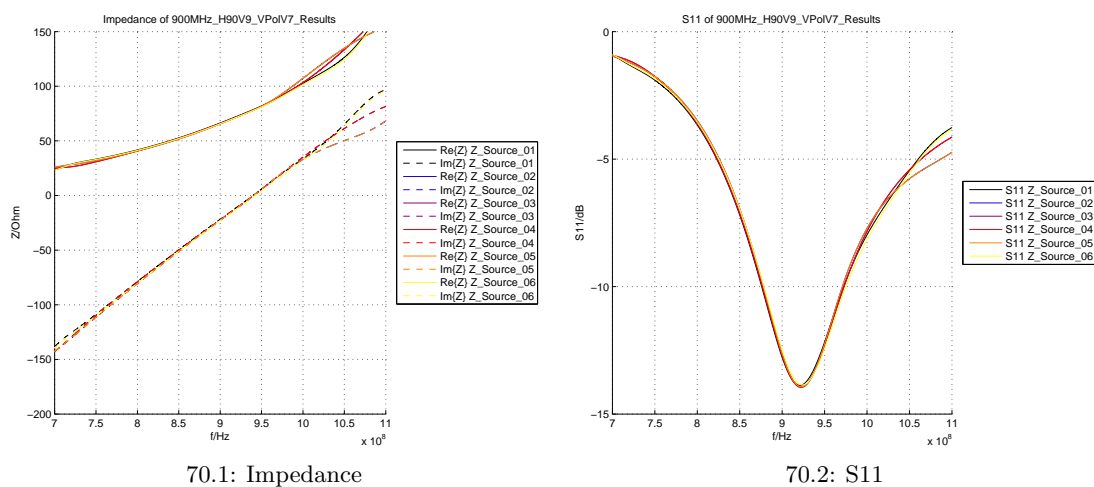
Figure 70: Results from SEMCAD 900MHz H90V9 VPolV7



71.1: Impedance                                      71.2: S11
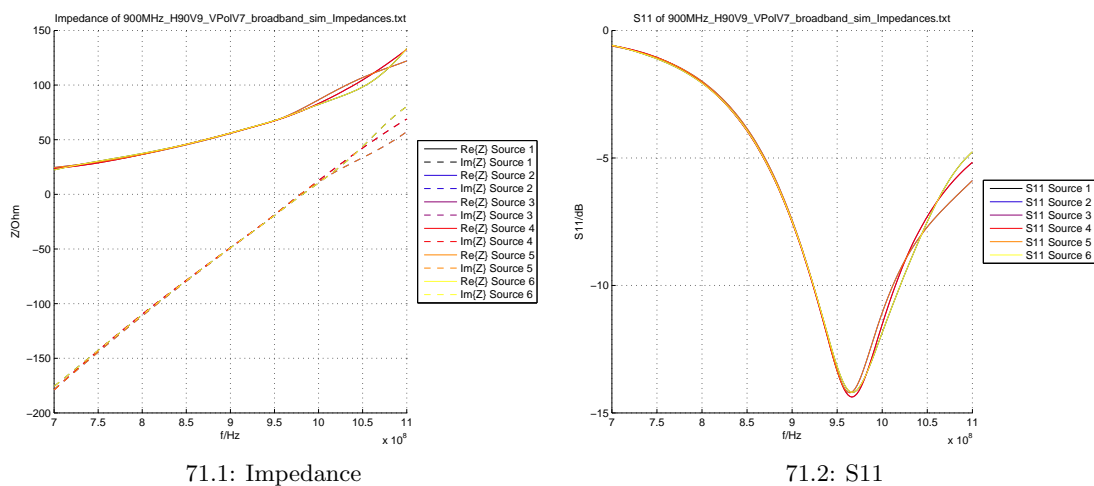
Figure 71: Results from FEKO 900MHz H90V9 VPolV7

### C.1.7    2100MHz H65V7 OutdoorXPolV3
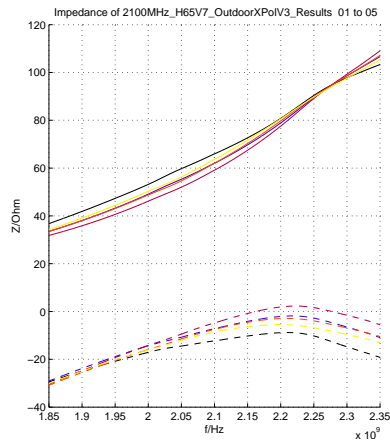
### Elements 1 to 5



72.1: Impedance
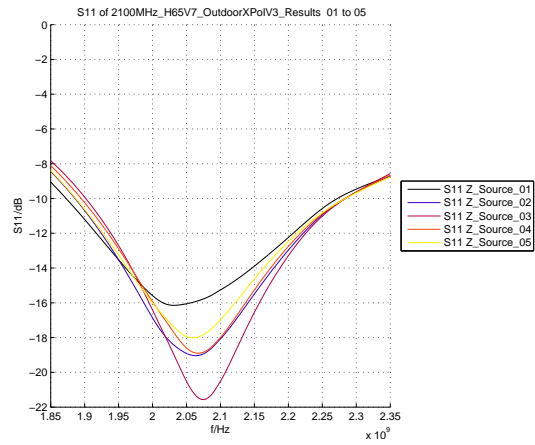
72.2: S11

Figure 72: Results from SEMCAD 2100MHz H65V7 OutdoorXPolV3, elements 1 to 5
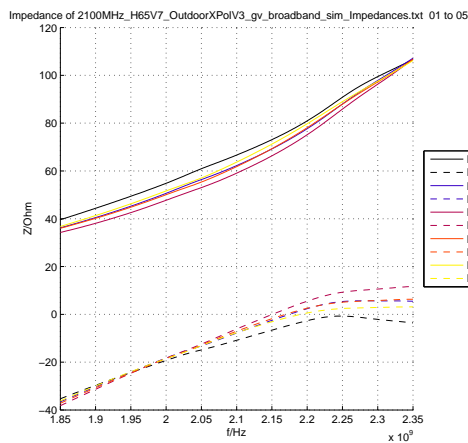


73.1: Impedance
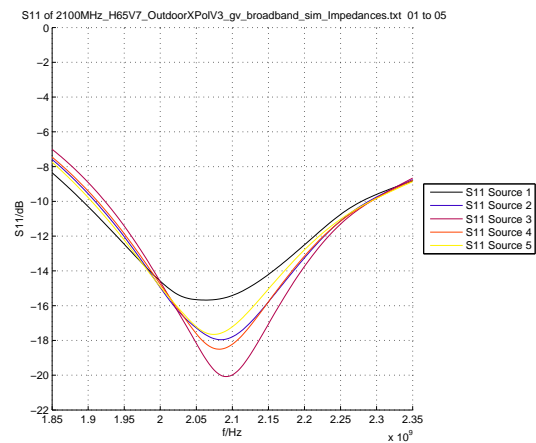
73.2: S11

Figure 73: Results from FEKO 2100MHz H65V7 OutdoorXPolV3, elements 1 to 5

**Elements 6 to 10**
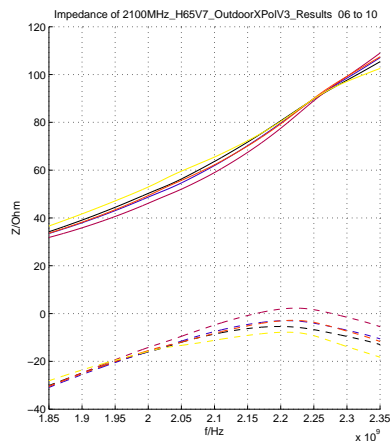


74.1: Impedance
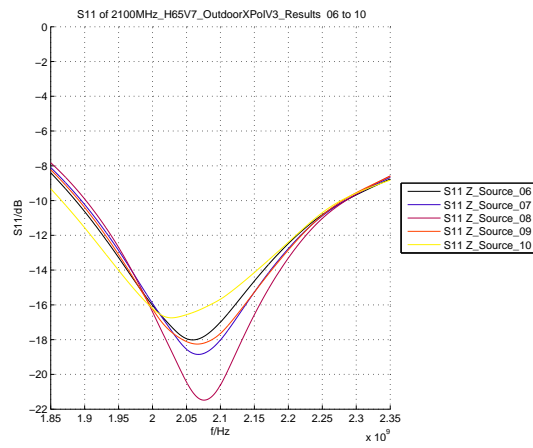
74.2: S11

Figure 74: Results from SEMCAD 2100MHz H65V7 OutdoorXPolV3, elements 6 to 10
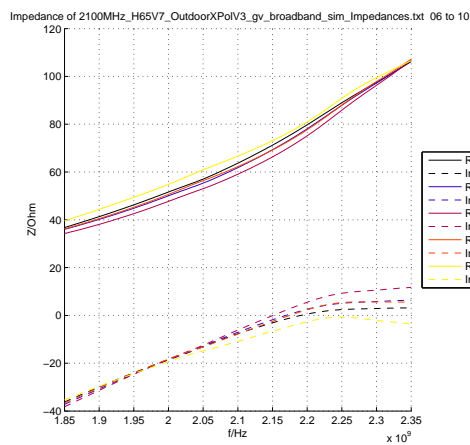


75.1: Impedance
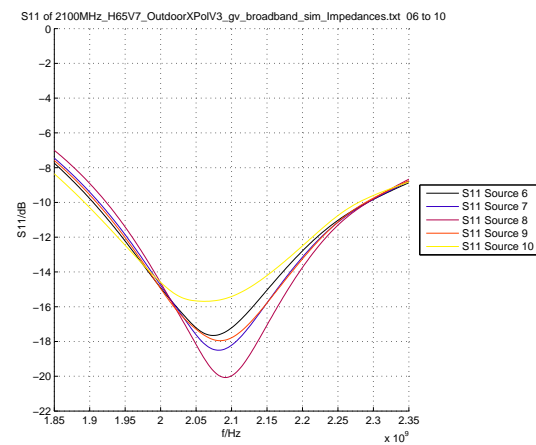
75.2: S11

Figure 75: Results from FEKO 2100MHz H65V7 OutdoorXPolV3, elements 6 to 10

### C.1.8   2100MHz H90V80 IndoorVPolV4



76.1: Impedance                                       76.2: S11
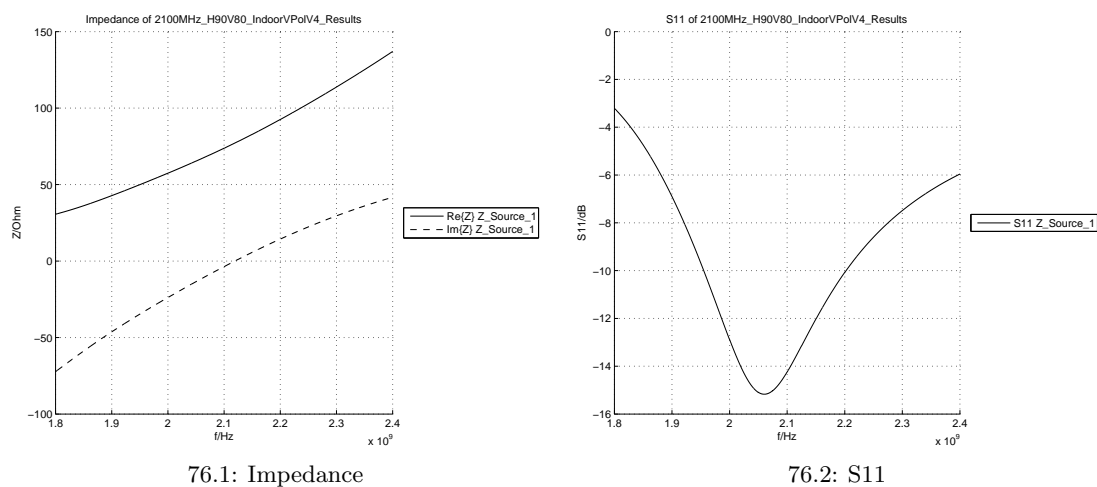
Figure 76: Results from SEMCAD 2100MHz H90V80 IndoorVPolV4



77.1: Impedance                                       77.2: S11
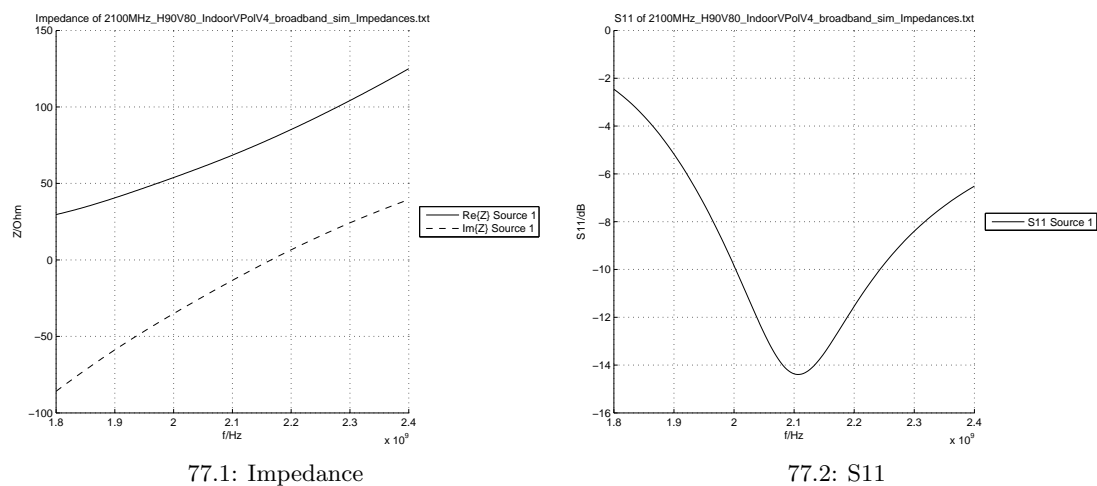
Figure 77: Results from FEKO 2100MHz H90V80 IndoorVPolV4

### C.1.9    3500MHz H18V18 VPol CPEV4

**Elements 1 to 8**



78.1: Impedance

78.2: S11
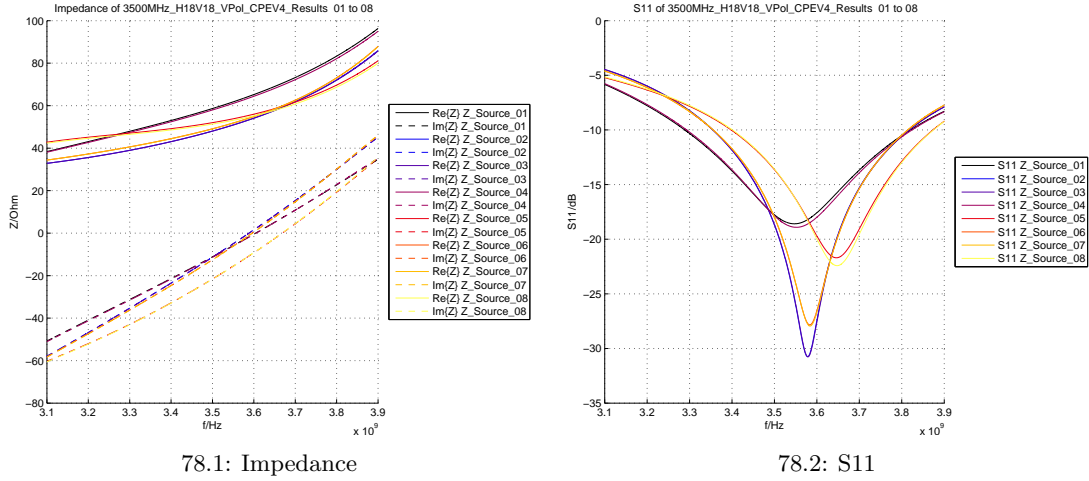
Figure 78: Results from SEMCAD 3500MHz H18V18 VPol CPEV4, elements 1 to 8



79.1: Impedance

79.2: S11
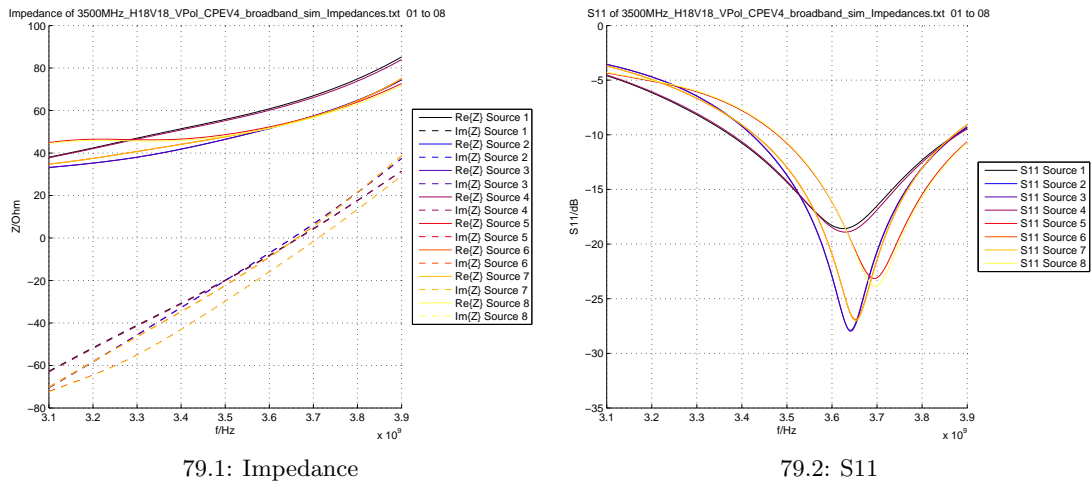
Figure 79: Results from FEKO 3500MHz H18V18 VPol CPEV4, elements 1 to 8

**Elements 9 to 16**



80.1: Impedance

80.2: S11
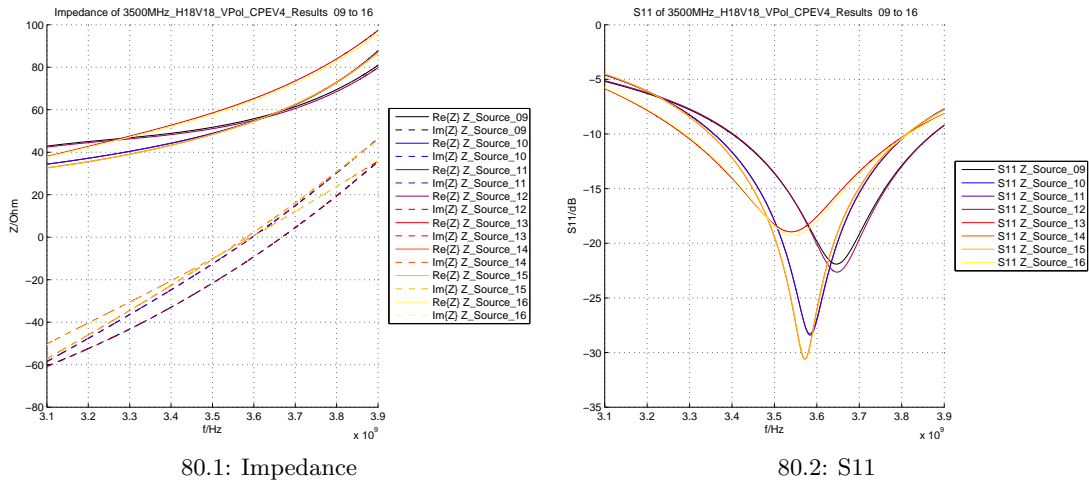
Figure 80: Results from SEMCAD 3500MHz H18V18 VPol CPEV4, elements 9 to 16



81.1: S11
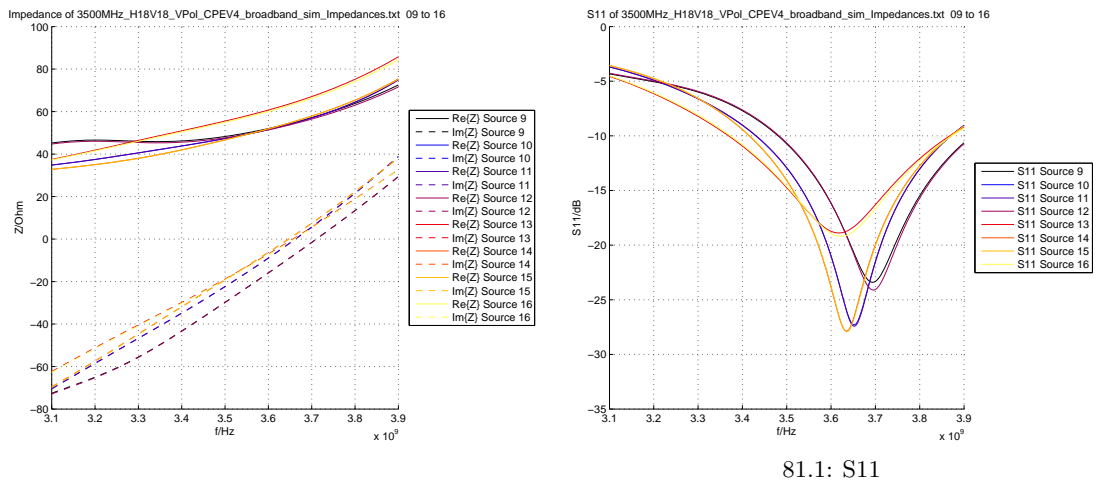
Figure 81: Results from FEKO 3500MHz H18V18 VPol CPEV4, elements 9 to 16

## C.1.10    3500MHz H65V9 VPol BTSV3
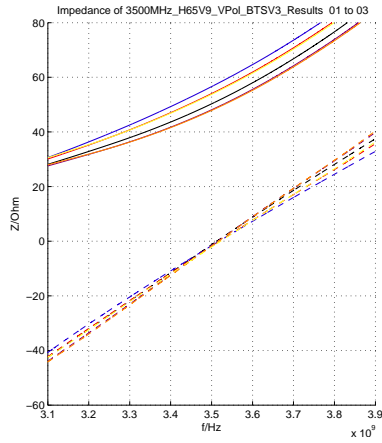
## Elements 1 to 6



82.1: Impedance
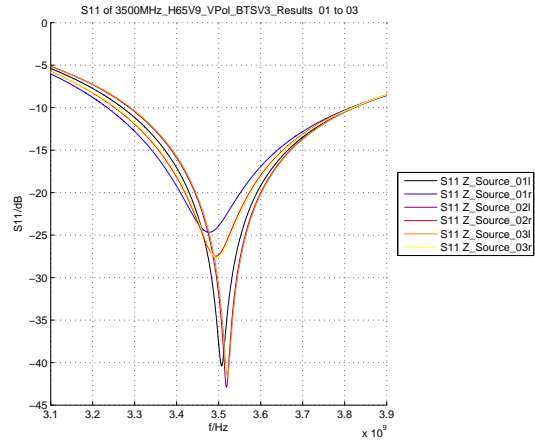
82.2: S11

Figure 82: Results from SEMCAD 3500MHz H65V9 VPol BTSV3, elements 1 to 6
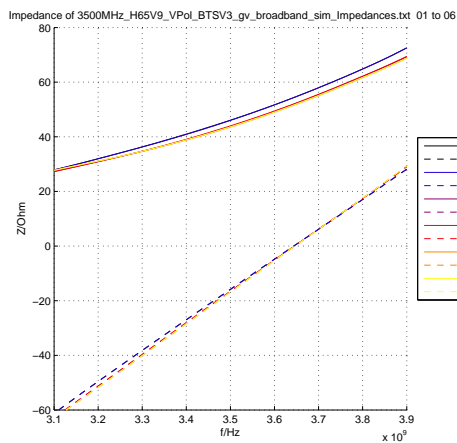


83.1: Impedance
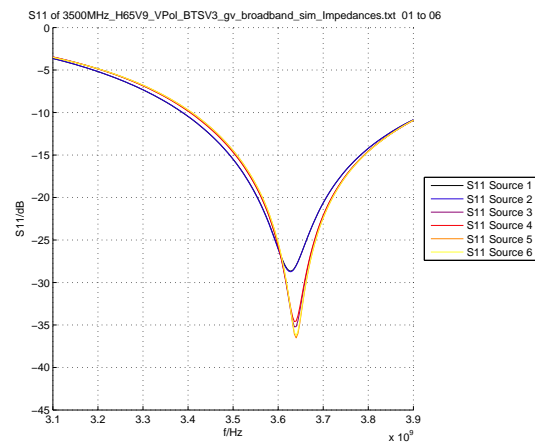
83.2: S11

Figure 83: Results from FEKO 3500MHz H65V9 VPol BTSV3, elements 1 to 6

**Elements 7 to 12**
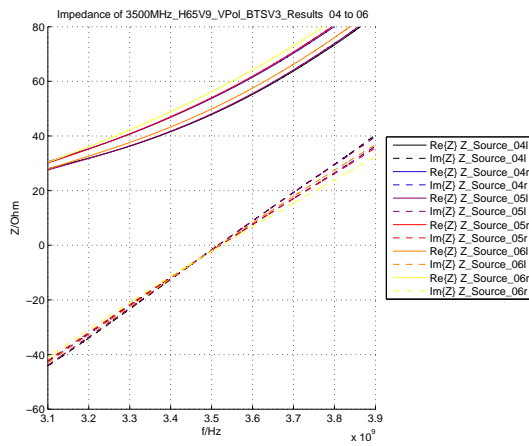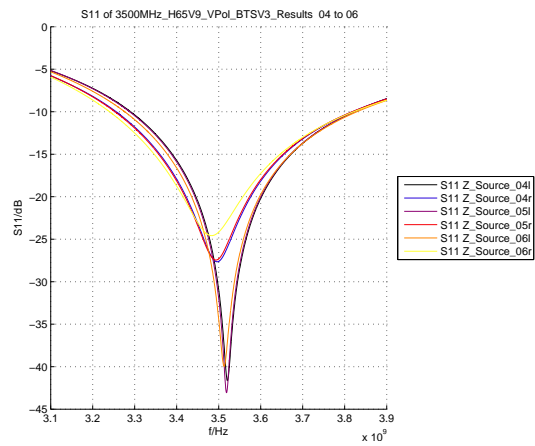


84.1: Impedance                                      84.2: S11

Figure 84: Results from SEMCAD 3500MHz H65V9 VPol BTSV3, elements 7 to 12
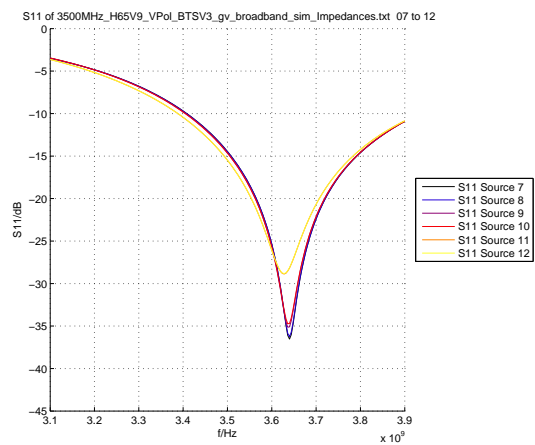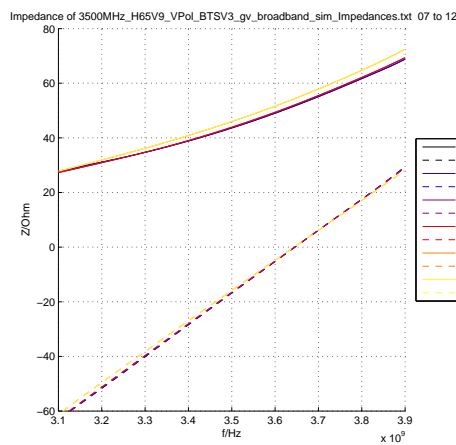


85.1: S11

Figure 85: Results from FEKO 3500MHz H65V9 VPol BTSV3, elements 7 to 12

### C.1.11  5000MHz H65V35 VPol DirectionalV5



86.1: Impedance

86.2: S11
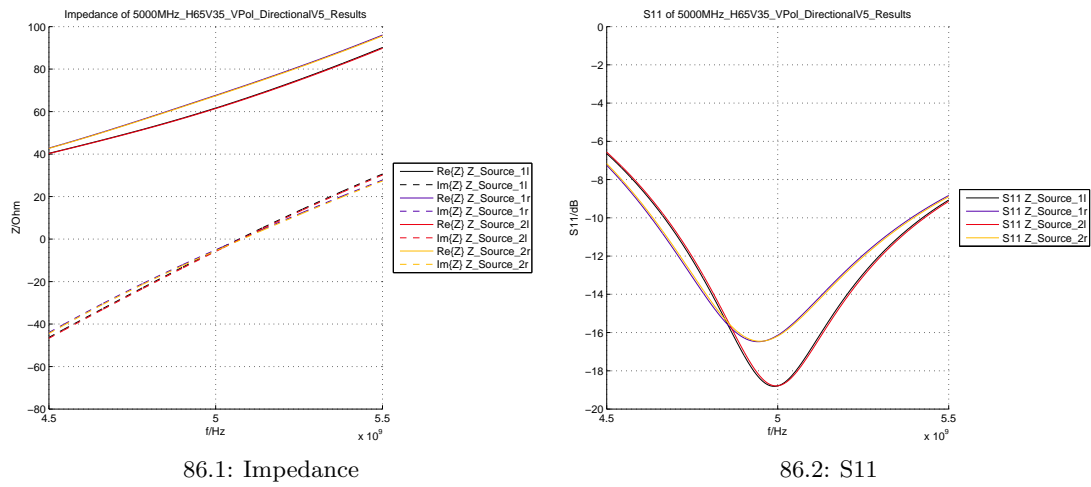
Figure 86: Results from SEMCAD 5000MHz H65V35 VPol DirectionalV5



87.1: Impedance

87.2: S11
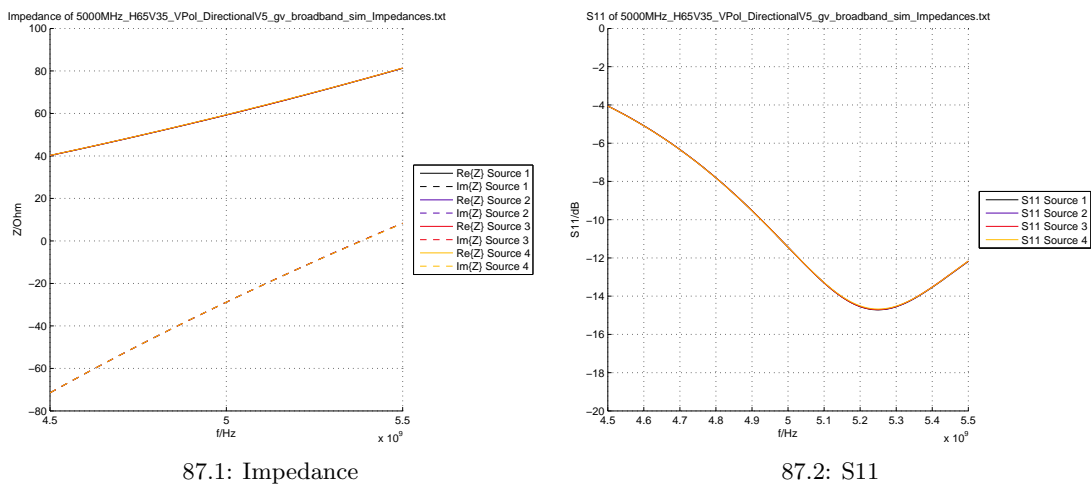
Figure 87: Results from FEKO 5000MHz H65V35 VPol DirectionalV5

### C.1.12  5000MHz H360V7 VPol OmniV4



88.1: Impedance                                           88.2: S11
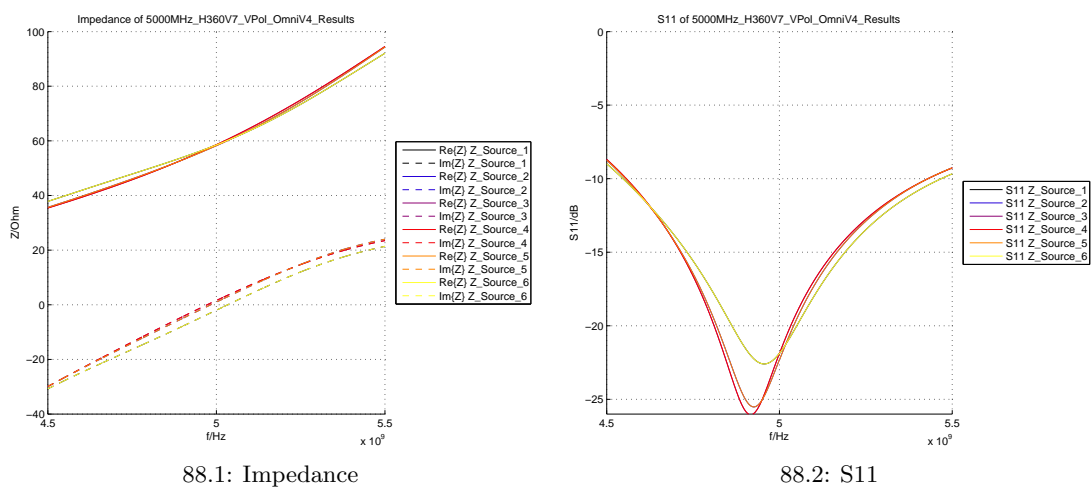
Figure 88: Results from SEMCAD 5000MHz H360V7 VPol OmniV4



89.1: Impedance                                           89.2: S11
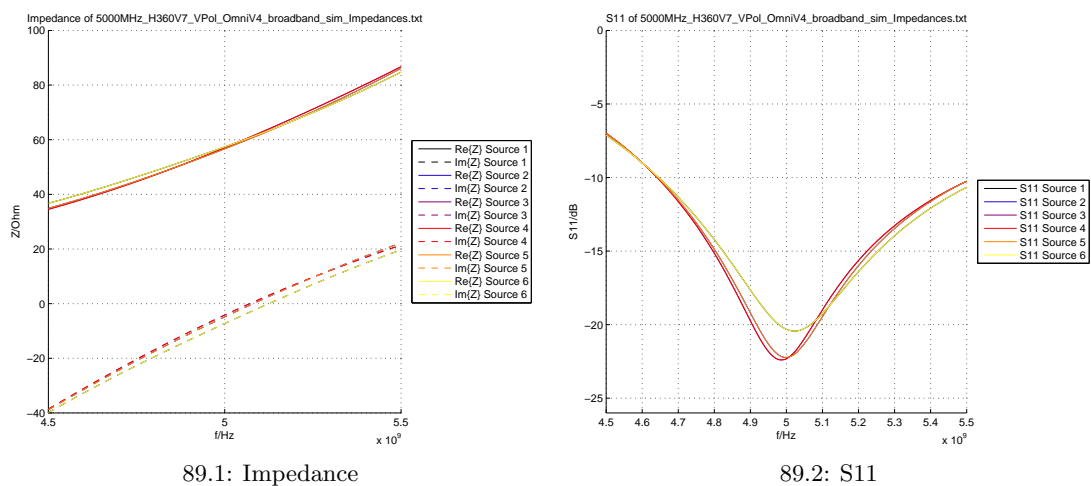
Figure 89: Results from FEKO 5000MHz H360V7 VPol OmniV4

## C.2    E- and H-fields

In this subsection, we compare the E- and H-field in planes parallel to the antennas, at distances of 10 mm, 50 mm, 300 mm, and 500 mm. The distance is calculated between the furthest point of the antenna and the plane. The planes are 1.9 m high and 0.6 m wide. The rms fields are normalized to an input power of 1 W. In SEMCAD X, this is directly done by extracting the value of the total input power. In Feko, the input power is computed by adding up the input power of every one of the sources:

$$P_{tot} = \sum_i P_i = 0.5 \sum_i \frac{|V_i|^2}{|Z_i|},$$

(69)

where $V_i$ is the voltage specified by the document describing the modelling of the antennas and $Z_i$ is the impedance of the source, displayed in subsection C.1.

### C.2.1    300MHz H65V64VPolV5



90.1: 10 mm        90.2: 50 mm        90.3: 300 mm        90.4: 500 mm
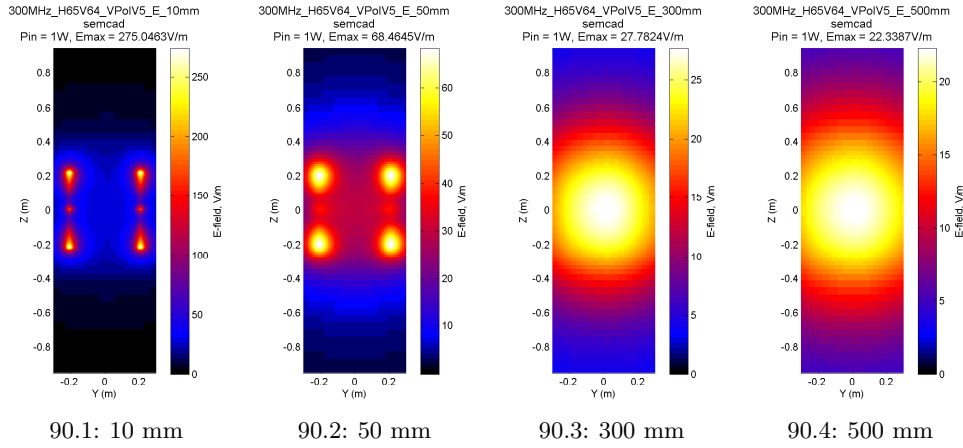
Figure 90: E-fields from SEMCAD 300MHz H65V64VPolV5



91.1: 10 mm        91.2: 50 mm        91.3: 300 mm        91.4: 500 mm
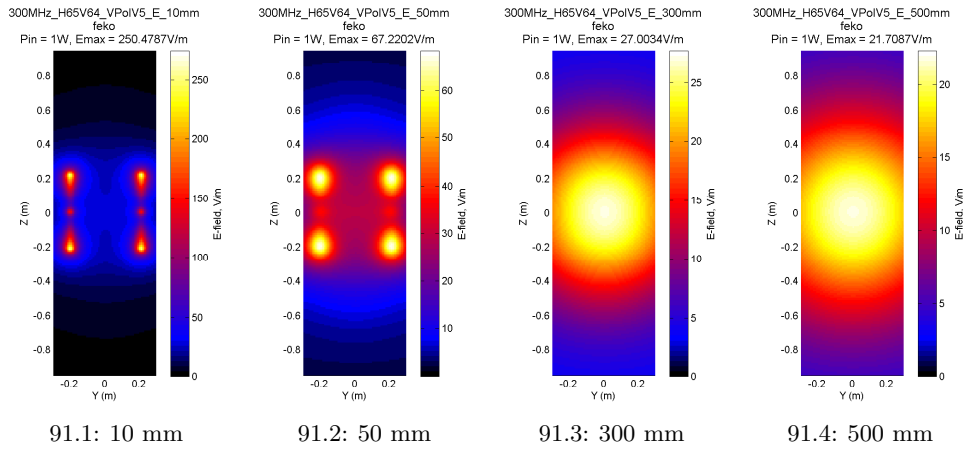
Figure 91: E-fields from FEKO 300MHz H65V64VPolV5

92.1: 10 mm    92.2: 50 mm    92.3: 300 mm    92.4: 500 mm
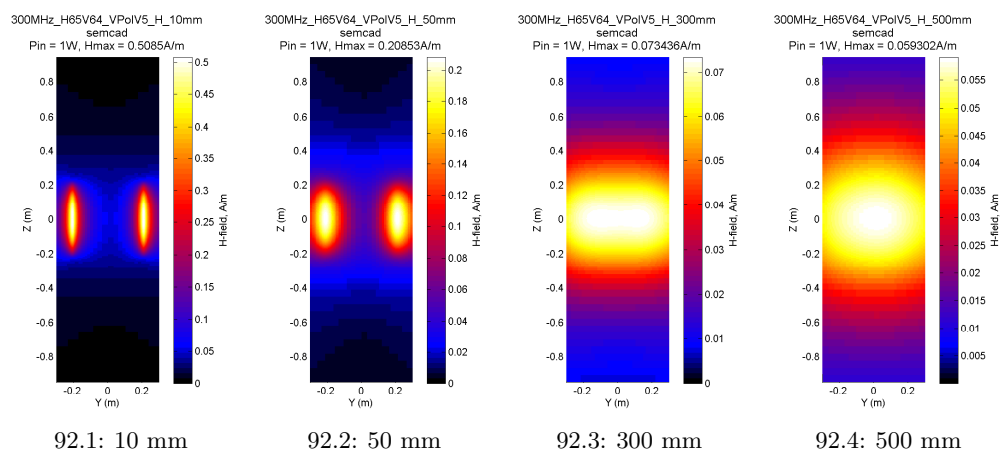
Figure 92: H-fields from SEMCAD 300MHz H65V64VPolV5



93.1: 10 mm    93.2: 50 mm    93.3: 300 mm    93.4: 500 mm
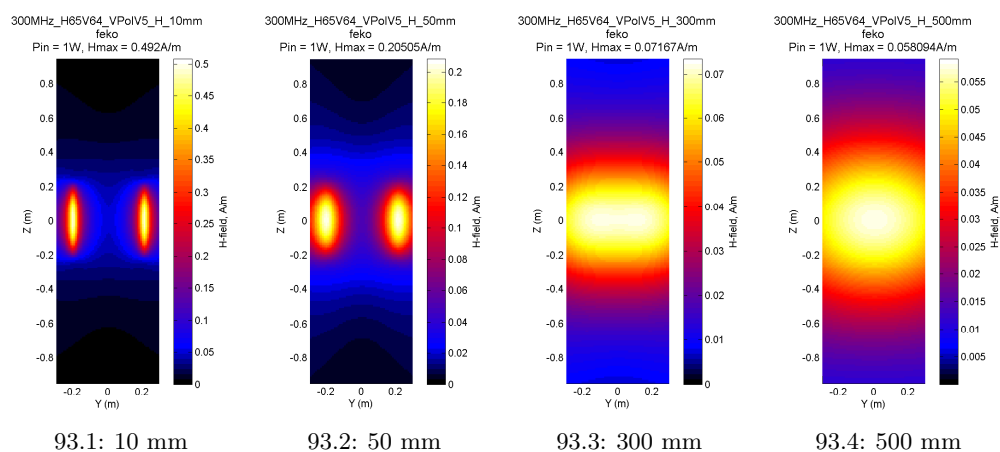
Figure 93: H-fields from FEKO 300MHz H65V64VPolV5

## C.2.2    300MHz H116V32 VPolV2



94.1: 10 mm          94.2: 50 mm          94.3: 300 mm          94.4: 500 mm
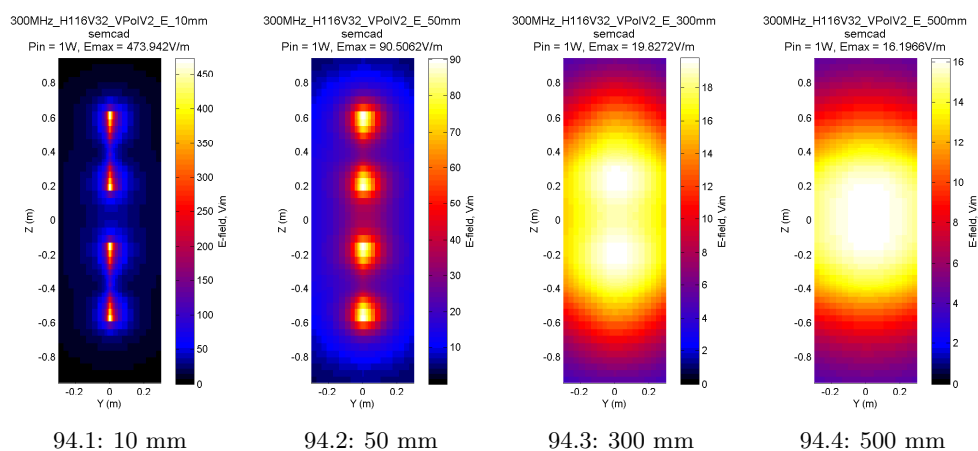
Figure 94: E-fields from SEMCAD 300MHz H116V32 VPolV2



95.1: 10 mm          95.2: 50 mm          95.3: 300 mm          95.4: 500 mm
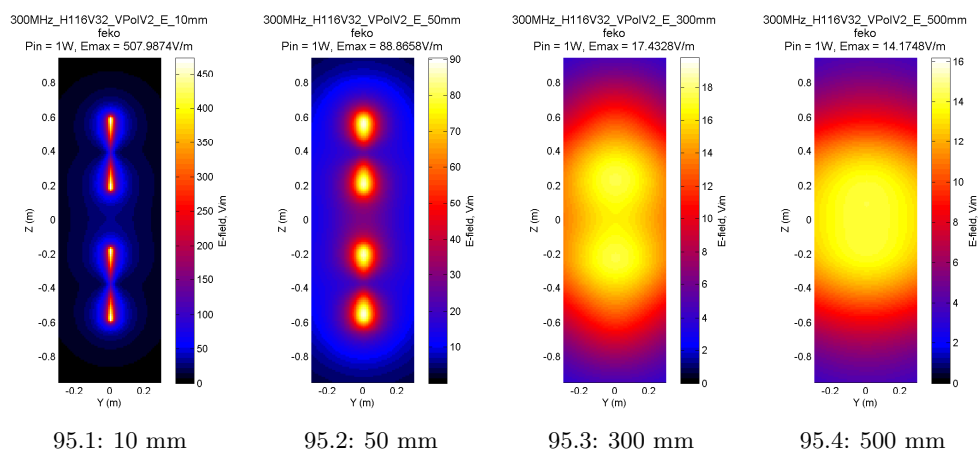
Figure 95: E-fields from FEKO 300MHz H116V32 VPolV2

96.1: 10 mm          96.2: 50 mm          96.3: 300 mm          96.4: 500 mm
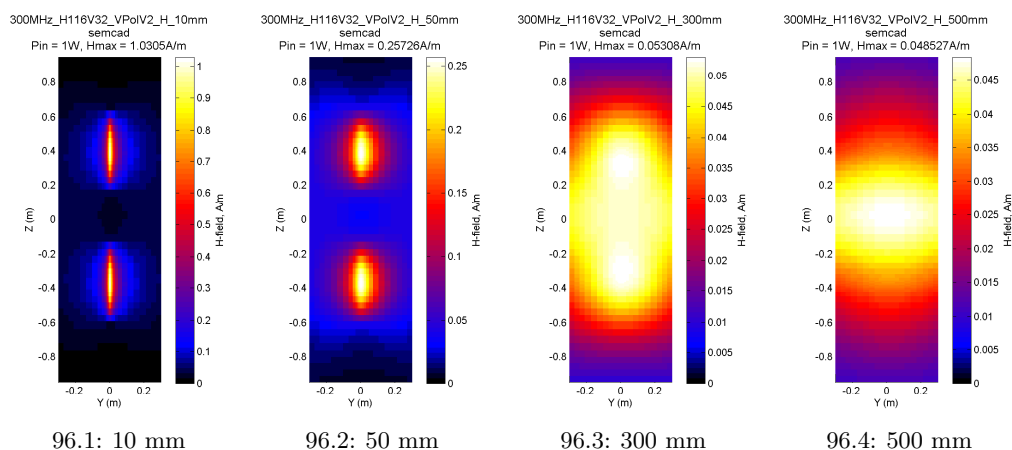
Figure 96: H-fields from SEMCAD 300MHz H116V32 VPolV2



97.1: 10 mm          97.2: 50 mm          97.3: 300 mm          97.4: 500 mm
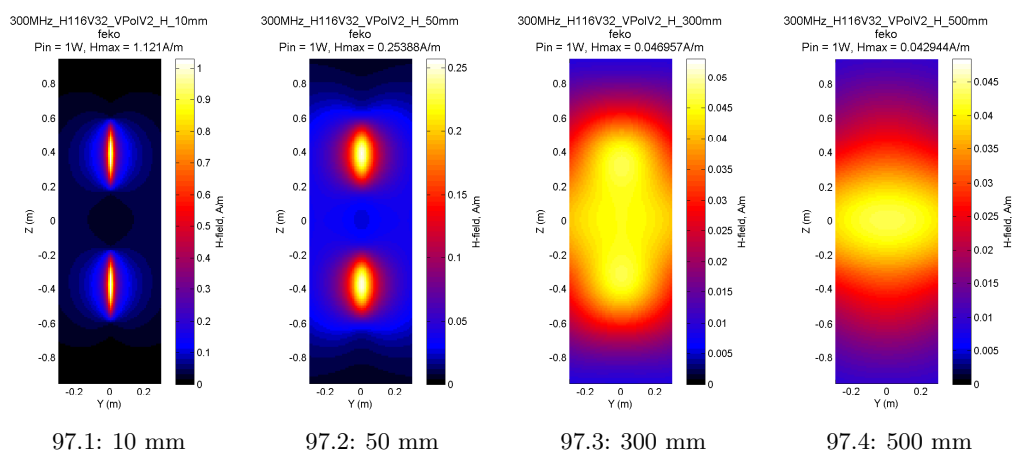
Figure 97: H-fields from FEKO 300MHz H116V32 VPolV2

### C.2.3 450MHz H118V35 VPolV4



98.1: 10 mm 98.2: 50 mm 98.3: 300 mm 98.4: 500 mm
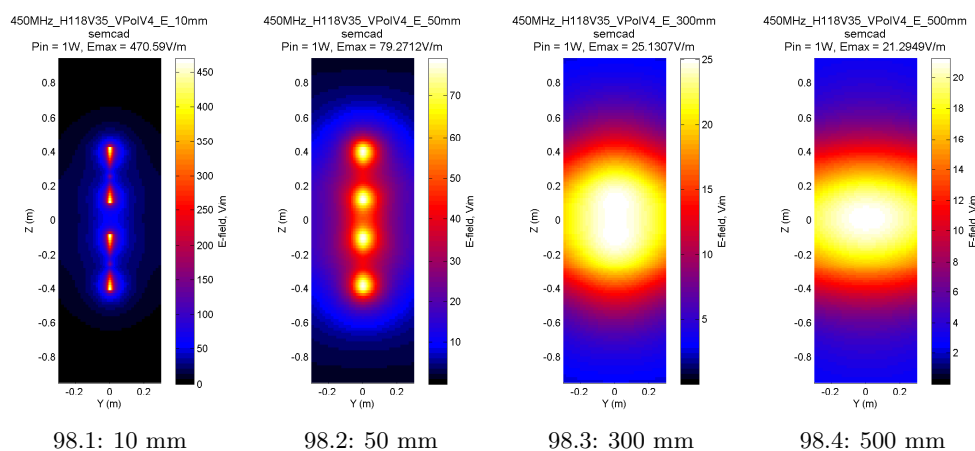
Figure 98: E-fields from SEMCAD 450MHz H118V35 VPolV4



99.1: 10 mm 99.2: 50 mm 99.3: 300 mm 99.4: 500 mm
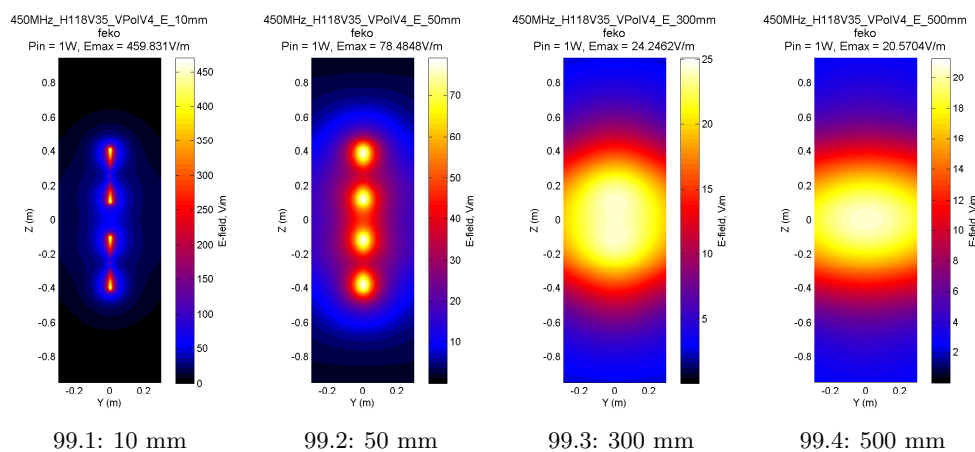
Figure 99: E-fields from FEKO 450MHz H118V35 VPolV4

100.1: 10 mm          100.2: 50 mm          100.3: 300 mm          100.4: 500 mm
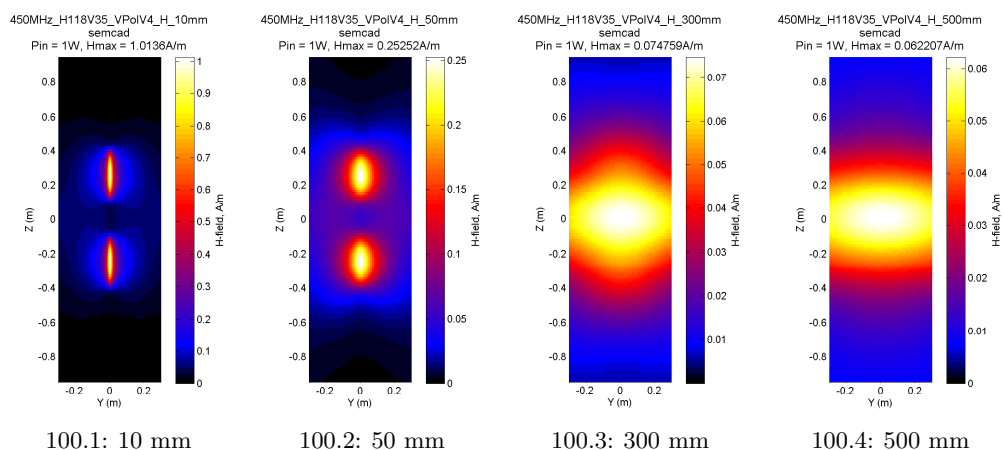
Figure 100: H-fields from SEMCAD 450MHz H118V35 VPolV4



101.1: 10 mm          101.2: 50 mm          101.3: 300 mm          101.4: 500 mm
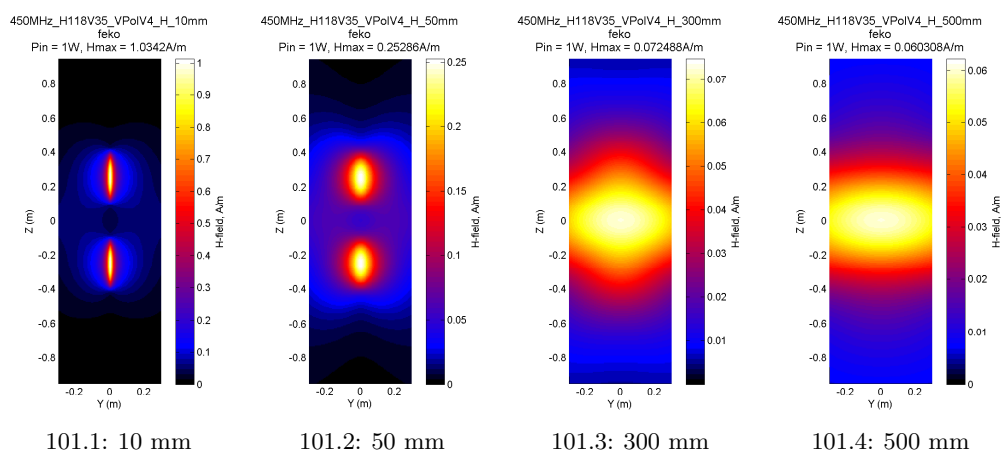
Figure 101: H-fields from FEKO 450MHz H118V35 VPolV4

### C.2.4 450MHz H180V19 VPolV4



| 102.1: 10 mm | 102.2: 50 mm | 102.3: 300 mm | 102.4: 500 mm |
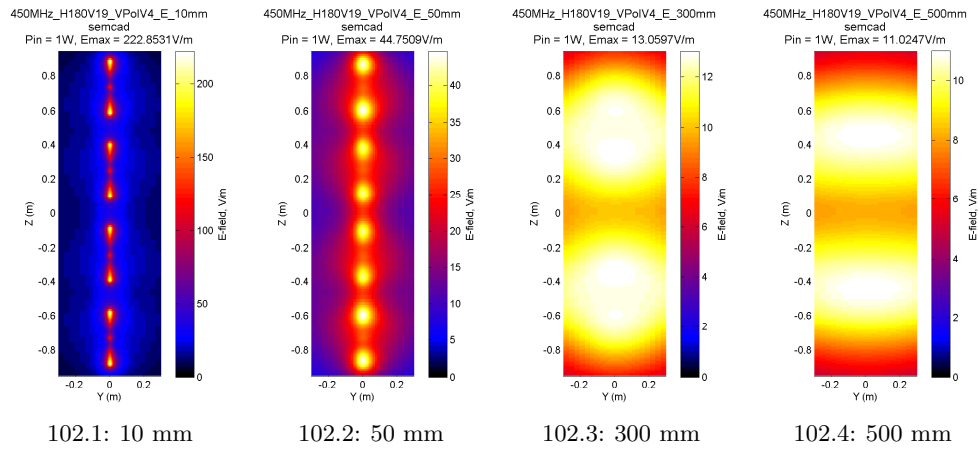
Figure 102: E-fields from SEMCAD 450MHz H180V19 VPolV4



| 103.1: 10 mm | 103.2: 50 mm | 103.3: 300 mm | 103.4: 500 mm |
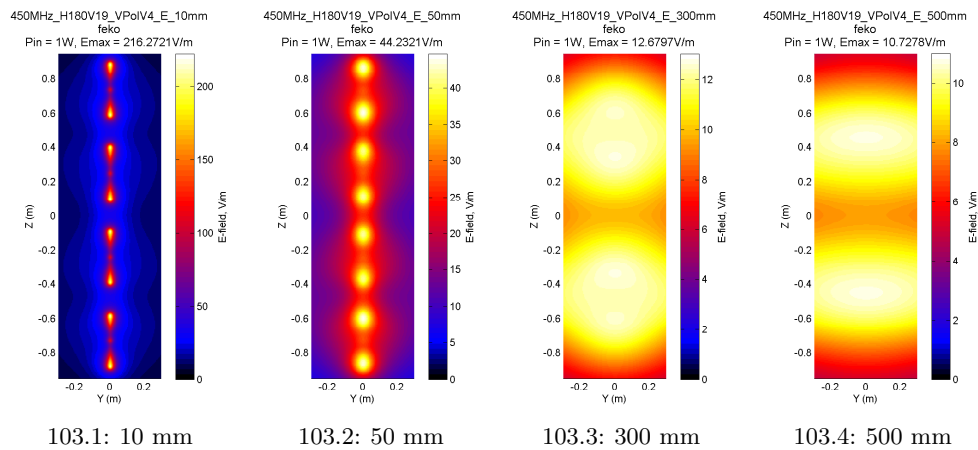
Figure 103: E-fields from FEKO 450MHz H180V19 VPolV4

104.1: 10 mm          104.2: 50 mm          104.3: 300 mm          104.4: 500 mm
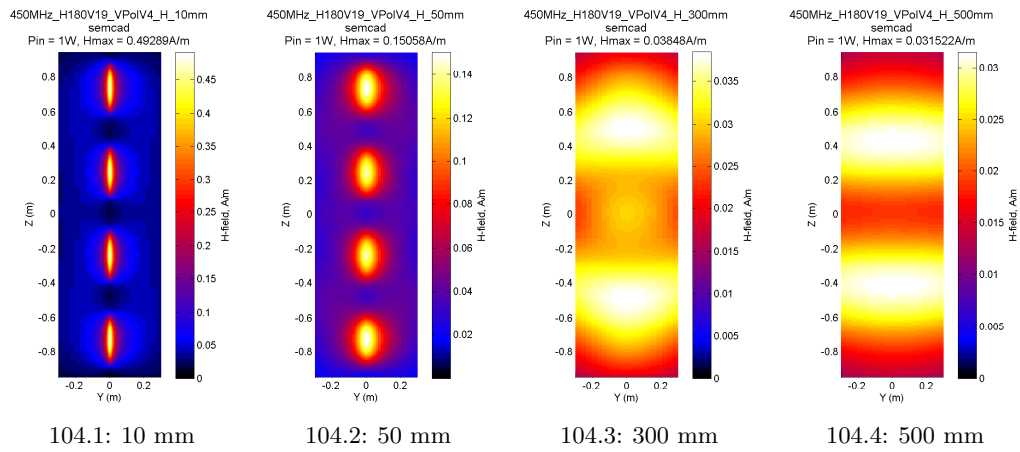
Figure 104: H-fields from SEMCAD 450MHz H180V19 VPolV4



105.1: 10 mm          105.2: 50 mm          105.3: 300 mm          105.4: 500 mm
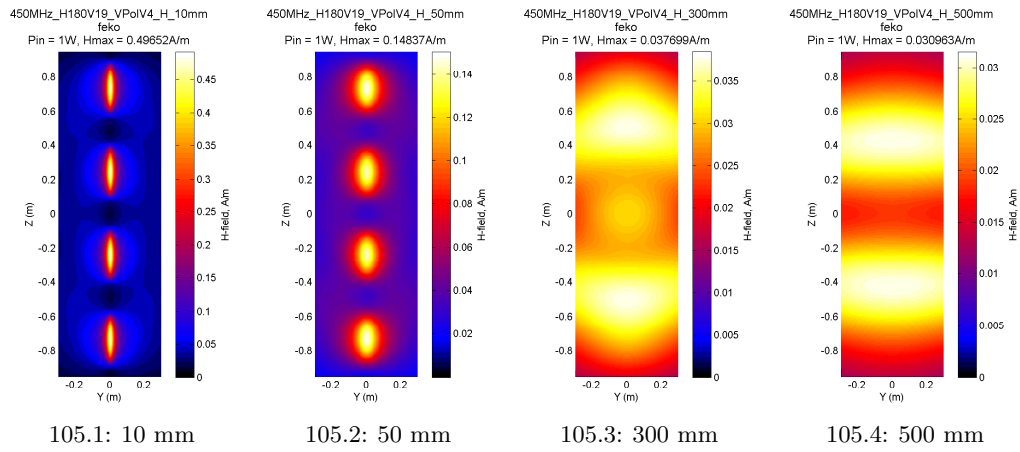
Figure 105: H-fields from FEKO 450MHz H180V19 VPolV4

## C.2.5 900MHz H65V7 X45V4



106.1: 10 mm | 106.2: 50 mm | 106.3: 300 mm | 106.4: 500 mm
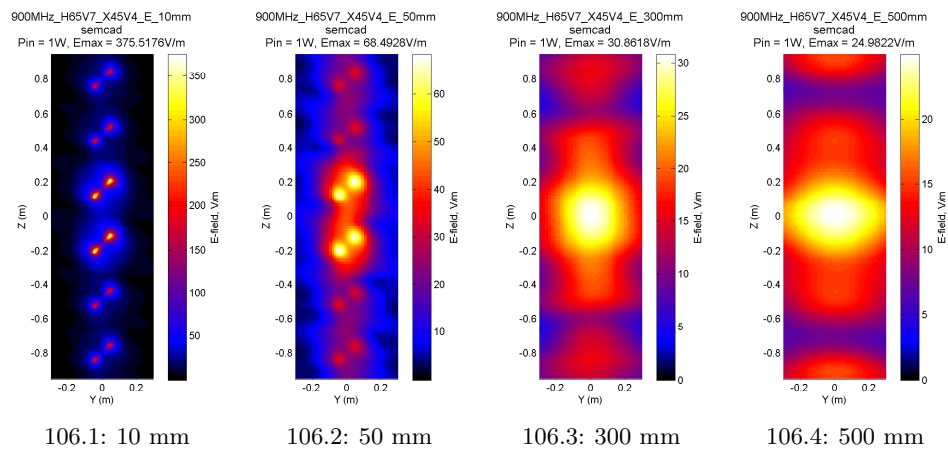
Figure 106: E-fields from SEMCAD 900MHz H65V7 X45V4



107.1: 10 mm | 107.2: 50 mm | 107.3: 300 mm | 107.4: 500 mm
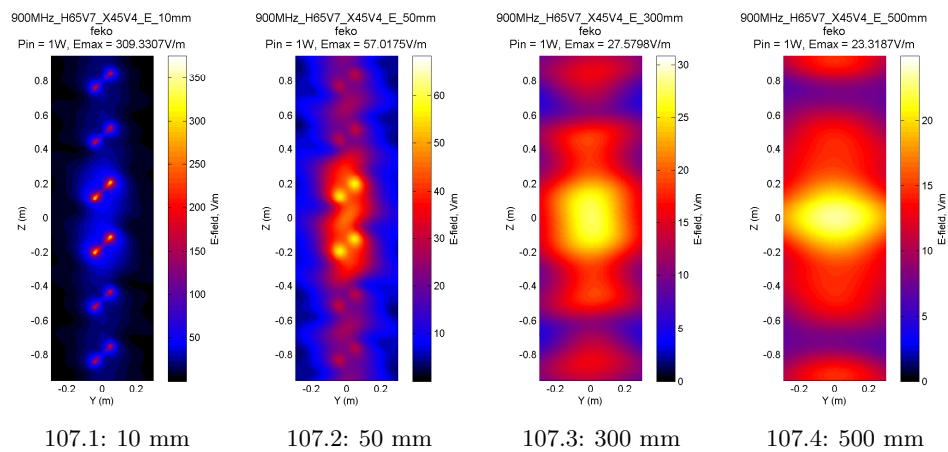
Figure 107: E-fields from FEKO 900MHz H65V7 X45V4

108.1: 10 mm        108.2: 50 mm        108.3: 300 mm        108.4: 500 mm
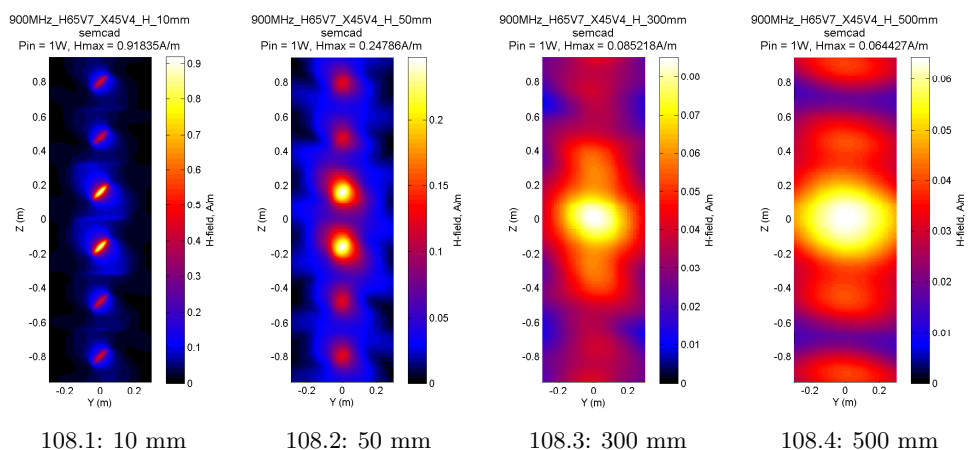
Figure 108: H-fields from SEMCAD 900MHz H65V7 X45V4



109.1: 10 mm        109.2: 50 mm        109.3: 300 mm        109.4: 500 mm
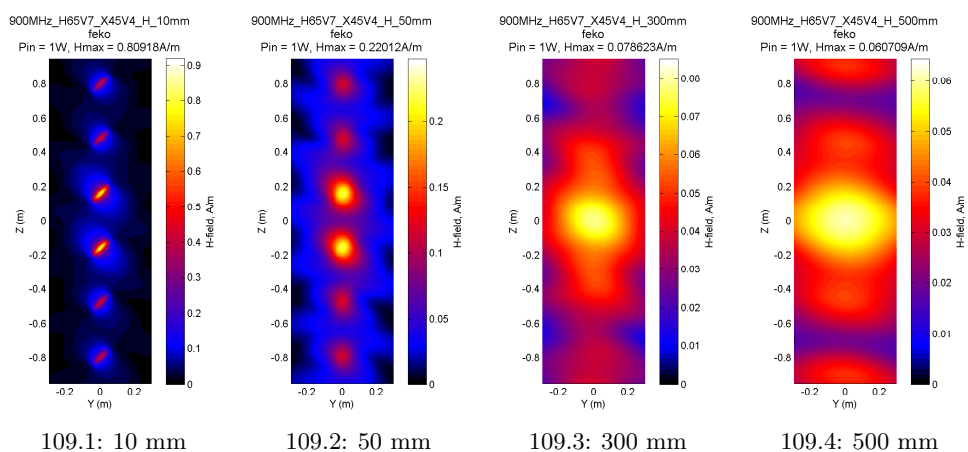
Figure 109: H-fields from FEKO 900MHz H65V7 X45V4

## C.2.6   900MHz H90V9 VPolV7



| 110.1: 10 mm | 110.2: 50 mm | 110.3: 300 mm | 110.4: 500 mm |
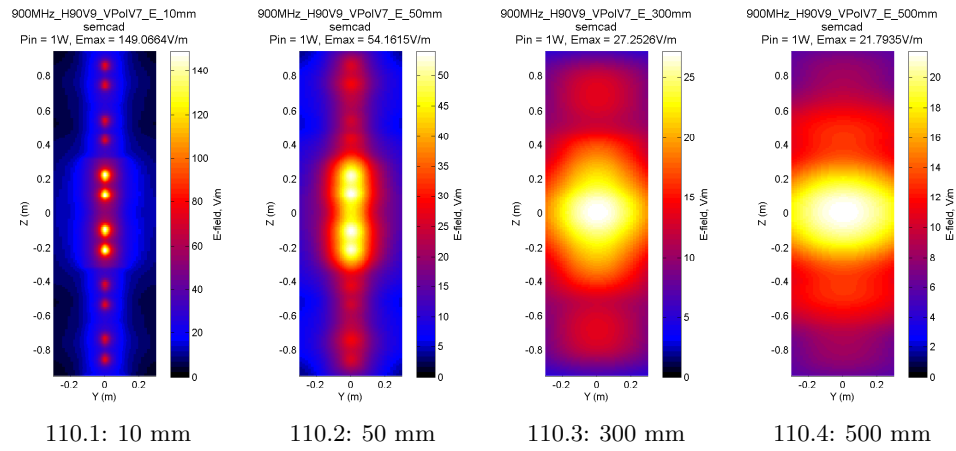
Figure 110: E-fields from SEMCAD 900MHz H90V9 VPolV7



| 111.1: 10 mm | 111.2: 50 mm | 111.3: 300 mm | 111.4: 500 mm |
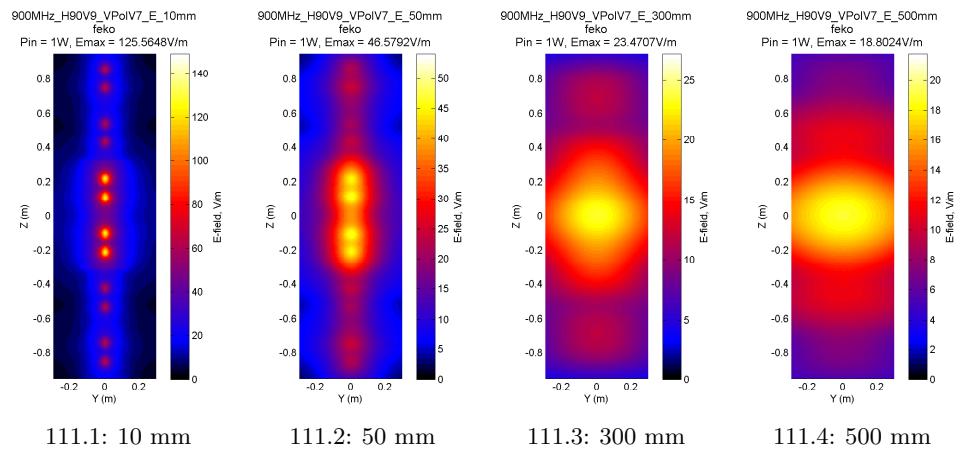
Figure 111: E-fields from FEKO 900MHz H90V9 VPolV7

| 112.1: 10 mm | 112.2: 50 mm | 112.3: 300 mm | 112.4: 500 mm |
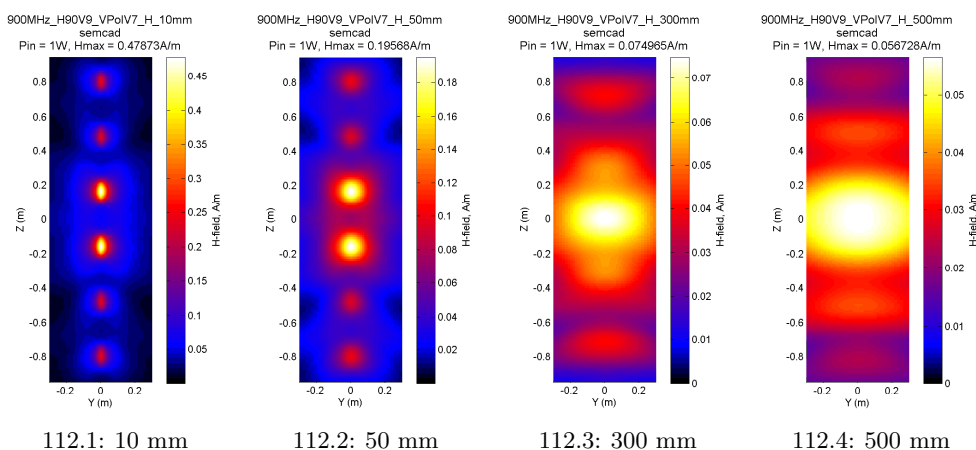
Figure 112: H-fields from SEMCAD 900MHz H90V9 VPolV7



| 113.1: 10 mm | 113.2: 50 mm | 113.3: 300 mm | 113.4: 500 mm |
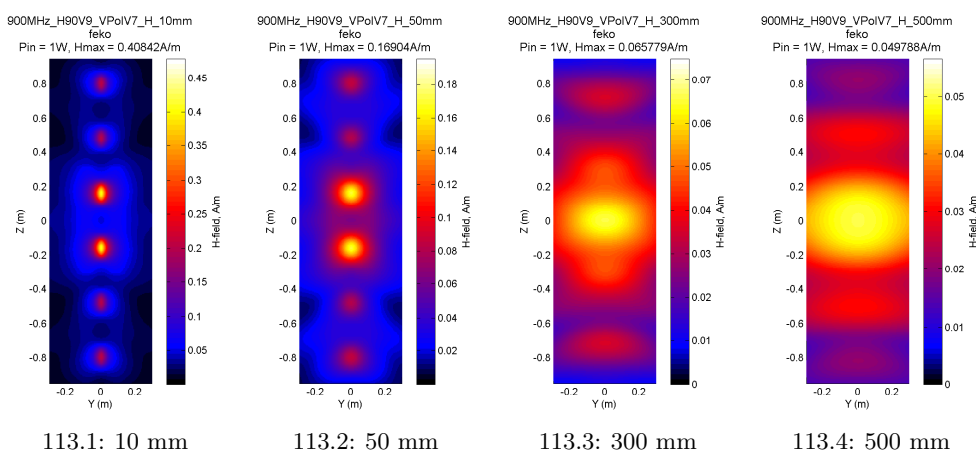
Figure 113: H-fields from FEKO 900MHz H90V9 VPolV7

### C.2.7  2100MHz H65V7 OutdoorXPolV3



114.1: 10 mm    114.2: 50 mm    114.3: 300 mm    114.4: 500 mm
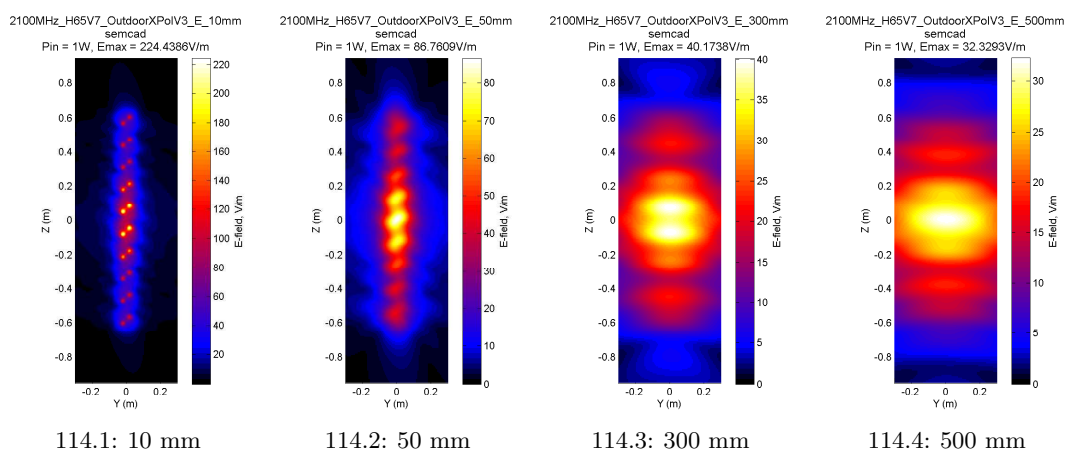
Figure 114: E-fields from SEMCAD 2100MHz H65V7 OutdoorXPolV3



115.1: 10 mm    115.2: 50 mm    115.3: 300 mm    115.4: 500 mm
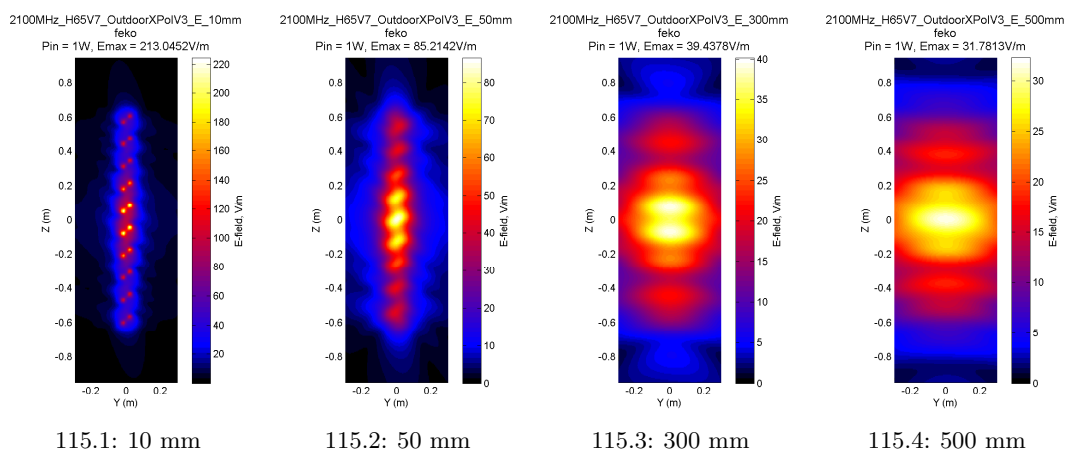
Figure 115: E-fields from FEKO 2100MHz H65V7 OutdoorXPolV3

116.1: 10 mm      116.2: 50 mm      116.3: 300 mm      116.4: 500 mm
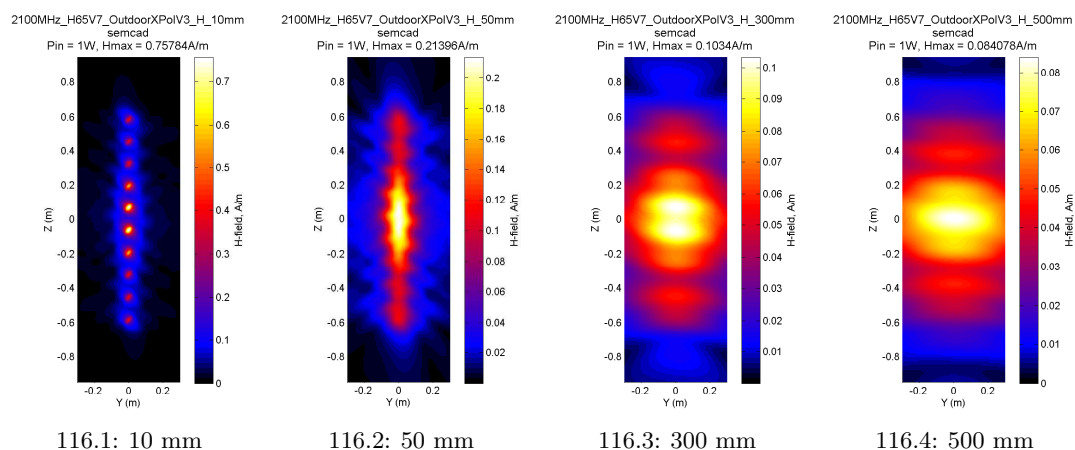
Figure 116: H-fields from SEMCAD 2100MHz H65V7 OutdoorXPolV3



117.1: 10 mm      117.2: 50 mm      117.3: 300 mm      117.4: 500 mm
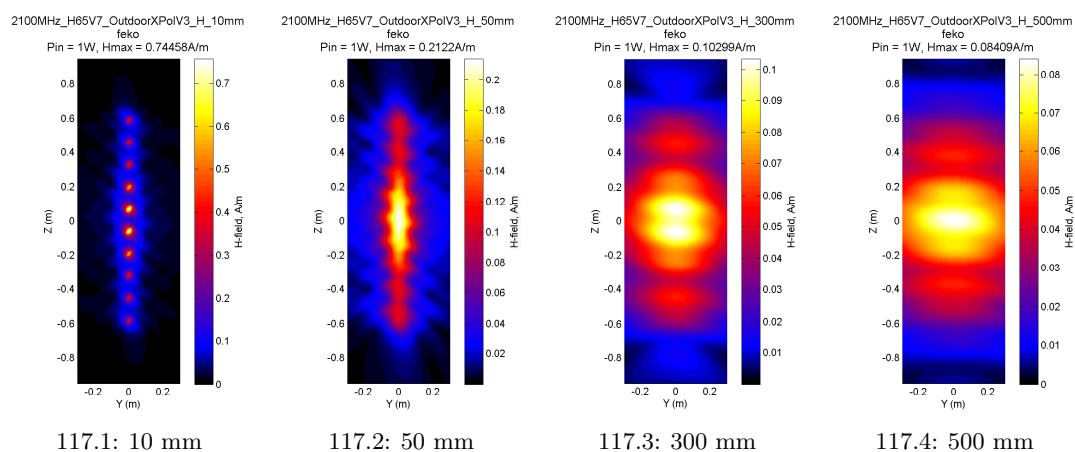
Figure 117: H-fields from FEKO 2100MHz H65V7 OutdoorXPolV3

## C.2.8 2100MHz H90V80 IndoorVPolV4



118.1: 10 mm      118.2: 50 mm      118.3: 300 mm      118.4: 500 mm
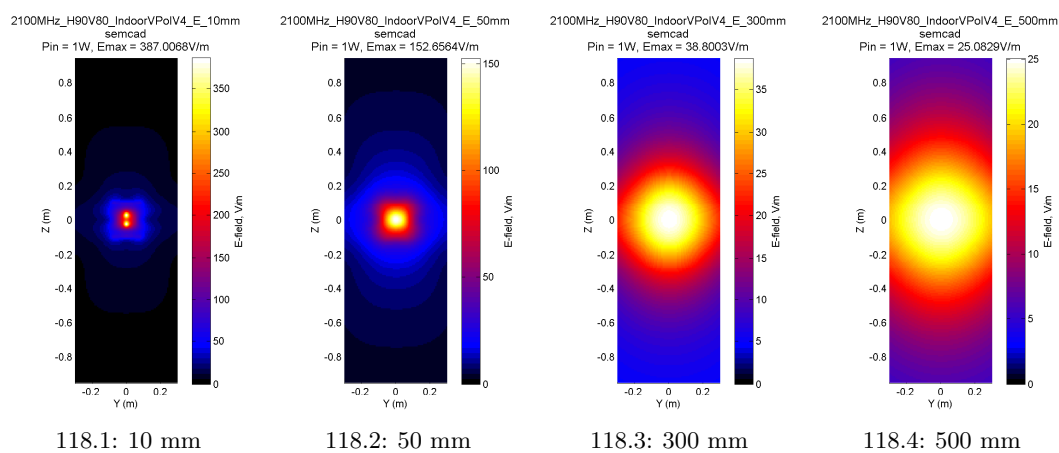
Figure 118: E-fields from SEMCAD 2100MHz H90V80 IndoorVPolV4



119.1: 10 mm      119.2: 50 mm      119.3: 300 mm      119.4: 500 mm
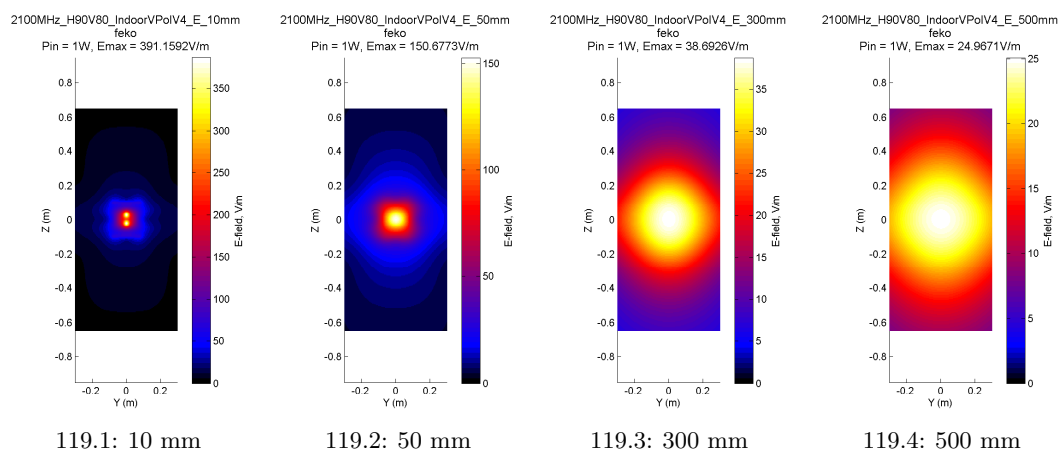
Figure 119: E-fields from FEKO 2100MHz H90V80 IndoorVPolV4

120.1: 10 mm    120.2: 50 mm    120.3: 300 mm    120.4: 500 mm
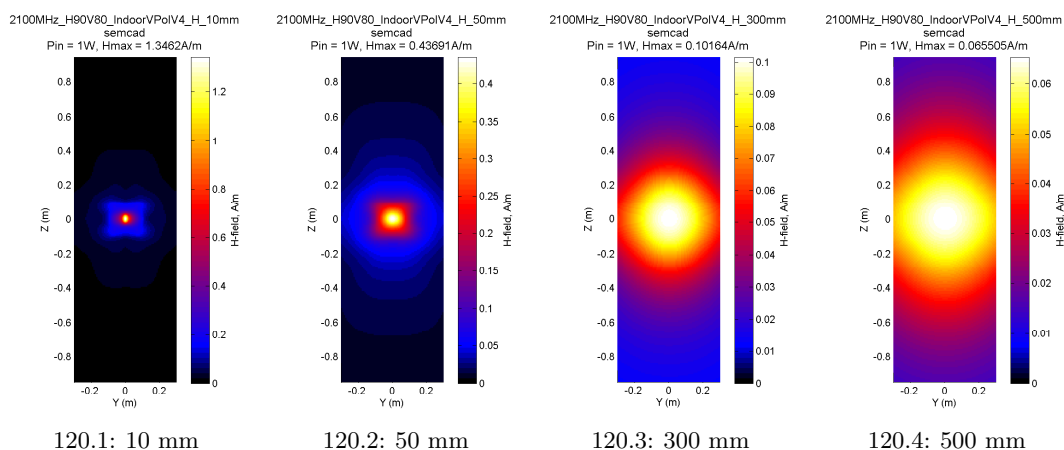
Figure 120: H-fields from SEMCAD 2100MHz H90V80 IndoorVPolV4



121.1: 10 mm    121.2: 50 mm    121.3: 300 mm    121.4: 500 mm
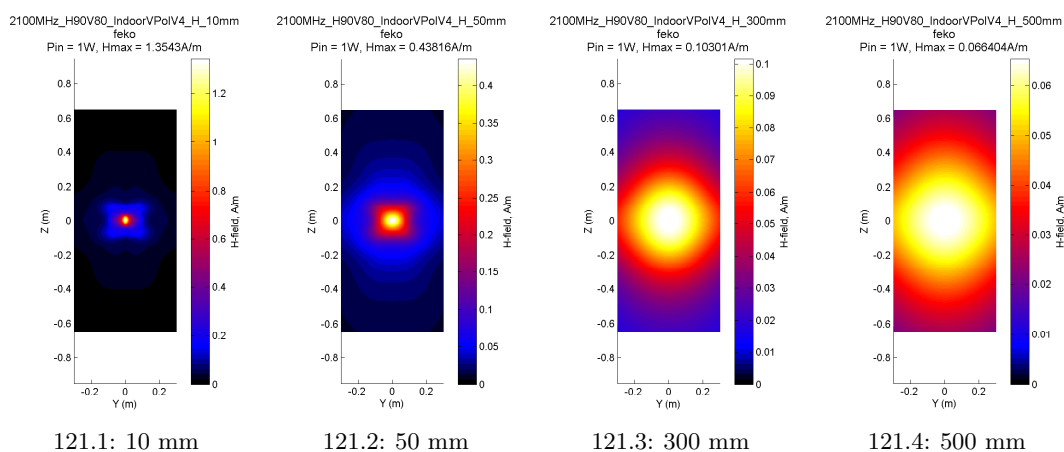
Figure 121: H-fields from FEKO 2100MHz H90V80 IndoorVPolV4

### C.2.9    3500MHz H18V18 VPol CPEV4



122.1: 10 mm          122.2: 50 mm          122.3: 300 mm          122.4: 500 mm
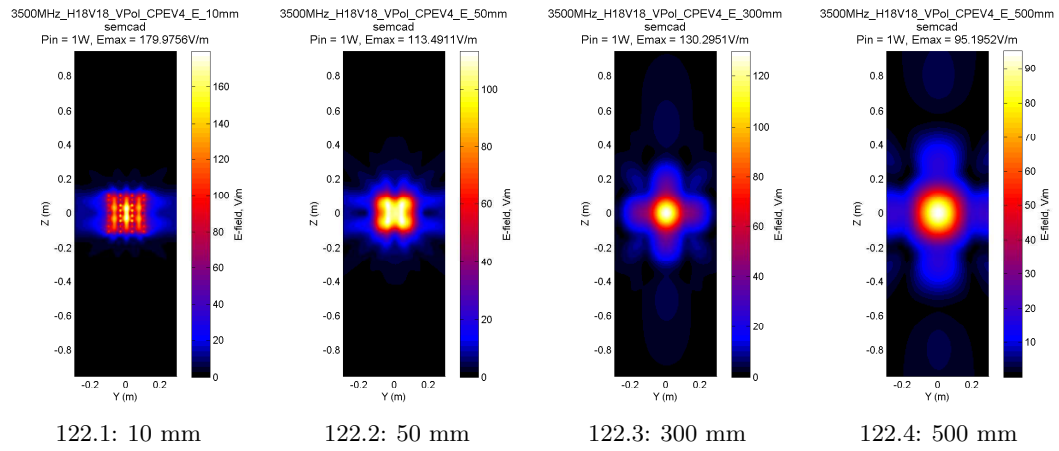
Figure 122: E-fields from SEMCAD 3500MHz H18V18 VPol CPEV4



123.1: 10 mm          123.2: 50 mm          123.3: 300 mm          123.4: 500 mm
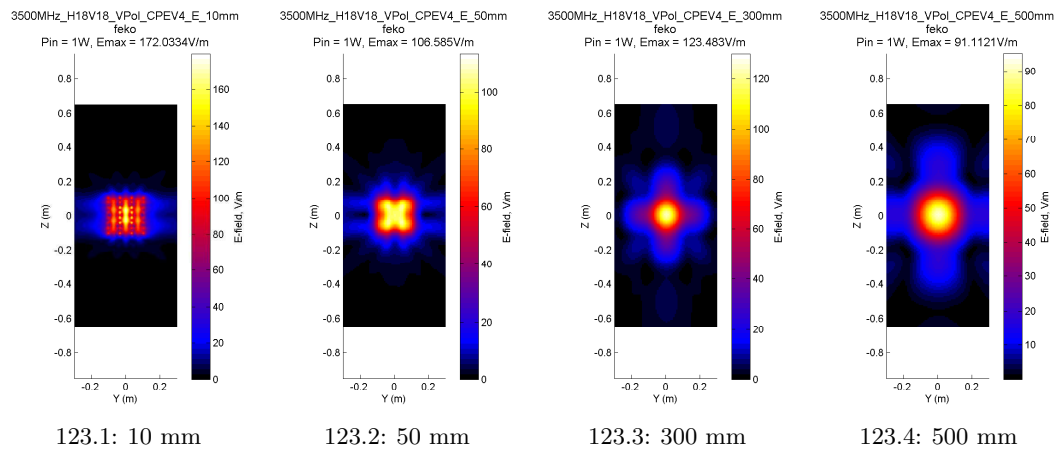
Figure 123: E-fields from FEKO 3500MHz H18V18 VPol CPEV4

124.1: 10 mm    124.2: 50 mm    124.3: 300 mm    124.4: 500 mm
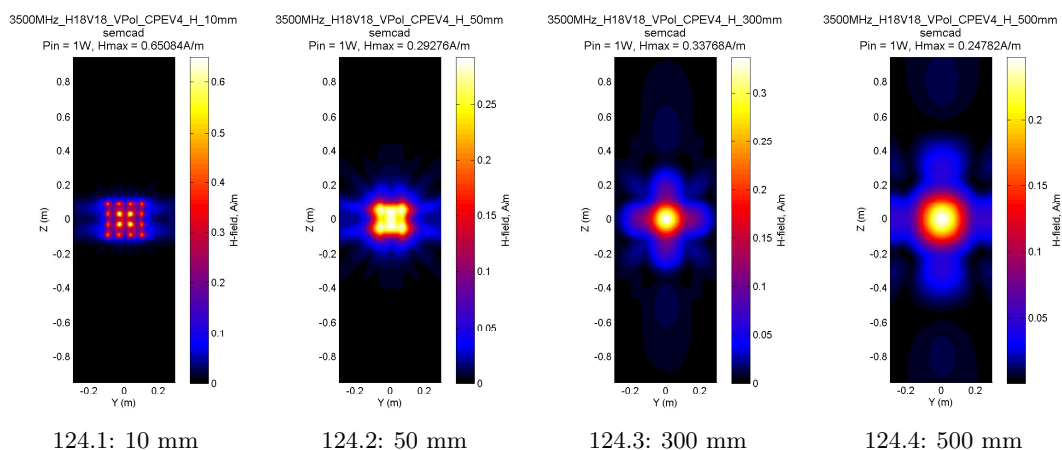
Figure 124: H-fields from SEMCAD 3500MHz H18V18 VPol CPEV4



125.1: 10 mm    125.2: 50 mm    125.3: 300 mm    125.4: 500 mm
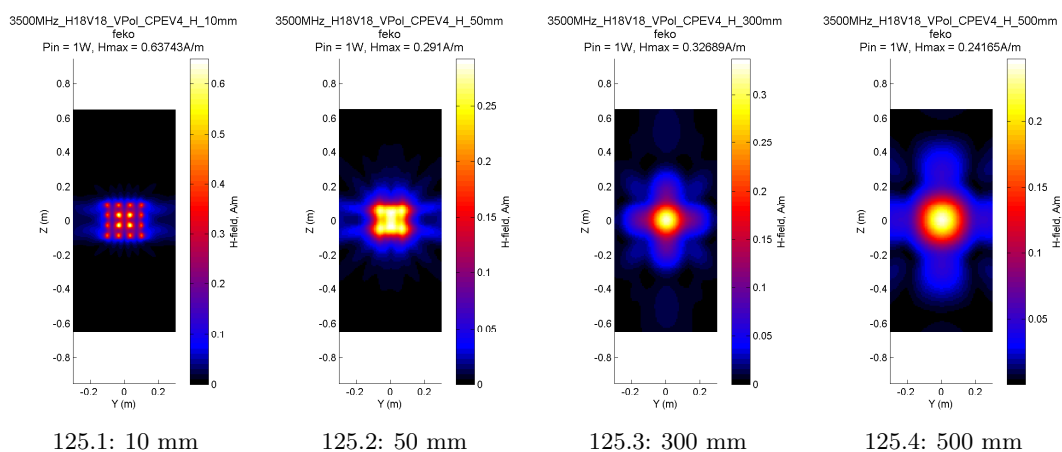
Figure 125: H-fields from FEKO 3500MHz H18V18 VPol CPEV4

## C.2.10    3500MHz H65V9 VPol BTSV3



126.1: 10 mm          126.2: 50 mm          126.3: 300 mm          126.4: 500 mm
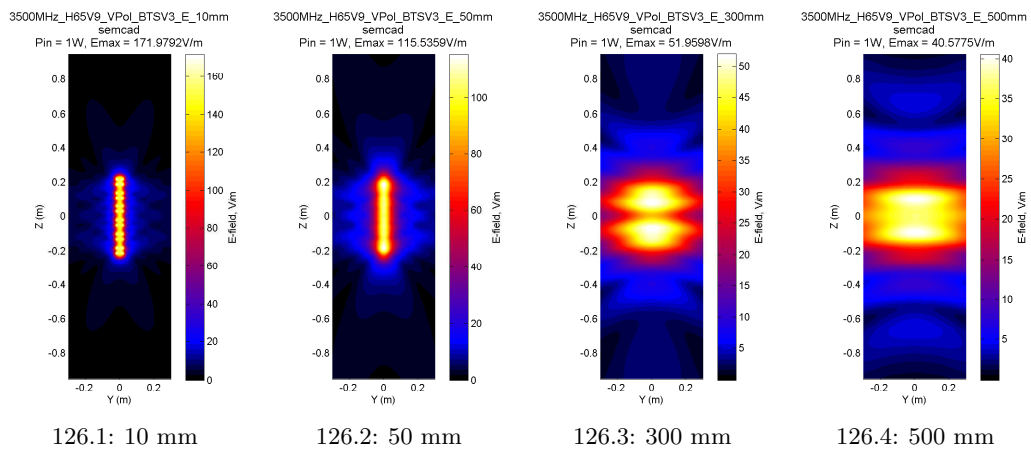
Figure 126: E-fields from SEMCAD 3500MHz H65V9 VPol BTSV3



127.1: 10 mm          127.2: 50 mm          127.3: 300 mm          127.4: 500 mm
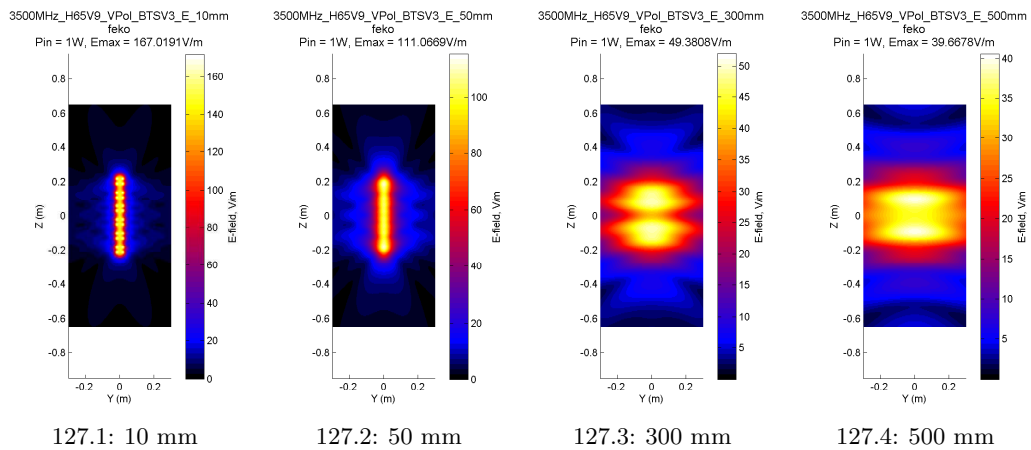
Figure 127: E-fields from FEKO 3500MHz H65V9 VPol BTSV3

128.1: 10 mm    128.2: 50 mm    128.3: 300 mm    128.4: 500 mm
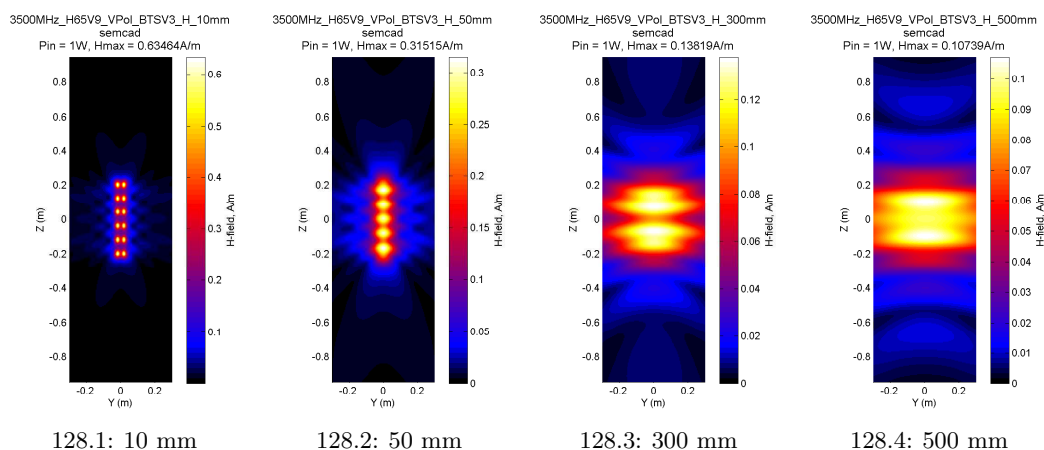
Figure 128: H-fields from SEMCAD 3500MHz H65V9 VPol BTSV3



129.1: 10 mm    129.2: 50 mm    129.3: 300 mm    129.4: 500 mm
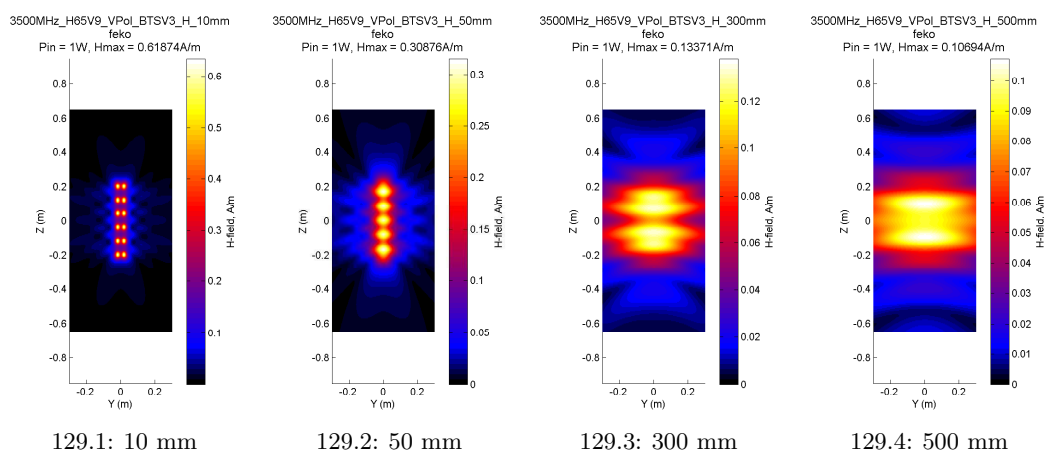
Figure 129: H-fields from FEKO 3500MHz H65V9 VPol BTSV3

### C.2.11    5000MHz H65V35 VPol DirectionalV5



130.1: 10 mm        130.2: 50 mm        130.3: 300 mm        130.4: 500 mm
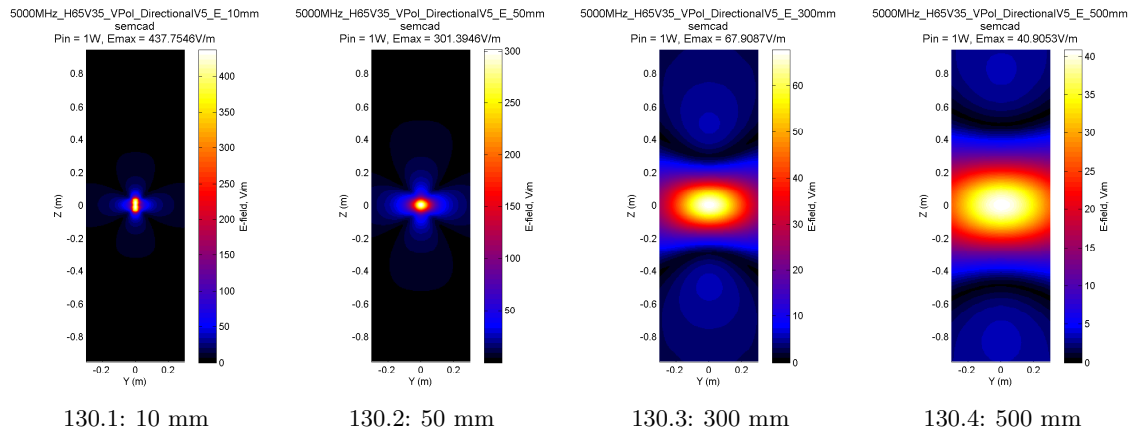
Figure 130: E-fields from SEMCAD 5000MHz H65V35 VPol DirectionalV5



131.1: 10 mm        131.2: 50 mm        131.3: 300 mm        131.4: 500 mm
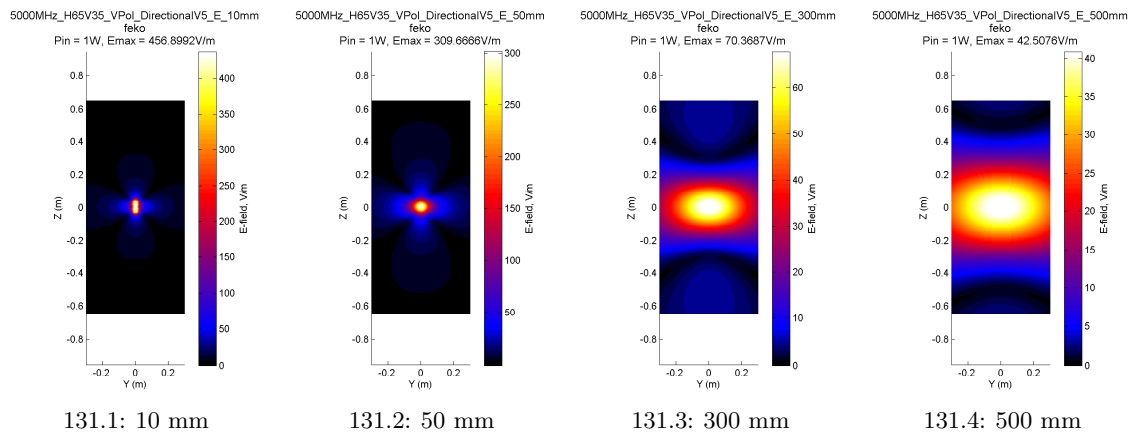
Figure 131: E-fields from FEKO 5000MHz H65V35 VPol DirectionalV5

132.1: 10 mm   132.2: 50 mm   132.3: 300 mm   132.4: 500 mm
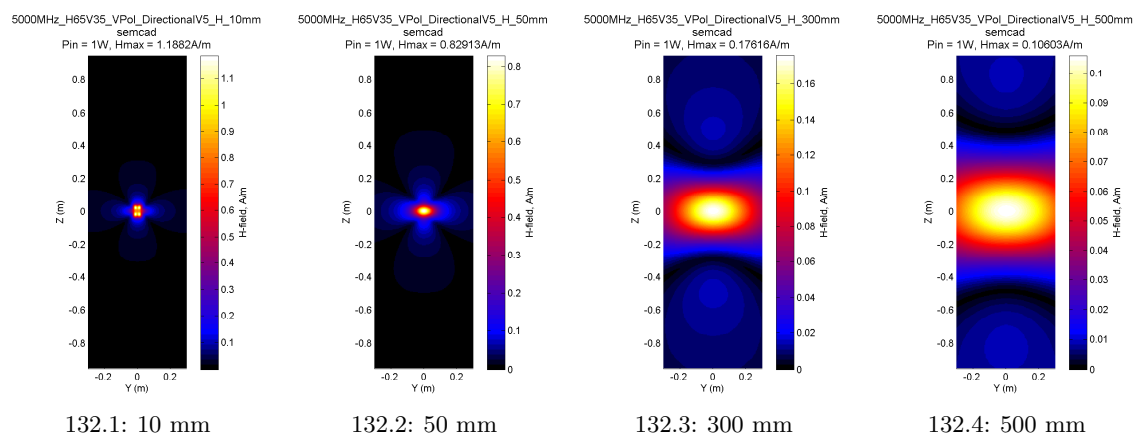
Figure 132: H-fields from SEMCAD 5000MHz H65V35 VPol DirectionalV5



133.1: 10 mm   133.2: 50 mm   133.3: 300 mm   133.4: 500 mm
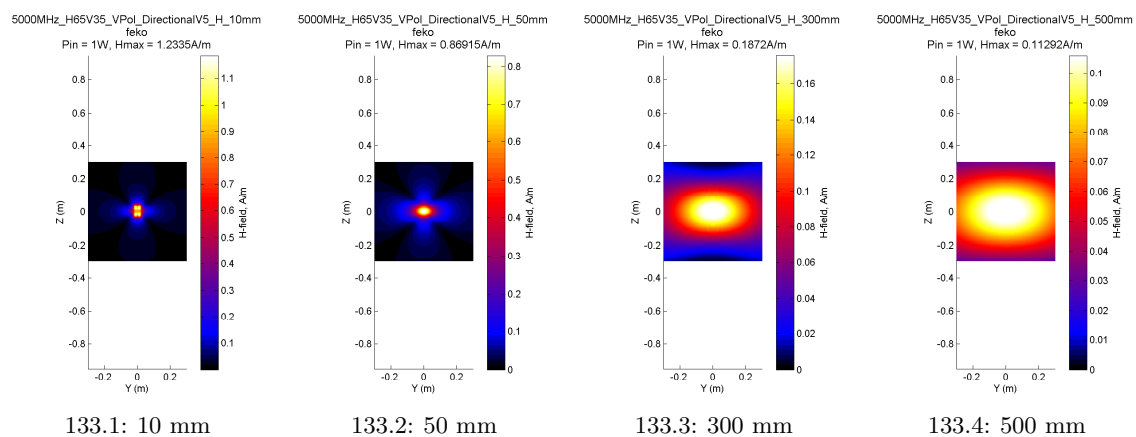
Figure 133: H-fields from FEKO 5000MHz H65V35 VPol DirectionalV5

## C.2.12 5000MHz H360V7 VPol OmniV4



134.1: 10 mm      134.2: 50 mm      134.3: 300 mm      134.4: 500 mm
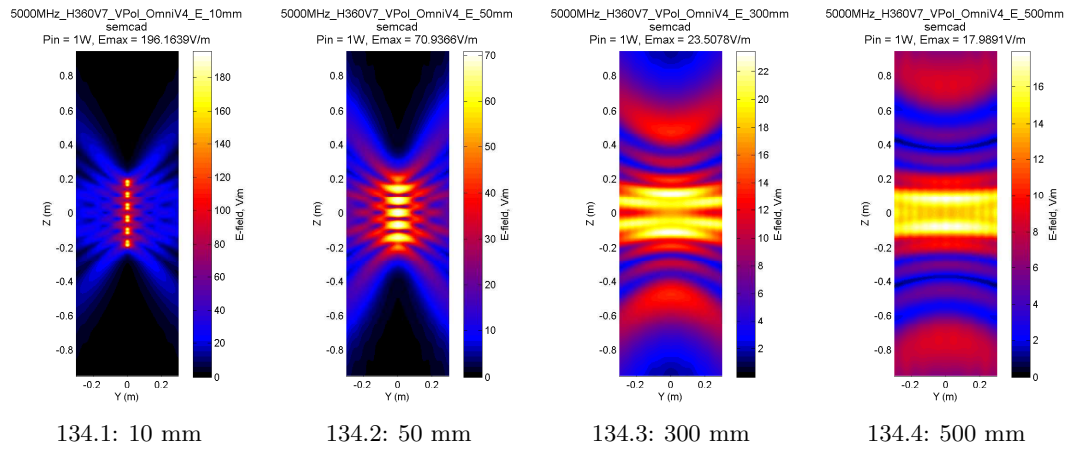
Figure 134: E-fields from SEMCAD 5000MHz H360V7 VPol OmniV4



135.1: 10 mm      135.2: 50 mm      135.3: 300 mm      135.4: 500 mm
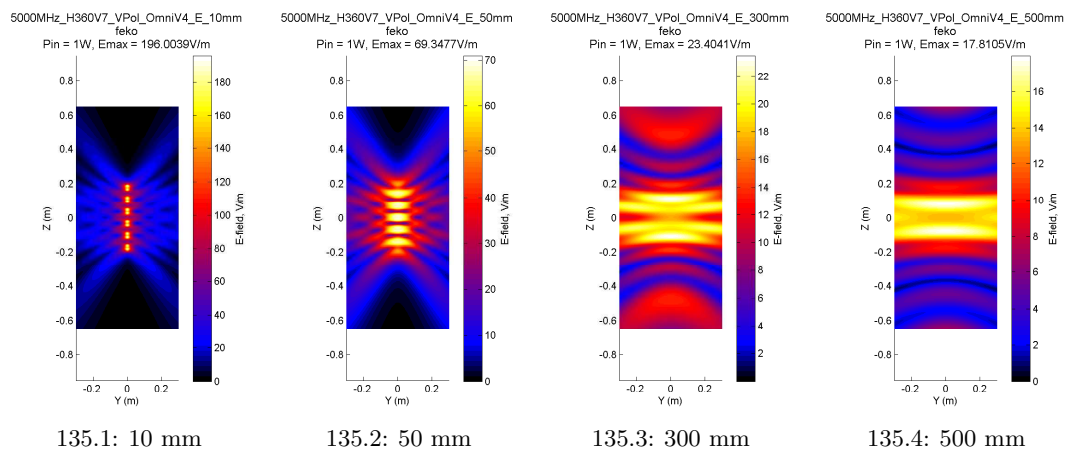
Figure 135: E-fields from FEKO 5000MHz H360V7 VPol OmniV4

136.1: 10 mm    136.2: 50 mm    136.3: 300 mm    136.4: 500 mm
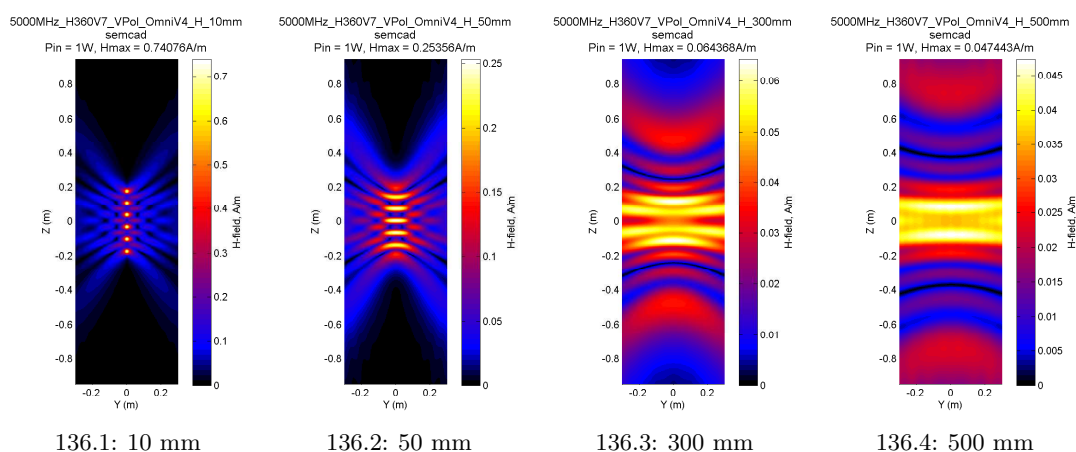
Figure 136: H-fields from SEMCAD 5000MHz H360V7 VPol OmniV4



137.1: 10 mm    137.2: 50 mm    137.3: 300 mm    137.4: 500 mm
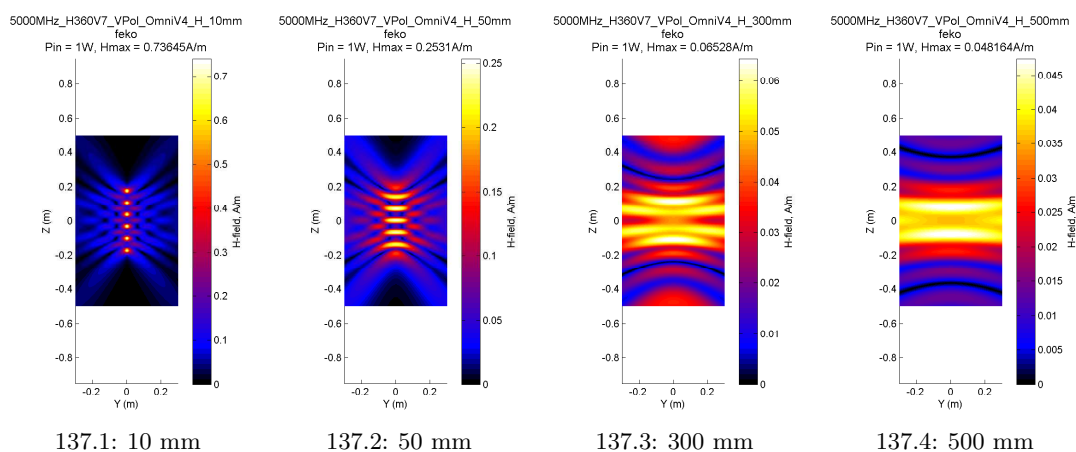
Figure 137: H-fields from FEKO 5000MHz H360V7 VPol OmniV4

## C.3 Directivity (SEMCAD only)

### C.3.1 300MHz H65V64 VPolV5



138.1: horizontal                    138.2: vertical
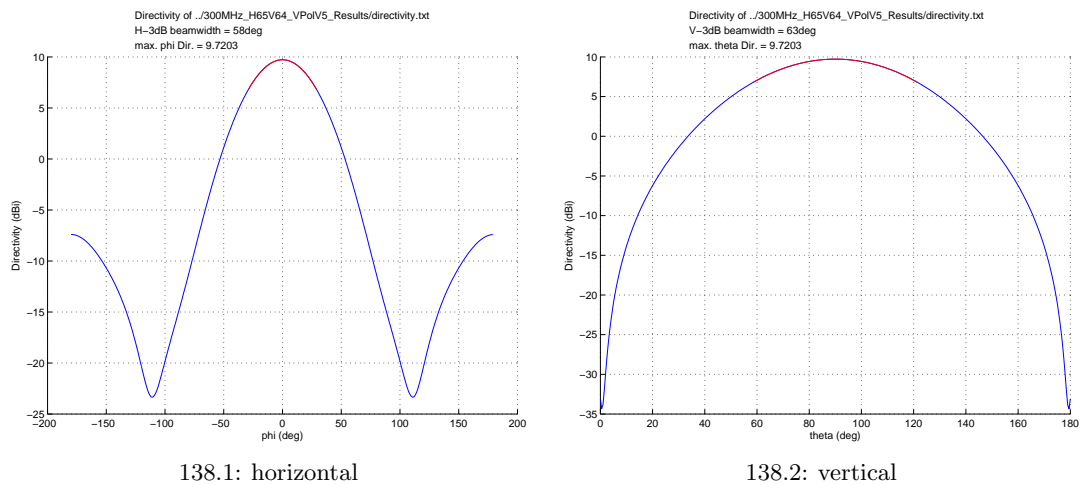
Figure 138: Results from SEMCAD 300MHz H65V64 VPolV5

### C.3.2 300MHz H116V32 VPolV2



139.1: horizontal                    139.2: vertical
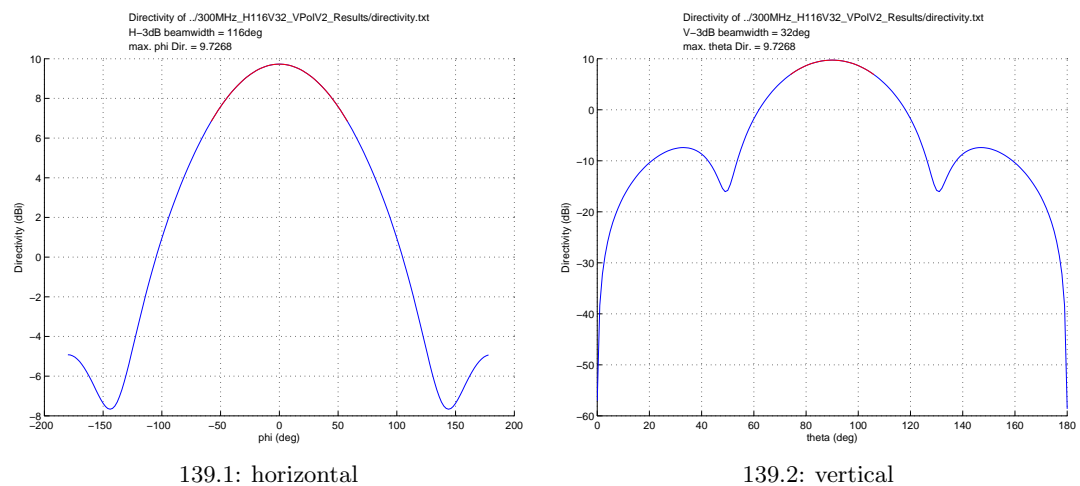
Figure 139: Results from SEMCAD 300MHz H116V32 VPolV2

### C.3.3 450MHz H118V35 VPolV4



140.1: horizontal

140.2: vertical
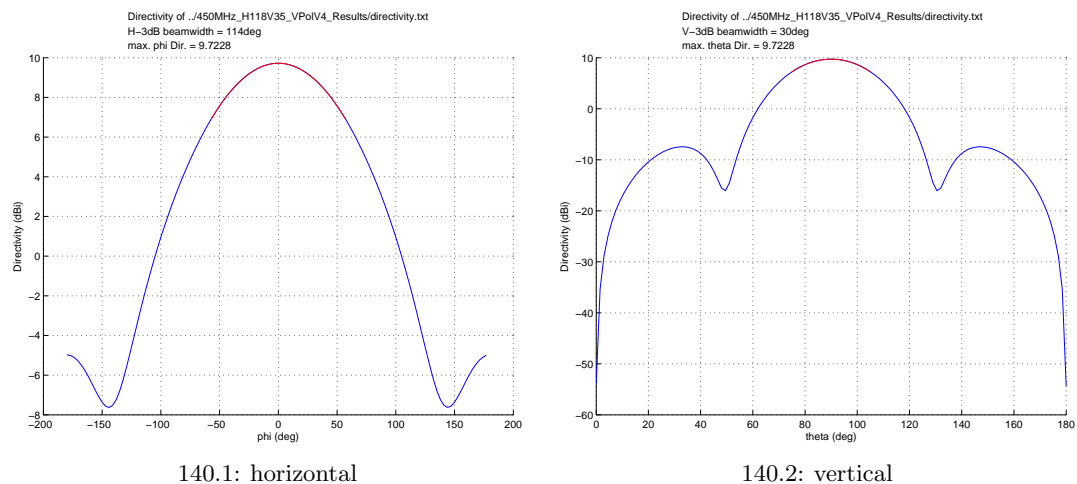
Figure 140: Results from SEMCAD 450MHz H118V35 VPolV4

### C.3.4 450MHz H180V19 VPolV4



141.1: horizontal

141.2: vertical
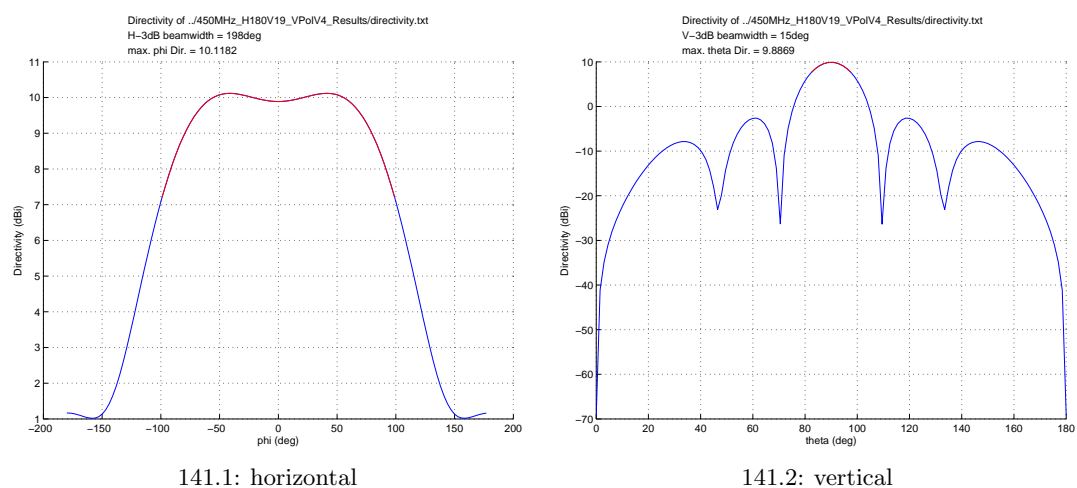
Figure 141: Results from SEMCAD 450MHz H180V19 VPolV4

### C.3.5  900MHz H65V7 X45V4



142.1: horizontal 142.2: vertical
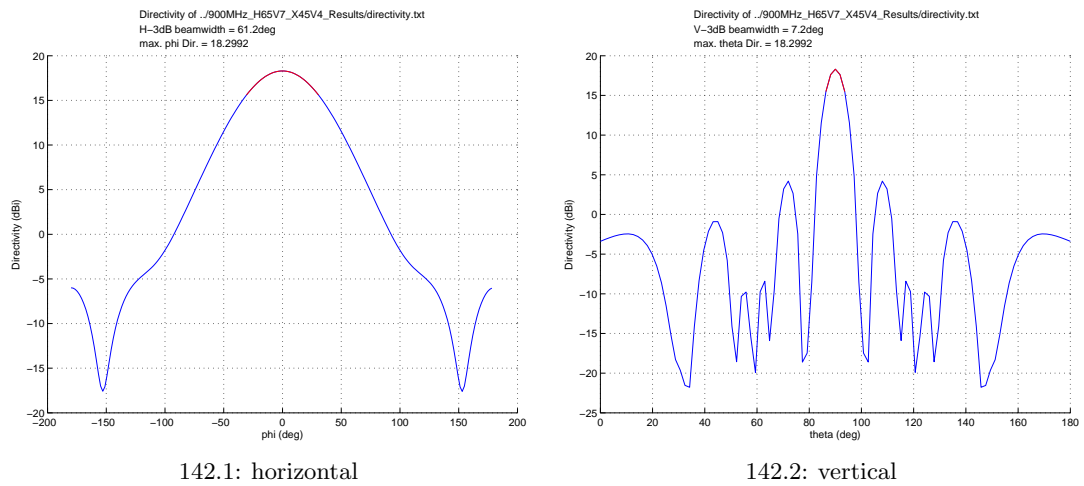
Figure 142: Results from SEMCAD 900MHz H65V7 X45V4

### C.3.6  900MHz H90V9 VPolV7



143.1: horizontal 143.2: vertical
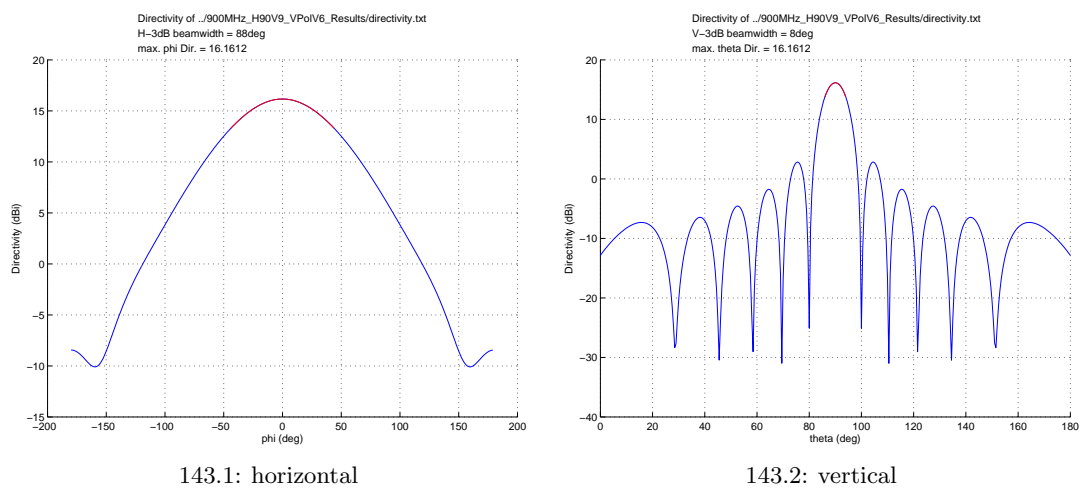
Figure 143: Results from SEMCAD 900MHz H90V9 VPolV7

### C.3.7 2100MHz H65V7 OutdoorXPolV3



144.1: horizontal
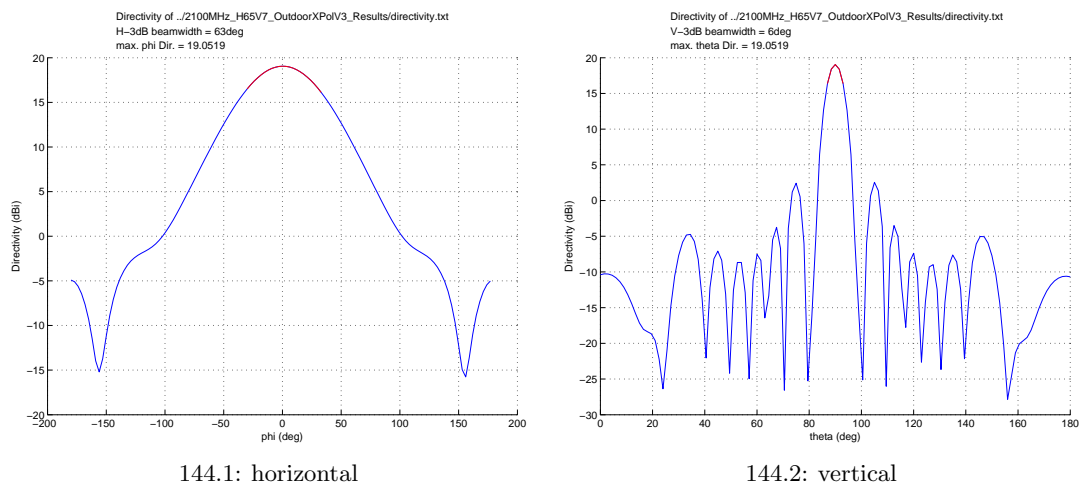
144.2: vertical

Figure 144: Results from SEMCAD 2100MHz H65V7 OutdoorXPolV3

### C.3.8 2100MHz H90V80 IndoorVPolV4



145.1: horizontal
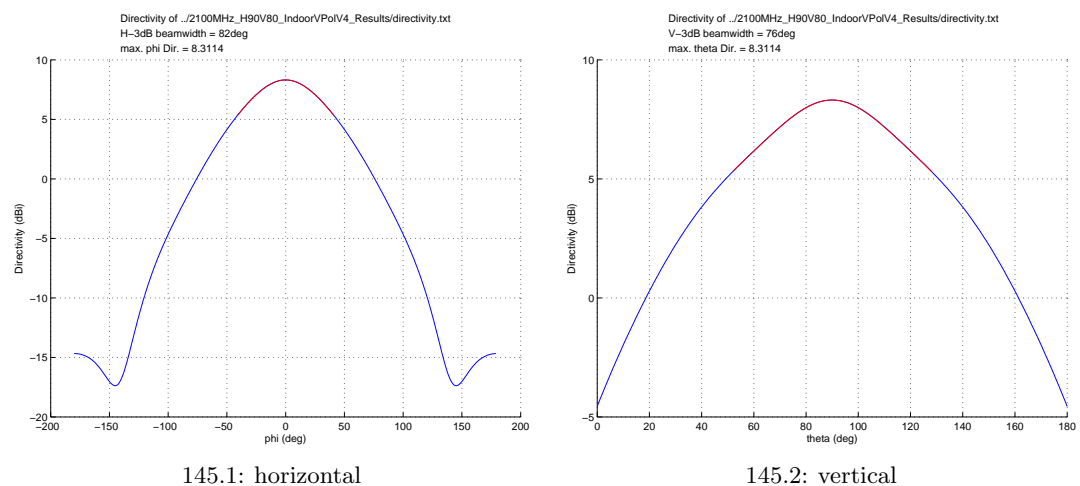
145.2: vertical

Figure 145: Results from SEMCAD 2100MHz H90V80 IndoorVPolV4

### C.3.9    3500MHz H18V18 VPol CPEV4
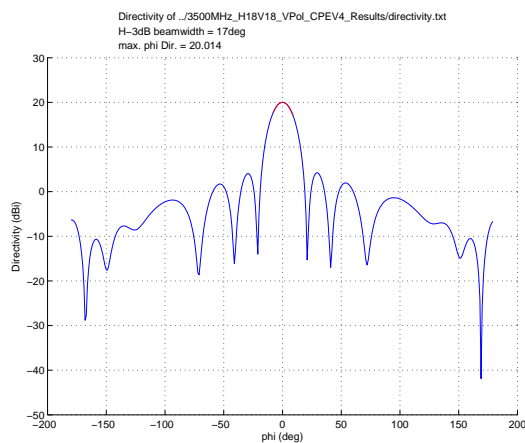


146.1: horizontal
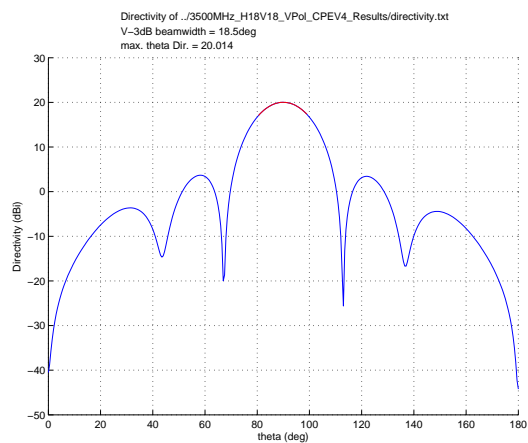
146.2: vertical

Figure 146: Results from SEMCAD 3500MHz H18V18 VPol CPEV4

### C.3.10    3500MHz H65V9 VPol BTSV3
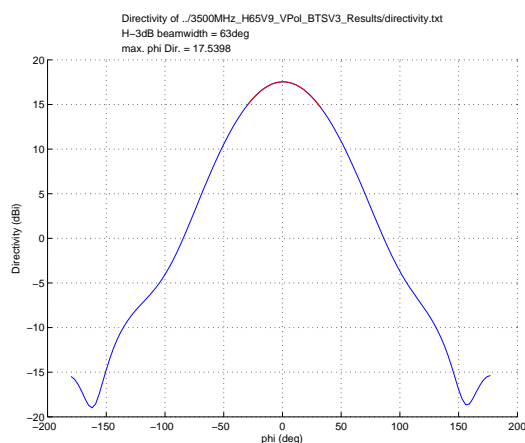


147.1: horizontal
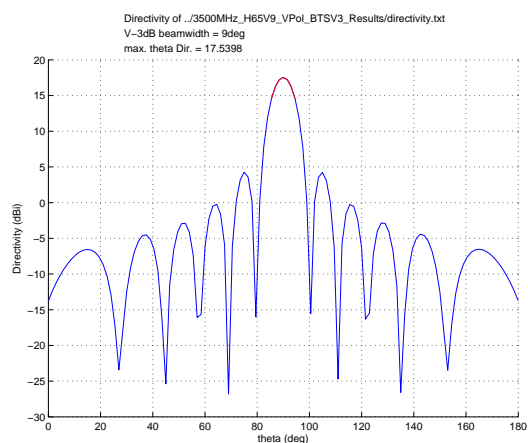
147.2: vertical

Figure 147: Results from SEMCAD 3500MHz H65V9 VPol BTSV3

### C.3.11    5000MHz H65V35 VPol DirectionalV5



148.1: horizontal

148.2: vertical
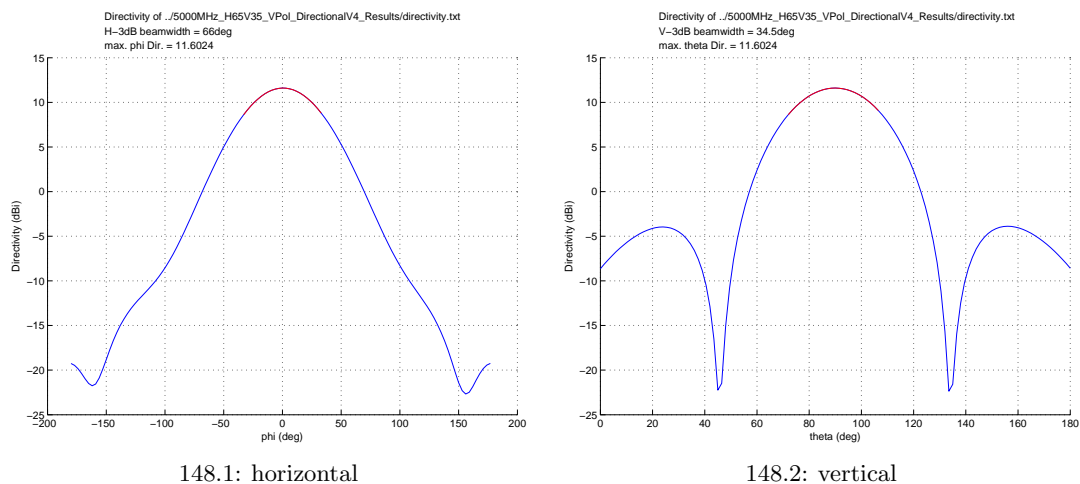
Figure 148: Results from SEMCAD 5000MHz H65V35 VPol DirectionalV5

### C.3.12    5000MHz H360V7 VPol OmniV4



149.1: horizontal

149.2: vertical
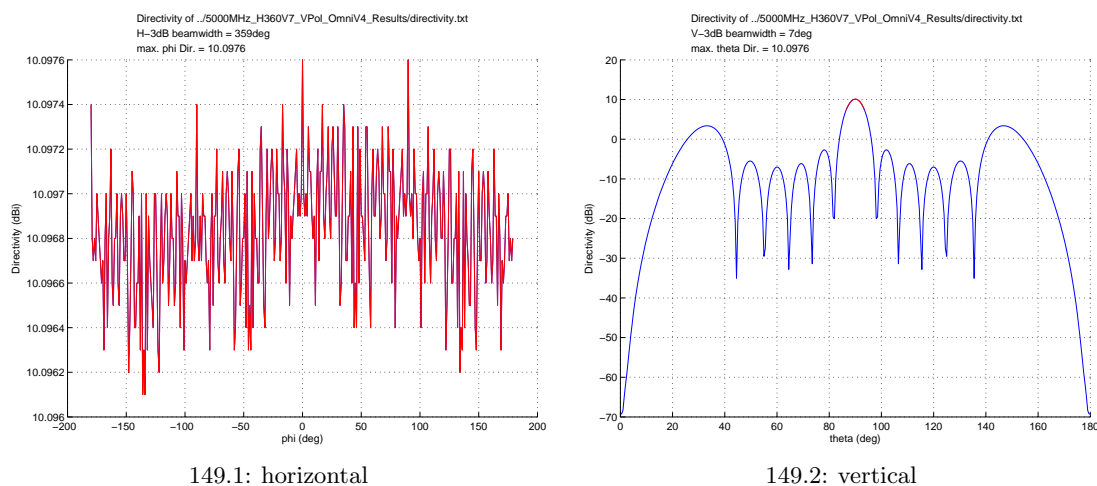
Figure 149: Results from SEMCAD 5000MHz H360V7 VPol OmniV4

# D   WP6 – Huygens Box Validation (FDTD, MoM)

This appendix presents the comparison of the electric field along straight lines passing through the VFB from SEMCAD X and FEKO for the validation of the GHB method.

## D.1   300 MHz
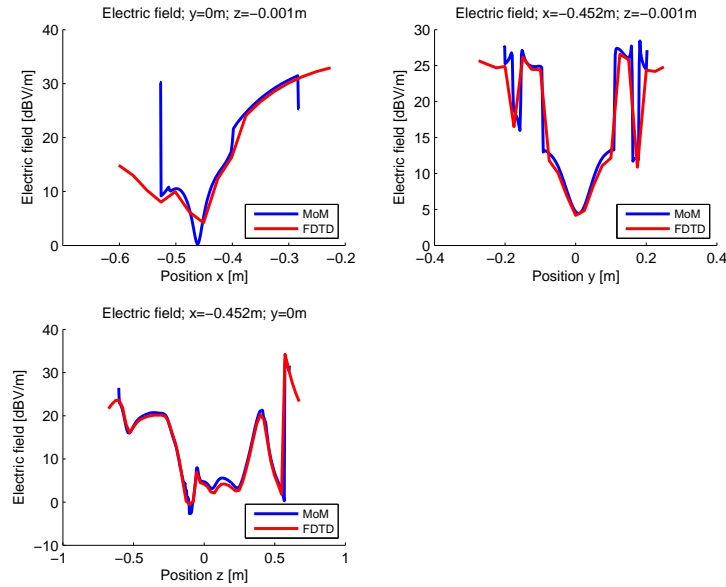


Figure 150: E-field along lines passing through the VFB model; 300 MHz, 0.3 m
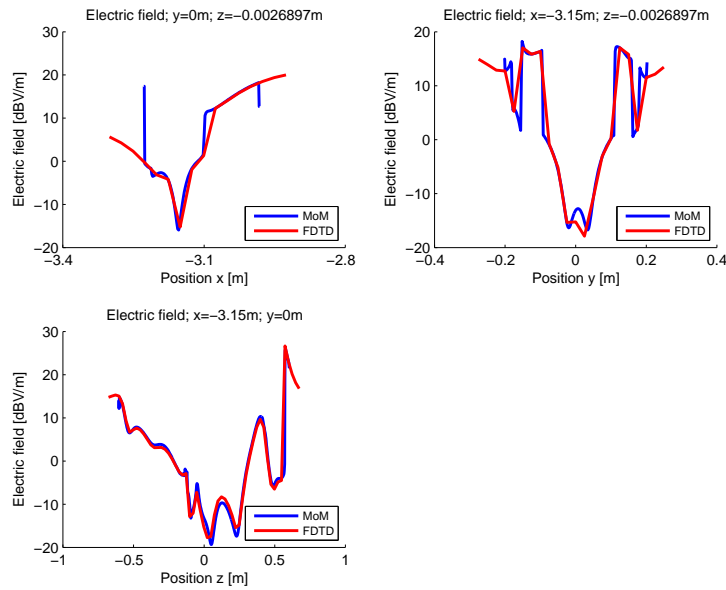


Figure 151: E-field along lines passing through the VFB model; 300 MHz, 3 m

## D.2 900 MHz
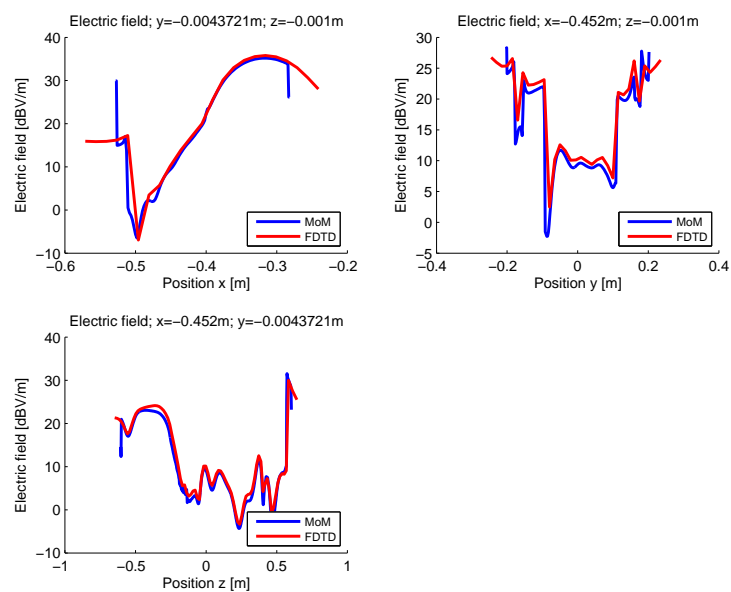


Figure 152: E-field along lines passing through the VFB model; 900 MHz, 0.3 m
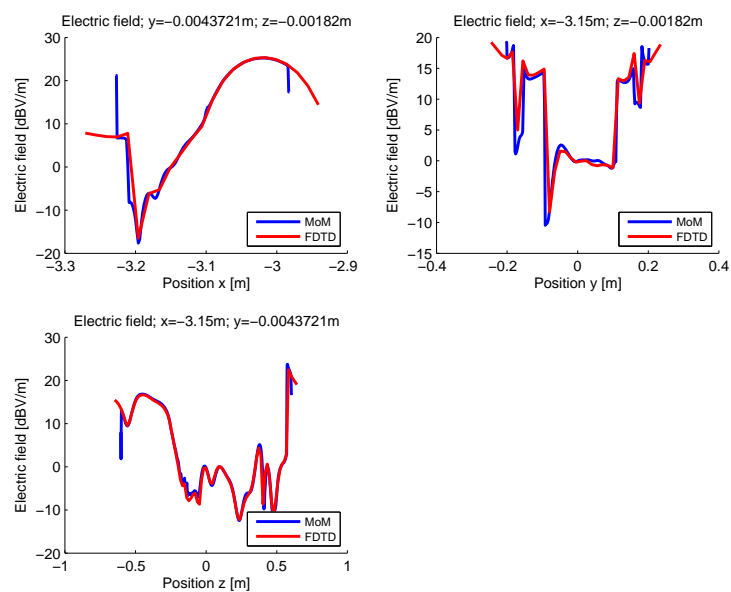


Figure 153: E-field along lines passing through the VFB model; 900 MHz, 3 m

## D.3   2100 MHz
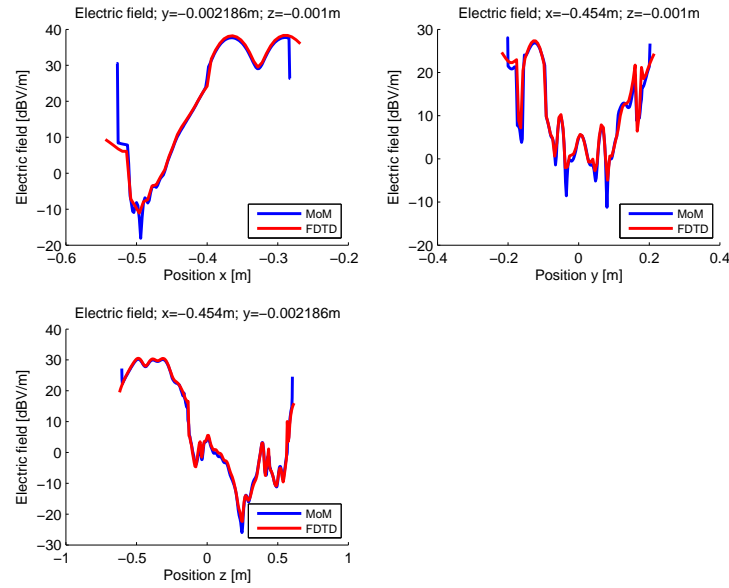


Figure 154: E-field along lines passing through the VFB model; 2100 MHz, 0.3 m
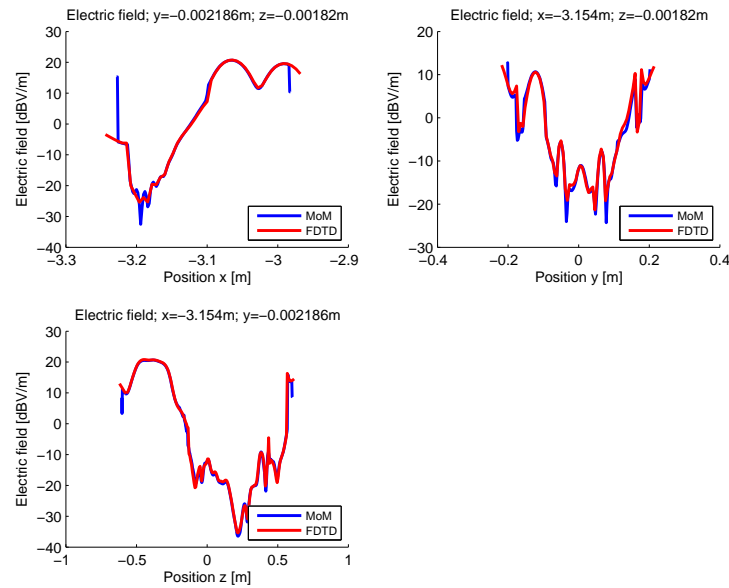


Figure 155: E-field along lines passing through the VFB model; 2100 MHz, 3 m

## D.4   Discussion

The resolution of the grid used for the computation using in MoM is much coarser than the one needed in FDTD. This can be observed on Figures 150 to 155. These figures show that, even if the maximum peak spatial average SAR (1 g and 10 g) did not compare well between the GHB FDTD method and the full-scenario MoM method, see Section 1.5.2, the electric field inside the

body does not present a significant variation. Also, for example at 900 MHz, it can be seen that the agreement is better at 3 m of distance between the human model and the antenna than at 0.3 m.

# E  WP6 – Comparison of All the Bulk Simulations Results with the Estimation Formula Using the Worst-case Human Dimensions

Figures 158 to 169 from this appendix presents the bulk simulation results of WP 6 (VFM, VFF, and VFB) together with the estimation formula for the worst-case human developed in Section 1.10. It should be kept in mind that the estimation formula is not meant to be conservative for child models.

Figures 156 and 157 present the histogram and the cumulative distribution function of all the models. It shows that the estimation formula based on the worst-case human is not conservative enough to be applicable to the VFB.
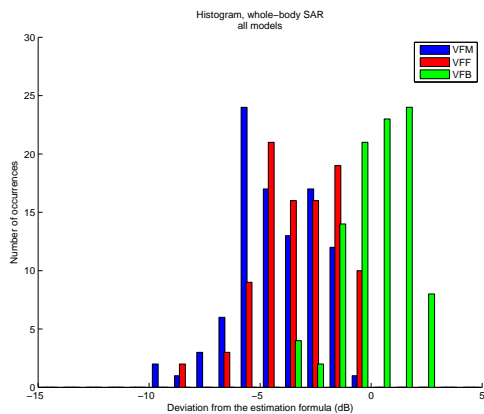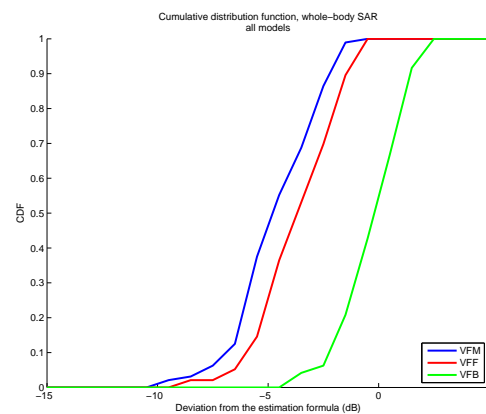


156.1: histogram  156.2: cumulative distribution function

Figure 156: Histogram and cumulative distribution function of the deviation between the bulk simulation whole-body SAR results of all the models ($> 20$ cm) and the estimation formula based on the worst-case human
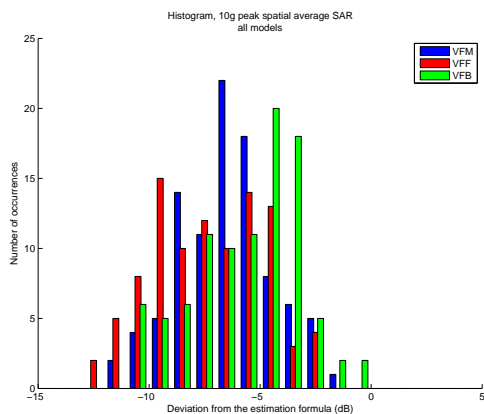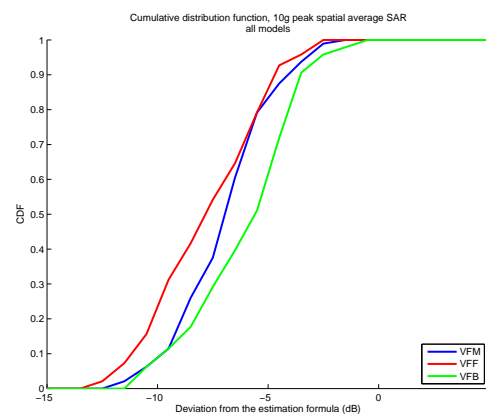


157.1: histogram  157.2: cumulative distribution function

Figure 157: Histogram and cumulative distribution function of the deviation between the bulk simulation 10 g peak spatial average SAR results of all the models ($> 20$ cm) and the estimation formula based on the worst-case human
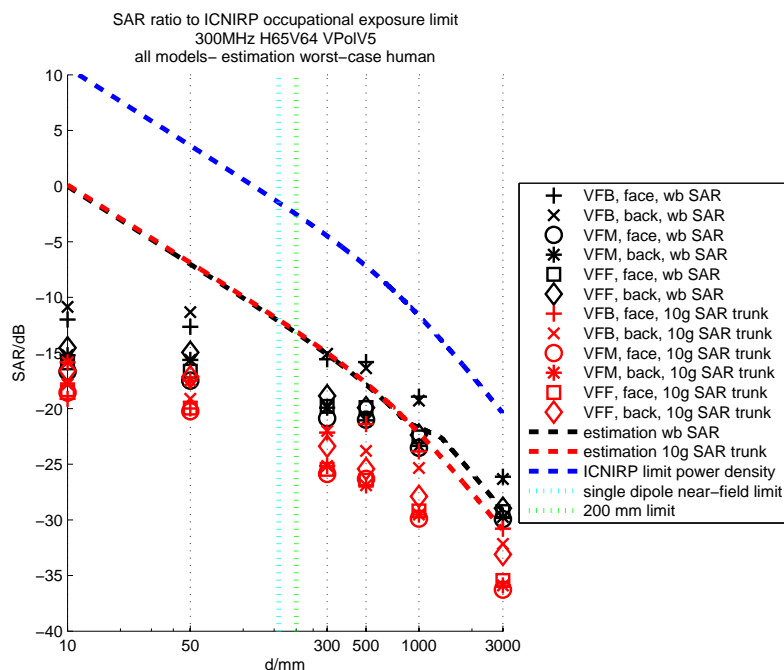
Figure 158: Bulk simulation results of all the models in front of the antenna 300MHz H65V64 VPolV5 and approximation formula using the dimensions of the worst-case human, for 1W radiated power
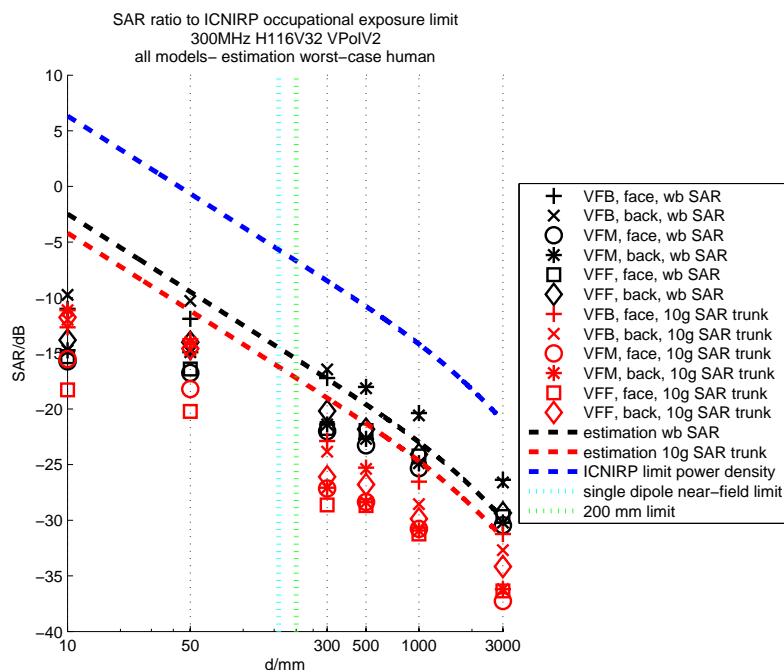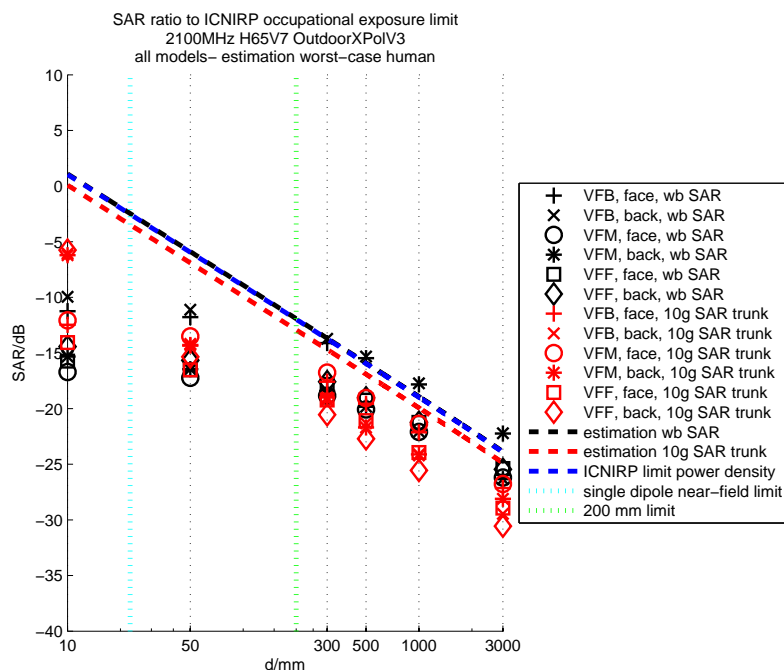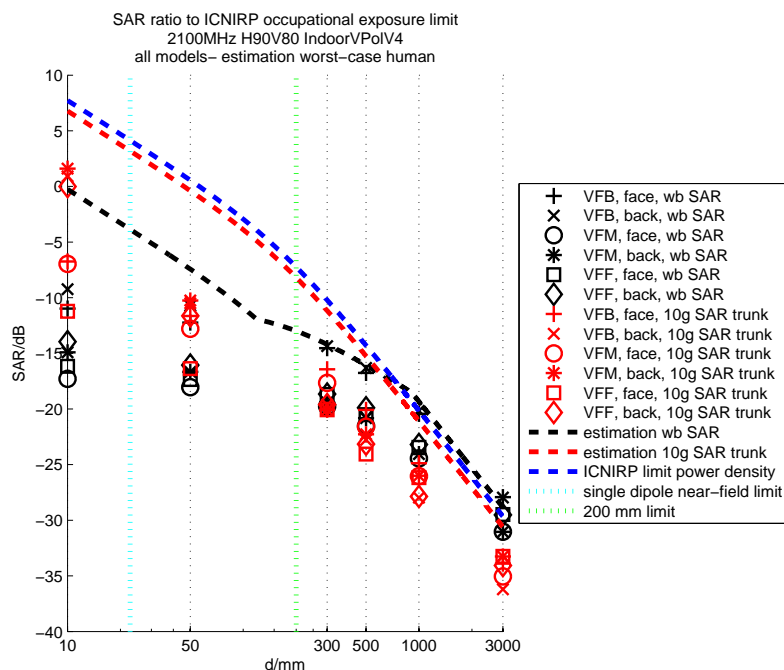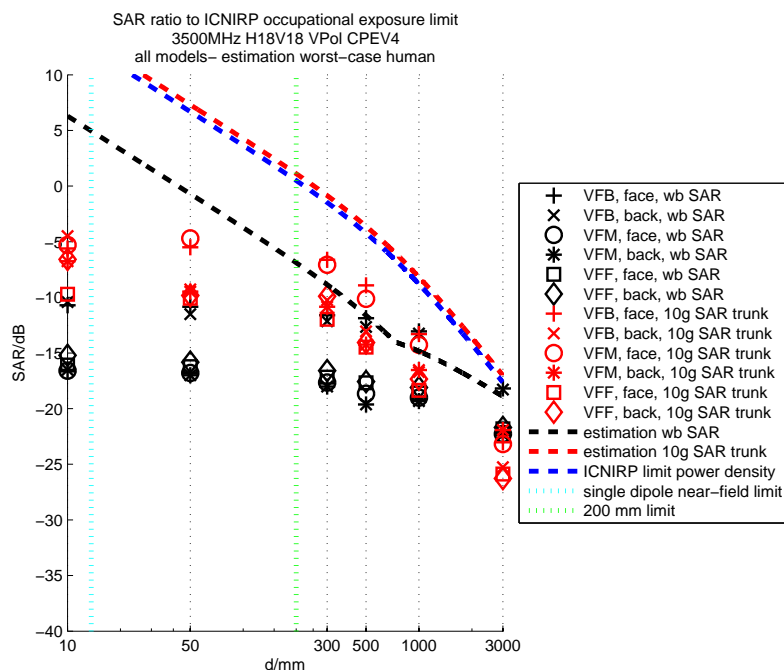


Figure 159: Bulk simulation results of all the models in front of the antenna 300MHz H116V32 VPolV2 and approximation formula using the dimensions of the worst-case human, for 1W radiated power
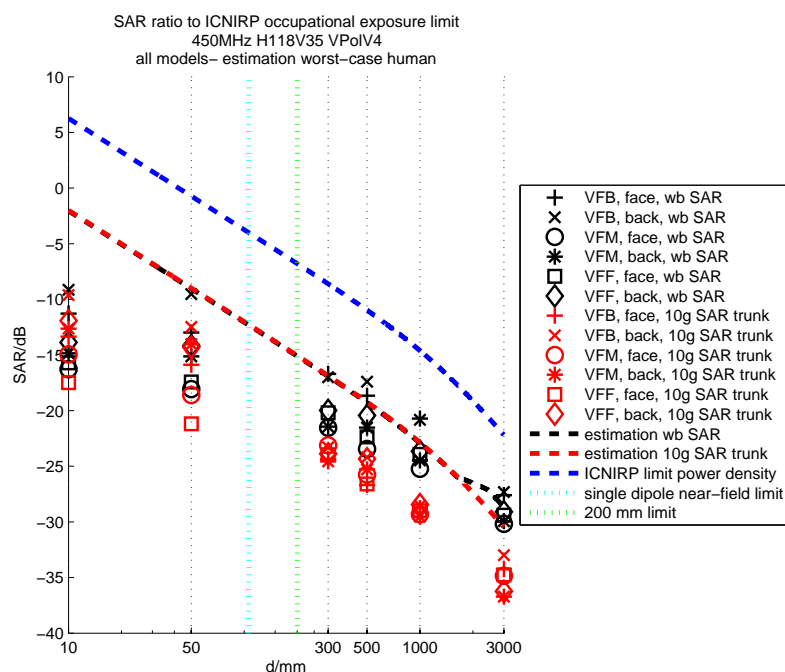
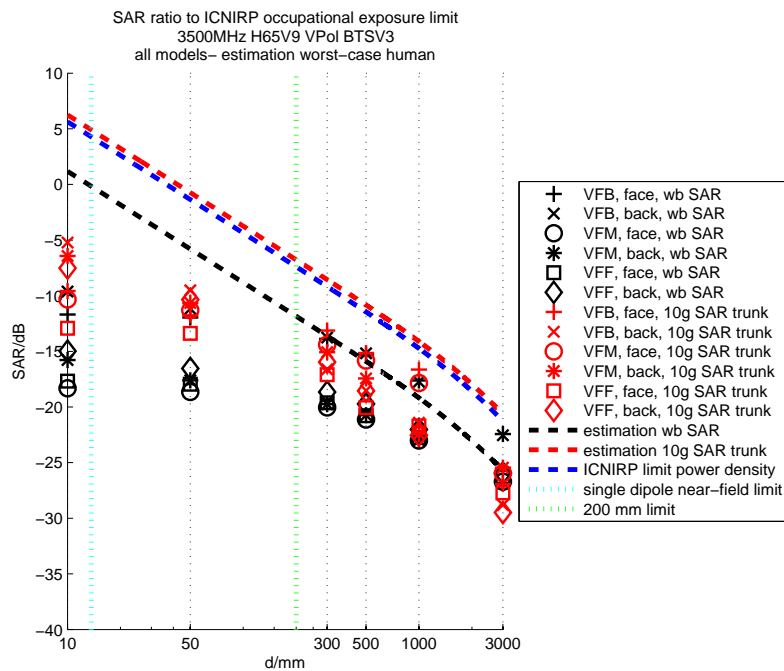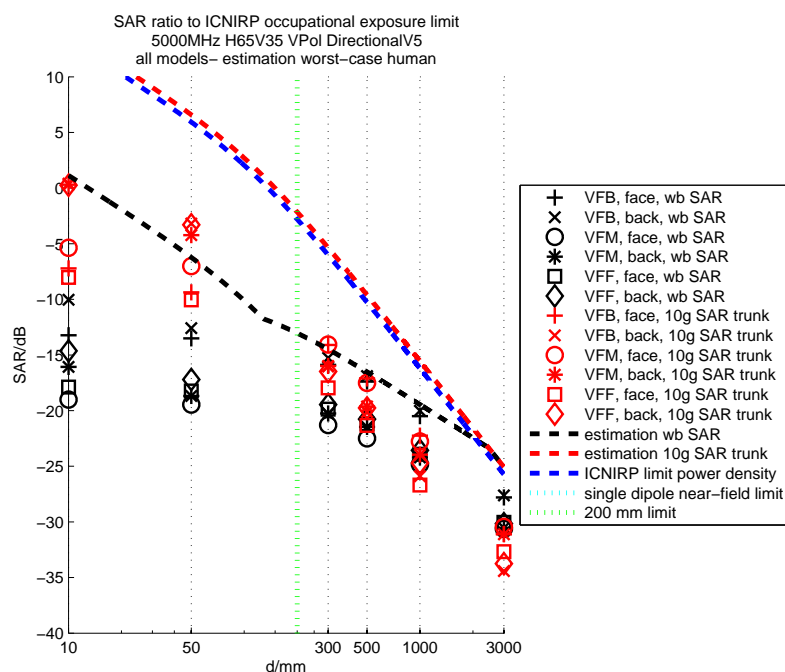Figure 160: Bulk simulation results of all the models in front of the antenna 450MHz H118V35 VPolV4 and approximation formula using the dimensions of the worst-case human, for 1W radiated power
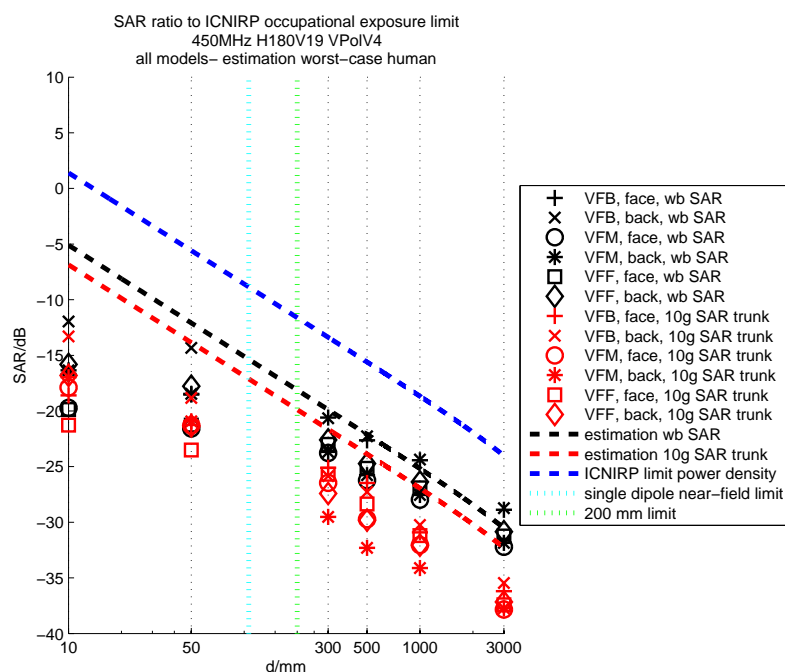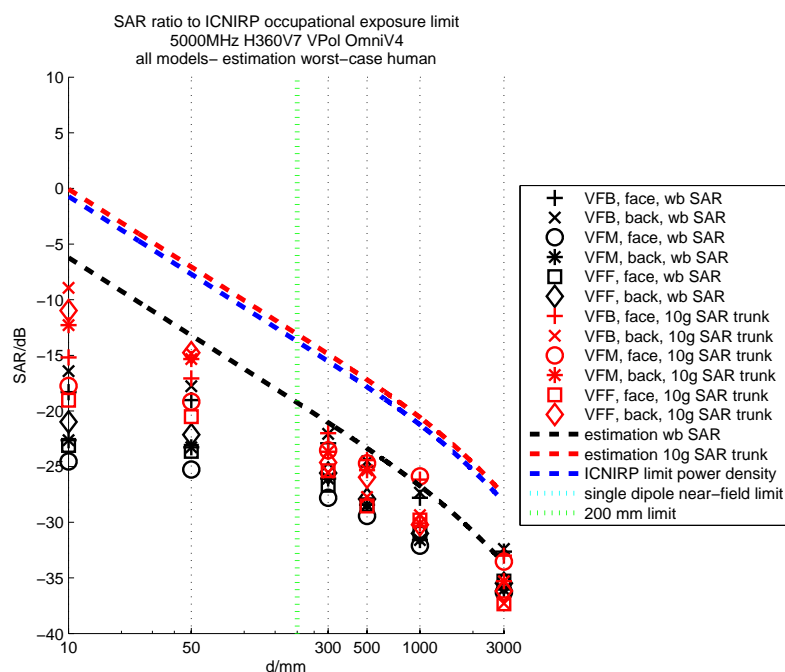


Figure 161: Bulk simulation results of all the models in front of the antenna 450MHz H180V19 VPolV4 and approximation formula using the dimensions of the worst-case human, for 1W radiated power
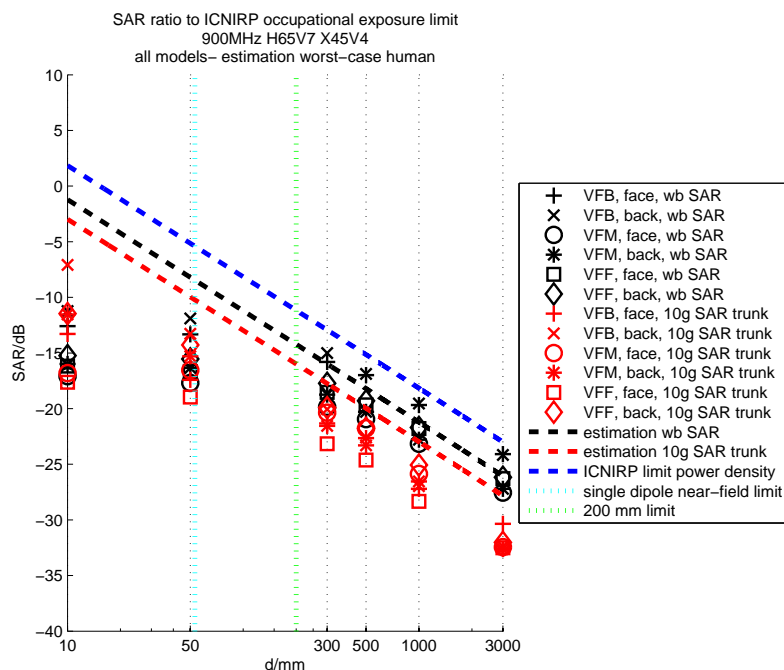
Figure 162: Bulk simulation results of all the models in front of the antenna 900MHz H65V7 X45V4 and approximation formula using the dimensions of the worst-case human, for 1W radiated power
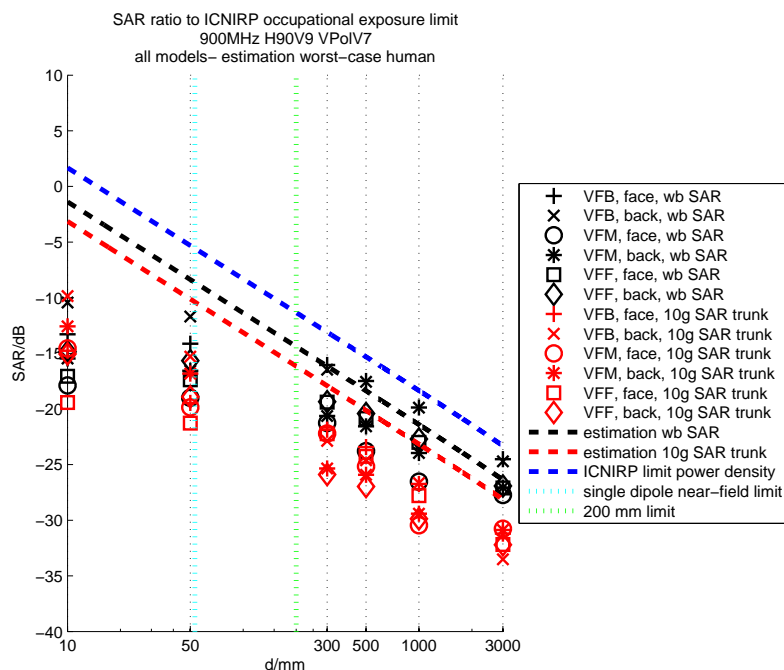


Figure 163: Bulk simulation results of all the models in front of the antenna 900MHz H90V9 VPolV7 and approximation formula using the dimensions of the worst-case human, for 1W radiated power

Figure 164: Bulk simulation results of all the models in front of the antenna 2100MHz H65V7 OutdoorXPolV3 and approximation formula using the dimensions of the worst-case human, for 1W radiated power

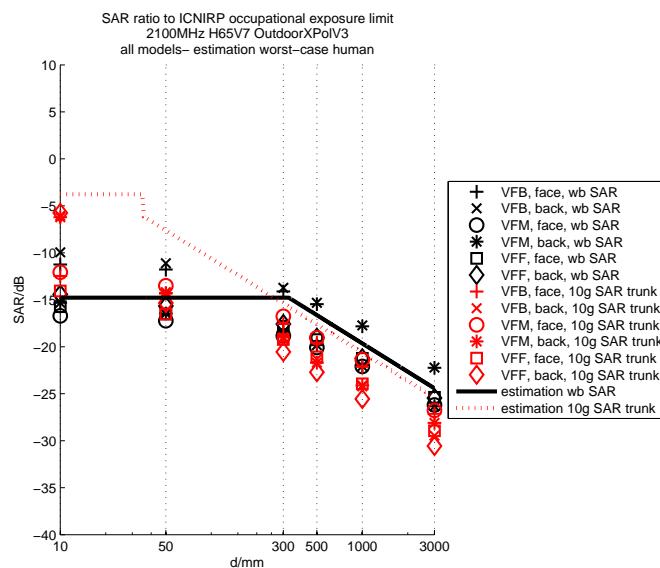

Figure 165: Bulk simulation results of all the models in front of the antenna 2100MHz H90V80 IndoorVPolV4 and approximation formula using the dimensions of the worst-case human, for 1W radiated power

Figure 166: Bulk simulation results of all the models in front of the antenna 3500MHz H18V18 VPol CPEV4 and approximation formula using the dimensions of the worst-case human, for 1W radiated power



Figure 167: Bulk simulation results of all the models in front of the antenna 3500MHz H65V9 VPol BTSV3 and approximation formula using the dimensions of the worst-case human, for 1W radiated power

Figure 168: Bulk simulation results of all the models in front of the antenna 5000MHz H65V35 VPol DirectionalV5 and approximation formula using the dimensions of the worst-case human, for 1W radiated power



Figure 169: Bulk simulation results of all the models in front of the antenna 5000MHz H360V7 VPol OmniV4 and approximation formula using the dimensions of the worst-case human, for 1W radiated power

## F  WP6 – Comparison of Estimation Formula from Ericsson with Bulk Results

This appendix presents the bulk simulation results of WP 6 together with the estimation formula developed in [Thors et al., 2008]. The range of validity of this estimation formula is between 800 MHz and 2200 MHz, so only these results have ben plotted here.
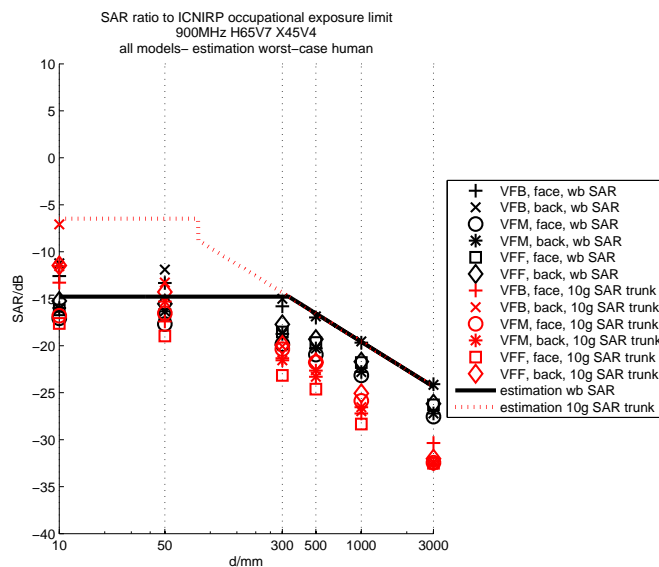


Figure 170: Bulk simulation results of all the models in front of the antenna 900MHz H65V7 X45V4 and approximation formula from [Thors et al., 2008], for 1W radiated power
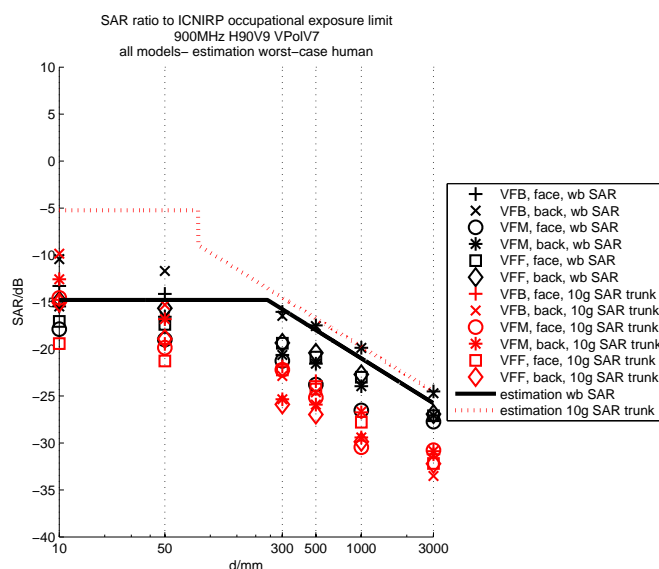


Figure 171: Bulk simulation results of all the models in front of the antenna 900MHz H90V9 VPolV7 and approximation formula from [Thors et al., 2008], for 1W radiated power

Figure 172: Bulk simulation results of all the models in front of the antenna 2100MHz H65V7 OutdoorXPolV3 and approximation formula from [Thors et al., 2008], for 1W radiated power
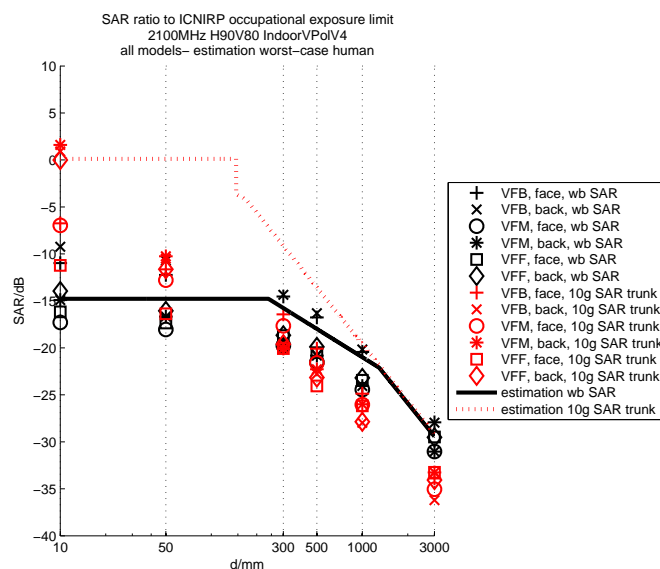


Figure 173: Bulk simulation results of all the models in front of the antenna 2100MHz H90V80 IndoorVPolV4 and approximation formula from [Thors et al., 2008], for 1W radiated power

## G    WP6 – Data from Ericsson's Study

This appendix presents the SAR results from exposure to base station antennas gathered by [Thors et al., 2008] together with the estimation formula that they propose. The approximation formulas developed in Section 1.7 are also represented on Figures 174 to 231. Equations (48) to (53), based on the $95^{th}$ percentile human, are plotted for every cases. Equations (39) to (47), based on the dimensions of the model, are plotted only for the cases where the weight and height of the simulated model was available.

### G.1    Data from the Ericsson's Study
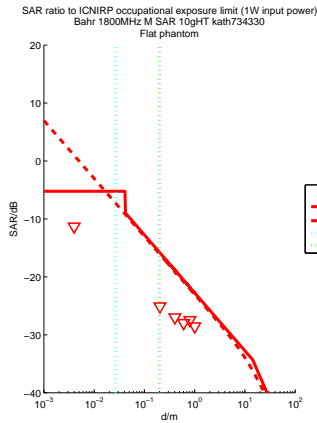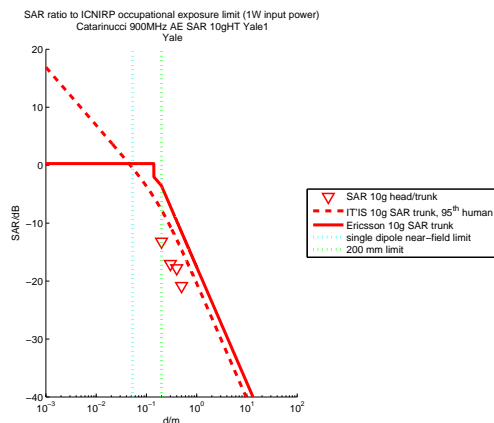


Figure 174:
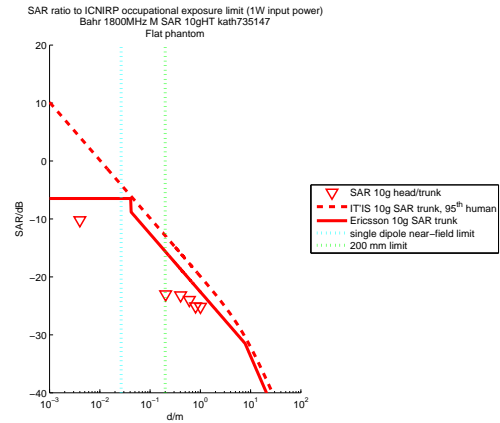


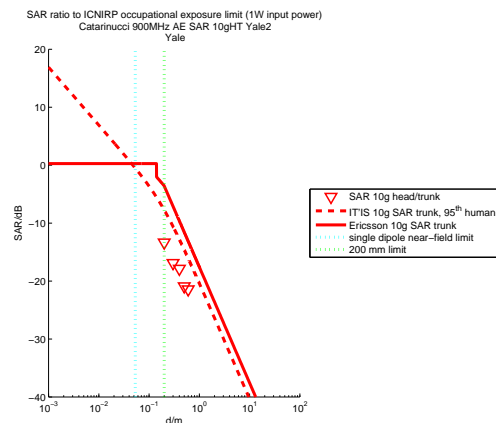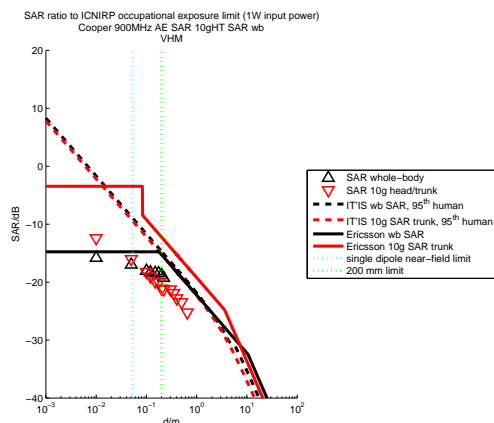Figure 175:
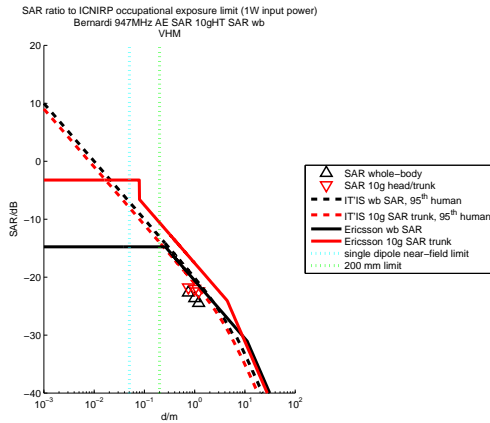


Figure 176:
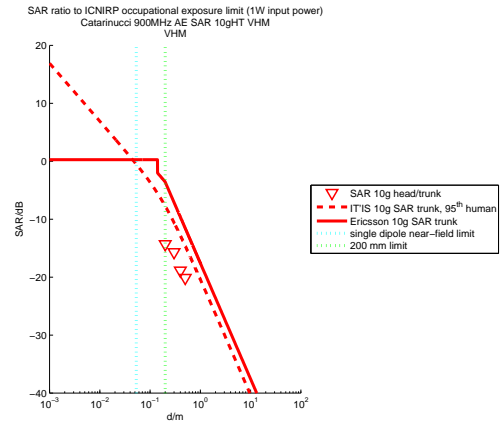


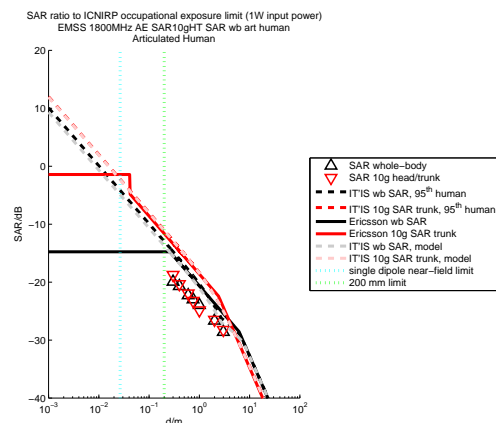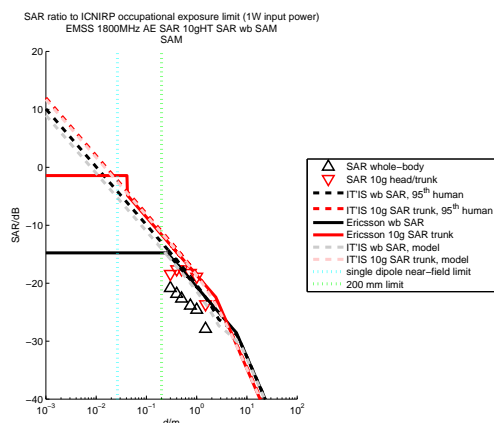Figure 177:

Figure 178:



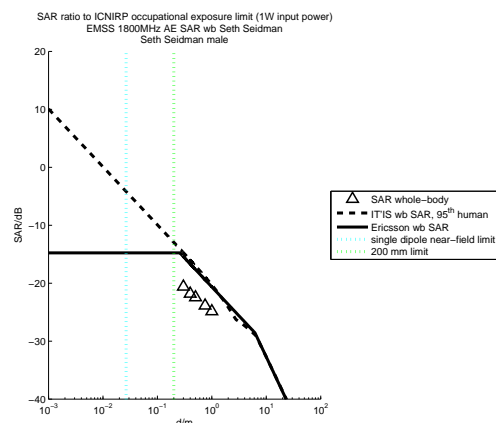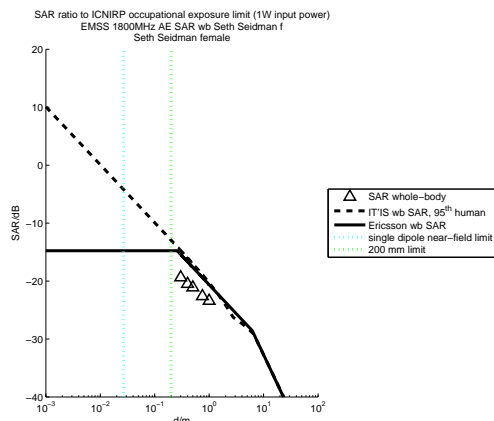Figure 179:



Figure 180:
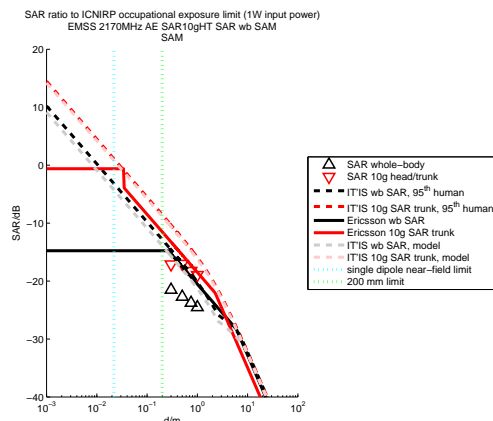


Figure 181:



Figure 182:



Figure 183:

Figure 184:



Figure 185:



Figure 186:



Figure 187:



Figure 188:



Figure 189:

Figure 190:



Figure 191:
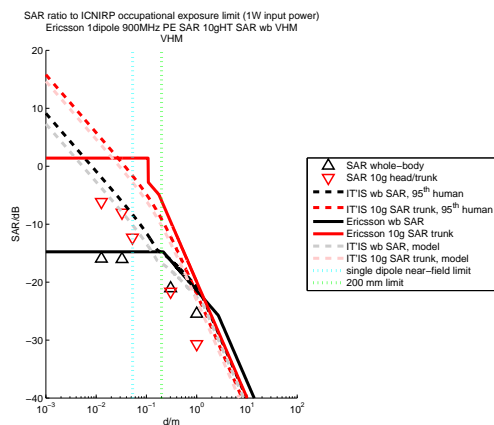


Figure 192:
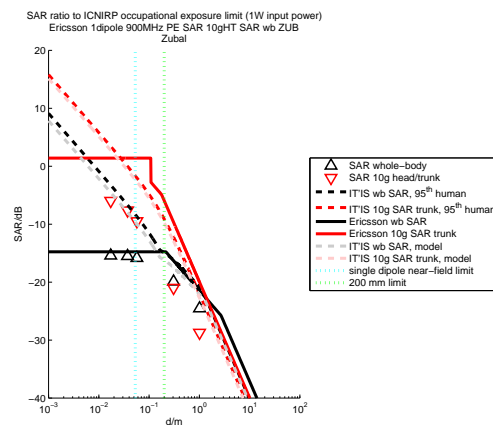


Figure 193:
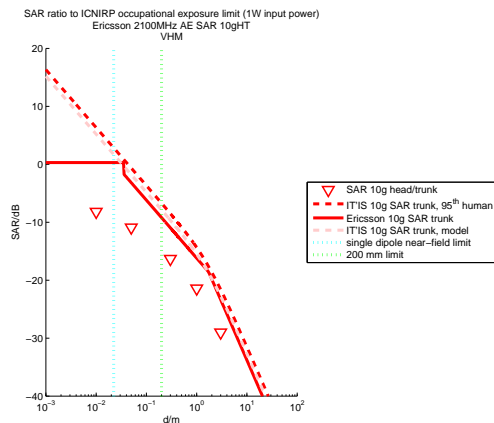


Figure 194:
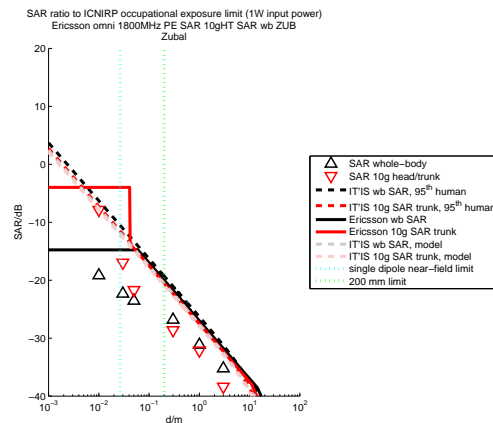


Figure 195:
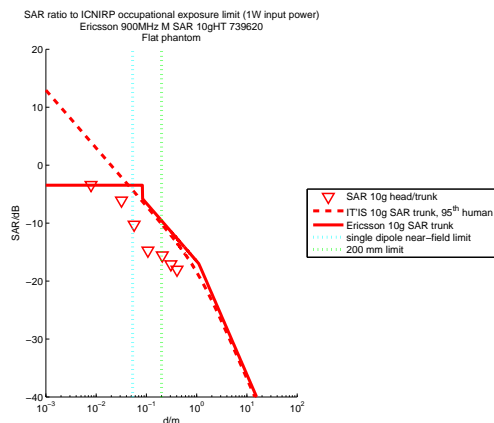
Figure 196:
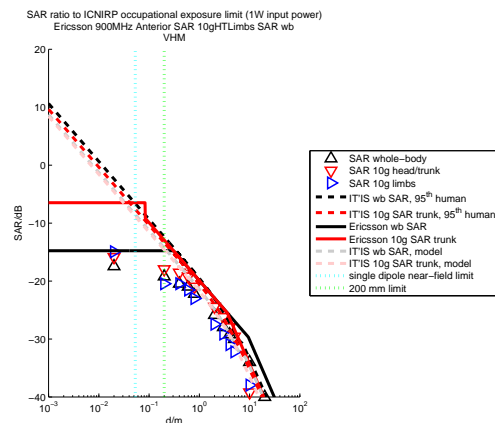


Figure 197:
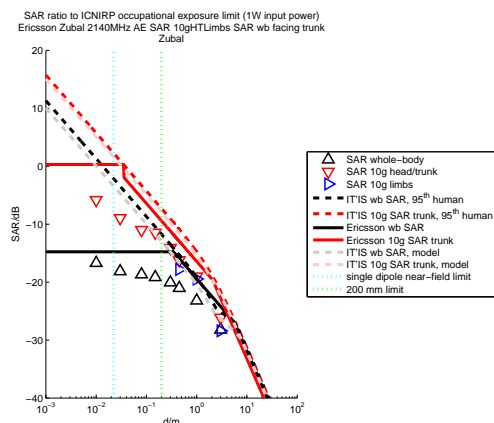


Figure 198:
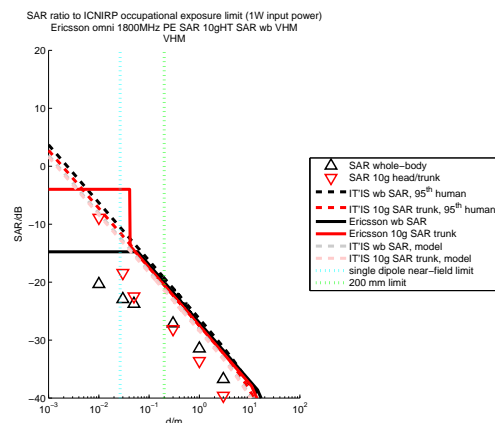


Figure 199:
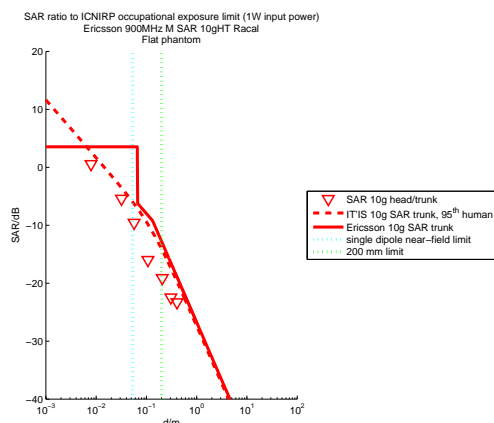


Figure 200:
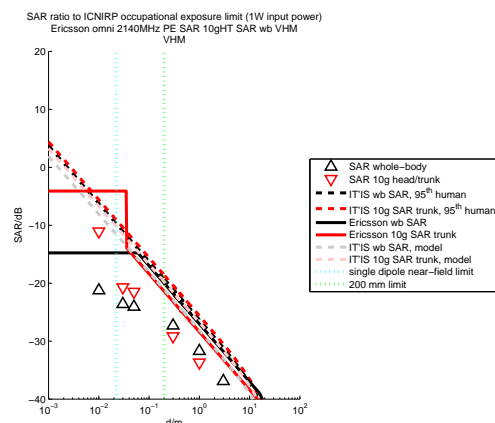


Figure 201:
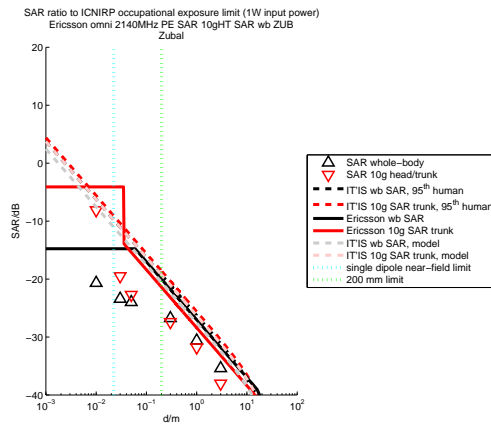
Figure 202:
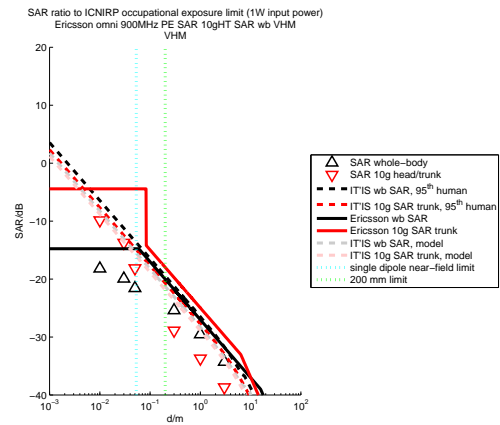


Figure 203:
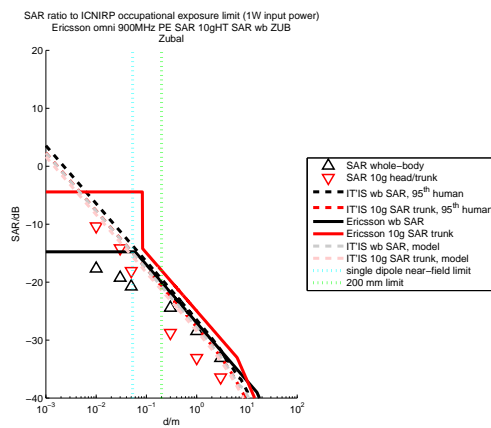


Figure 204:
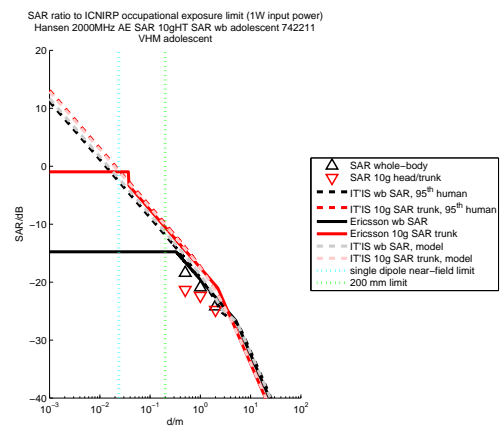


Figure 205:
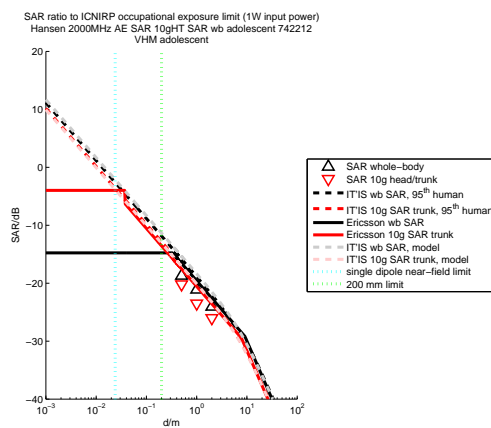


Figure 206:
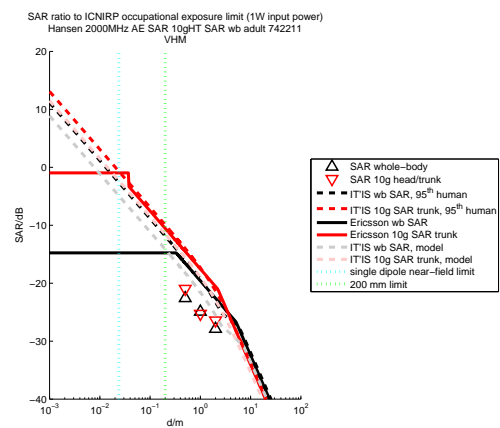


Figure 207:
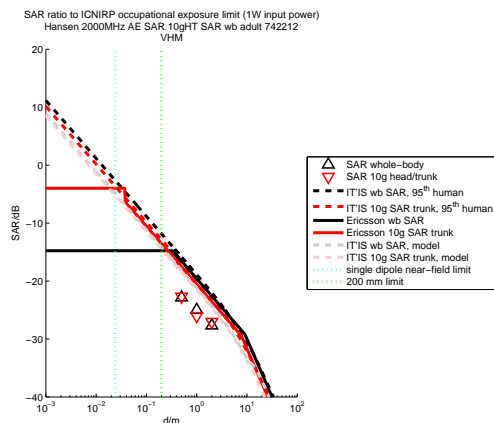
Figure 208:
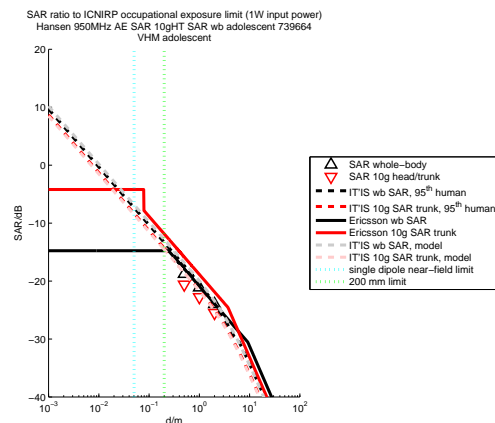


Figure 209:
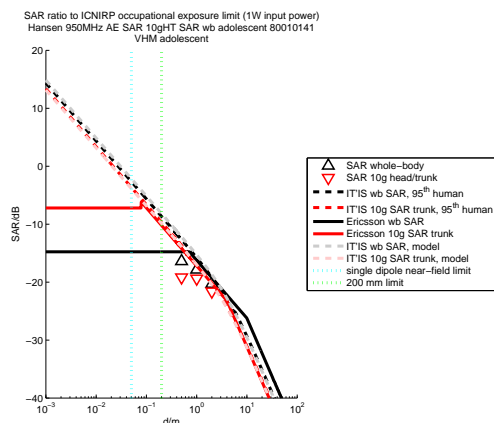


Figure 210:
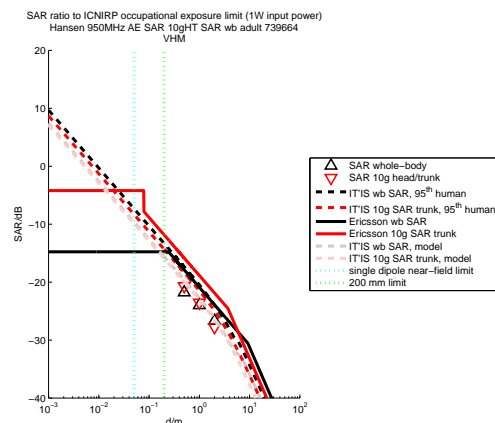


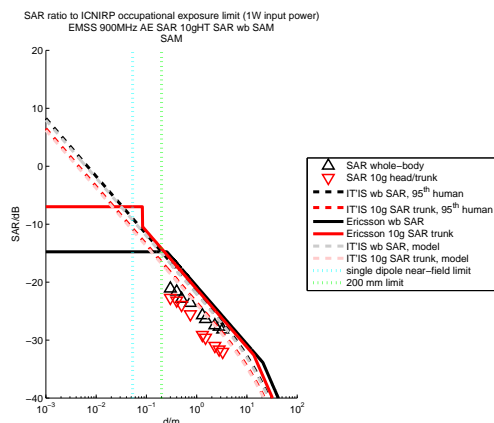Figure 211:
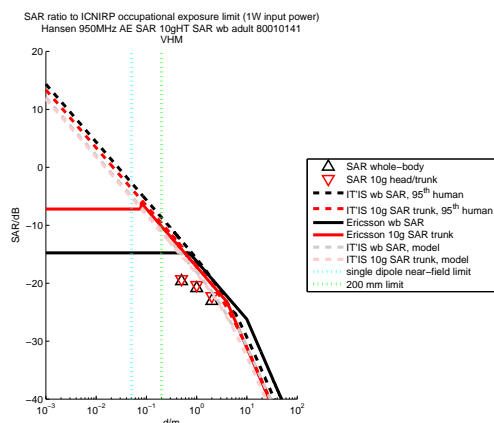


Figure 212:
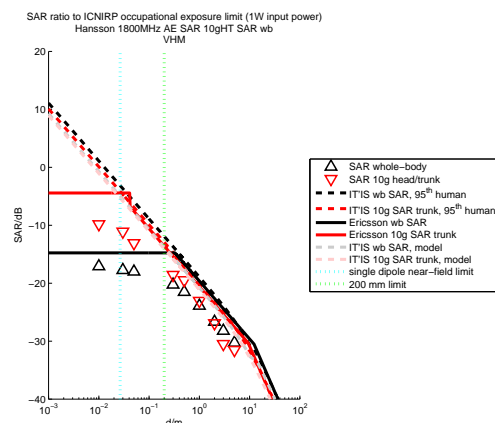
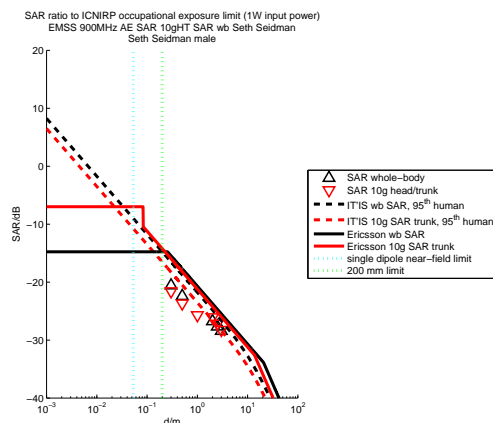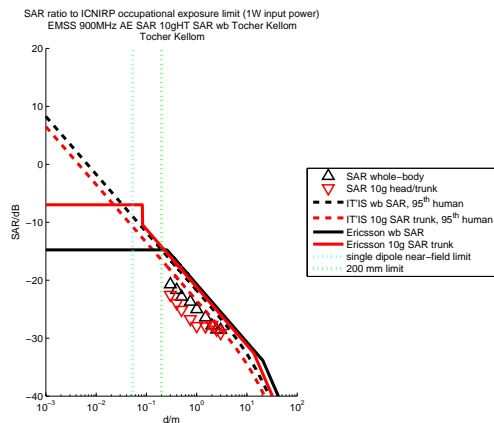

Figure 213:
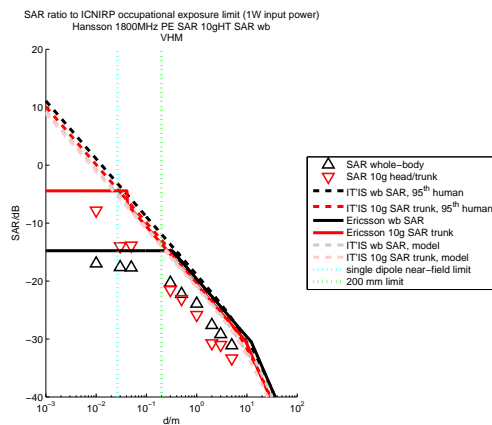
Figure 214:
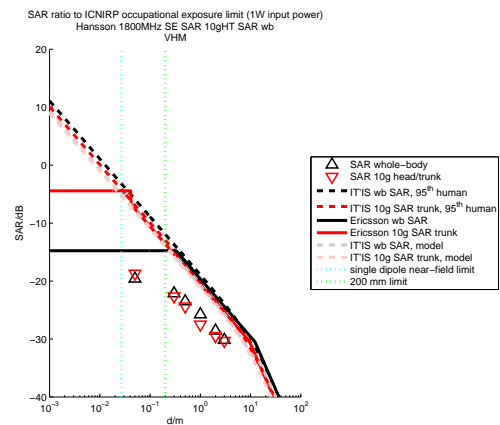


Figure 215:
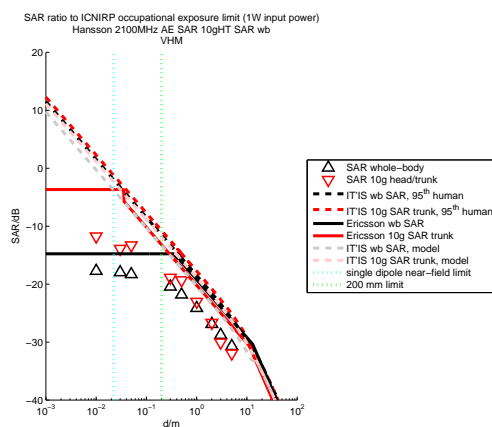


Figure 216:
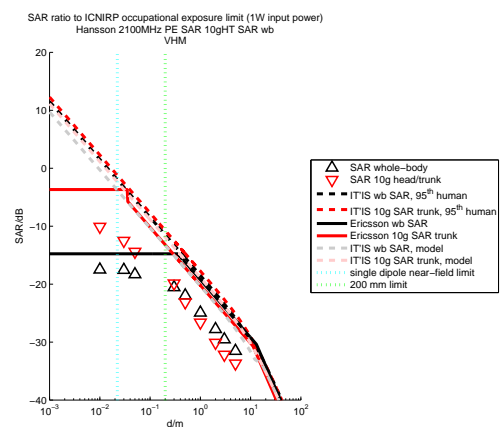


Figure 217:
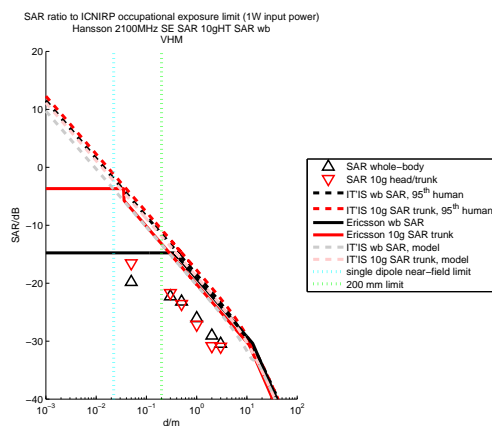


Figure 218:



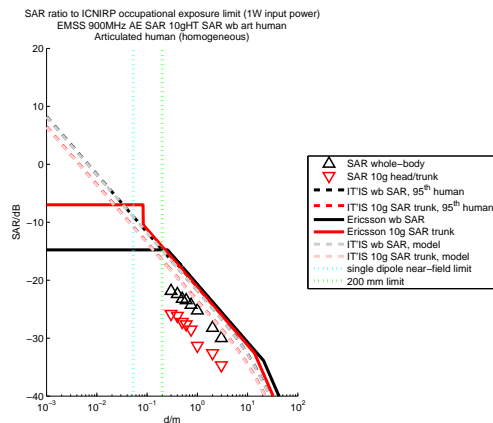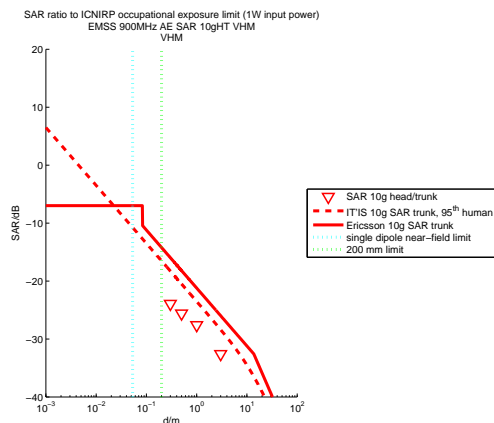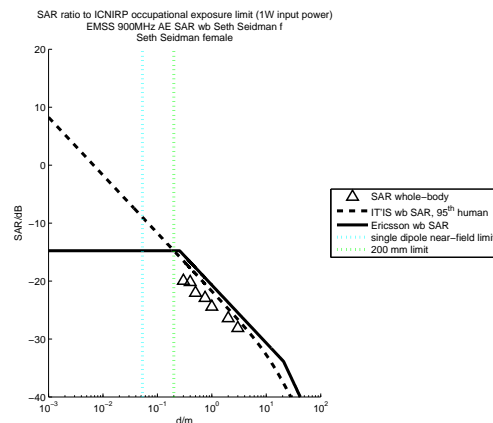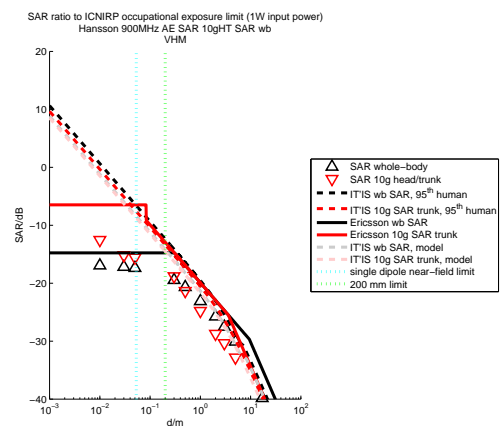Figure 219:
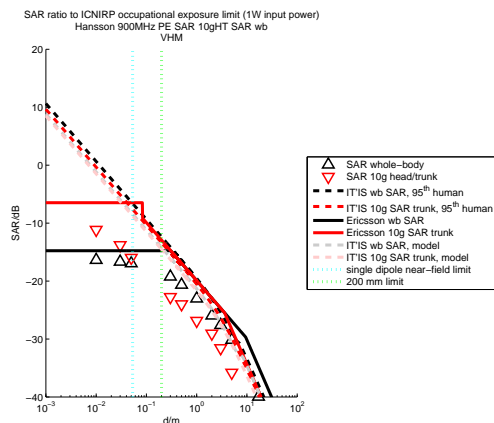
Figure 220:
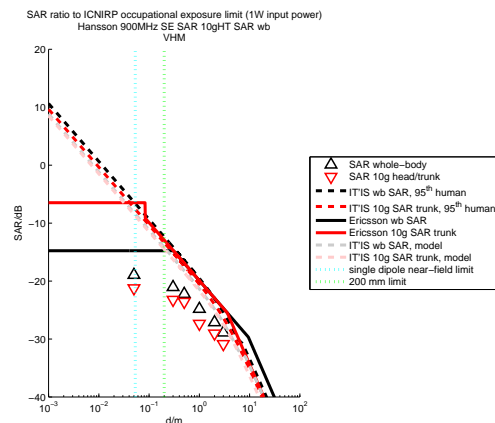


Figure 221:
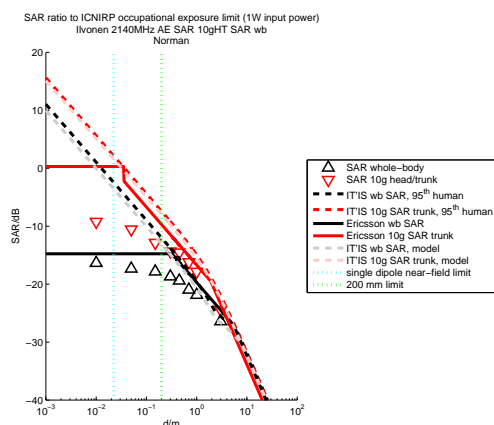


Figure 222:
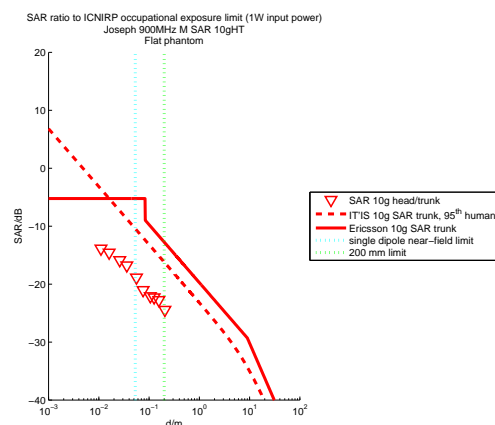


Figure 223:
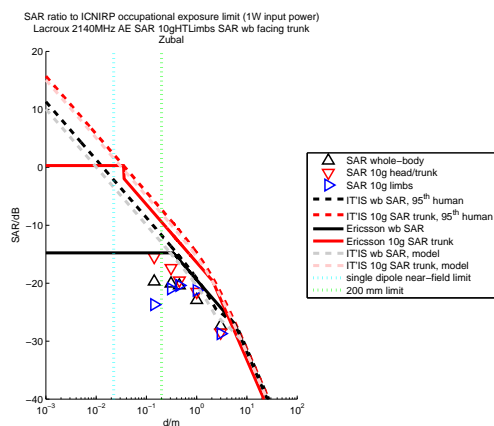


Figure 224:
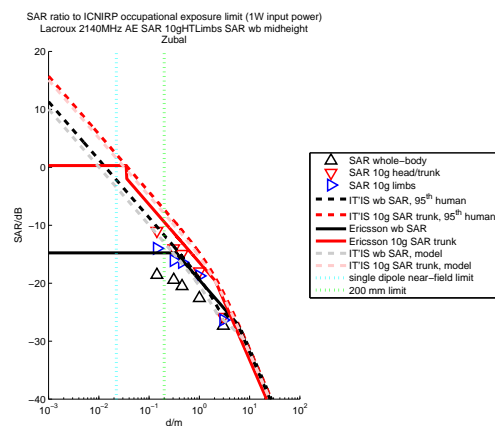


Figure 225:
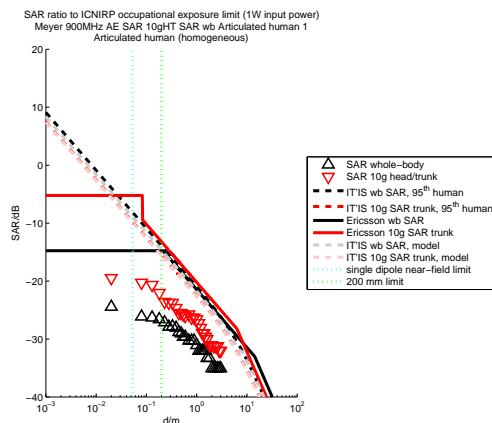
Figure 226:
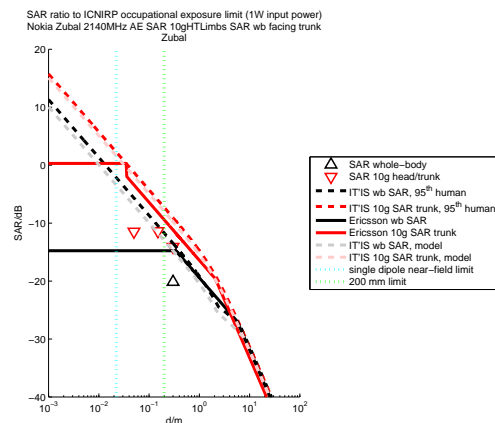


Figure 227:
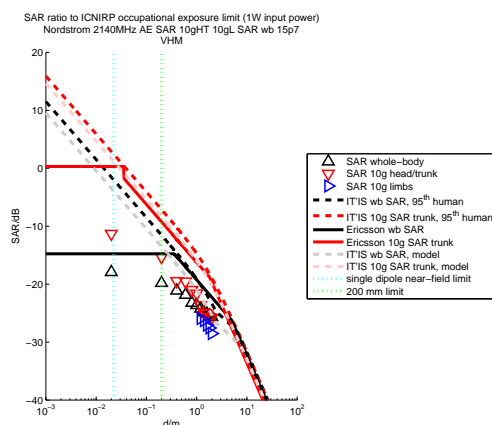


Figure 228:
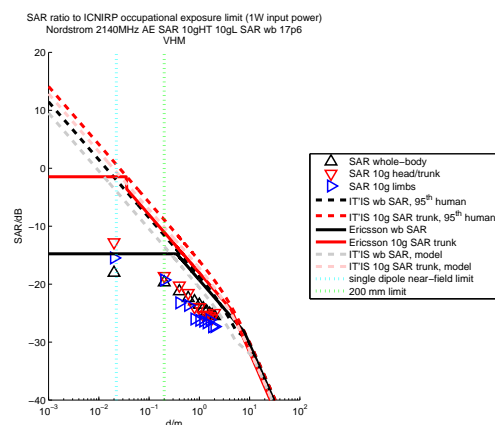


Figure 229:
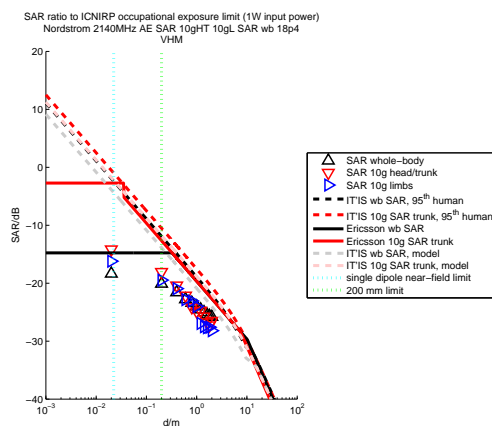


Figure 230:
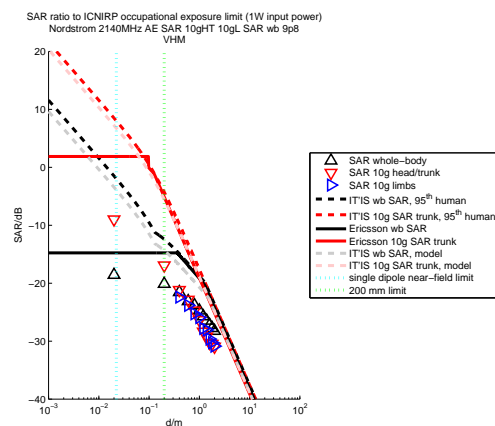


Figure 231:

## G.2    Discussion

In the figures of Section G.1, the estimation formulas are generally conservative for distances larger than 200 mm. As expected, using the weight and height of the simulated model leads to as less conservative estimation.

One can also observe that there is a group of data for which the whole-body SAR approximation is far too conservative (below -9 dB). These data are all associated to homogeneous models, which should not be approximated by formulas including a layering enhancement factor.



232.1: whole-body SAR                       232.2: 10 g SAR
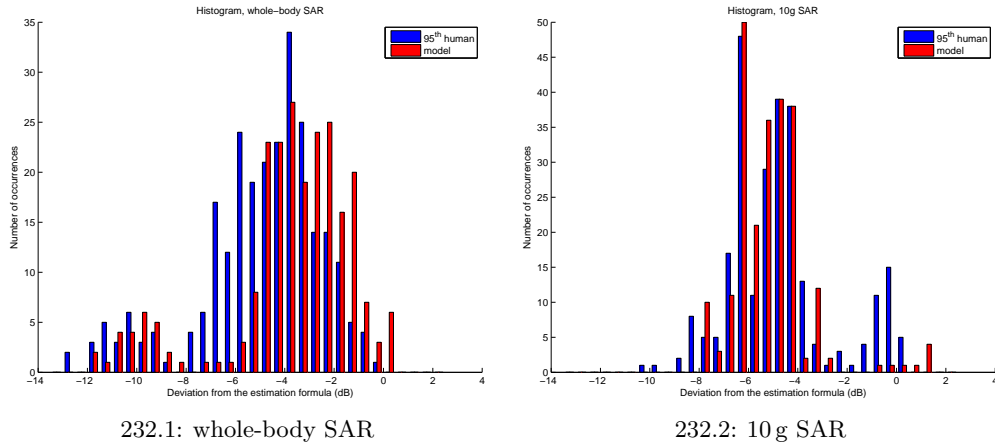
Figure 232: Histogram the deviation between the bulk simulation results of the adult models (> 200 mm) and the estimation formula based on the $95^{th}$ percentile human body and the simulated model cuboids

# H   WP7 – Huygens' Box Validation (Reflective Environment)

Further validation has been done in WP 7 regarding the use of the GHB method in a reflective environment. In addition to the comparison of the 10 g SAR and whole-body average SAR values, electric fields have been extracted along lines passing through the body. This section presents the e-field plots.

Figures 234 - 251 show the rms electric field along three perpendicular lines directed along $x$-, $y$- and $z$-axis running through the body of the homogeneous VFB. The results are shown for two positions of the intersection of the three lines. The position of these two intersections are listed in Table 24 and shown in Figure 233.

| $(x, y, z)$ (m) |
| --- |
| $p_c = (0.106, 0.185, 0.588)$ |
| $p_1 = (0.08, 0.19, 0.7)$ |

Table 24: Two positions for the intersection of the lines along which the fields are evaluated.
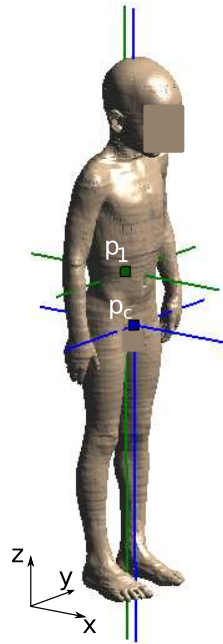


Figure 233: Two sets of three perpendicular where the electric fields are evaluated. The lines are directed along $x$-, $y$- and $z$-axis. The intersections are designated by $p_c$ and $p_1$.

The coordinate system was defined as follows (see Figure 233: *The anatomical model is bounded by a box. From the front, looking into the eyes of the model, the lower, left, back corner of this bounding box is the origin of a right handed coordinate system. The z axis is aligned with the vertical axis of the anatomical model. The positive direction of the z axis is orientated from the legs to the head. The y axis goes in positive direction to the right when looking into the eyes of the model, i.e. from the right hand of the model to the left hand.* Position $p_c$ coincides with the center of the bounding box around the VFB. However, for this position the line along the y-direction lies almost completely outside the body. Therefore, a second position $p_1$ has been chosen.

A good agreement is observed between EMSS and IT'IS for the ground plane and a frequecy of 900 MHz and 2100 MHz. At 300 MHz the results of GHB (IT'IS) deviate from the fully coupled

simulations (EMSS). So, coupling between the body and the environment cannot be completely neglected at 300 MHz. Remark also that the results for the fields along the y-direction and the intersection in the center of the VFB do not agree well because this line lies almost completely outside the body. For the vertical wall, no agreement has been observed between the fully coupled simulations and the GHB for all the considered configurations. This is mainly due to the shadowing of the body for the incident fields.



234.1: Ground - x-line

234.2: Wall - x-line

234.3: Ground - y-line

234.4: Wall - y-line

234.5: Ground - z-line

234.6: Wall - z-line
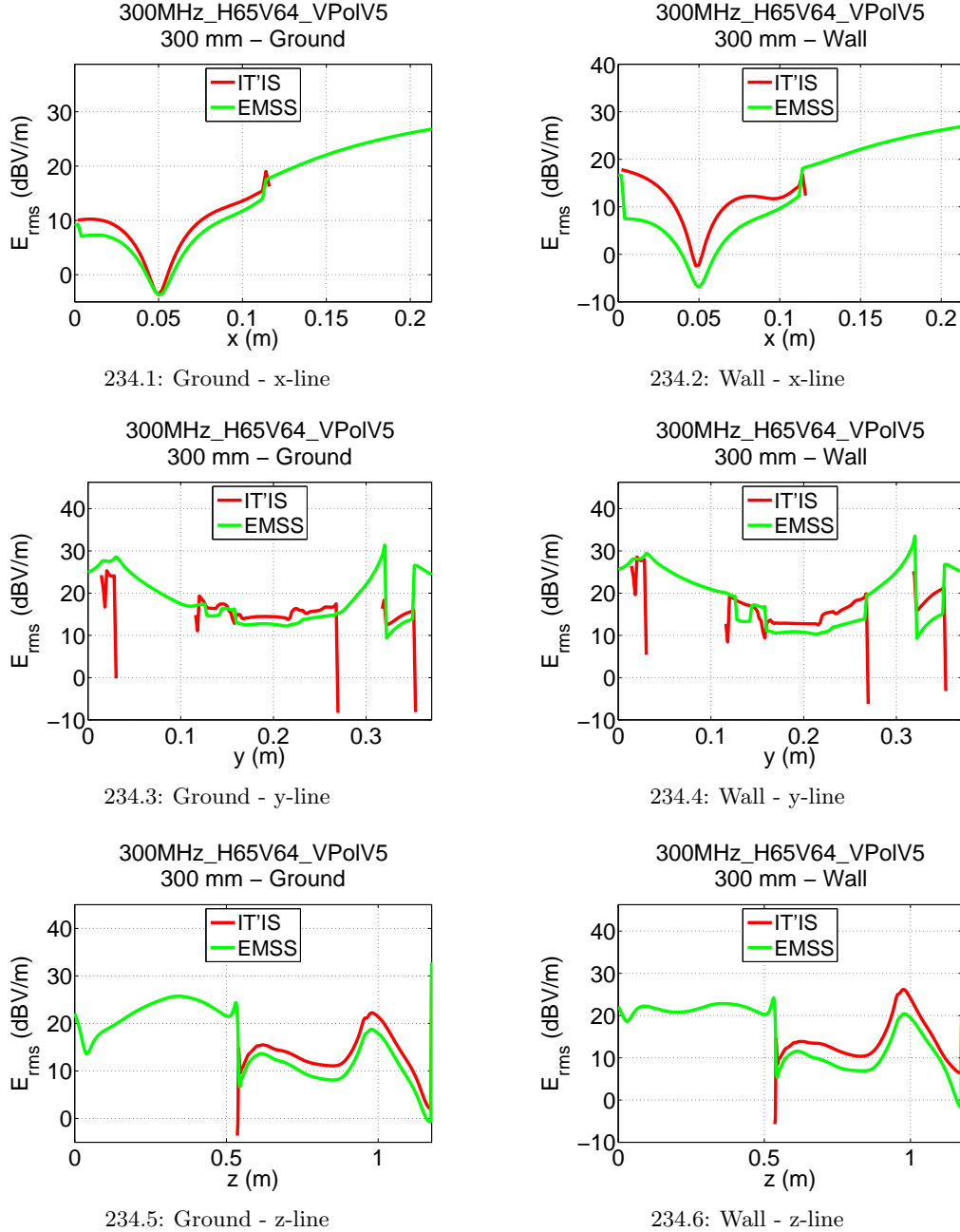
Figure 234: The rms electric field through the center of the VFB along x-, y- and z-direction for 300MHz_H65V64_VPolV5 base station antenna in a reflective environment at a distance of 0.3 m from VFB.

235.1: Ground - x-line

235.2: Wall - x-line

235.3: Ground - y-line

235.4: Wall - y-line

235.5: Ground - z-line

235.6: Wall - z-line

Figure 235: The rms electric field through the center of the VFB along x-, y- and z-direction for 300MHz_H65V64_VPolV5 base station antenna in a reflective environment at a distance of 3 m from VFB.

236.1: Ground - x-line

236.2: Wall - x-line

236.3: Ground - y-line

236.4: Wall - y-line

236.5: Ground - z-line

236.6: Wall - z-line

Figure 236: The rms electric field through the center of the VFB along x-, y- and z-direction for 300MHz_H65V64_VPolV5 base station antenna in a reflective environment at a distance of 10 m from VFB.
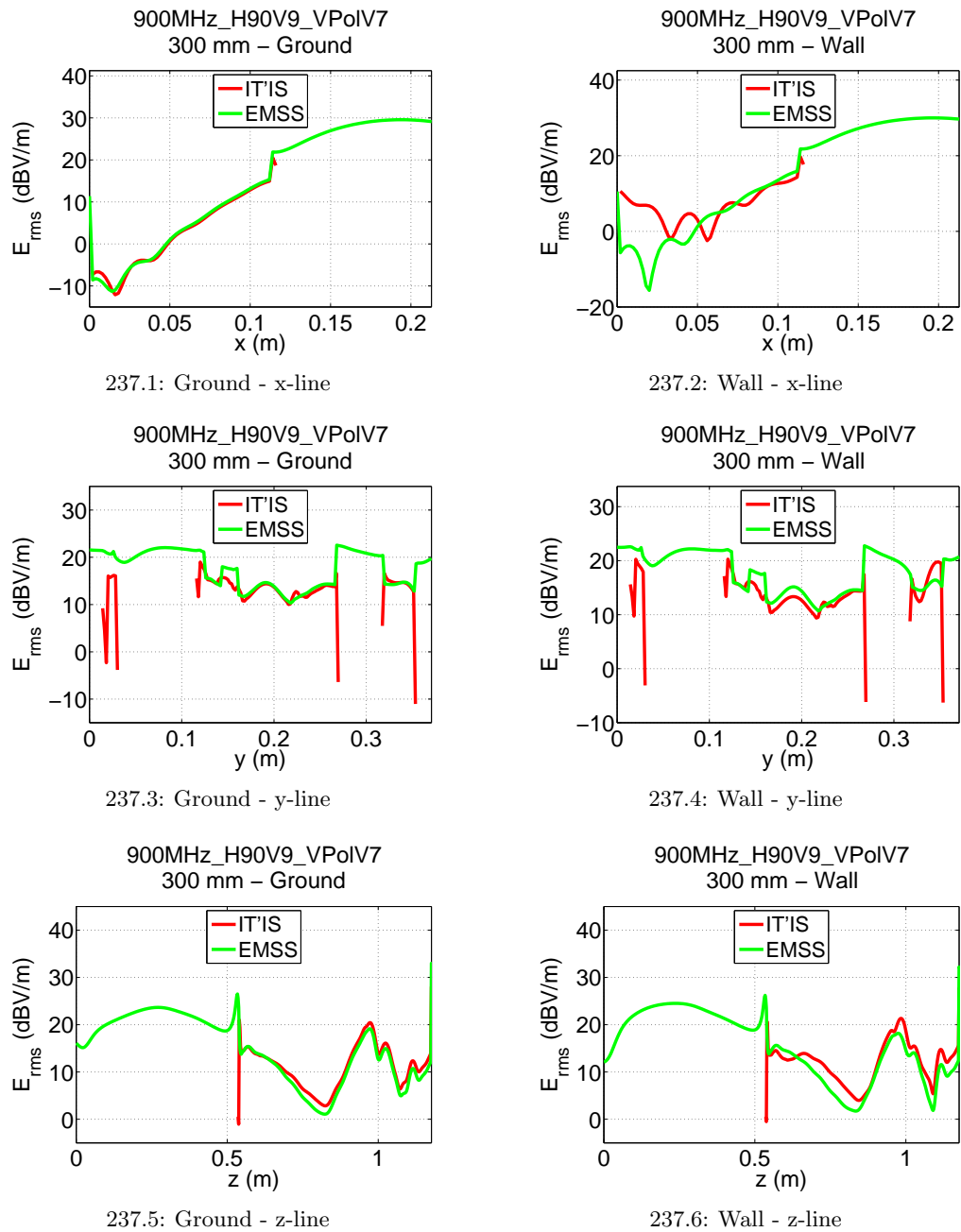
Figure 237: The rms electric field through the center of the VFB along x-, y- and z-direction for 900MHz_H90V9_VPolV7 base station antenna in a reflective environment at a distance of 0.3 m from VFB.

238.1: Ground - x-line

238.2: Wall - x-line

238.3: Ground - y-line

238.4: Wall - y-line

238.5: Ground - z-line

238.6: Wall - z-line

Figure 238: The rms electric field through the center of the VFB along x-, y- and z-direction for 900MHz_H90V9_VPolV7 base station antenna in a reflective environment at a distance of 3 m from VFB.

239.1: Ground - x-line

239.2: Wall - x-line

239.3: Ground - y-line

239.4: Wall - y-line

239.5: Ground - z-line

239.6: Wall - z-line

Figure 239: The rms electric field through the center of the VFB along x-, y- and z-direction for 900MHz_H90V9_VPolV7 base station antenna in a reflective environment at a distance of 10 m from VFB.

2100MHz_H90V80_IndoorVPolV4
300 mm – Ground

240.1: Ground - x-line

2100MHz_H90V80_IndoorVPolV4
300 mm – Wall

240.2: Wall - x-line

2100MHz_H90V80_IndoorVPolV4
300 mm – Ground

240.3: Ground - y-line

2100MHz_H90V80_IndoorVPolV4
300 mm – Wall

240.4: Wall - y-line

2100MHz_H90V80_IndoorVPolV4
300 mm – Ground

240.5: Ground - z-line

2100MHz_H90V80_IndoorVPolV4
300 mm – Wall

240.6: Wall - z-line

Figure 240: The rms electric field through the center of the VFB along x-, y- and z-direction for 2100MHz_H90V80_IndoorVPolV4 base station antenna in a reflective environment at a distance of 0.3 m from VFB.

241.1: Ground - x-line

241.2: Wall - x-line

241.3: Ground - y-line

241.4: Wall - y-line

241.5: Ground - z-line

241.6: Wall - z-line

Figure 241: The rms electric field through the center of the VFB along x-, y- and z-direction for 2100MHz_H90V80_IndoorVPolV4 base station antenna in a reflective environment at a distance of 3 m from VFB.

242.1: Ground - x-line

242.2: Wall - x-line

242.3: Ground - y-line

242.4: Wall - y-line

242.5: Ground - z-line

242.6: Wall - z-line

Figure 242: The rms electric field through the center of the VFB along x-, y- and z-direction for 2100MHz_H90V80_IndoorVPolV4 base station antenna in a reflective environment at a distance of 10 m from VFB.

243.1: Ground - x-line

243.2: Wall - x-line

243.3: Ground - y-line

243.4: Wall - y-line

243.5: Ground - z-line

243.6: Wall - z-line

Figure 243: The rms electric field through $p_1$ along x-, y- and z-direction for 300MHz_H65V64_VPolV5 base station antenna in a reflective environment at a distance of 0.3 m from VFB.

244.1: Ground - x-line

244.2: Wall - x-line

244.3: Ground - y-line

244.4: Wall - y-line

244.5: Ground - z-line

244.6: Wall - z-line

Figure 244: The rms electric field through $p_1$ along x-, y- and z-direction for 300MHz_H65V64_VPolV5 base station antenna in a reflective environment at a distance of 3 m from VFB.

245.1: Ground - x-line

245.2: Wall - x-line

245.3: Ground - y-line

245.4: Wall - y-line

245.5: Ground - z-line

245.6: Wall - z-line
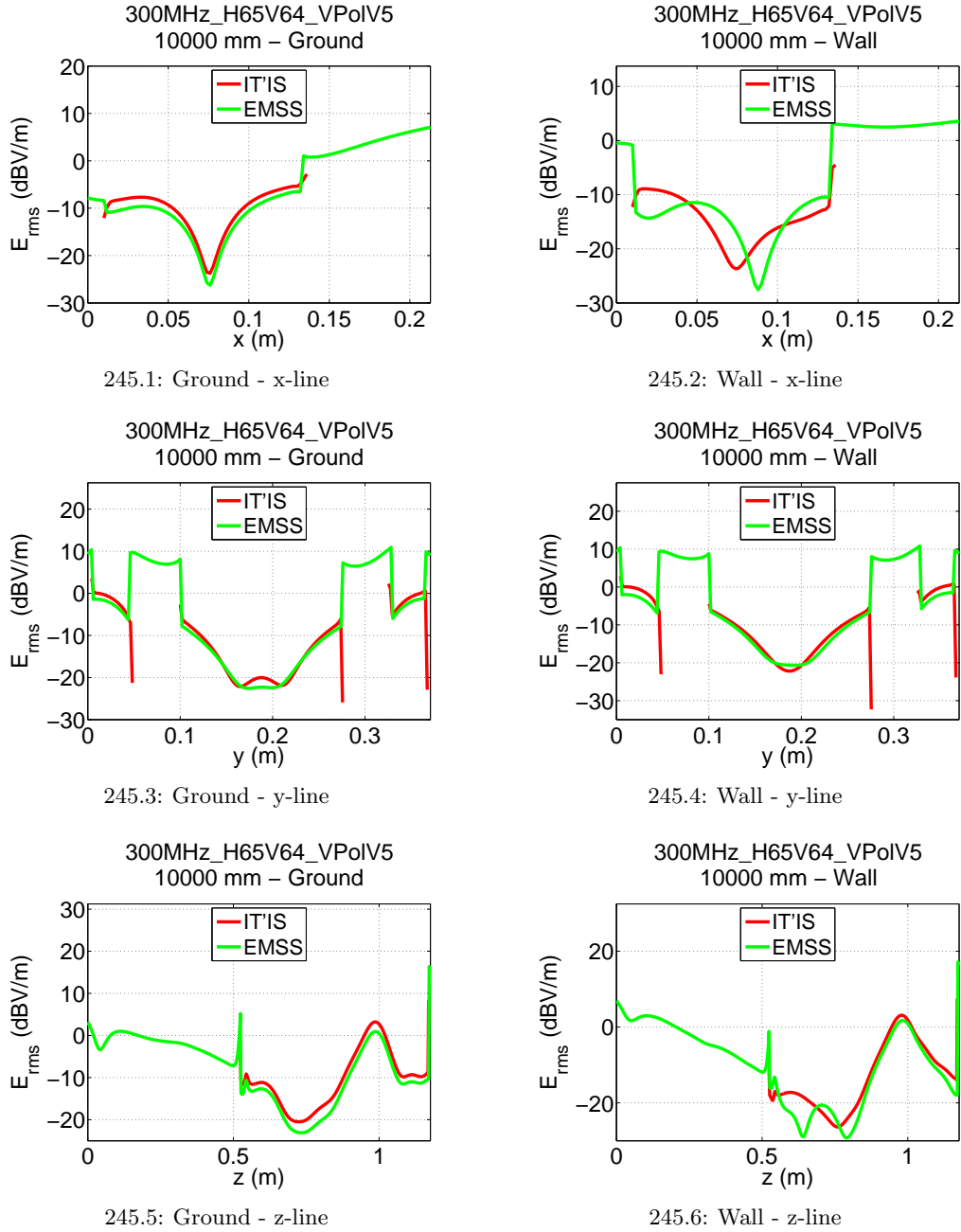
Figure 245: The rms electric field through $p_1$ along x-, y- and z-direction for 300MHz_H65V64_VPolV5 base station antenna in a reflective environment at a distance of 10 m from VFB.

246.1: Ground - x-line

246.2: Wall - x-line

246.3: Ground - y-line

246.4: Wall - y-line

246.5: Ground - z-line

246.6: Wall - z-line
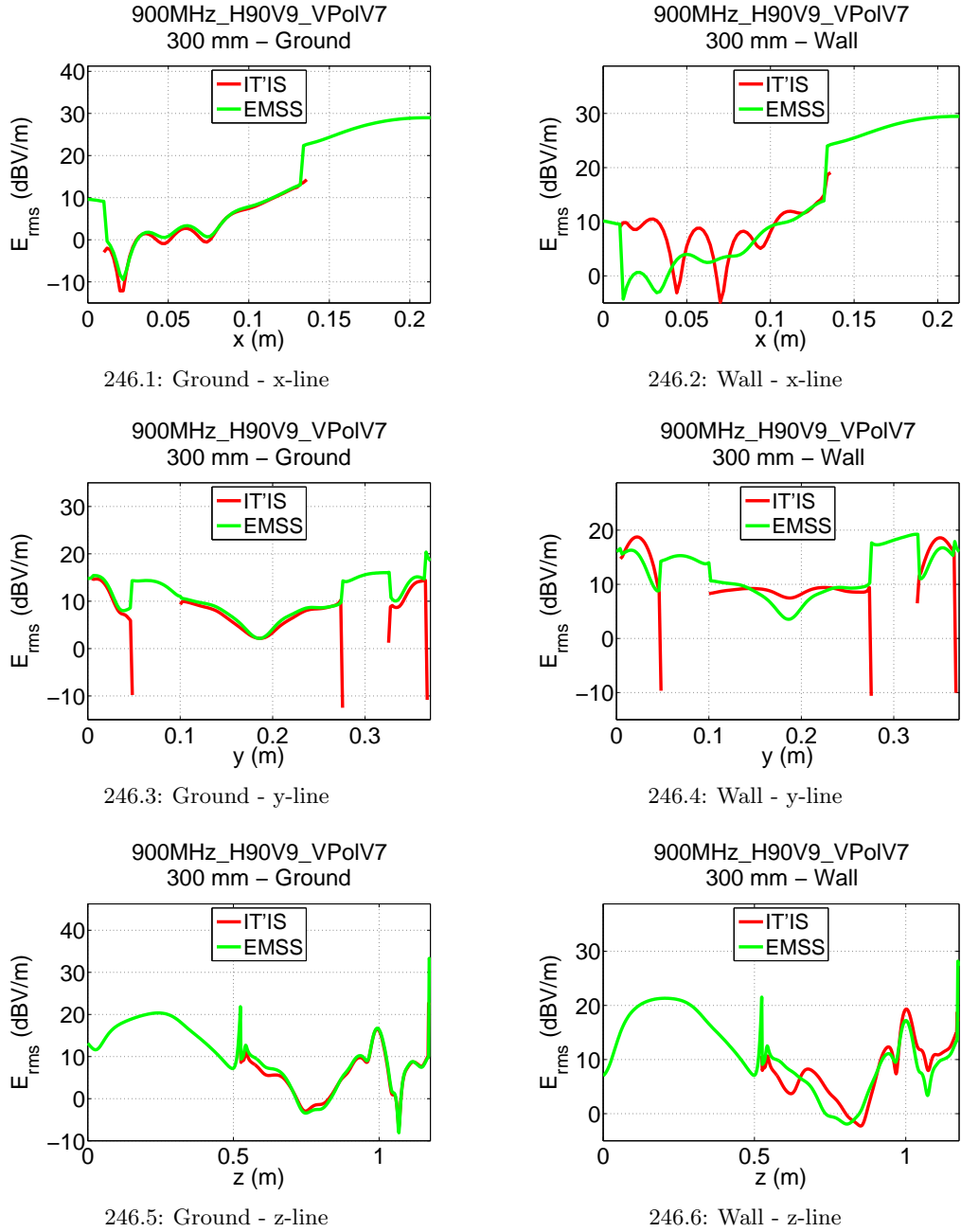
Figure 246: The rms electric field through $p_1$ along x-, y- and z-direction for 900MHz_H90V9_VPolV7 base station antenna in a reflective environment at a distance of $0.3\,\mathrm{m}$ from VFB.

247.1: Ground - x-line

247.2: Wall - x-line

247.3: Ground - y-line

247.4: Wall - y-line

247.5: Ground - z-line

247.6: Wall - z-line
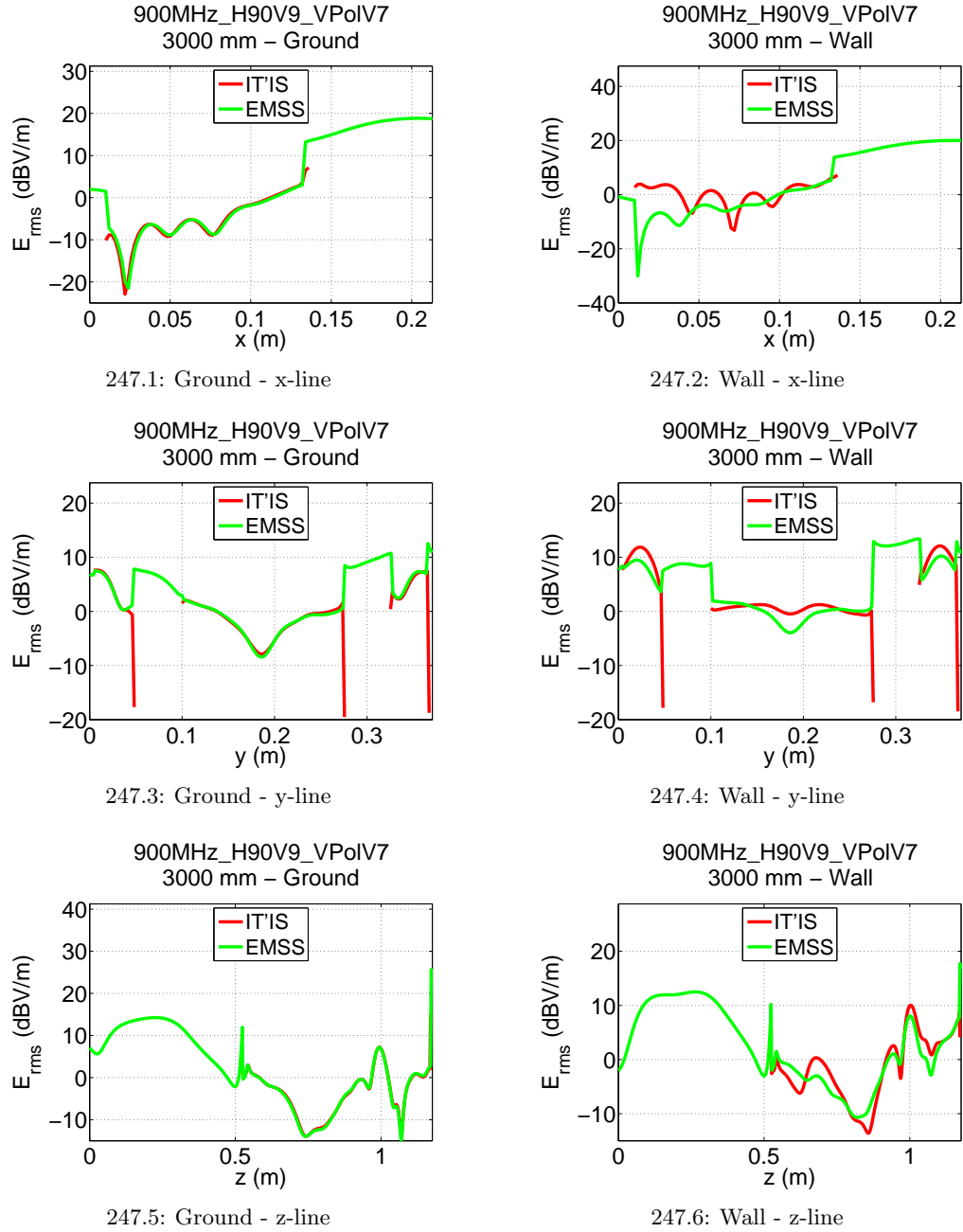
Figure 247: The rms electric field through $p_1$ along x-, y- and z-direction for 900MHz_H90V9_VPolV7 base station antenna in a reflective environment at a distance of $3\,\mathrm{m}$ from VFB.

248.1: Ground - x-line

248.2: Wall - x-line

248.3: Ground - y-line

248.4: Wall - y-line

248.5: Ground - z-line

248.6: Wall - z-line
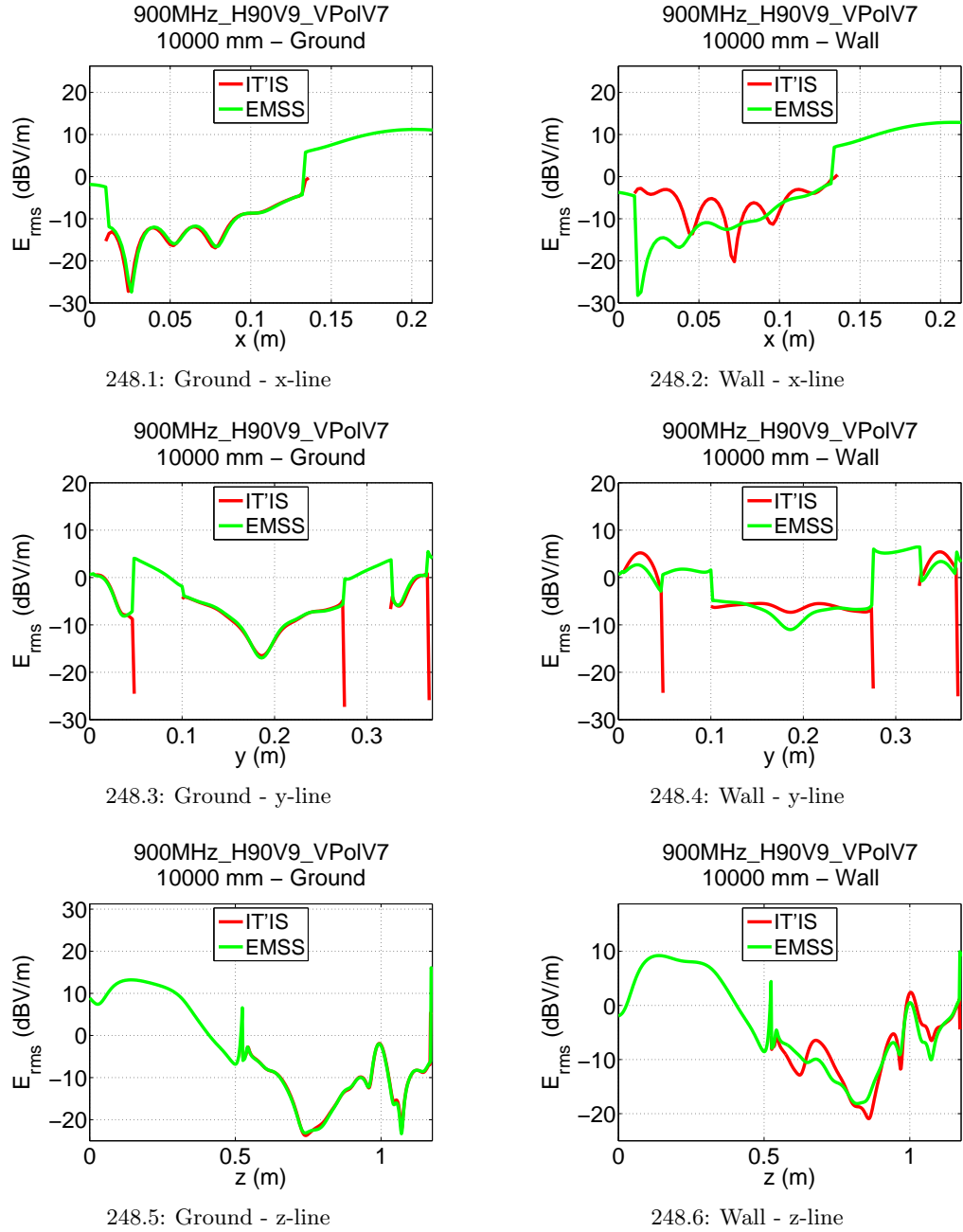
Figure 248: The rms electric field through $p_1$ along x-, y- and z-direction for 900MHz_H90V9_VPolV7 base station antenna in a reflective environment at a distance of $10\,\mathrm{m}$ from VFB.

2100MHz_H90V80_IndoorVPolV4
300 mm – Ground

2100MHz_H90V80_IndoorVPolV4
300 mm – Wall

249.1: Ground - x-line

249.2: Wall - x-line

2100MHz_H90V80_IndoorVPolV4
300 mm – Ground

2100MHz_H90V80_IndoorVPolV4
300 mm – Wall

249.3: Ground - y-line

249.4: Wall - y-line

2100MHz_H90V80_IndoorVPolV4
300 mm – Ground

2100MHz_H90V80_IndoorVPolV4
300 mm – Wall

249.5: Ground - z-line

249.6: Wall - z-line
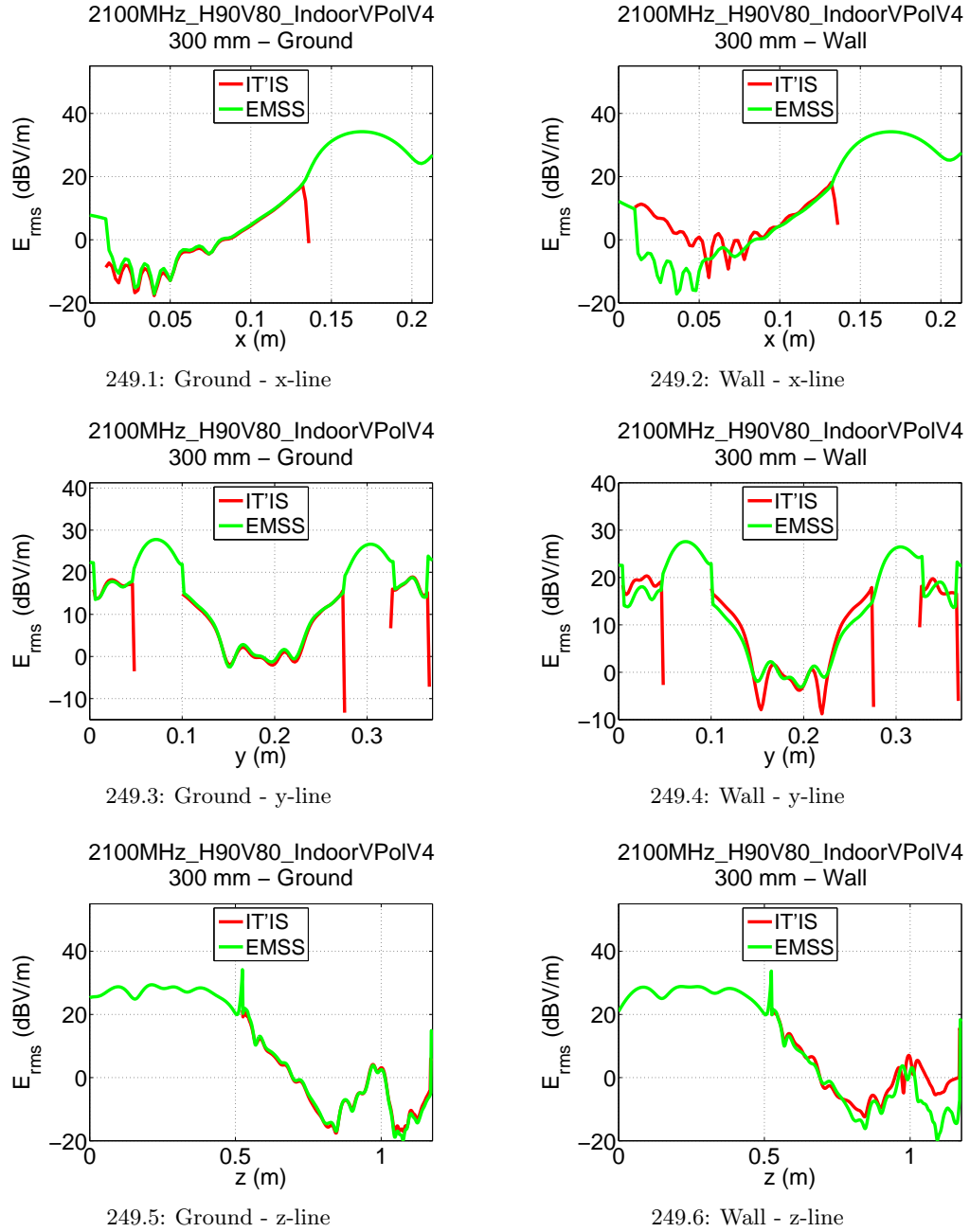
Figure 249: The rms electric field through $p_1$ along x-, y- and z-direction for 2100MHz_H90V80_IndoorVPolV4 base station antenna in a reflective environment at a distance of 0.3 m from VFB.

250.1: Ground - x-line

250.2: Wall - x-line

250.3: Ground - y-line

250.4: Wall - y-line

250.5: Ground - z-line

250.6: Wall - z-line
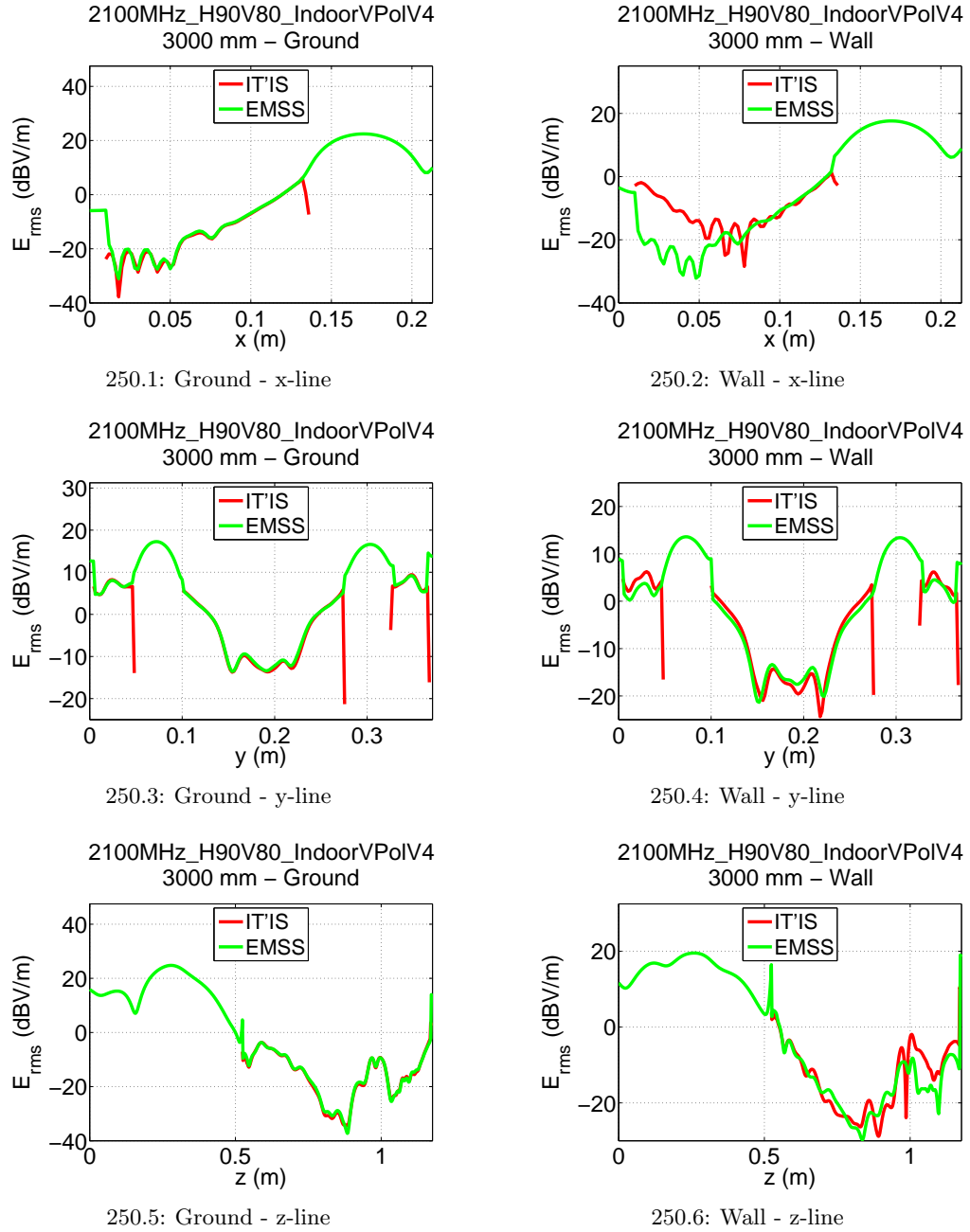
Figure 250: The rms electric field through $p_1$ along x-, y- and z-direction for 2100MHz_H90V80_IndoorVPolV4 base station antenna in a reflective environment at a distance of 3 m from VFB.

251.1: Ground - x-line

251.2: Wall - x-line

251.3: Ground - y-line

251.4: Wall - y-line

251.5: Ground - z-line

251.6: Wall - z-line
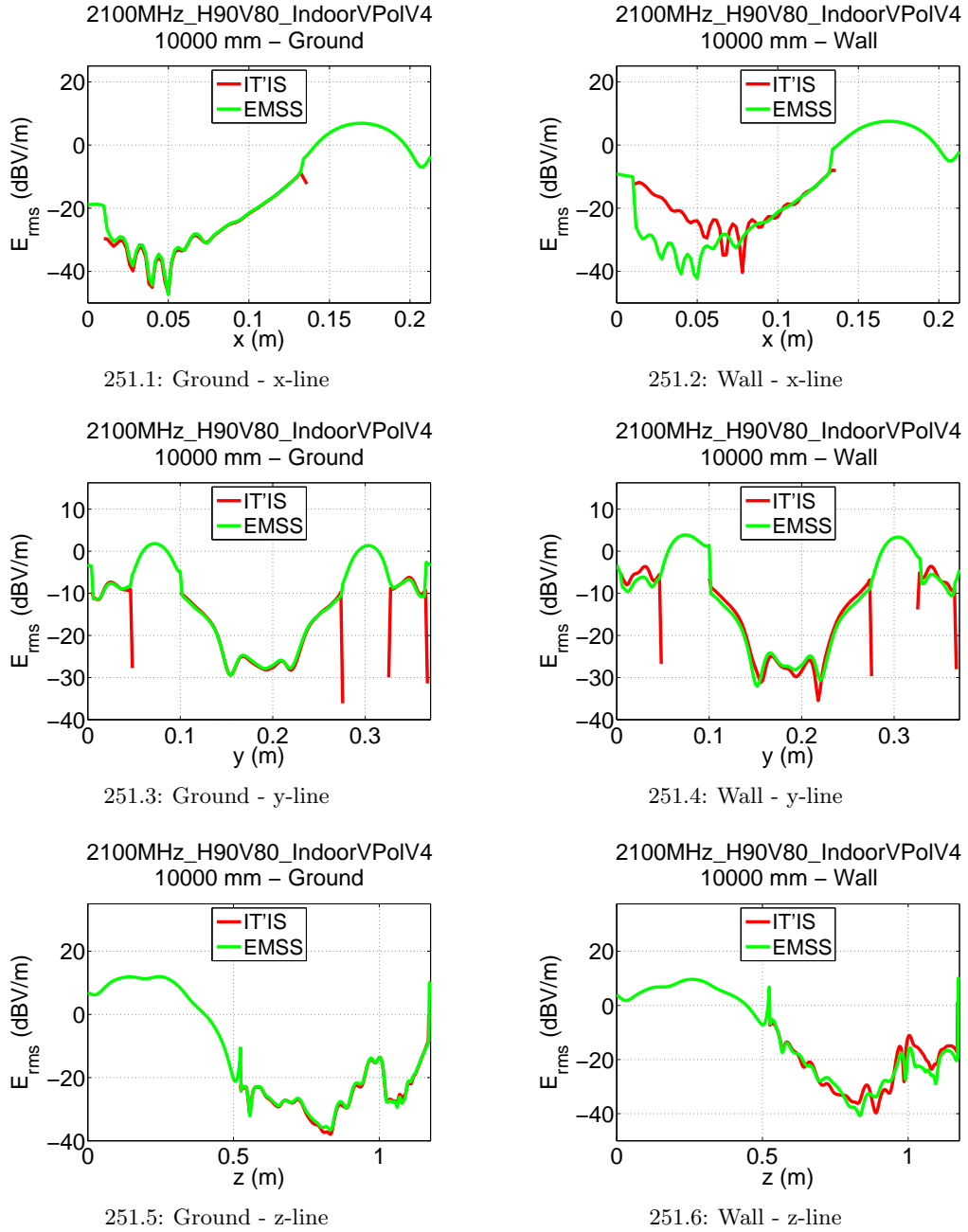
Figure 251: The rms electric field through $p_1$ along x-, y- and z-direction for 2100MHz_H90V80_IndoorVPolV4 base station antenna in a reflective environment at a distance of 10 m from VFB.
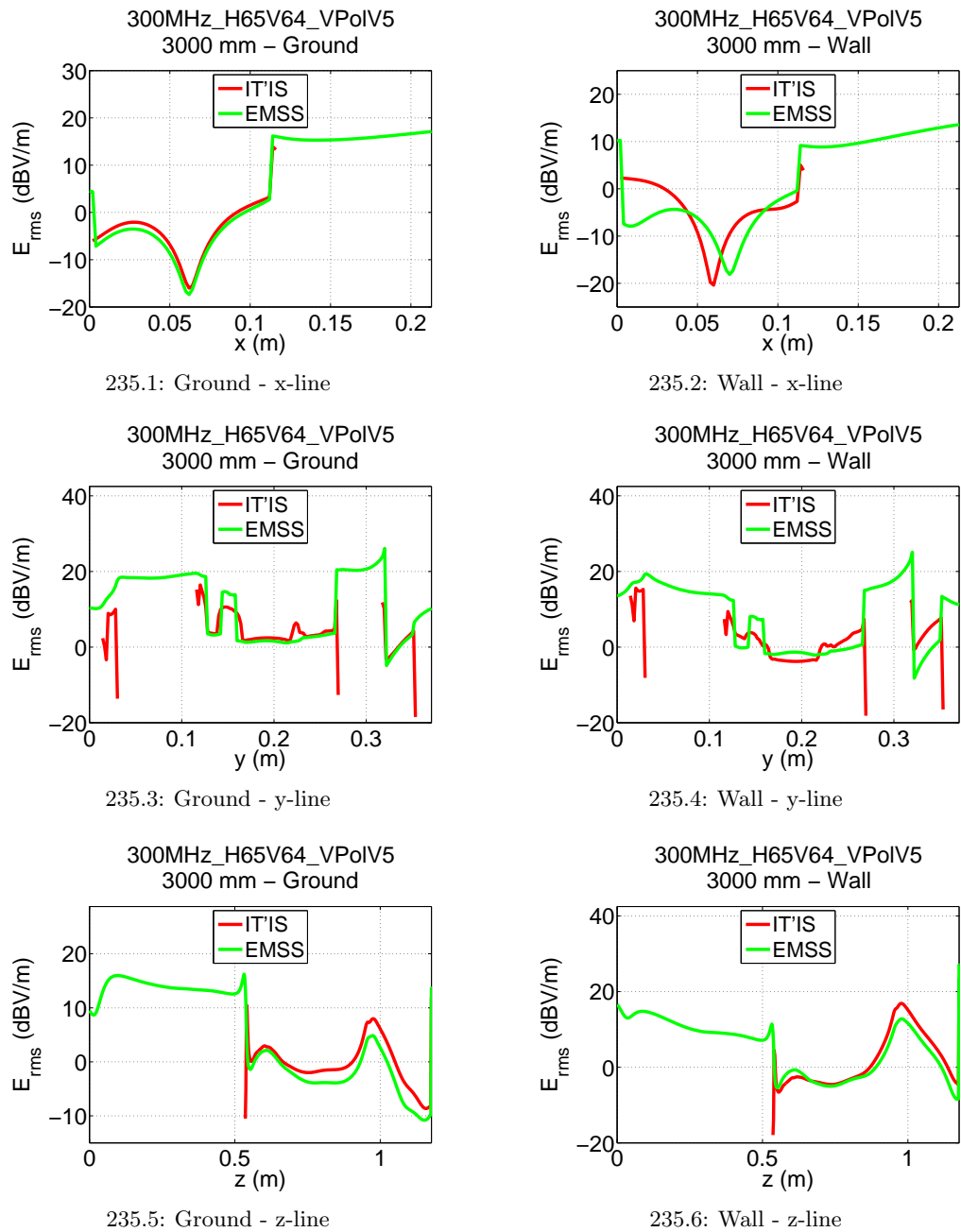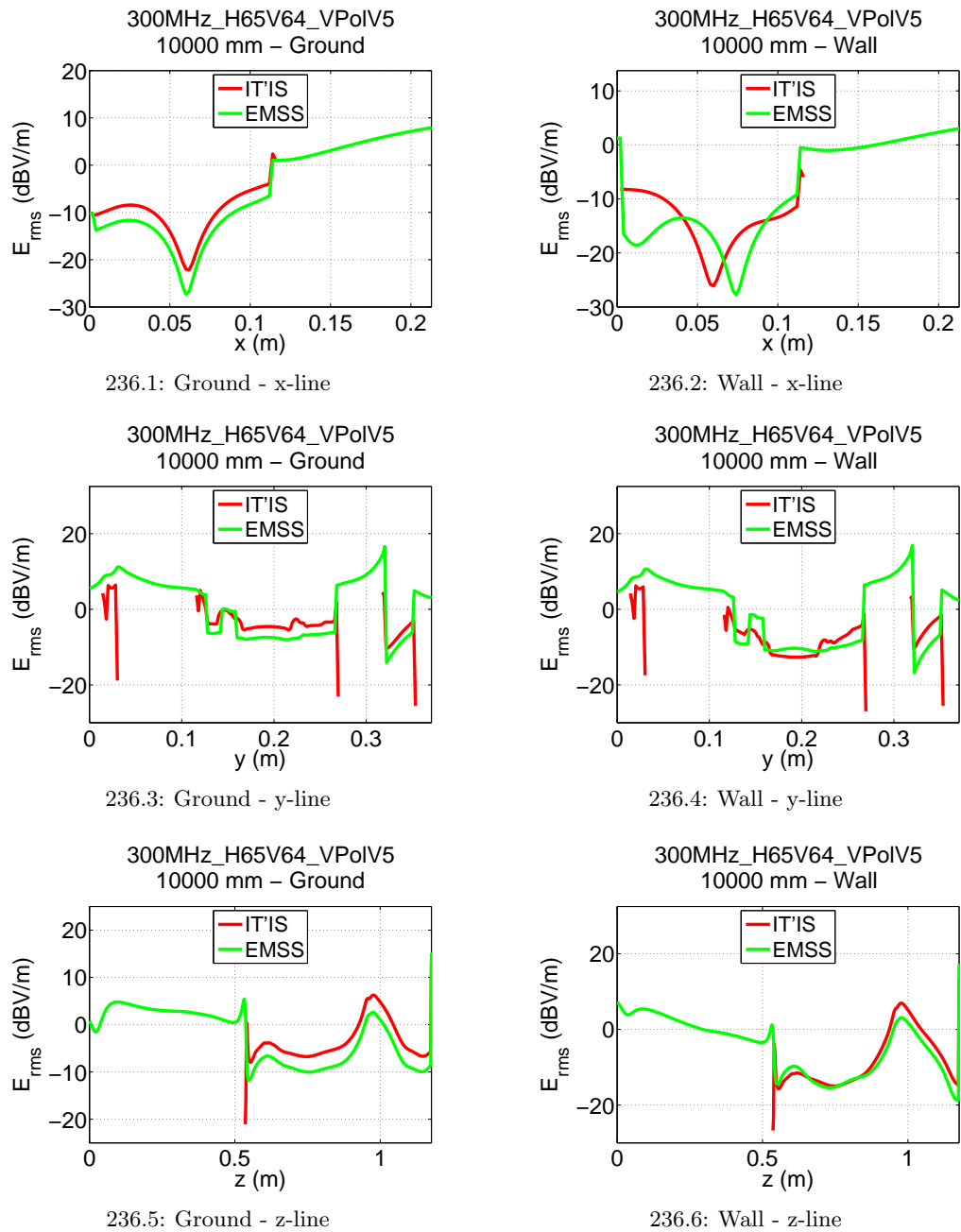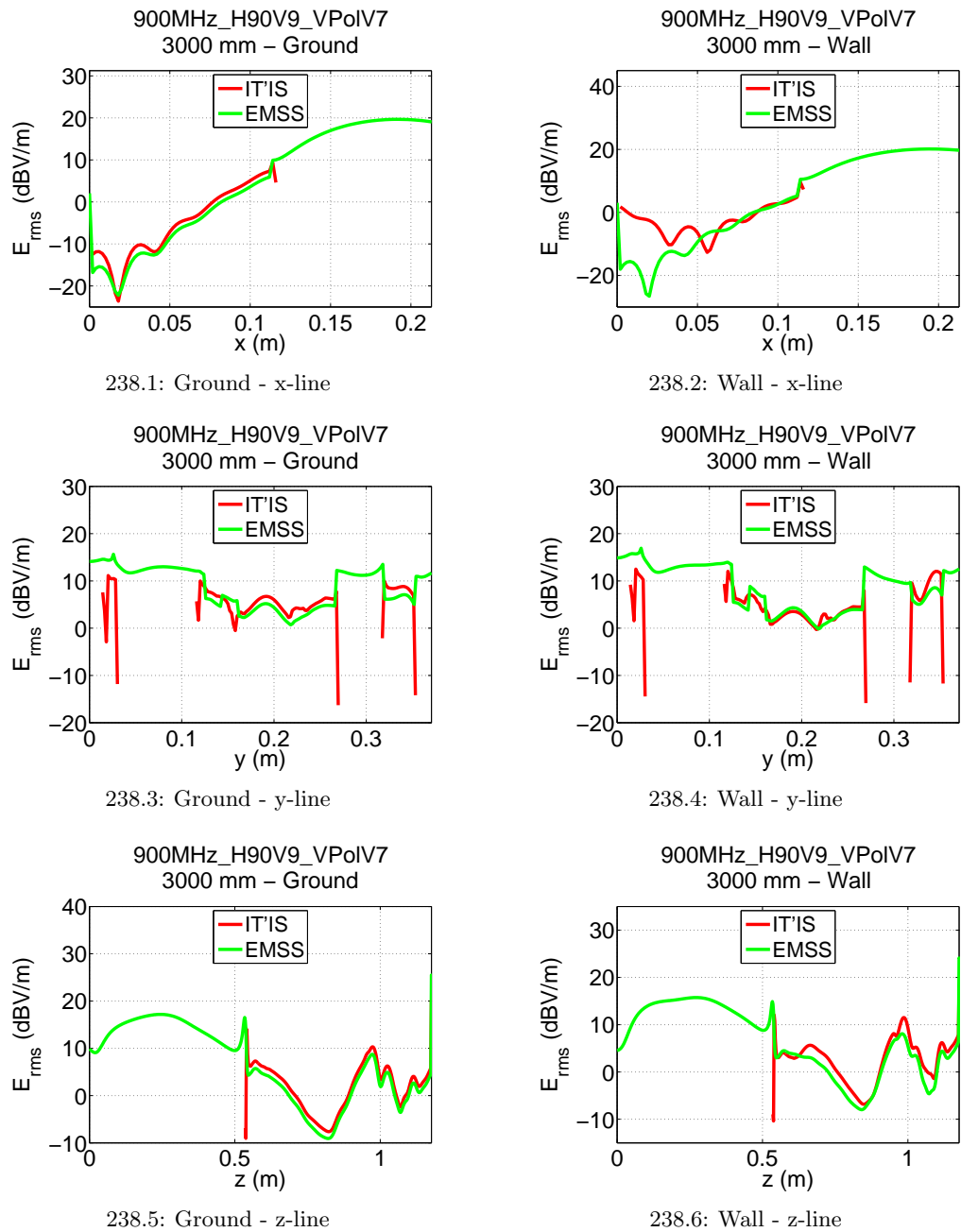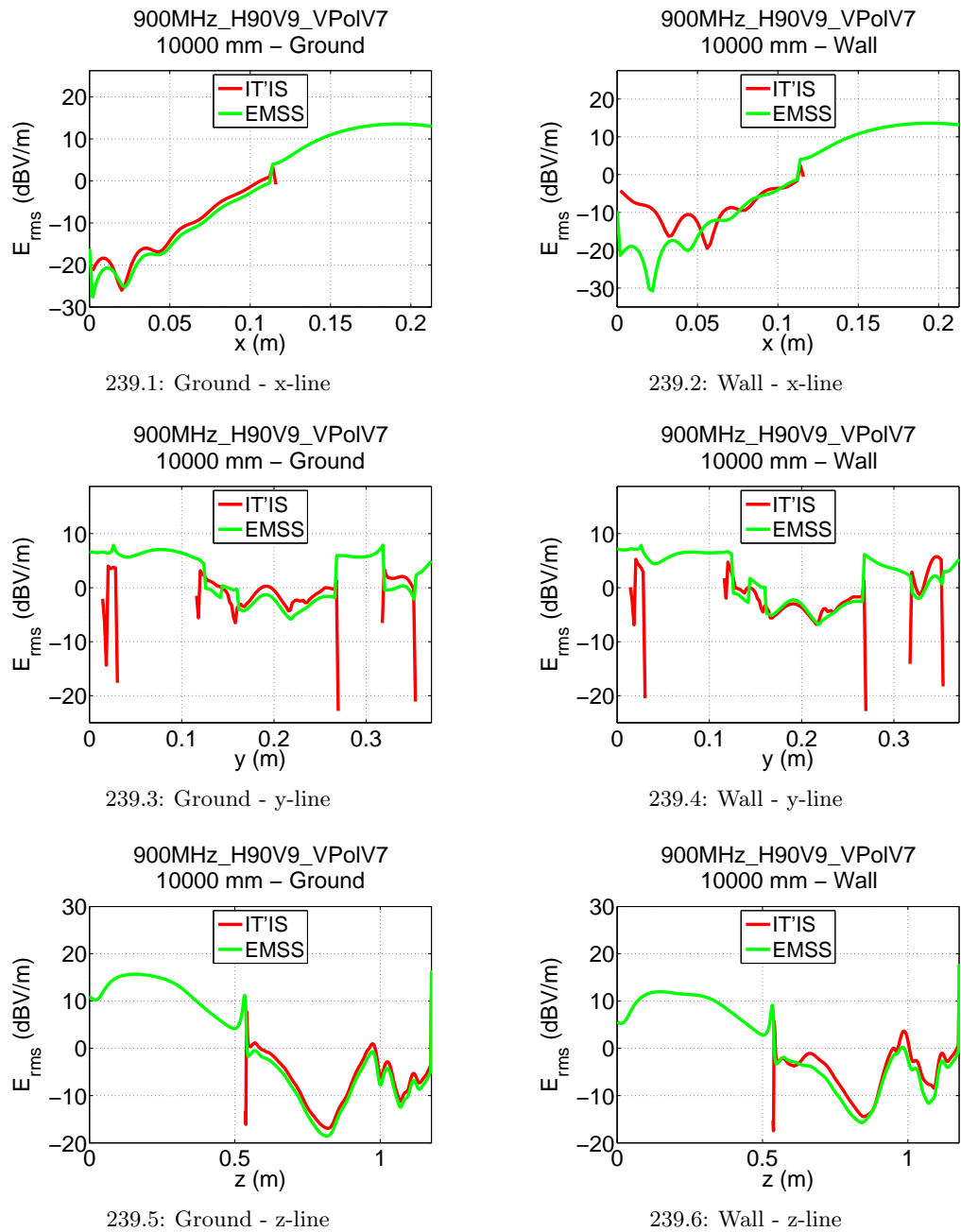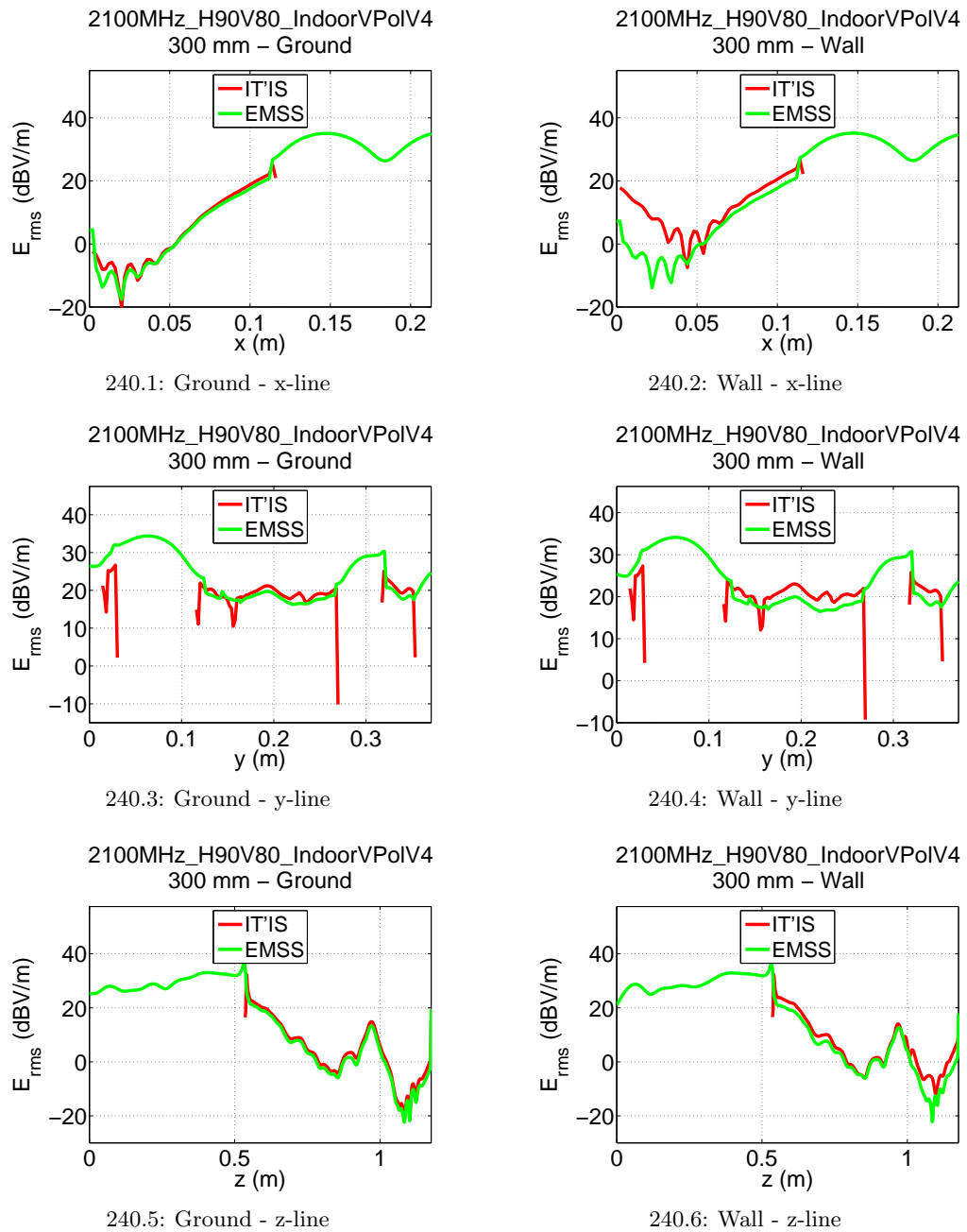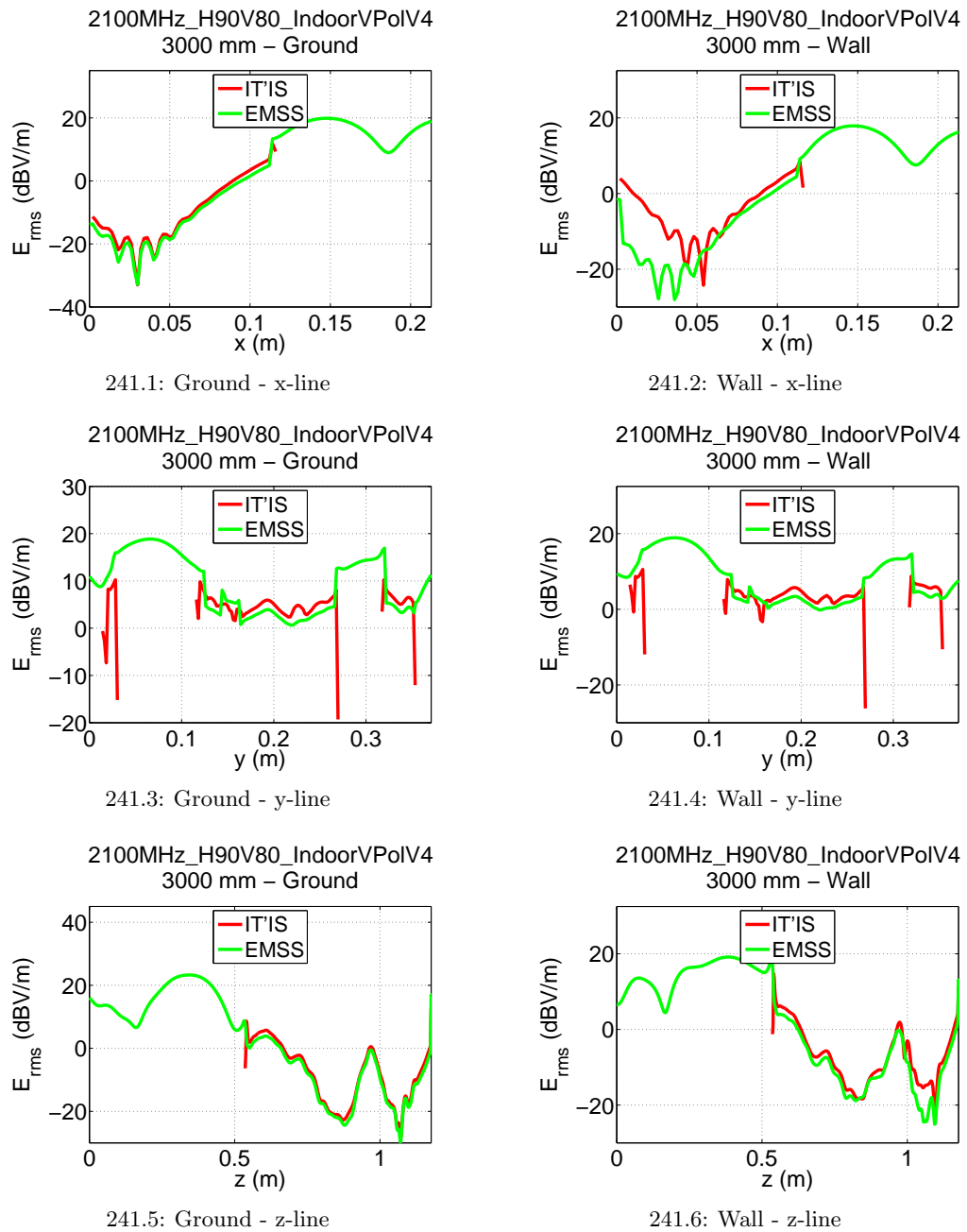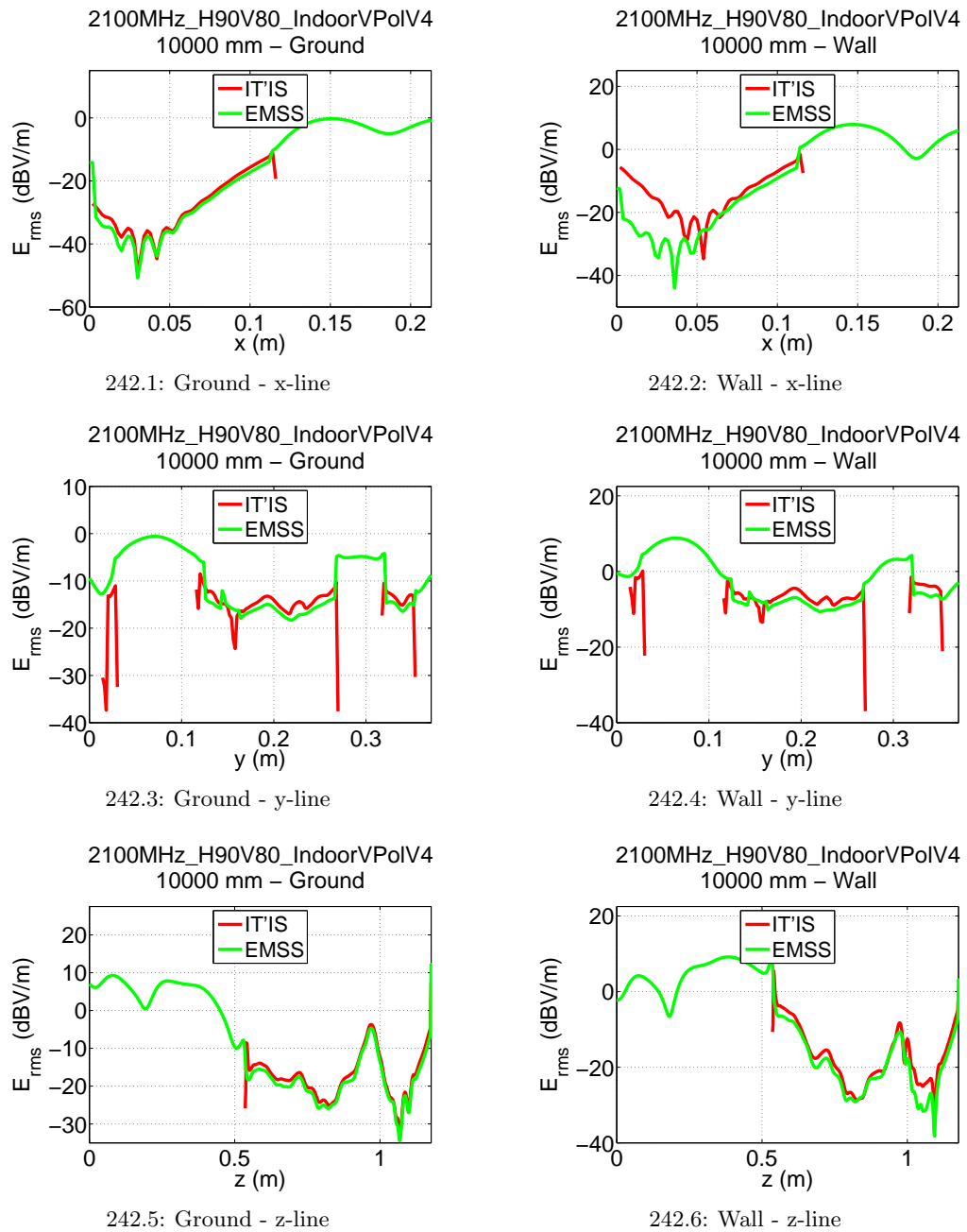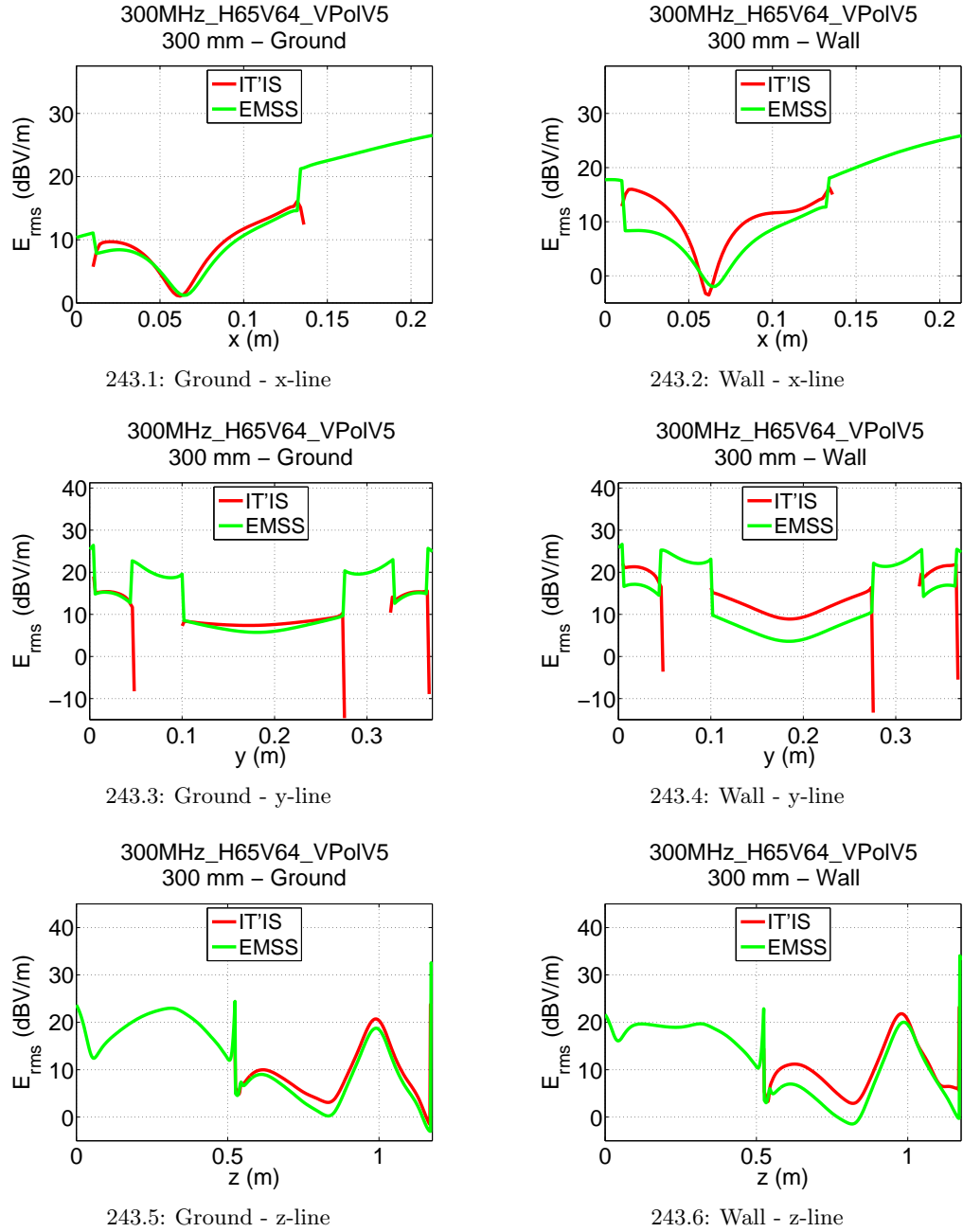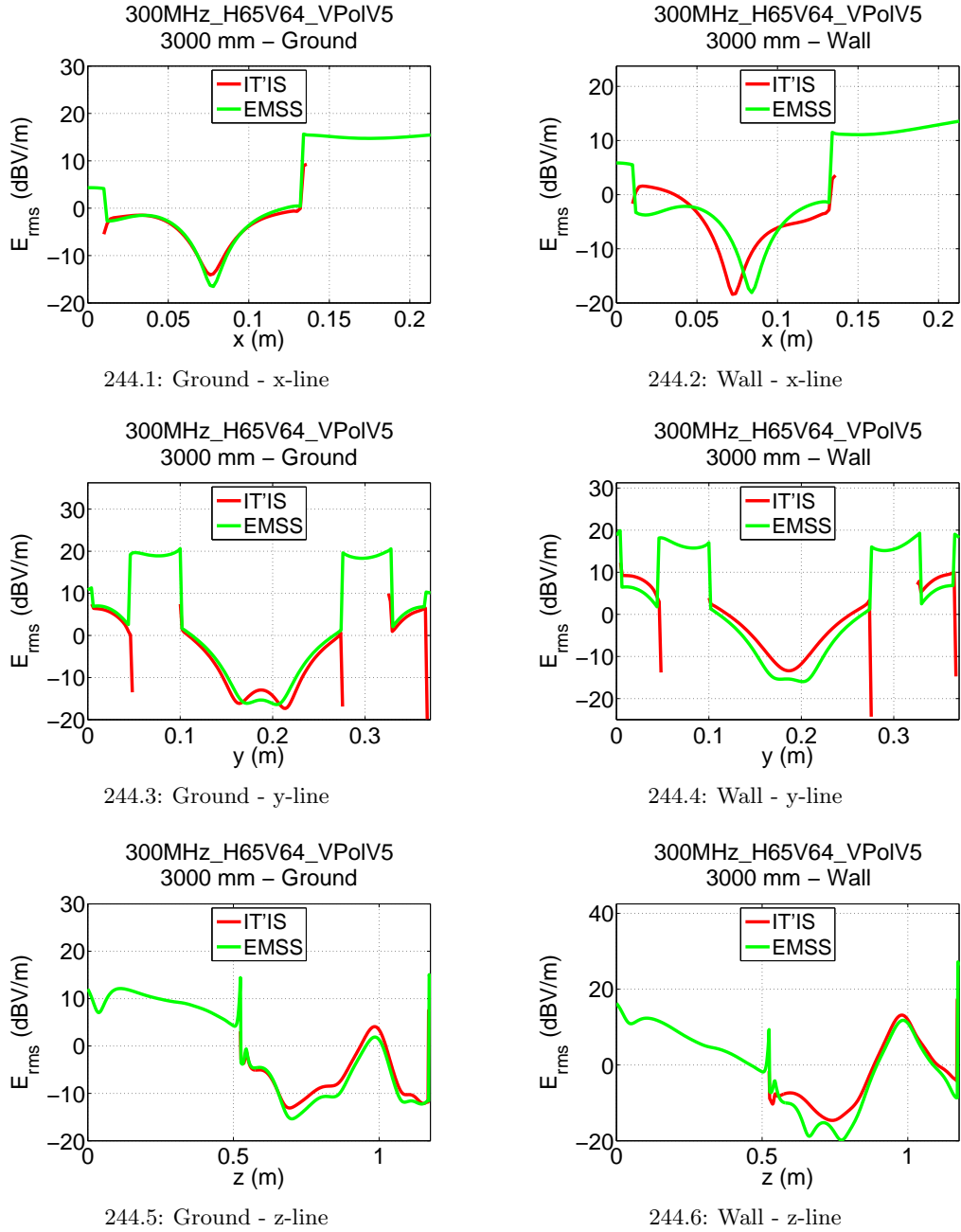
# I Inter-laboratory Comparison Results Sheet

**Full Wave SAR Evaluations – Plane Waves**

| Anatomical Model from Virtual Family | Antenna | Frequency GHz | Resolution mm | | 1g SAR W/kg | location 1g SAR x m | y m | z m | 10g SAR W/kg | location 10g SAR x m | y m | z m | whole body averaged SAR W/kg | Total Mass [Kg] |
|---|---|---|---|---|---|---|---|---|---|---|---|---|---|---|
| homogeneous | male adult: Duke | plane wave | 0.9 | 2 | | | | | | | | | | | |
| | child boy 6y: Thelonious | plane wave | 0.9 | 2 | | | | | | | | | | | |
| | child boy 6y: Thelonious | plane wave | 2.1 | 2 | | | | | | | | | | | |
| | child boy 6y: Thelonious | plane wave | 5.0 | 1 | | | | | | | | | | | |

**Full Wave SAR Evaluations – Representative Base Station Antenna**

| Anatomical Model from Virtual Family | Antenna | Frequency GHz | Resolution mm | | 1g SAR W/kg | location 1g SAR x m | y m | z m | 10g SAR W/kg | location 10g SAR x m | y m | z m | whole body averaged SAR W/kg | Total Mass [Kg] |
|---|---|---|---|---|---|---|---|---|---|---|---|---|---|---|---|
| homogeneous | male adult: Duke | 900MHz-H90V9 VPol Outdoor | 0.9 | 2 | | | | | | | | | | | |
| | child boy 6y: Thelonious | 900MHz-H90V9 VPol Outdoor | 0.9 | 2 | | | | | | | | | | | |
| | child boy 6y: Thelonious | 2100MHz-H90V80 VPol Indoor base station | 2.1 | 2 | | | | | | | | | | | |
| | child boy 6y: Thelonious | 5000MHz-H65V35 VPol Directional Panel | 5 | 1 | | | | | | | | | | | |

**Full Wave SAR Evaluations – Plane Waves**

| Anatomical Model from Virtual Family | Antenna | Frequency GHz | Resolution mm | | 1g SAR W/kg | location 1g SAR x m | y m | z m | 10g SAR W/kg | location 10g SAR x m | y m | z m | whole body averaged SAR W/kg | Total Mass [Kg] |
|---|---|---|---|---|---|---|---|---|---|---|---|---|---|---|---|
| in-homogeneous | male adult: Duke | plane wave | 0.9 | 2 | | | | | | | | | | | |
| | child boy 6y: Thelonious | plane wave | 0.9 | 2 | | | | | | | | | | | |
| | child boy 6y: Thelonious | plane wave | 2.1 | 2 | | | | | | | | | | | |
| | child boy 6y: Thelonious | plane wave | 5 | 1 | | | | | | | | | | | |

**Full Wave SAR Evaluations – Representative Base Station Antenna**

| Anatomical Model from Virtual Family | Antenna | Frequency GHz | Resolution mm | | 1g SAR W/kg | location 1g SAR x m | y m | z m | 10g SAR W/kg | location 10g SAR x m | y m | z m | whole body averaged SAR W/kg | Total Mass [Kg] |
|---|---|---|---|---|---|---|---|---|---|---|---|---|---|---|---|
| in-homogeneous | male adult: Duke | 900MHz-H90V9 VPol Outdoor | 0.9 | 2 | | | | | | | | | | | |
| | child boy 6y: Thelonious | 900MHz-H90V9 VPol Outdoor | 0.9 | 2 | | | | | | | | | | | |
| | child boy 6y: Thelonious | 2100MHz-H90V80 VPol Indoor base station | 2.1 | 2 | | | | | | | | | | | |
| | child boy 6y: Thelonious | 5000MHz-H65V35 VPol Directional Panel | 5 | 1 | | | | | | | | | | | |

**Free space simultions**

| | Antenna | Frequency GHz | free space antenna input impedance Re Ohm | Im Ohm | Re Ohm | Im Ohm | Re Ohm | Im Ohm | Re Ohm | Im Ohm | far-field pattern horizontal half power beamwidth (-3dB) degrees | vertical half-power beamwidth (-3dB) degrees | directivity dBi |
|---|---|---|---|---|---|---|---|---|---|---|---|---|---|
| Free space simultions | 900MHz-H90V9 VPol Outdoor | 0.9 | | | | | | | | | | | |
| | 2100MHz-H90V80 VPol Indoor base station | 2.1 | | | | | | | | | | | |
| | 5000MHz-H65V35 VPol Directional Panel | 5 | | | | | | | | | | | |

Peak value of Erms in a plane with a height of

| 1cm V/m | 5cm V/m | 30cm V/m | 50cm V/m |
|---|---|---|---|

Peak value of Hrms in a plane with a height of

| 1cm A/m | 5cm A/m | 30cm A/m | 50cm A/m |
|---|---|---|---|

jpg picture

jpg pictures: directivity in dBi in planes xy (horizontal) and xz (vertical), plotted in a rectangular coordinates system

scale for jpg pictures: dB scale 0/-20dBm where 0dB = max field rms in this plane

# J  WP6 – Generalized Huygen's Box Validation Sheet

| Anatomical model from Virtual Family | Antenna | Distance | Method | Antenna input impedance | | | | | | | | Weight | whole-body averaged SAR | 10g SAR | maximum 10g SAR in whole phantom | | | 1g SAR | maximum 1g SAR in whole phantom | | |
|---|---|---|---|---|---|---|---|---|---|---|---|---|---|---|---|---|---|---|---|---|---|
| | | | | Re | Im | Re | Im | Re | Im | Re | Im | | | | x | y | z | | x | y | z |
| | | m | | Ohm | Ohm | Ohm | Ohm | Ohm | Ohm | Ohm | Ohm | kg | W/kg | W/kg | m | m | m | W/kg | m | m | m |
| **300 MHz** | | | | | | | | | | | | | | | | | | | | | |
| child boy 6y: Thelonious, homogeneous | 300MHz_H65V64_VPolV5 | 0.3 | Whole System / Huygens Box | | | | | | | | | | | | | | | | | | |
| child boy 6y: Thelonious, homogeneous | 300MHz_H65V64_VPolV5 | 3 | Whole System / Huygens Box | | | | | | | | | | | | | | | | | | |
| **900MHz** | | | | | | | | | | | | | | | | | | | | | |
| child boy 6y: Thelonious, homogeneous | 900MHz_H90V9_VPolV7 | 0.3 | Whole System / Huygens Box | | | | | | | | | | | | | | | | | | |
| child boy 6y: Thelonious, homogeneous | 900MHz_H90V9_VPolV7 | 3 | Whole System / Huygens Box | | | | | | | | | | | | | | | | | | |
| **2100 MHz** | | | | | | | | | | | | | | | | | | | | | |
| child boy 6y: Thelonious, homogeneous | 2100MHz_H90V80_IndoorVPolV4 | 0.3 | Whole System / Huygens Box | | | | | | | | | | | | | | | | | | |
| child boy 6y: Thelonious, homogeneous | 2100MHz_H90V80_IndoorVPolV4 | 3 | Whole System / Huygens Box | | | | | | | | | | | | | | | | | | |

## K   WP7 – Generalized Huygen's Box Validation Sheet

| Human body model | Reflector | f (MHz) | antenna | Distance between antenna and anatomical model | Total mass of phantom (kg) | Whole-body SAR (W/kg) | 1g SAR (W/kg) | Location of 1g SAR (m) x | y | z | 10g SAR (W/kg) | Location of 10g SAR (m) x | y | z |
|---|---|---|---|---|---|---|---|---|---|---|---|---|---|---|
| Homogeneous VFB | Ground reflector | 300 | 300MHz_H65V64_VPolV5 | 0.3 | | | | | | | | | | |
| Homogeneous VFB | Ground reflector | 300 | 300MHz_H65V64_VPolV5 | 3 | | | | | | | | | | |
| Homogeneous VFB | Ground reflector | 300 | 300MHz_H65V64_VPolV5 | 10 | | | | | | | | | | |
| Homogeneous VFB | Vertical reflector | 300 | 300MHz_H65V64_VPolV5 | 0.3 | | | | | | | | | | |
| Homogeneous VFB | Vertical reflector | 300 | 300MHz_H65V64_VPolV5 | 3 | | | | | | | | | | |
| Homogeneous VFB | Vertical reflector | 300 | 300MHz_H65V64_VPolV5 | 10 | | | | | | | | | | |
| Homogeneous VFB | Ground reflector | 900 | 900MHz_H90V9_VPolV7 | 0.3 | | | | | | | | | | |
| Homogeneous VFB | Ground reflector | 900 | 900MHz_H90V9_VPolV7 | 3 | | | | | | | | | | |
| Homogeneous VFB | Ground reflector | 900 | 900MHz_H90V9_VPolV7 | 10 | | | | | | | | | | |
| Homogeneous VFB | Vertical reflector | 900 | 900MHz_H90V9_VPolV7 | 0.3 | | | | | | | | | | |
| Homogeneous VFB | Vertical reflector | 900 | 900MHz_H90V9_VPolV7 | 3 | | | | | | | | | | |
| Homogeneous VFB | Vertical reflector | 900 | 900MHz_H90V9_VPolV7 | 10 | | | | | | | | | | |
| Homogeneous VFB | Ground reflector | 2100 | 2100MHz_H90V80_IndoorVPolV4 | 0.3 | | | | | | | | | | |
| Homogeneous VFB | Ground reflector | 2100 | 2100MHz_H90V80_IndoorVPolV4 | 3 | | | | | | | | | | |
| Homogeneous VFB | Ground reflector | 2100 | 2100MHz_H90V80_IndoorVPolV4 | 10 | | | | | | | | | | |
| Homogeneous VFB | Vertical reflector | 2100 | 2100MHz_H90V80_IndoorVPolV4 | 0.3 | | | | | | | | | | |
| Homogeneous VFB | Vertical reflector | 2100 | 2100MHz_H90V80_IndoorVPolV4 | 3 | | | | | | | | | | |
| Homogeneous VFB | Vertical reflector | 2100 | 2100MHz_H90V80_IndoorVPolV4 | 10 | | | | | | | | | | |